Forschungszentrum Jülich
in der Helmholtz-Gemeinschaft

Institut für Kernphysik

Strong Interactions and Electromagnetism in Low-Energy Hadron Physics

Bastian Kubis

Jül-4007

Strong Interactions and Electromagnetism in Low-Energy Hadron Physics

Bastian Kubis

Berichte des Forschungszentrums Jülich ; 4007
ISSN 0944-2952
Institut für Kernforschung Jül-4007
D 5 (Diss., Bonn, Univ., 2002)

Zu beziehen durch: Forschungszentrum Jülich GmbH · Zentralbibliothek
D-52425 Jülich · Bundesrepublik Deutschland
☎ 02461/61-5220 · Telefax: 02461/61-6103 · e-mail: zb-publikation@fz-juelich.de

Strong Interactions and Electromagnetism in Low–Energy Hadron Physics

In the present work, we study various aspects of the entanglement of the strong and electromagnetic interactions as it is manifest in low–energy hadron physics. In the framework of chiral perturbation theory, two aspects are investigated: the test of the structure of baryons as probed by external electromagnetic currents, and the modification of reactions mediated by the strong interactions in the presence of internal (virtual) photons. In the first part of this work, we study the electromagnetic form factors of nucleons and the ground state baryon octet, as well as strangeness form factors of the nucleon. Emphasis is put on the comparison of a new relativistic scheme for the calculation of loop diagrams to the heavy baryon formalism, and on the convergence of higher order corrections in both schemes. The new scheme is shown to yield both a phenomenologically more successful description of the data and better convergence behaviour. In the second part, we study isospin violation in pion–kaon scattering as mediated by virtual photon effects and the light quark mass difference. This investigation is of particular importance for the extraction of scattering lengths from measurements of lifetime and energy levels in pion–kaon atoms. The isospin breaking corrections are shown to be small and sufficiently well under control.

Starke Wechselwirkung und Elektromagnetismus in niederenergetischer Hadronenphysik

In dieser Arbeit werden verschiedene Aspekte des Zusammenspiels von starker und elektromagnetischer Wechselwirkung studiert, wie sie in niederenergetischer Hadronenphysik studiert werden können. Im Rahmen der chiralen Störungstheorie werden dabei zwei Aspekte untersucht: die Struktur von Baryonen, wie sie von äußeren elektromagnetischen Strömen getestet werden kann, sowie die Modifikation starker Reaktionen durch innere (virtuelle) Photonen. Im ersten Teil der Arbeit werden elektromagnetische Formfaktoren untersucht, sowohl die der Nukleonen als auch die des baryonischen Grundzustandsoktetts; des weiteren analysieren wir die sogenannten seltsamen Formfaktoren des Nukleons. Schwerpunkte liegen auf dem Vergleich eines neuen relativistischen Rechenschemas für Schleifendiagramme mit dem Formalismus schwerer Baryonen, und auf der Untersuchung der Konvergenz von Korrekturen höherer Ordnung in beiden Formalismen. Es wird gezeigt, dass das neue Schema sowohl zu einer phänomenologisch erfolgreicheren Beschreibung führt als auch ein besseres Konvergenzverhalten aufweist. Im zweiten Teil wird Isospinverletzung in Pion–Kaon Streuung untersucht, verursacht sowohl durch virtuelle Photonen als auch durch den Massenunterschied der leichten Quarks. Diese Rechnung ist besonders wichtig für die Extraktion von Streulängen aus den Messungen von Lebensdauer und Energieniveaus von Pion–Kaon Atomen. Es wird gezeigt, dass die isospinbrechenden Korrekturen klein und hinreichend gut unter Kontrolle sind.

Contents

Introduction

The quantum field theory of electromagnetism, Quantum Electrodynamics (QED), is one of the most precise theories in all of modern physics. Originally formulated in the 1940s, it has yielded calculations of higher and higher accuracy up to this very day, and has provoked experimental efforts to test it to incredible precision. This theory has produced some of the most stunning agreements ever between theoretical predictions and experiments. To quote but two, the magnetic moment of the electron and the muon are known to thirteen and eleven significant decimal places [PDG02], respectively!

However, the successes of the description of electromagnetic properties in particle physics began to falter as soon as they were interwoven with the strong interactions. Victor Weisskopf relates the story (see [Dr00] and references therein) how Otto Stern, during a seminar in Göttingen shortly before his famous measurement of the magnetic moment of the proton, received no other prediction among the present theoreticians than $\mu_p = 1$ (as given by the Dirac equation), where we today know $\mu_p \approx 2.793$. The measurement of a large anomalous magnetic moment of the proton (and, subsequently, of other baryons) was the first sign of the fact that the proton is no "elementary" particle, but has a rich substructure that can be studied e.g. by electromagnetic probes.

Although we think we know today what the underlying theory for such a strongly interacting system like the proton is: Quantum Chromodynamics (QCD), and although we think we know what the substructure consists of: quarks and gluons, such time honored experimental findings as the one about μ_p still pose tremendous problems to contemporary theoretical physics. QCD in some ways closely mirrors many of the properties of QED, the great role model for all subsequently developed field theories in particle physics, but it often fails completely in coming anywhere close to the accuracy quoted above for certain QED calculations: current results from lattice QCD computations aim at (but do not necessarily reach) an accuracy of 10–15% [LWD91, GJJ01] for the proton magnetic moment, and as we shall see in the course of this work, even in theoretical frameworks that do not attempt to compute magnetic moments *ab initio*, but rather relate moments of different hadrons to each other based on symmetry considerations, struggle hard to get beyond such a precision.

There is another aspect to the history of strong interactions "spoiling" the successes of Quantum Electrodynamics. Even for such quantities like the abovementioned magnetic moments of electron and muon that characterise the electromagnetic properties of leptons, hence particles that do not interact strongly, higher order corrections do involve virtual quark/antiquark or hadronic states. In fact, the uncertainty about the hadronic contributions to these corrections are now the limiting factor for theoretical predictions of the anomalous magnetic moment of the muon (for a review linked to the recent experimental results [G201], see [Me01]). This is a new quality of the entanglement of hadronic physics and electromagnetism: both influence each other to a certain degree via virtual effects, and neither can be ignored in high–precision tests of the other.

In the previous paragraphs we have sketched the subject of all of this work: the interplay of strong and electromagnetic interactions in the low energy domain of particle physics. This interplay can be studied under the two different aspects, partly outlined above. First, electromagnetism can be used as an *external* probe to test the structure of hadrons, which itself is essentially given by the strong interactions. Experiments of such type can involve real or virtual photons, the latter usually provided by electron scattering, and the reaction on the target can be either elastic or inelastic. Predictions for such experiments can be made by any kind of theory or model for the strong interactions that can be consistently coupled to external electromagnetic currents, obeying gauge invariance etc.

The second aspect also concerns seemingly purely strong reactions such as hadron hadron scattering. Although the strong interactions may vastly dominate the behaviour of such reactions, the inclusion of electromagnetic corrections proves essential as soon as the experimental accuracy allows for high precision tests. These corrections can be viewed as *internal* electromagnetic effects, as they are based on the exchange of virtual photons either between charged hadrons, or between the charged quarks within (even neutral) hadrons. The challenge for theory is to simultaneously and consistently treat strong and electromagnetic interactions, both in order to make sufficiently accurate predictions for precision tests in hadron physics, and in order to be able to isolate the purely strong part of physical observables from experimental data.

The theoretical framework we shall employ to study such questions in this work is Chiral Perturbation Theory (ChPT). Usually apostrophised as the effective field theory of the strong interactions at low energies, it is ideally suited to address exactly the problems of the interplay of QCD and QED because it is more than just that. As it is a quantum field theory, the formalism of coupling its degrees of freedom to external currents is well–established and strictly equivalent to the coupling of QCD degrees of freedom to such sources [We79, Le94]. Furthermore, the formalism can include the most general virtual photon effects and therefore allows for the desired consistent treatment of electromagnetic corrections to strong processes. The more formal aspects of how QCD in the presence of QED can be related to "pure" QCD have been readdressed recently and are not yet fully understood [Ga02].

This work is organised as follows: After an introduction to the basics of Chiral Perturbation Theory in Chapter 1, all of Part I will be devoted to a study of electromagnetic form factors, the observables parameterising the hadronic structure as reveiled in elastic electron scattering experiments. Chapter 2 starts out with a low–energy analysis of the form factors for proton and neutron, Chapter 3 extends this investigation to the whole baryon ground state octet. The leading moments of these form factors, magnetic moments and both electric and magnetic radii, will feature prominently in these studies. Chapter 4 provides an extension in a slightly different direction by considering strangeness form factors of the nucleon, going beyond pure electromagnetism.

Part II switches focus to the second aspect of photons in strong–interaction physics and studies their impact on pion kaon scattering. Chapter 5 summarises the main work in this part and gives an analysis of isospin violation in this reaction. It is followed by a more technical Chapter 6 that investigates some particular aspects of amplitudes involving virtual photon exchanges.

Both parts are supplemented by appendices that collect formulae or technical details. A final outlook hints at future directions for research related to these results.

Chapter 1

Chiral Perturbation Theory

In this chapter, we wish to give a very brief introduction to the ideas and basic features of the theory underlying all calculations in this thesis, Chiral Perturbation Theory. We restrict ourselves to the basic principles for the construction of chiral Lagrangians and defer all the higher order terms needed for particular calculations to the later chapters, which we try to keep as self–contained as possible.

1.1 Chiral symmetry of QCD

The widely accepted theory of the strong interactions within the Standard Model is a non–abelian gauge theory, Quantum Chromodynamics (QCD). It describes quarks as the elementary matter fields and gluons as the gauge bosons of an SU(3) colour symmetry. The QCD Lagrangian has the form

$$\mathcal{L}_{\rm QCD} = -\frac{1}{4} G_{a,\mu\nu} G_a^{\mu\nu} + \bar{q}\Big(i\not{D} - \mathcal{M}\Big) q + \frac{\theta\, g^2}{64\pi^2} G_{a,\mu\nu} \tilde{G}_a^{\mu\nu} \quad , \tag{1.1}$$

where q comprises all quark flavours, $q^T = (u, d, s, \ldots)$, chosen such that the mass matrix is diagonal, $\mathcal{M} = \text{diag}(m_u, m_d, m_s, \ldots)$. The covariant derivative is given by $D^\mu = \partial^\mu - ig\, T_a G_a^\mu$, G_a^μ is the gluon field, $G_a^{\mu\nu}$ the corresponding field strength tensor, T_a are the SU(3) generators, e.g. linked to the Gell-Mann matrices by $T_a = \frac{\lambda_a}{2}$, and g is the strong coupling constant. The last term in Eq. (1.1) contains the dual field strength tensor $\tilde{G}_a^{\mu\nu} = 1/2\, \epsilon^{\mu\nu\alpha\beta}\, G_{a,\alpha\beta}$ and is related to the problem of strong *CP* violation (for a review, see [Pe89]). The parameter θ parameterising its strength has not (yet) been shown to be non–vanishing experimentally, so we shall drop this term in everything that follows. Furthermore, we have neglected gauge fixing terms altogether in Eq. (1.1).

In the limit of the masses of N_f quark flavours being set to zero, the left– and right–handed components of these N_f quark fields decouple according to

$$\mathcal{L}_{\rm QCD} \to \bar{q}_L\, i\not{D}\, q_L + \bar{q}_R\, i\not{D}\, q_R \tag{1.2}$$

(only the quark parts of the Lagrangian are displayed), where we define the left– and right–handed fields using the projection operators $P_{L/R}$,

$$q_{L/R} = P_{L/R}\, q = \frac{1}{2}(1 \mp \gamma_5) q \quad . \tag{1.3}$$

This Lagrangian displays an additional (global) $U(N_f)_L \times U(N_f)_R$ symmetry. The abelian subgroups are of no interest for what follows: one decomposes the symmetry group into irreducible subgroups according to

$$U(N_f)_L \times U(N_f)_R \to \underbrace{SU(N_f)_L \times SU(N_f)_R}_{\text{chiral group}} \times U(1)_V \times U(1)_A \quad , \tag{1.4}$$

and notes that $U(1)_V$ is realised in the conserved baryon number, while $U(1)_A$ is anomalously broken and is no symmetry of QCD [tHo76].

If the remaining $SU(N_f)_L \times SU(N_f)_R$ symmetry (which is of course only approximate in the real world as the quark masses are not exactly zero) was realised in the Wigner–Weyl mode, we should expect to observe parity doubling of the low–lying hadron spectrum, e.g. baryons with J^P quantum numbers $\frac{1}{2}^-$ (nearly) degenerate in mass with the observed $\frac{1}{2}^+$ ones. Nothing like this is found experimentally. Therefore, there are strong indications that the symmetry is realised in the Goldstone mode, namely via spontaneous symmetry breaking (SSB), yielding Goldstone bosons that carry the same quantum numbers as the broken generators. With the chiral group broken down to its vectorial subgroup, $SU(N_f)_L \times SU(N_f)_R \stackrel{\text{SSB}}{\longrightarrow} SU(N_f)_V$, there should be $N_f^2 - 1$ pseudoscalar ($J^P = 0^-$) Goldstone bosons corresponding to the broken axial generators. For $N_f = 3$, these can be identified with the pions, the kaons, and the eta. In the low–energy regime, one should be able to describe the properties of these Goldstone bosons and their interactions with the help of effective Lagrangians, constructed on the principle of chiral symmetry as well as other general symmetries of the strong interactions such as Lorentz invariance, parity, charge conjugation symmetry, etc.

1.2 The meson Lagrangian

1.2.1 Construction

Let us first briefly introduce the formalism to deal with effective Lagrangians for spontaneously broken symmetries as worked out by Callan, Coleman, Wess, and Zumino [CCWZ69]. Consider a symmetry group G spontaneously broken down to a subgroup H. One chooses a vacuum ground state ψ_0 for the fields $\psi(x)$ that is invariant under H, such that an arbitrary vector can be written as

$$\psi(x) = \Xi(x)\, \psi_0 \tag{1.5}$$

with $\Xi(x) \in G$. $\Xi(x)$ is not unique as $\Xi(x)\,\psi_0 = \Xi(x)\,\tilde{h}(x)\,\psi_0$ for any $\tilde{h}(x) \in H$. In the CCWZ formalism, one picks a set of broken generators X^a and chooses

$$\Xi(x) = e^{i\phi^a(x)X^a} \quad . \tag{1.6}$$

Under a global symmetry transformation $\psi(x) \to \tilde{g}\,\psi(x)$, $\Xi(x)$ behaves according to $\Xi(x) \to \tilde{g}\,\Xi(x)$ which is now not necessarily in the standard form, but in general

$$\tilde{g}\,\Xi(x) = \Xi'(x)\,\tilde{h} \tag{1.7}$$

for some $\tilde{h} \in H$ and a $\Xi'(x) \in G$ of the form (1.6), different from $\Xi(x)$. Hence the transformation of $\Xi(x)$ can be written as

$$\Xi(x) \to \tilde{g}\,\Xi(x)\,\tilde{h}^{-1}(\tilde{g}, \Xi(x)) \quad , \tag{1.8}$$

where $\tilde{h}^{-1}$ is a complicated nonlinear function of $\tilde{g}$ and $\Xi(x)$ (and hence implicitly depending on x).

In the $SU(3)_L \times SU(3)_R \xrightarrow{\text{SSB}} SU(3)_V$ case, the generators of the full symmetry group are T_L^a and T_R^a, those of the unbroken subgroup $T^a = T_L^a + T_R^a$. $SU(3)_L \times SU(3)_R$ transformations may be represented by block diagonal matrices

$$\tilde{g} = \begin{pmatrix} g_R & 0 \\ 0 & g_L \end{pmatrix} \tag{1.9}$$

where $g_L \in SU(3)_L$ and $g_R \in SU(3)_R$. The unbroken transformations are of the form $g_L = g_R = K$,

$$\tilde{h} = \begin{pmatrix} K & 0 \\ 0 & K \end{pmatrix} \quad . \tag{1.10}$$

One chooses the broken symmetry operators to be $X^a = T_L^a - T_R^a$. The resulting Ξ field, according to the general CCWZ prescription Eq. (1.6), is now

$$\Xi(x) = e^{i\phi^a(x)X^a/2F} = \exp\frac{i}{2F}\begin{pmatrix} \phi^a(x)T^a & 0 \\ 0 & -\phi^a(x)T^a \end{pmatrix} = \begin{pmatrix} u(x) & 0 \\ 0 & u^\dagger(x) \end{pmatrix} \tag{1.11}$$

where

$$u(x) = e^{i\phi^a(x)T^a/2F} \quad , \tag{1.12}$$

and F is a constant of mass dimension 1 introduced in order to make the $\phi^a(x)$ have mass dimension 1 like ordinary spin–zero fields. The value of F for the $\phi^a(x)$ interpreted as physical meson fields will be determined later on. The matrix ϕ in terms of physical particles can be written as

$$\phi = \phi^a T^a = \sqrt{2}\begin{pmatrix} \frac{1}{\sqrt{2}}\phi_3 + \frac{1}{\sqrt{6}}\phi_8 & \pi^+ & K^+ \\ \pi^- & -\frac{1}{\sqrt{2}}\phi_3 + \frac{1}{\sqrt{6}}\phi_8 & K^0 \\ K^- & \bar{K}^0 & -\frac{2}{\sqrt{6}}\phi_8 \end{pmatrix} \quad , \tag{1.13}$$

where the fields ϕ_3 and ϕ_8 correspond to the physical particles π^0 and η when neglecting some mixing (induced by $m_u \neq m_d$, see Eq. (1.51)). (Mixing with the η', which is no Goldstone boson, has been neglected altogether.)

The transformation rule for $\Xi(x)$, Eq. (1.8), now reads

$$\begin{pmatrix} u(x) & 0 \\ 0 & u^\dagger(x) \end{pmatrix} \to \begin{pmatrix} g_R & 0 \\ 0 & g_L \end{pmatrix} \begin{pmatrix} u(x) & 0 \\ 0 & u^\dagger(x) \end{pmatrix} \begin{pmatrix} K^{-1}(g,u) & 0 \\ 0 & K^{-1}(g,u) \end{pmatrix} , \tag{1.14}$$

yielding

$$u(x) \to g_R\, u(x)\, K^{-1}(g,u) = K(g,u)\, u(x)\, g_L^\dagger \tag{1.15}$$

which defines $K(g,u)$ in terms of g_L, g_R, and $u(x)$.

Another basis combining the meson fields in a unitary matrix is given by

$$U(x) = u^2(x) = e^{i\phi^a(x)T^a/F} , \tag{1.16}$$

which is seen to transform linearly as

$$U(x) \to g_R\, U(x)\, g_L^\dagger . \tag{1.17}$$

In both cases, the ϕ–fields transform in a complicated nonlinear way.

For the case of SU(2) chiral symmetry, a different way of combining the pion fields in a matrix representation is often more convenient than the exponential gauge given so far, since certain vertices vanish. In the so–called σ–model gauge, one defines

$$\begin{aligned} U(x) &= \sigma(x)\, \mathbf{1}_2 + i\, \frac{\vec{\tau}\cdot\vec{\pi}(x)}{F} , \\ \sigma(x) &= \sqrt{1-\frac{\pi^2(x)}{F^2}} , \quad \pi = \vec{\tau}\cdot\vec{\pi} = \begin{pmatrix} \pi^0 & \sqrt{2}\pi^+ \\ \sqrt{2}\pi^- & -\pi^0 \end{pmatrix} , \end{aligned} \tag{1.18}$$

which, upon expansion in the pion fields, yields

$$U(\pi) = 1 + \frac{i\,\pi}{F} - \frac{\pi^2}{2F^2} - \frac{\pi^4}{8F^4} + \mathcal{O}(\pi^6) , \tag{1.19}$$

$$u(\pi) = 1 + \frac{i\,\pi}{2F} - \frac{\pi^2}{8F^2} + \frac{i\,\pi^3}{16F^3} - \frac{5\,\pi^4}{128F^4} + \mathcal{O}(\pi^5) . \tag{1.20}$$

According to the usual procedure for low–energy effective theories, we now want to construct the most general Lagrangian, invariant under $SU(3)_L \times SU(3)_R$ symmetry transformations, as an expansion in terms of (small) momenta, or equivalently, of derivatives of the meson fields:

$$\mathcal{L}_\phi = \mathcal{L}_\phi^{(0)} + \mathcal{L}_\phi^{(2)} + \mathcal{L}_\phi^{(4)} + \ldots , \tag{1.21}$$

where the superscripts denote the number of derivatives in the respective terms. As there are no other four–vectors available, the number of derivatives always has to be even in order to form a Lorentz scalar. In fact, $\mathcal{L}_\phi^{(0)}$ is zero as U is unitary and hence terms like $\langle U^\dagger U\rangle$ (where $\langle \ldots \rangle$ denotes the trace in flavour space) are just constant. (Such terms only play a role when gravity is involved.) There is just one term of second order:

$$\mathcal{L}_\phi^{(2)} = \frac{F^2}{4}\langle \partial_\mu U^\dagger \partial^\mu U\rangle \quad , \tag{1.22}$$

where the coefficient has been chosen such as to reproduce the standard normalisation for the kinetic terms when Eq. (1.22) is expanded in terms of the meson fields,

$$\begin{aligned}\mathcal{L}_\phi^{(2)} &= \langle \partial_\mu \phi \partial^\mu \phi\rangle + \frac{1}{3F^2}\langle [\phi, \partial_\mu \phi]^2\rangle + \ldots \\ &= \frac{1}{2}\partial_\mu \pi^0 \partial^\mu \pi^0 + \partial_\mu \pi^+ \partial^\mu \pi^- + \partial_\mu K^+ \partial^\mu K^- + \partial_\mu \bar{K}^0 \partial^\mu K^0 + \frac{1}{2}\partial_\mu \eta \partial^\mu \eta + \ldots \quad ,\end{aligned} \tag{1.23}$$

where the ellipsis denotes terms of higher powers in the meson fields. The second term of order ϕ^4 is the lowest order contribution to the meson–meson scattering amplitude; we note that the meson fields are derivatively coupled, so the amplitude vanishes in the low–energy limit. Finally, we remark that introducing the chiral vielbein

$$u_\mu = i\left(u^\dagger \partial_\mu u - u \partial_\mu u^\dagger\right) = i u^\dagger \partial_\mu U u^\dagger \quad , \tag{1.24}$$

which behaves according to $u_\mu \to K u_\mu K^\dagger$ under chiral transformations, the Lagrangian (1.22) may be rewritten as

$$\mathcal{L}_\phi^{(2)} = \frac{F^2}{4}\langle u_\mu u^\mu\rangle \quad . \tag{1.25}$$

The Lagrangian of fourth order in momenta has three contributions and looks like [GL85a]

$$\mathcal{L}_\phi^{(4)} = L_1\langle \partial_\mu U^\dagger \partial^\mu U\rangle^2 + L_2\langle \partial_\mu U^\dagger \partial_\nu U\rangle\langle \partial^\mu U^\dagger \partial^\nu U\rangle + L_3\langle \partial_\mu U^\dagger \partial^\mu U \partial_\nu U^\dagger \partial^\nu U\rangle \quad , \tag{1.26}$$

where the coefficients L_i, the so–called low–energy constants (LECs), are not restrained by symmetries and have to be determined from experiment, calculated from lattice QCD, or estimated by some model.

1.2.2 Power counting and chiral symmetry breaking scale

In order for Chiral Perturbation Theory to be a predictive effective field theory, we have to convince ourselves that there exists a way to organise the perturbative expansion, based on the Lagrangians given in the last section, and to consistently truncate it in order to describe low–energy processes to a certain desired accuracy. The way to do this was introduced by Weinberg [We79].

Consider the case of pion–pion scattering. We have contributions from the different terms in the chiral Lagrangian

$$\mathcal{L}_\phi = \sum_d \mathcal{L}_\phi^{(d)} \quad , \tag{1.27}$$

where $\mathcal{L}_\phi^{(d)}$ is of d-th order in derivatives and gives a contribution to the four pion vertex proportional to q^d. Note that d is even and $d \geq 2$, the chiral Lagrangian starts out at order q^2, as discussed in the previous section. In an arbitrarily complicated loop graph, let there be L loops, I internal lines, and V_d vertices of order d. The amplitude is then of the form

$$\mathcal{A} \sim \int (d^4q)^L \frac{1}{(q^2)^I} \prod_d (q^d)^{V_d} \quad . \tag{1.28}$$

If $\mathcal{A}$ is to be of order q^ν, we have the relation

$$\nu = 4L - 2I + \sum_d d\, V_d \quad . \tag{1.29}$$

Using the topological identity for the number of loops

$$L = I - \sum_d V_d + 1 \tag{1.30}$$

to eliminate I, we obtain

$$\nu = \sum_d V_d(d-2) + 2L + 2 \quad . \tag{1.31}$$

The point to note about this expression is that all the terms on the right–hand side are positive because of $d \geq 2$, and for fixed ν there is always just a finite number of combinations of V_d and L that obey the condition of Eq. (1.31). For instance, for the pion–pion scattering amplitude at next–to–leading order, i.e. $\nu = 4$, one only has to consider one loop graphs involving lowest order interactions and tree graphs with one insertion from $\mathcal{L}_\phi^{(4)}$.

In effective field theories where heavy particles have explicitly been integrated out, the low energy expansion proceeds in powers of q/M, with M the mass of one of the particles eliminated from the theory. Equally, the coefficients L_i of the terms of order q^4 in Eq. (1.26) for example have to include negative powers of some dimensionful quantity which we shall call Λ_χ, the chiral symmetry breaking scale. The effective Lagrangian then looks like

$$\mathcal{L}_\phi = \frac{F^2}{4}\left\{ \langle \partial_\mu U^\dagger \partial^\mu U \rangle + \frac{\mathcal{L}_\phi^{(4)}}{\Lambda_\chi^2} + \frac{\mathcal{L}_\phi^{(6)}}{\Lambda_\chi^4} + \ldots \right\} \quad . \tag{1.32}$$

Let us try to find some heuristic arguments for the size of Λ_χ. For this purpose, we compare the two aforementioned contributions of order q^4 to the pion–pion scattering amplitude: the loop graphs with lowest order interactions ($I = 2$, $V_2 = 2$, $L = 1$) give a contribution like

$$I \sim \int \frac{d^4p}{(2\pi)^4} \frac{1}{(q^2)^2} \left(\frac{q^2}{F^2}\right)^2 \sim \frac{1}{(4\pi)^2} \frac{q^4}{F^4} \log \frac{M_\phi}{\lambda} \tag{1.33}$$

(in a mass independent renormalisation scheme such as dimensional regularisation), whereas the tree graphs with one insertion from $\mathcal{L}_\phi^{(4)}$ are proportional to

$$\frac{F^2}{\Lambda_\chi^2} \frac{q^4}{F^4} \quad . \tag{1.34}$$

As the total amplitude has to be independent of the renormalisation scale λ, a shift in λ in Eq. (1.33) of order 1 has to be compensated for by a shift in the coefficient in Eq. (1.34) of order $1/(4\pi)^2$. Therefore it would be unnatural for this coefficient to be smaller than the shift due to a change of the renormalisation scale which yields the condition for Λ_χ

$$\Lambda_\chi \leq 4\pi F \quad . \tag{1.35}$$

Later on, the constant F will be identified with the pion decay constant $F_\pi = 92.4$ MeV such that we obtain numerically $\Lambda_\chi \approx 1160$ MeV.

A more physical way of arguing ensues from the fact that Chiral Perturbation Theory does not incorporate any meson resonances as dynamical fields, therefore the validity of the chiral expansion is certainly limited to the energy regime below the resonance masses. Hence one could argue for a chiral symmetry breaking scale of about the mass of the lowest lying resonance, the ρ,

$$\Lambda_\chi \sim M_\rho \approx 770 \text{ MeV} \quad . \tag{1.36}$$

1.2.3 External sources

A convenient way to calculate matrix elements from chiral Lagrangians is to use external sources in the path integral formalism, a method well known from other quantum field theories. For this purpose, we introduce scalar (s), pseudoscalar (p), vector (v_μ), and axial vector (a_μ) sources. These are coupled to the QCD Lagrangian according to

$$\mathcal{L} = \mathcal{L}_{QCD} + \bar{q}\,\gamma^\mu\Big(v_\mu + \gamma_5\, a_\mu\Big)q - \bar{q}\,\Big(s - i\,\gamma_5\, p\Big)q \quad . \tag{1.37}$$

The effective generating functional is then of the form

$$\exp\Big\{i\,\mathcal{Z}[v_\mu, a_\mu, s, p]\Big\} = \int \mathcal{D}u \exp\Big\{i \int d^4x\, \mathcal{L}_{\text{eff}}[u, v_\mu, a_\mu, s, p]\Big\} \quad , \tag{1.38}$$

and matrix elements can be retrieved by functional derivation with respect to the external sources. Generalising the chiral symmetry transformations to *local*, i.e. gauge transformations, the left– and right–handed vector currents (that combine vector and axial vector currents) have the chiral transformation behaviour

$$l_\mu = v_\mu - a_\mu \quad \longrightarrow \quad g_L l_\mu g_L^\dagger + i g_L \partial_\mu g_L^\dagger \quad , \tag{1.39}$$

$$r_\mu = v_\mu + a_\mu \quad \longrightarrow \quad g_R r_\mu g_R^\dagger + i g_R \partial_\mu g_R^\dagger \quad . \tag{1.40}$$

These can be coupled to the chiral Lagrangian as gauge fields, in the form of covariant derivatives [GL85a]

$$\nabla_\mu U = \partial_\mu U - i[v_\mu, U] - i\{a_\mu, U\} \quad , \tag{1.41}$$

with Eq. (1.24) taking the new form

$$u_\mu \;=\; i\Big(u^\dagger(\partial_\mu - i\, r_\mu)u - u(\partial_\mu - i\, l_\mu)u^\dagger\Big) \;=\; i u^\dagger \nabla_\mu U u^\dagger \quad , \tag{1.42}$$

The scalar and pseudoscalar sources can be combined into the field χ,

$$\chi = 2B(s + i\, p) \quad , \tag{1.43}$$

which has to transform according to

$$\chi \longrightarrow g_R\, \chi\, g_L^\dagger \quad , \tag{1.44}$$

or further into fields

$$\chi_\pm = u^\dagger \chi u^\dagger \pm u \chi^\dagger u \tag{1.45}$$

that obey the transformation rule

$$\chi_\pm \longrightarrow K \chi_\pm K^\dagger \quad , \tag{1.46}$$

with the compensator field K determined in Eq. (1.15). The scalar source s incorporates the explicit symmetry breaking terms due to the non–vanishing quark masses,

$$s = \mathcal{M} + \ldots \quad , \qquad \mathcal{M} = \begin{pmatrix} m_u & 0 & 0 \\ 0 & m_d & 0 \\ 0 & 0 & m_s \end{pmatrix} \quad . \tag{1.47}$$

The transformation law Eq. (1.44) can be motivated by considering the QCD mass term

$$\mathcal{L}_\mathcal{M} = -\bar{q}_R\, \mathcal{M}\, q_L + \text{h.c.} \quad , \tag{1.48}$$

written in terms of left– and right–handed quark fields. Eq. (1.44) is made such as to leave the Lagrangian Eq. (1.48) invariant. The lowest order mass term in the chiral Lagrangian is hence given by

$$\mathcal{L}_\mathcal{M}^{(2)} = \frac{F^2}{4}\langle \chi_+ \rangle \quad , \tag{1.49}$$

which, expanded in the meson fields, results in the lowest order hadronic mass formulae for the mesons,

$$\begin{aligned} M^2_{\pi^-} &= B(m_u + m_d) + \mathcal{O}(m_q^2) \quad , \\ M^2_{K^\pm} &= B(m_u + m_s) + \mathcal{O}(m_q^2) \quad , \\ M^2_{K^0,\bar{K}^0} &= B(m_d + m_s) + \mathcal{O}(m_q^2) \quad , \end{aligned} \tag{1.50}$$

and for ϕ_3 and ϕ_8 in the mass matrix

$$B \begin{pmatrix} m_u + m_d & \frac{1}{\sqrt{3}}(m_u - m_d) \\ \frac{1}{\sqrt{3}}(m_u - m_d) & \frac{1}{3}(m_u + m_d + 4m_s) \end{pmatrix} \quad , \tag{1.51}$$

where the diagonal elements can be taken as the approximate mass eigenvalues of π^0 and η, neglecting mixing corrections that are of second order in the isospin violation parameter $(m_u - m_d)$. The constant B is related to the vacuum expectation value of the scalar quark density,

$$\langle 0|\,\bar{q}q\,|0\rangle = -F^2\,B\{1 + \mathcal{O}(m_q)\} \quad . \tag{1.52}$$

Note that B is only real if CP is conserved. We always assume $B \gg F$ (standard ChPT) such that, by comparison of both sides of the mass formulae, the quark masses are counted as $\mathcal{O}(q^2)$.

In [FSS91], a different scheme (called "generalised ChPT") was put up in which both B and m_q are counted as $\mathcal{O}(q)$. Because of the relation of the low energy constant B to the quark condensate in Eq. (1.52), this scenario allows for a different pattern of chiral symmetry breaking with a small quark condensate. This of course results in a different power counting, but will not be regarded in what follows, although the question of large versus small quark condensate is of high interest for the motivation of the investigations in Chapter 5.

In order to determine the omnipresent dimensionful quantity F, we have to calculate the two–point function of the axial–vector current

$$A^a_\mu = \bar{q}\,\gamma_\mu\gamma_5 T^a\,q \quad , \tag{1.53}$$

where T^a are the group generators, $T^a = \frac{1}{2}\lambda^a$ for SU(3) or $T^a = \frac{1}{2}\tau^a$ for SU(2). We find

$$\langle 0|A^a_\mu|\phi^b(p)\rangle = i\,F\,p_\mu\,\delta^{ab}\{1 + \mathcal{O}(m_q)\} \quad , \tag{1.54}$$

from which we immediately read off that F is the pion decay constant in the chiral limit,

$$F \approx 88 \text{ MeV} \quad , \tag{1.55}$$

see [GL83, GL84].

1.2.4 Inclusion of virtual photon effects

In the last section, the emphasis has been on coupling the QCD degrees of freedom to static external sources, which may in practice be provided (for the case of vector/axialvector sources) by gauge bosons of the electroweak interactions. We have not yet allowed for dynamically propagating gauge bosons, in particular for the propagation of (virtual) photons which, due to their masslessness, should in principle always be present in any low–energy theory. One might be tempted to think that it suffices to add the free Lagrangian for the electromagnetic field,

$$\mathcal{L}^{\mathrm{em}} = -\frac{1}{4}F_{\mu\nu}F^{\mu\nu} - \frac{\lambda}{2}(\partial \cdot A)^2 \quad , \tag{1.56}$$

where A_μ represents the photon field and $F_{\mu\nu} = \partial_\mu A_\nu - \partial_\nu A_\mu$ is the conventional electromagnetic field strength tensor, with λ the gauge fixing parameter. One then has to couple photons to the Goldstone boson fields through a once–more modified covariant derivative,

$$\nabla_\mu U = \partial_\mu U - i[v_\mu, U] - i\mathcal{Q}[A_\mu, U] - i\{a_\mu, U\} \tag{1.57}$$

(with $\mathcal{Q} = e\,\mathrm{diag}(2/3, -1/3, -1/3)$ the SU(3) quark charge matrix), and then proceed from the usual lowest order chiral Lagrangian

$$\mathcal{L}^{(2)} = \frac{F^2}{4}\langle \nabla_\mu U \nabla^\mu U^\dagger + \chi U^\dagger + \chi^\dagger U \rangle \quad . \tag{1.58}$$

It has been noted since long that this Lagrangian cannot possibly comprise all effects stemming from virtual photons. Suppose the charged to neutral pion mass difference was completely generated by virtual photon loops. On dimensional grounds, this mass contribution has to be of the form

$$(\Delta M_\pi^2)_{\mathrm{em}} = e^2 M_{\pi^+}^2 f(d) \tag{1.59}$$

(where d denotes the dimension of space time). This vanishes in the chiral limit $m_u = m_d = 0$. However, a low energy theorem ensures that the mass of the charged pion *in the chiral limit* should be given by the integral over the difference of the vector and axial vector spectral functions [Da67]. Saturating these by the lowest lying resonances ρ and a_1 and using the Weinberg sum rule $M_{a_1}^2 F_{a_1}^2 = M_\rho^2 F_\rho^2$ to link mass and decay constant of the a_1 to those of the ρ [We67], one arrives at [GL82]

$$(\Delta M_\pi^2)_{\mathrm{em}} = \frac{3\alpha}{32\pi F_\pi^2} F_\rho^2 M_\rho^2 \log\frac{F_\rho^2}{F_\rho^2 - F_\pi^2} \quad , \tag{1.60}$$

where $\alpha = e^2/4\pi$ is the fine structure constant. The (non–vanishing) low–energy limit of this expression should be represented in counterterms incorporating electromagnetic effects. Therefore, including virtual photons via minimal substitution in the covariant derivative only does not yield an accurate description of electromagnetism in the meson sector.

In order to construct the most general Lagrangian involving pions and virtual photons, one introduces spurions $Q_{L,R}$ with the transformation properties

$$Q_I \to g_I \, Q_I \, g_I^\dagger \quad , \quad g_I \in SU(3)_I \quad , \quad I = L, R \quad , \tag{1.61}$$

[Ur95, MMS97]. These are deduced from the decomposition of the quark level vector current in terms of left and right handed fields,

$$\bar{q} \, \gamma^\mu Q \, q = \bar{q}_L \, \gamma^\mu Q_L \, q_L + \bar{q}_R \, \gamma^\mu Q_R \, q_R \quad , \tag{1.62}$$

which is invariant under $SU(3)_L \times SU(3)_R$ exactly with the transformation law as given in Eq. (1.61). In the end, one sets $Q_{L,R} \to Q$.

The leading order electromagnetic Lagrangian constructed this way reads[Ec89]

$$\mathcal{L}^{(2,\mathrm{em})} = -\frac{1}{4} F_{\mu\nu} F^{\mu\nu} - \frac{\lambda}{2} (\partial \cdot A)^2 + C \, \langle Q_R \, U \, Q_L \, U^\dagger \rangle \quad . \tag{1.63}$$

In the σ–model gauge for the pions, the last term of this Lagrangian leads only to a term quadratic in pion fields. Consequently, the LEC C can be calculated from the charged to neutral pion mass difference,

$$(M_{\pi^\pm}^2 - M_{\pi^0}^2)_{\mathrm{em}} = (\Delta M_\pi^2)_{\mathrm{em}} = \frac{2e^2 C}{F^2} = 2Z e^2 F^2 \quad , \quad Z = \frac{C}{F^4} \quad . \tag{1.64}$$

We have $Z = 0.89$ if we use for F its value in the chiral limit, $F = 88\,\mathrm{MeV}$.

Note again recent work [Ga02] that attempts to put this formalism on a firmer theoretical ground.

1.3 Baryon fields

Up to now, we have seen how to construct the chirally invariant effective Lagrangian for the Goldstone bosons, how to include explicit symmetry breaking by mass terms, and how to systematically incorporate electromagnetism. The next thing we would like to do is to include fields for other low–lying hadrons, especially for the lightest baryon fields, the spin–1/2 baryon octet. We shall proceed in a similar way as for the mesons: choose a suitable representation and construct the most general Lagrangian allowed by symmetries.

In the SU(3) case, we may allow the octet of baryon fields

$$B = \begin{pmatrix} \frac{1}{\sqrt{2}}\Sigma^0 + \frac{1}{\sqrt{6}}\Lambda & \Sigma^+ & p \\ \Sigma^- & -\frac{1}{\sqrt{2}}\Sigma^0 + \frac{1}{\sqrt{6}}\Lambda & n \\ \Xi^- & \Xi^0 & -\frac{2}{\sqrt{6}}\Lambda \end{pmatrix} \tag{1.65}$$

to transform in any way under $SU(3)_L \times SU(3)_R$ that reduces to the adjoint (octet) representation of $SU(3)_V$ after spontaneous symmetry breakdown. It turns out that a particularly convenient transformation law is

$$B(x) \to K(x)\, B(x)\, K^\dagger(x) \quad , \tag{1.66}$$

where $K(x)$ is determined by Eq. (1.15). For an $SU(3)_V$ transformation with $g_L = g_R = K$, this is indeed the adjoint transformation law. Other allowed representations can be linked to this one by multiplying B with u or U (as discussed in [Ge84]).

Furthermore, it is convenient for the construction of the baryon Lagrangian to introduce the connection Γ^μ

$$\Gamma^\mu = \frac{1}{2}\left(u\partial^\mu u^\dagger + u^\dagger \partial^\mu u\right) \quad , \tag{1.67}$$

and use the chiral vielbein u^μ given before, Eq. (1.24). Their respective transformation properties under $SU(3)_L \times SU(3)_R$ are

$$\Gamma^\mu \;\to\; K\,\Gamma^\mu\, K^\dagger - (\partial^\mu K)\, K^\dagger \quad , \tag{1.68}$$

$$u^\mu \;\to\; K\, u^\mu\, K^\dagger . \tag{1.69}$$

Using (1.68), we can construct a covariant derivative of the baryon field according to

$$D^\mu B = \partial^\mu B + [\Gamma^\mu, B] \tag{1.70}$$

transforming as

$$D^\mu B \to K\,(D^\mu B)\, K^\dagger \quad . \tag{1.71}$$

To first order in derivatives/momenta, the most general baryon Lagrangian describing processes with no more than one incoming and one outgoing baryon is

$$\mathcal{L}^{(1)}_{\phi B} = \langle \bar{B}\,(i\not{D} - m)\, B\rangle + \frac{D}{2}\langle \bar{B}\gamma^\mu\gamma_5\,\{u_\mu, B\}\rangle + \frac{F}{2}\langle \bar{B}\gamma^\mu\gamma_5\,[u_\mu, B]\rangle \tag{1.72}$$

with m the average baryon mass, and D and F the axial vector coupling constants.[#1] $\langle \ldots \rangle$ again denotes the trace in flavour space.

In the case of SU(2) chiral symmetry, the nucleon doublet

$$\Psi = \begin{pmatrix} p \\ n \end{pmatrix} \quad , \tag{1.73}$$

consisting of proton and neutron, transforms according to the fundamental representation of SU(2),

$$\Psi \to K\Psi \quad . \tag{1.74}$$

[#1] Note that the symbol D is used for the covariant derivative and for one of the axial coupling constants. From the context it is, however, always obvious which one is meant. Similarly, the axial vector coupling F should not be confused with the pion decay constant in the chiral limit.

With the same definition of Γ^μ as before, the covariant derivative is now

$$D^\mu \Psi = \partial^\mu \Psi + \Gamma^\mu \Psi \quad , \tag{1.75}$$

and the most general pion nucleon Lagrangian to first order in derivatives turns out to be

$$\mathcal{L}_{\pi N}^{(1)} = \bar{\Psi}\Big(i\not{D} - m + \frac{g_A}{2}\not{u}\gamma_5\Big)\Psi \quad , \tag{1.76}$$

where the axial coupling g_A is related to the SU(3) couplings by $g_A = D + F$.

One severe drawback occurs in the formalism for including baryon fields as spelled out in this section: the introduction of a new mass scale that does not vanish in the chiral limit, comparable in size to the chiral symmetry breaking scale (average nucleon mass $m_N = \frac{1}{2}(m_p + m_n) = 939$ MeV, average baryon octet mass $m_B = \frac{1}{8}\sum_B m_B = 1151$ MeV, $4\pi F_\pi = 1161$ MeV), spoils the power counting argument, loop diagrams of arbitrary order can contribute to low energy processes. To remedy this problem, Jenkins and Manohar [JM91] suggested a procedure similar to the one used in heavy quark effective field theories, which consists in expanding around the extreme non relativistic limit and shifting the baryon mass dependence from the propagator to a series of new vertices suppressed by powers of $1/m$. Due to the observation made above that we have $m \sim 4\pi F$, it is sensible to generalise the chiral expansion to a twofold expansion both in $1/(4\pi F)$ and $1/m$ and adopt a power counting scheme treating both scales on an equal footing. This procedure was put on a more formally secure footing by [BKKM92] where a general formalism to construct the $1/m$ corrections on the Lagrangian level was developed, making use of path integral techniques.

A completely different technique that avoids the non relativistic expansion and allows for a manifestly Lorentz invariant calculation in ChPT with baryon fields has been developed in [BL99], building on work by [ET98] and since then extended also to processes involving more than one (conserved) baryon line [Go01b, LP01]. This procedure employs a different regularisation scheme for loop diagrams involving "heavy" propagators and allows for a neat separation of true low–energy singularities and those "regular" contributions that defy naive power counting arguments. As the work presented in Chapters 2, 3 (and also in Chapter 6) is mainly devoted to an exploration of this technique called "infrared regularisation" as well as comparisons to the heavy–baryon scheme, we defer a more detailed description of it to those chapters.

We only briefly mention that the transformation law Eq. (1.74) also allows to construct Lagrangians with more than just one incoming and outgoing nucleon involved, see e.g. [We90, EGM98]. Such Lagrangians have been used extensively to investigate nucleon–nucleon scattering and properties of the deuteron, and are subsequently extended to studies of three, four… nucleon systems. In this way, an effective field theory of the nuclear forces incorporating all constraints from chiral symmetry is systematically developed. The application of such multi–nucleon Lagrangians involves some new subtleties, however. Already in the two–nucleon system, the appearance of a bound state in the $^3S_1$ channel, the deuteron, as well as an unnaturally large $^1S_0$ scattering length ($a \gg 1/M_\pi$) signal the breakdown of perturbation theory, and one has to resort to (partial) resummations and/or to the construction of a non relativistic NN potential. Different approaches how this can be done have been proposed, compare [KSW98]. We shall not investigate any multi nucleon systems in this work and hence do not discuss these aspects any further.

Part I

Form Factors

Chapter 2

Low–energy analysis of the nucleon electromagnetic form factors[#1]

2.1 Introduction

The electromagnetic structure of the nucleon as revealed in elastic electron–nucleon scattering is parameterised in terms of four form factors.The understanding of these form factors is of utmost importance in any theory or model of the strong interactions. Abundant data on these form factors over a large range of momentum transfer already exist, and this data base will considerably improve in the few GeV region as soon as further experiments at CEBAF will be completed and analysed. In addition, experiments involving polarised beams and/or targets are also performed at lower energies to give better data in particular for the electric form factor of the neutron, but also for the magnetic proton and neutron ones. Such kinds of experiments have been performed or are under way at NIKHEF, MAMI, ELSA, MIT–Bates and other places. Clearly, theory has to provide a tool to interpret these data in a model–independent fashion. For small momentum transfer, this can be done in the framework of baryon chiral perturbation theory, which is the effective field theory of the Standard Model at low energies. This will be the main topic of the present investigation.

To put our work presented here into a better perspective, let us recall what is already known from chiral perturbation theory studies of the electromagnetic form factors. Already a long time ago it was established that the isovector (Dirac and Pauli) charge radii diverge in the chiral limit of vanishing pion mass [BZ72]. The first systematic investigation in the framework of relativistic baryon ChPT was given in [GSS88], in particular, it was shown that the analytic structure of the one–loop representation of the isovector spectral functions is in agreement with the one deduced from unitarity (in the low energy region, that is on the left wing of the rho resonance). That approach, however, suffers from the fact that due to the use of standard dimensional

[#1]The contents of this chapter have been published in [KM01a].

regularisation, the one–to–one correspondence between the expansion in loops and the one in small momenta was upset. If one considers the nucleon as a very heavy static source, a consistent power counting is possible, the so called heavy baryon chiral perturbation theory (HBChPT). Within that approach, the electromagnetic form factors were studied in [BKKM92, BFHM98], the latter also containing the extension to an effective field theory including the delta resonance. It was found that the chiral description already fails for values of the four–momentum transfer squared of about $Q^2 \simeq 0.2\,\mathrm{GeV}^2$. In [BKM96c], the isovector and isoscalar spectral functions were investigated in the heavy–nucleon approach. It was pointed out that due to the heavy–mass expansion, the analytic structure of the isovector spectral function is distorted, making the chiral expansion fail to converge in certain regions of small momentum transfer. This can be overcome in the recently proposed Lorentz invariant formulation of [BL99] making use of the so called "infrared regularisation". Being relativistic, this approach leads by construction to the correct behaviour of the spectral functions in the low energy domain. Furthermore, it is expected to improve the convergence of the chiral expansion. This will be one of the main issues to be addressed here. We perform a complete one loop analysis of the form factors, i.e. taking into account all terms up to fourth order. We will demonstrate that one can achieve a good description of the neutron charge form factor for momentum transfer squared up to about $Q^2 = 0.4\,\mathrm{GeV}^2$. The other three form factors cannot be precisely reproduced by the pion cloud plus local contact terms to this order. The source of this deficiency is readily located – it stems from the contribution of vector mesons. We show how to incorporate these in a chirally symmetric manner without introducing additional free parameters (the new parameters related to the vector mesons are taken from dispersion theoretical analyses of the form factors, see [Ho76, MMD96, HMD96]). Within that framework, we obtain a very precise description of the large "dipole–like" form factors without destroying the good result for the neutron form factor obtained in the pure chiral expansion. It is also important to stress that the results obtained in the heavy–baryon approach can be straightforwardly deduced from the framework employed here, shedding some more light on previous HBChPT results.

This chapter is organised as follows. In Section 2.2, some basic definitions concerning the electromagnetic form factors are collected. The one loop representation of the nucleon form factors is given in Section 2.3. The effective Lagrangian on which our investigation is based is briefly reviewed in Section 2.3.1. In particular, infrared regularisation and the treatment of loop integrals are discussed in some detail in Section 2.3.2. The pertinent results based on this complete one loop representation are presented and discussed in Sections 2.3.3 and 2.3.4. Particular emphasis is put on a direct comparison with the results obtained in heavy–baryon chiral perturbation theory, which is a limiting case of the procedure employed here. Section 2.3.5 contains a brief discussion of higher–order scale dependence in these results. The inclusion of vector mesons in harmony with chiral symmetry is presented in Section 2.4. We give some technicalities in Section 2.4.1 and display the results for the form factors in 2.4.2, followed by some remarks on resonance saturation in 2.4.3. Concluding remarks are given in Section 2.5. Some further technical aspects are relegated to App. A.

2.2 Nucleon form factors

The structure of the nucleon (denoted by 'N') as probed by virtual photons is parameterised in terms of four form factors,

$$\langle N(p') \,|\, \mathcal{J}_\mu \,|\, N(p)\rangle = e\,\bar{u}(p') \left\{ \gamma_\mu F_1^N(t) + \frac{i\sigma_{\mu\nu}q^\nu}{2m_N} F_2^N(t) \right\} u(p) \,, \quad N = p, n \,, \tag{2.1}$$

with $t = q_\mu q^\mu = (p'-p)^2$ the invariant momentum transfer squared, $\mathcal{J}_\mu$ the isovector vector quark current, $\mathcal{J}_\mu = \bar{q}\mathcal{Q}\gamma_\mu q$ ($\mathcal{Q}$ is the quark charge matrix), and m_N the mean nucleon mass. In electron scattering, t is negative and it is often convenient to define the positive quantity $Q^2 = -t > 0$. F_1 and F_2 are called the Dirac and the Pauli form factor, respectively, with the normalisations $F_1^p(0) = 1$, $F_1^n(0) = 0$, $F_2^p(0) = \kappa_p$ and $F_2^n(0) = \kappa_n$. Here, κ denotes the anomalous magnetic moment. One also uses the electric and magnetic Sachs form factors,

$$G_E(t) = F_1(t) + \frac{t}{4m_N^2} F_2(t) \,, \quad G_M(t) = F_1(t) + F_2(t) \,. \tag{2.2}$$

In the Breit–frame, G_E and G_M are nothing but the Fourier–transforms of the charge and the magnetisation distribution, respectively. In a relativistic framework, as it is used throughout this text, the Dirac and Pauli form factors arise if one constructs the most general nucleonic matrix element of the electromagnetic current consistent with Lorentz invariance, parity and charge conjugation. In the non–relativistic limit on the other hand, in which the nucleon can be considered as a very heavy static source, one naturally deals with the Sachs form factors. Therefore, as first stressed in [BKKM92], these arise in the heavy–baryon approach to chiral perturbation theory. Since we will frequently compare our results to those obtained in that framework, we will consider both Pauli and Dirac and the Sachs form factors. For the theoretical analysis, it is advantageous to work in the isospin basis,

$$F_i^{s,v}(t) = F_i^p(t) \pm F_i^n(t) \;, \quad (i = 1, 2) \;, \tag{2.3}$$

since the photon has an isoscalar ($I = s$) and an isovector ($I = v$) component (and similarly for the Sachs form factors). It is important to note that the lowest hadronic states to which the isovector and isoscalar photons couple are the two and three pion systems, respectively. These are the corresponding thresholds for the absorptive parts of the isovector and isoscalar nucleon form factors.

The slope of the form factors at $t = 0$ is conventionally expressed in terms of a nucleon radius $\langle r^2\rangle^{1/2}$,

$$F(t) = F(0)\left(1 + \frac{1}{6}\langle r^2\rangle\, t + \ldots\right) \tag{2.4}$$

which is rooted in the non–relativistic description of the scattering process in which a point–like charged particle interacts with a given charge distribution $\rho(r)$. The mean square radius of this charge distribution is given by

$$\langle r^2 \rangle = 4\pi \int_0^\infty dr\, r^2 \rho(r) = -\frac{6}{F(0)} \frac{dF(Q^2)}{dQ^2}\bigg|_{Q^2=0} . \tag{2.5}$$

Eq. (2.5) can be used for all form factors except G_E^n and F_1^n which vanish at $t = 0$. In these cases, one simply drops the normalisation factor $1/F(0)$ and defines e.g. the neutron charge radius via

$$\langle (r_E^n)^2 \rangle = -6\, \frac{dG_E^n(Q^2)}{dQ^2}\bigg|_{Q^2=0} . \tag{2.6}$$

It is important to note that the slopes of G_E^n and F_1^n are related via

$$\frac{dG_E^n(Q^2)}{dQ^2}\bigg|_{Q^2=0} = \frac{dF_1^n(Q^2)}{dQ^2}\bigg|_{Q^2=0} - \frac{F_2^n(0)}{4m_N^2} , \tag{2.7}$$

where the second term in Eq. (2.7) is called the Foldy term. It gives the dominant contribution to the slope of G_E^n.

The large body of electron scattering data spanning momentum transfers from $Q^2 \simeq 0$ to $Q^2 \simeq 35\,\text{GeV}^2$ can be analysed in a largely model independent fashion using dispersion relations [Ho76, MMD96, HMD96]. Here, we are interested in the region of small momentum transfer, $Q^2 \leq 0.5\,\text{GeV}^2$. Nevertheless, since there is still some substantial scatter in the data in this range of momentum transfer, we will also use the results of the dispersive analysis for comparison to the ones obtained in the chiral expansion. A recent review on the theory of the form factors is given in [Me00], the status of the data as of 1999 is discussed in [Pe00].

2.3 One–loop representation

2.3.1 Effective Lagrangian

Our starting point is an effective field theory of asymptotically observable relativistic spin 1/2 fields, the nucleons, chirally coupled to the pseudo Goldstone bosons of QCD, the pions, and external sources (like e.g. the photon field). The theory shares the symmetries of QCD (spontaneously and explicitly broken chiral symmetry, parity, charge conjugation, time reversal invariance, and Lorentz covariance) and can be formulated in such a way as to obey systematic power counting, which will be discussed at length in the following section. External momenta and quark (pion) mass insertions are treated as small quantities in comparison to the scale of chiral symmetry breaking, $\Lambda_\chi \simeq 1$ GeV. The most direct link of the effective field theory to the underlying one, QCD, comes from the analysis of the chiral Ward identities as stressed by

Leutwyler [Le94]. Any contribution to S–matrix elements or transition currents has the form

$$\mathcal{M} = q^\nu f\left(\frac{q}{\lambda}, g\right) \ , \tag{2.8}$$

where q is a generic symbol for any small quantity, f a function of order one, λ a regularisation scale, and g a collection of coupling constants. Chiral symmetry demands that the power ν is bounded from below. The expansion in increasing powers of this parameter is called the *chiral* expansion. At a given order, one has to consider tree as well as loop diagrams, the latter ones restoring unitarity in a perturbative fashion. The machinery to perform this is based on an effective Lagrangian, which consists of a string of terms of increasing (chiral) dimension,

$$\mathcal{L}_{\rm eff} = \mathcal{L}_{\pi\pi}^{(2)} + \mathcal{L}_{\pi N}^{(1)} + \mathcal{L}_{\pi N}^{(2)} + \mathcal{L}_{\pi N}^{(3)} + \mathcal{L}_{\pi N}^{(4)} + \ldots \ , \tag{2.9}$$

where the ellipsis denotes terms of higher order not needed here. We note that we perform a complete one–loop analysis, i.e. taking tree graphs with insertions from all terms indicated in Eq. (2.9) and *one*–loop diagrams with insertions from $\mathcal{L}_{\pi N}^{(1)}$ and at most one insertion from $\mathcal{L}_{\pi N}^{(2)}$.

We will now consider the terms relevant to our problem (for a more detailed description, we refer the reader to [BKM95a]). The chiral effective pion Lagrangian, which to leading order contains two parameters, the pion decay constant (in the chiral limit) F and the pion mass (its leading term in the quark mass expansion) M, is given by

$$\mathcal{L}_{\pi\pi}^{(2)} = \frac{F^2}{4}\langle u_\mu u^\mu + \chi_+\rangle \ , \tag{2.10}$$

where the triplet of pion fields is collected in the SU(2) valued matrix $U(x) = u^2(x)$, and the chiral vielbein is related to u via $u_\mu = i\{u^\dagger, \nabla_\mu u\}$. The covariant derivative ∇_μ as well as the scalar field χ_+ containing the quark mass matrix correspond to their definitions in Section 1.2.3. $\langle\ldots\rangle$ again denotes the trace in flavour space.

The pion–nucleon Lagrangian at leading order reads

$$\mathcal{L}_{\pi N}^{(1)} = \bar\Psi\Big(i\not{D} - m + \frac{g_A}{2}\not{u}\gamma_5\Big)\Psi \ , \tag{2.11}$$

where the bi spinor Ψ collects the proton and neutron fields and g_A is the axial vector coupling constant measured in neutron β decay, $g_A = 1.26$. Strictly speaking, the nucleon mass and the axial coupling should be taken at their values in the two flavour chiral limit ($m_u = m_d = 0$, m_s fixed at its physical value). To this order, the photon field only couples to the charge of the nucleon. It resides in the chiral covariant derivative, $D_\mu\Psi = \partial_\mu\Psi + \Gamma_\mu\Psi$, with the chiral connection given by $\Gamma_\mu = \frac{1}{2}[u^\dagger, \partial_\mu u] - \frac{i}{2}u^\dagger(v_\mu + a_\mu)u - \frac{i}{2}u(v_\mu - a_\mu)u^\dagger$.

The minimal Lagrangians at second and third order have been given in [FMS98]. We only show the terms needed for the calculation of the form factors,

$$\begin{aligned}\mathcal{L}_{\pi N}^{(2)} &= \bar{\Psi}\left\{c_1\langle\chi_+\rangle - \frac{c_2}{8m^2}\Big(\langle u_\mu u_\nu\rangle\{D^\mu, D^\nu\} + \text{h.c.}\Big) + \frac{i\,c_4}{4}\sigma^{\mu\nu}[u_\mu, u_\nu]\right. \\ &\qquad \left. +\frac{c_6}{8m}\sigma^{\mu\nu}F_{\mu\nu}^+ + \frac{c_7}{8m}\sigma^{\mu\nu}\langle F_{\mu\nu}^-\rangle\right\}\Psi \quad , \qquad (2.12)\\ \mathcal{L}_{\pi N}^{(3)} &= \bar{\Psi}\left\{\frac{i\,d_6}{2m}\Big([D^\mu, \hat{F}_{\mu\nu}^+]D_\nu + \text{h.c.}\Big) + \frac{i\,d_7}{2m}\Big([D^\mu, \langle F_{\mu\nu}^+\rangle]D_\nu + \text{h.c.}\Big)\right\}\Psi \quad . \qquad (2.13)\end{aligned}$$

Here, $F_{\mu\nu}^+ = u^\dagger F_{\mu\nu} u + u F_{\mu\nu} u^\dagger$, and $F_{\mu\nu} = \partial_\mu A_\nu - \partial_\nu A_\mu$ is the conventional photon field strength tensor. Furthermore, we have adopted the notation introduced in [FMS98] for traceless operators in SU(2), $\hat{A} = A - \frac{1}{2}\langle A\rangle$. The c_i and d_i are low energy constants that encode information about the more massive states not contained in the effective field theory or other short distance effects. These parameters have to be pinned down from data. In our case, the LECs c_1, c_2, c_4, which only appear in loop diagrams, can be taken from analyses of πN–scattering, whereas c_6, c_7 parameterise the leading magnetic photon coupling to the nucleon, and d_6, d_7 have to be fitted to the charge radii of proton and neutron.

The minimal pion–nucleon Lagrangian to fourth order has been worked out in [FMMS00]. Of the 118 terms given there, we only show the four which are of interest for this calculation,

$$\begin{aligned}\mathcal{L}_{\pi N}^{(4)} &= \bar{\Psi}\left\{-\frac{e_{54}}{2}[D^\lambda, [D_\lambda, \langle F_{\mu\nu}^+\rangle]]\,\sigma^{\mu\nu} - \frac{e_{74}}{2}[D^\lambda, [D_\lambda, \hat{F}_{\mu\nu}^+]]\,\sigma^{\mu\nu}\right. \\ &\qquad \left. -\frac{e_{105}}{2}\langle F_{\mu\nu}^+\rangle\,\langle\chi_+\rangle\,\sigma^{\mu\nu} - \frac{e_{106}}{2}\hat{F}_{\mu\nu}^+\langle\chi_+\rangle\,\sigma^{\mu\nu}\right\}\Psi \quad . \qquad (2.14)\end{aligned}$$

Two more terms (numbered 107 and 108 respectively in [FMMS00]) only contribute when taking into account effects due to $m_u \neq m_d$. We shall disregard these in what follows. We also note that the terms $\sim e_{105}, e_{106}$ only amount to a quark mass renormalisation of the leading magnetic couplings $\sim c_6$, c_7,

$$\begin{aligned} c_6 &\rightarrow \bar{c}_6 = c_6 - 16\,m\,M^2\,e_{106} \ , \\ c_7 &\rightarrow \bar{c}_7 = c_7 - 8\,m\,M^2\Big(2e_{105} - e_{106}\Big) \ . \qquad (2.15)\end{aligned}$$

When it comes to numerical evaluation, we will just use the renormalised constants $\bar{c}_6$ and $\bar{c}_7$ and will not regard e_{105} and e_{106} as additional parameters to be fitted. This leaves us with just two new parameters of fourth order (e_{54}, e_{74}) that have to be determined.

2.3.2 Infrared regularisation

Chiral perturbation theory in the meson sector as an effective theory for weakly interacting Goldstone bosons allows for a systematic expansion of physical observables simultaneously in powers of small momenta and quark masses. For example, in the isospin limit ($m_u = m_d$) the quark mass expansion of the pion mass takes the form

$$M_\pi^2 = M^2 \left\{ 1 - \frac{M^2}{32\pi^2 F^2} \bar{\ell}_3 \right\} + \mathcal{O}(M^6) \; , \tag{2.16}$$

where the renormalised coupling $\bar{\ell}_3$ depends logarithmically on the quark mass, $M^2 d\bar{\ell}_3 / dM^2 = -1$. The infinite contribution of the pion tadpole $\sim 1/(d-4)$, see graph (a) in Fig. 2.1, has been absorbed in the infinite part of this LEC. In this scheme, there is a consistent power counting since the only mass scale (i.e. the pion mass) vanishes in the chiral limit $m_u = m_d = 0$. If one uses the same method in

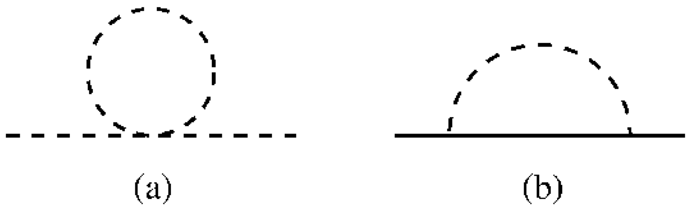

Figure 2.1: Lowest order loop diagrams contributing to the mass renormalisation of (a) the pion at $\mathcal{O}(q^4)$, and (b) the nucleon at $\mathcal{O}(q^3)$. Solid and dashed lines refer to nucleons and pions, respectively.

the nucleon case, one encounters a scale problem: for instance, if the nucleon field is treated relativistically based on standard dimensional regularisation, the nucleon mass shift calculated from the self–energy diagram (see graph (b) in Fig. 2.1) can be expressed as [GSS88]

$$m_N - m = \frac{3 g_A^2 m^2}{32\pi^2 F^2} m \left\{ \bar{c}_0 + \bar{c}_1 \mu^2 - \pi \mu^3 - \mu^4 \log \mu + \sum_{\nu=4}^{\infty} a_\nu \mu^\nu \right\} \; , \tag{2.17}$$

where m_N corresponds to the observable nucleon mass up to one loop accuracy, while m is the "bare" nucleon mass in the chiral limit as defined in the Lagrangian Eq. (2.11). In addition, we have used $\mu = M/m$, and $\bar{c}_0$, $\bar{c}_1$ are renormalised LECs (the precise relation of which to previously defined LECs is of no relevance here). This expansion is very different from the one for the pion mass, in that the nucleon mass already receives a (infinite) renormalisation in the chiral limit. This difference is due to the fact that the nucleon mass does not vanish in the chiral limit and thus introduces a new mass scale apart from the one set by the quark masses. Therefore, any power of the quark masses can be generated by chiral loops in the nucleon case, whereas in the meson case a loop order corresponds to a definite number of quark mass insertions. This is the reason why one has introduced the heavy mass expansion in the nucleon case. Since in that formalism the nucleon mass is transformed from the propagator into a string of vertices with increasing powers of $1/m$, a consistent power counting can be formulated. However, this method has the disadvantage that certain types of diagrams are at odds with strictures from analyticity. The best example is the so–called triangle graph, which enters e.g. the scalar form factor or the isovector electromagnetic form factors of the nucleon (see graph (6) in Fig. 2.2). This diagram has its threshold at $t_0 = 4M_\pi^2$ but also a singularity on the second Riemann sheet, at $t_c = 4M_\pi^2 - M_\pi^4/m_N^2 = 3.98M_\pi^2$, i.e. very close to threshold. To leading order in the heavy baryon approach, this singularity coalesces with the threshold and thus causes problems (a more detailed discussion can be found e.g. in [BKM96c, Me98]). In a fully relativistic treatment, such constraints from analyticity are automatically fulfilled.

It was recently argued in [ET98] that relativistic one loop integrals can be separated into "soft" and "hard" parts. While for the former, a similar power counting as in HBChPT applies, the contributions from the latter can be absorbed in certain LECs. In this way, one can combine the advantages of both methods. A more formal and rigorous implementation of such a program is due to Becher and Leutwyler [BL99]. They call their method, which we shall also use here, "infrared regularisation". Any one–loop integral H is split into an infrared singular and a regular part by a particular choice of Feynman parameterisation. Consider first the regular part, called R. If one chirally expands these terms, one generates polynomials in momenta and quark masses. Consequently, to any order, R can be absorbed in the LECs of the effective Lagrangian. The regular part incorporates singularities of the *heavy* mass going to zero, which therefore lie outside the low energy region. On the other hand, the infrared singular part I has the same analytical properties as the full integral H in the low energy region and its chiral expansion leads to the non trivial momentum and quark mass dependences of ChPT, like e.g. the chiral logarithms or fractional powers of the quark masses. It is this infrared singular part I that is closely related to the heavy–baryon expansion: there, the relativistic nucleon propagator is replaced by a heavy–baryon propagator plus a series of $1/m$–suppressed insertions. Summing up all heavy–baryon diagrams with all internal–line insertions yields the infrared singular part of the corresponding relativistic diagram.

To be specific, consider the self–energy diagram (b) of Fig. 2.1. In d dimensions, the corresponding scalar loop integral is

$$H(p^2) = \frac{1}{i}\int \frac{d^dk}{(2\pi)^d}\frac{1}{[M^2 - k^2 - i\epsilon][m^2 - (p-k)^2 - i\epsilon]} \; . \tag{2.18}$$

At threshold, $p^2 = s_0 = (M+m)^2$, this results in

$$H(s_0) = c(d)\frac{M^{d-3}+m^{d-3}}{M+m} = I + R\ , \tag{2.19}$$

with $c(d)$ some constant depending on the dimensionality of space–time. The infrared singular piece I is characterised by fractional powers in the pion mass and generated by loop momenta of order M. For these soft contributions, the power counting is fine. On the other hand, the infrared regular part R is characterised by fractional powers of the nucleon mass (hence divergent in m for $d < 3$), but by integer powers when expanded in the pion mass and generated by internal momenta of the order of the nucleon mass (the large mass scale). These are the terms that lead to the violation of the power counting in the standard dimensional regularisation discussed above. For the self–energy integral, this splitting can be achieved in the following way:

$$\begin{aligned} H &= \int \frac{d^dk}{(2\pi)^d}\frac{1}{AB} = \int_0^1 dz \int \frac{d^dk}{(2\pi)^d}\frac{1}{[(1-z)A+zB]^2} \\ &= \left\{\int_0^\infty - \int_1^\infty\right\} dz \int \frac{d^dk}{(2\pi)^d}\frac{1}{[(1-z)A+zB]^2} = I + R\ , \end{aligned} \tag{2.20}$$

with $A = M^2 - k^2 - i\epsilon$, $B = m^2 - (p-k)^2 - i\epsilon$. Any general one loop diagram with arbitrary many insertions from external sources can be brought into this form by combining the propagators to a single pion– and a single nucleon–propagator. It was also shown that this procedure leads to a unique, i.e. process–independent result, in accordance with the chiral Ward identities of QCD [BL99]. This is essentially based on the fact that terms with fractional versus integer powers in the pion mass must be separately chirally symmetric. Consequently, the transition from any one–loop graph H to its infrared singular piece I defines a symmetry preserving regularisation. A generalisation of this method to higher loop orders (and also to an arbitrary number of heavy particles) has been discussed in [LP01]. However, its phenomenological consequences have not been explored in great detail so far, while it is expected that this approach will be applicable in a larger energy range than the heavy baryon approach. Recent applications of the infrared regularisation scheme include pion–nucleon scattering [ET98, BL00, TE02] as well as an investigation of the generalised Gerasimov–Drell–Hearn sum rule and Compton scattering on the nucleon [BHM02].

Some remarks concerning renormalisation within this scheme are in order. To leading order, the infrared singular parts coincide with the heavy baryon expansion, in particular the infinite parts of loop integrals are the same. Therefore, the β functions for low–energy constants which absorb these infinities are identical. However, infrared singular parts of relativistic loop integrals also contain infinite parts which are suppressed by powers of μ, which hence cannot be absorbed as long as one only introduces counterterms to a finite order: exact renormalisation only works up to the order at which one works, higher order divergences have to be removed by hand.

Closely related to this problem is the one of the new mass scale λ which one has to introduce in the process of regularisation and renormalisation. In dimensional regularisation and related schemes, loop diagrams depend logarithmically on λ. This $\log\lambda$ dependence is compensated for by running coupling constants, the running behaviour being determined by the corresponding β functions. In the same way as the contact terms cannot consistently absorb higher order divergences, their β functions cannot compensate for scale dependence which is suppressed by powers of μ. In order to avoid this unphysical scale dependence in physical results, the authors of [BL99] have argued that the nucleon mass m_N serves as a "natural" scale in a relativistic baryon ChPT loop calculation and that therefore one should set $\lambda = m_N$ everywhere when using the infrared regularisation scheme. This was already suggested in [BKKM92] for the framework of a relativistic theory with ordinary dimensional regularisation. We will follow this idea most of the time, hence in our formulae, what would actually be $\log(M_\pi/\lambda)$ will always be spelled out as $\log\mu$. In addition, we will study the phenomenological consequences of this higher order scale variation in Section 2.3.5.

In the following calculation, we frequently compare our results to the equivalent heavy–baryon ones. We wish to emphasise that one can always regain the heavy–baryon result from the infrared regularised relativistic one by performing a strict chiral expansion of all involved loop functions. As a simple example, we again show the expansion of the nucleon mass up to third order corresponding to Eq. (2.17), but this time using infrared regularisation. The result is

$$m_N - m = -4c_1 M^2 + \frac{3g_A^2}{2F^2} m M^2 I(m^2) \quad , \tag{2.21}$$

where the loop integral $I(m^2)$ is given by

$$I(m^2) = -\mu^2\Big(L + \frac{1}{16\pi^2}\log\mu\Big) + \frac{\mu}{16\pi^2}\Big\{\frac{\mu}{2} - \sqrt{4-\mu^2}\arccos\Big(-\frac{\mu}{2}\Big)\Big\} \quad . \tag{2.22}$$

Here, L contains the pole in $d-4$,

$$L = \frac{m^{d-4}}{16\pi^2}\Big\{\frac{1}{d-4} + \frac{1}{2}\Big(\gamma_E - 1 - \log 4\pi\Big)\Big\} \quad , \tag{2.23}$$

and γ_E is Euler's constant. (Definitions and results for this and all other loop functions needed in this work can be found in Appendix A.1.) Expanding to leading order, one finds

$$I(m^2) = -\frac{\mu}{16\pi} + \mathcal{O}(\mu^2) \quad , \tag{2.24}$$

which leads to the well known result

$$m_N - m = -4c_1 M^2 - \frac{3g_A^2 M^3}{32\pi F^2} + \mathcal{O}(\mu^4) \ , \tag{2.25}$$

yielding a contribution non–analytic in the quark masses. As explained before, the loop function $I(m^2)$ contains a non–leading divergence which cannot be absorbed to this order, but will be by an appropriate contact term at fourth order. The calculation of the nucleon mass to fourth order and the reduction to the heavy baryon limit is done in detail in [BL99].

An essential ingredient to the treatment of loop integrals as described in the previous paragraphs is the fact that higher order effects are included as compared to the "strict" chiral expansion in the heavy baryon formalism. This was justified in [BL99] by improved convergence properties in the low–energy region, it introduces however a certain amount of arbitrariness as to which of these higher order terms to keep and which to dismiss. It is therefore mandatory to exactly describe our treatment of these terms. The philosophy in [BL99] was, above all, to preserve the correct relativistic analyticity properties. This was achieved by keeping the full *denominators* of loop integrals (and evaluating them by the infrared regularisation prescription), while expanding the *numerators* to the desired chiral order only. In addition, e.g. crossing symmetry is to be conserved. We explore a different approach here: as we anticipate the neutron electric form factor to be highly sensitive to recoil effects, we keep *all* terms which occur according to the infrared regularisation prescription and do not even expand the numerators of loop integrals. However, three effects involving low–energy constants have to be discussed separately, all in the spirit of avoiding "artificial" higher order counterterms:

- Loop diagrams with second order insertions proportional to c_1 can easily be summarised by a shift of the "bare" nucleon mass to its renormalised value at second order, $m \to m_N = m - 4c_1 M_\pi^2 + \mathcal{O}(q^3)$. In principle, this does *not* occur in those loop diagrams which have insertions from other second order low energy constants. As we do not want to artificially introduce this additional LEC by discriminating between m and m_N in our formulae, we allow for this renormalisation everywhere.

- As detailed in the previous section, the second order LECs c_6, c_7 receive a renormalisation $\sim M_\pi^2$ at fourth order. In principle, to this order only the unrenormalised c_i appear in loop diagrams. We disregard this difference and use the same values both on tree level and for the loops.

- From the definitions of the various electromagnetic form factors, it is obvious that these are not all calculated to the same accuracy in terms of chiral orders. A calculation employing chiral Lagrangians up to and including $\mathcal{O}(q^4)$ will be able to give the Dirac form factor F_1 to $\mathcal{O}(q^3)$ and the Pauli form factor F_2 to $\mathcal{O}(q^2)$. When combining these to the Sachs form factors G_E and G_M, the chiral orders are "mixed", see Eq. (2.2). When we, in the following, talk about "third"/"fourth" order calculations of the various form factors, we always refer to the projections of the third/fourth order *amplitude* onto these observables. We truncate exactly one kind of term in this process: the $\mathcal{O}(q^3)$ counterterms which enter the electric (charge) radii are really "G_E counterterms" in the sense that they appear in F_1 and F_2 with opposite signs in order to cancel exactly in G_M. In addition, there are, at $\mathcal{O}(q^4)$, F_2 counterterms fixing the magnetic radii. Therefore, G_E receives q^4 counterterms inherited from $(q^2/4m^2)F_2$. As a genuine polynomial contribution of this kind only appears in an $\mathcal{O}(q^5)$ calculation, we drop these terms in G_E.

2.3.3 Chiral expansion of the nucleon form factors

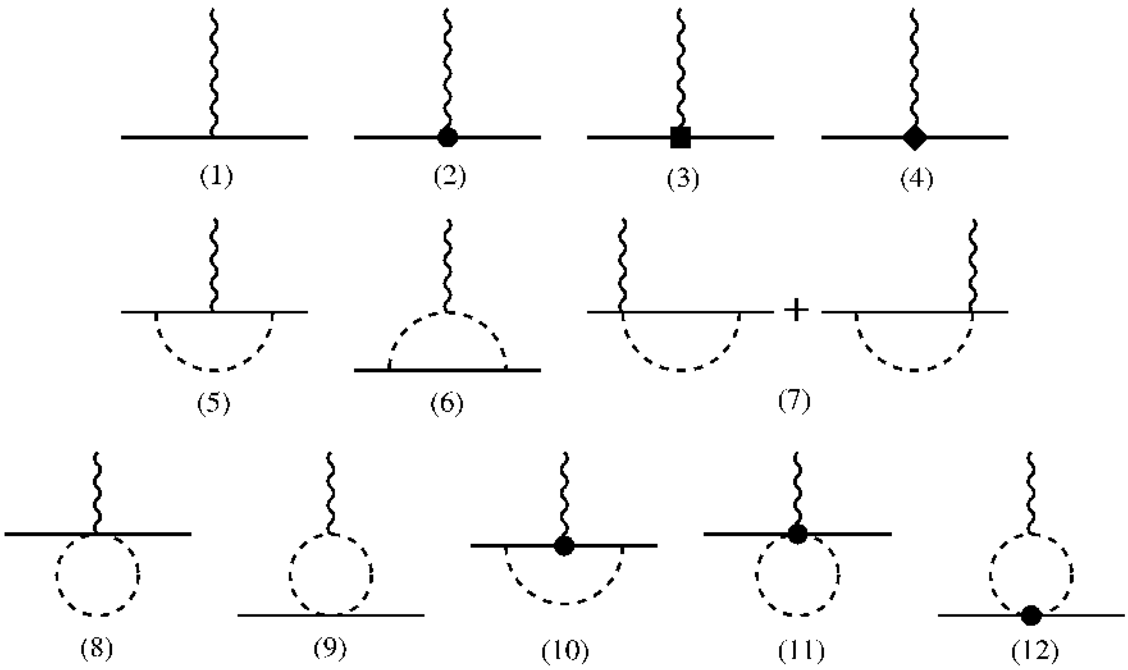

Figure 2.2: Feynman diagrams contributing to the electromagnetic form factors up to fourth order. Solid, dashed, and wiggly lines refer to nucleons, pions, and the vector source, respectively. Vertices denoted by a heavy dot/a square/a diamond refer to insertions from the second/third/fourth order chiral Lagrangian, respectively. Diagrams contributing via wave function renormalisation only are not shown.

The chiral expansion of a form factor F (being a genuine symbol for any of the four electromagnetic nucleon form factors) consists of two contributions, tree and loop graphs. The tree graphs comprise that of lowest order with a fixed coupling (the nucleon charge) as well as counterterms from the second, third, and fourth order Lagrangians. As one–loop graphs, we have both those with just lowest order couplings and those with exactly one insertion from $\mathcal{L}_{\pi N}^{(2)}$. The pertinent tree and loop graphs are depicted in Fig. 2.2 (we have not shown the diagrams leading to wave function renormalisation only). The first four of these comprise the tree graphs with insertions up to dimension four, and diagrams (5) to (9) ((10) to (12)) are the third (fourth) order loop graphs. Consequently, any form factor can be written as

$$F(t) = F^{\text{tree}}(t) + F^{\text{loop}}(t) \ . \tag{2.26}$$

In Appendix A.3, we have listed the contributions to the Dirac and Pauli form factors from the various diagrams, including the nucleon Z factor. This allows to reconstruct the pertinent expressions for $F_{1,2}^{p,n}$ in a straightforward manner. We refrain from giving the complete expressions here. The corresponding Sachs form factors $G_{E,M}^{p,n}$ are obtained by use of Eq. (2.2) under the restrictions discussed in the preceding section. We only show the explicit formulae for the magnetic moments, the electric and the magnetic radii (in terms of renormalised, i.e. physical, masses and coupling constants). The magnetic moments read

$$\begin{aligned}
\kappa^v &= \bar{c}_6^r \\
&- \frac{\mu^2 g_A^2 m_N^2}{(4\pi F_\pi)^2}\Bigg\{\frac{3}{2}\mu^2 + \Big(2-\frac{\mu^2}{4}\Big)c_6 \\
&\qquad + \frac{\arccos(-\frac{\mu}{2})}{\mu\sqrt{4-\mu^2}}\Big[2\Big(8-13\mu^2+3\mu^4\Big)-\mu^2\Big(8-\frac{5}{2}\mu^2\Big)c_6\Big] \\
&\qquad + \Big[2\Big(7-3\mu^2\Big)+\Big(4-\frac{5}{2}\mu^2\Big)c_6\Big]\log\mu\Bigg\} \\
&+ \frac{\mu^2 m_N^2}{(4\pi F_\pi)^2}\Bigg\{\frac{3}{4}\mu^2 m_N\, c_2 - \Big(3\mu^2 m_N\, c_2 - 8 m_N\, c_4 + 2c_6\Big)\log\mu\Bigg\} \ , \qquad (2.27) \\
\kappa^s &= c_6^r + 2c_7^r \\
&- \frac{3\mu^2 g_A^2 m_N^2}{(4\pi F_\pi)^2}\Bigg\{\frac{\mu^2}{4}\Big(2+c_6+2c_7\Big) \\
&\qquad - \frac{\mu\arccos(-\frac{\mu}{2})}{\sqrt{4-\mu^2}}\Big[2\Big(3-\mu^2\Big)+\Big(4-\frac{3}{2}\mu^2\Big)\Big(c_6+2c_7\Big)\Big] \\
&\qquad + \Big[2\Big(1-\mu^2\Big)+\Big(2-\frac{3}{2}\mu^2\Big)\Big(c_6+2c_7\Big)\Big]\log\mu\Bigg\} \\
&+ \frac{3\mu^4 m_N^3\, c_2}{(4\pi F_\pi)^2}\Big(\frac{1}{4}-\log\mu\Big) \ , \qquad (2.28)
\end{aligned}$$

with $\mu = M_\pi/m_N \simeq 1/7$. Note that the magnetic moments are finite in the chiral limit. We remind the reader of the definitions of c_6 and c_7 in Eq. (2.15). We have distinguished between the renormalised and the unrenormalised LECs (at tree level and in loop contributions, respectively) only for reasons of formal exactitude, and will disregard this difference from now on. Note however that, in contrast to c_6, c_7, these renormalised LECs inherit infinite parts from e_{105}, e_{106} which are needed in order to remove the leading order divergences in the magnetic moments (as explained in Section 2.3.2). Their poles in $(d-4)$ are determined by the corresponding β functions,

$$\beta_{e_{105}} = -\frac{3g_A^2}{16m_N}\Big(1+c_6+2c_7\Big) \ , \tag{2.29}$$

$$\beta_{e_{106}} = -\frac{1}{8m_N}\Big[7g_A^2 - 4m_N c_4 + (1+2g_A^2)c_6\Big] \quad . \tag{2.30}$$

$\bar{c}_6^r$, $\bar{c}_7^r$ in Eqs. (2.27), (2.28) denote the finite LECs, i.e. with the poles subtracted. Next, the charge radii can be brought into the form

$$\begin{aligned}
(r_E^v)^2 &= -12\, d_6^r + \frac{3\,\kappa^v}{2m_N^2} \\
&- \frac{g_A^2}{(4\pi F_\pi)^2}\Bigg\{7 - 8\mu^2 - \frac{3}{4}\mu^4\Big(1 - c_6\Big) \\
&\qquad - \frac{\mu\arccos(-\frac{\mu}{2})}{\sqrt{4-\mu^2}}\Big[70 - 74\mu^2 + 15\mu^4 + 3\mu^2\Big(3-\mu^2\Big)c_6\Big] \\
&\qquad + \Big[10 - 44\mu^2 + 15\mu^4 + 3\mu^2\Big(1-\mu^2\Big)c_6\Big]\log\mu\Bigg\} \\
&- \frac{1}{(4\pi F_\pi)^2}\Big(1 + 2\log\mu\Big) \quad , \qquad (2.31) \\
(r_E^s)^2 &= -24\, d_7 + \frac{3\,\kappa^s}{2m_N^2} \\
&+ \frac{3\mu^2 g_A^2}{(4\pi F_\pi)^2}\Bigg\{\frac{2}{4-\mu^2} + \frac{\mu^2}{4}\Big[1 + 3\Big(c_6 + 2c_7\Big)\Big] \\
&\qquad - \frac{\mu\arccos(-\frac{\mu}{2})}{(4-\mu^2)^{3/2}}\Big[54 - 34\mu^2 + 5\mu^4 + 3\Big(12 - 7\mu^2 + \mu^4\Big)\Big(c_6 + 2c_7\Big)\Big] \\
&\qquad + \Big[4 - 5\mu^2 + 3\Big(1-\mu^2\Big)\Big(c_6 + 2c_7\Big)\Big]\log\mu\Bigg\} \quad . \qquad (2.32)
\end{aligned}$$

The isovector charge radius diverges logarithmically in the chiral limit, while the isoscalar one is finite. d_6^r denotes the renormalised LEC d_6, i.e. without the infinite part that removes the leading order divergence in the isovector electric form factor, the corresponding β–function being given by [Ec94, FMS98]

$$\beta_{d_6} = -\frac{1+5g_A^2}{6} \quad . \tag{2.33}$$

The LEC d_7 entering the isoscalar radius is, in contrast, finite. Finally, the magnetic radii are given by

$$\begin{aligned}
\mu^v(r_M^v)^2 &= 24\, m_N\, e_{74}^r \\
&+ \frac{g_A^2}{(4\pi F_\pi)^2}\Bigg\{\frac{1}{4(4-\mu^2)}\Big[112 - 36\mu^2 - 8\mu^4 + 3\mu^6 - \mu^2\Big(8 - 8\mu^2 + \mu^4\Big)\,c_6\Big] \\
&\qquad + \frac{\arccos(-\frac{\mu}{2})}{\mu(4-\mu^2)^{3/2}}\Big[32 - 152\mu^2 + 126\mu^4 - 34\mu^6 + 3\mu^8 \\
&\qquad\quad -\mu^4\Big(6 - 6\mu^2 + \mu^4\Big)\,c_6\Big]
\end{aligned}$$

$$
\begin{aligned}
& \qquad + \Big[14 - 16\mu^2 + 3\mu^4\Big(3 - c_6\Big)\Big] \log\mu \Bigg\} \\
& - \frac{1}{(4\pi F_\pi)^2}\Big(1 + 2\log\mu\Big)\Big(1 + 4m_N\, c_4\Big) \ , \qquad (2.34) \\
\mu^s (r_M^s)^2 &= 48\, m_N\, e_{54} \\
& - \frac{3\mu^2 g_A^2}{(4\pi F_\pi)^2}\left\{\frac{8 - 8\mu^2 + \mu^4}{4(4-\mu^2)} + \frac{\mu \arccos(-\frac{\mu}{2})}{(4-\mu^2)^{3/2}}\Big(6 - 6\mu^2 + \mu^4\Big) + \mu^2 \log\mu\right\} \\
& \qquad \times\Big(1 + c_6 + 2c_7\Big) \ , \qquad (2.35)
\end{aligned}
$$

where, again, e_{74}^r has the infinite part, which is given by[#2]

$$
\beta_{e_{74}} = -\frac{7g_A^2 - 1}{12m_N} + \frac{c_4}{3} \ , \qquad (2.36)
$$

subtracted, while e_{54} in the isoscalar radius (in analogy to d_7 for the electric isoscalar radius) is finite. The isovector magnetic radius explodes like $1/M_\pi$ as the pion mass goes to zero, while, again, the isoscalar radius is finite in the chiral limit. These chiral limit results are to be expected because the Sachs form factors inherit the well known chiral singularities of the isovector Dirac and Pauli form factors, more precisely, the corresponding radii diverge in the chiral limit as

$$
\begin{aligned}
(r_1^v)^2 &= -\frac{10g_A^2 + 2}{(4\pi F_\pi)^2} \log\frac{M_\pi}{m_N} + \ldots \ , \\
(r_2^v)^2 &= \frac{g_A^2 m_N}{8\pi F_\pi^2 \kappa_v M_\pi} + \ldots \ , \qquad (2.37)
\end{aligned}
$$

where the ellipsis denotes subleading terms as the pion mass vanishes. This dominant pion loop effect in the nucleon form factors has already been established a long time ago [BZ72]. It can also be expected on physical grounds: the pion cloud, which is Yukawa suppressed for finite pion mass, becomes long ranged in the chiral limit leading to a divergent contribution. Such phenomena are also observed in two photon observables like e.g. the electromagnetic polarisabilities of the nucleon.

As a consequence of analyticity, in the heavy–baryon approach (i.e. in a strict chiral expansion) the isoscalar form factors are, to one–loop order, given simply by a polynomial subsuming tree and counterterm contributions. There *are*, however, isoscalar loop effects as higher order corrections, as is obvious from the above. These stem from the diagrams with the photon coupling to the nucleons (see graphs (5) and (10) in Fig. 2.2), which only yield constant terms needed for renormalisation in HBChPT, but also contain higher order t dependent terms. As the spectral function corresponding

[#2]Unfortunately, [KM01a] quotes an erroneous β-function for e_{74}^r, displaying really the divergent piece in the combination $e_{74} + d_6/(2m_N)$, the linear combination of counterterms arising in the isovector radius $(r_2^v)^2$.

to these diagrams only starts to contribute for $t \geq 4m_N^2$, these t–dependent terms (in the real part) are highly suppressed.

In Section 2.3.2, we already mentioned the marked difference in the threshold behaviour of the isovector spectral functions in the relativistic and the heavy baryon approach. We only quote the results for the threshold behaviour here and relegate the full results to Appendix A.6. Note that these have already been given in the literature, the relativistic results to third order in [GSS88], the additional fourth order contribution as well as the heavy–baryon expansions in [BKM96c]. We reemphasise that the imaginary parts in the infrared regularisation approach do not differ from those in a fully relativistic calculation. For $\mathrm{Im}\, F_1^v(t)$, the relativistic threshold expansion is given by

$$\mathrm{Im}\, F_1^v(t) = \frac{1}{192\pi F_\pi^2 M_\pi^3}\Big\{g_A^2\Big(4m_N^2 - M_\pi^2\Big) + M_\pi^2\Big\}\,(t-4M_\pi^2)^{3/2} + \mathcal{O}\Big((t-4M_\pi^2)^{5/2}\Big)\,, \tag{2.38}$$

and for $\mathrm{Im}\, F_2^v(t)$, one finds

$$\mathrm{Im}\, F_2^v(t) = \frac{m_N\, c_4}{48\pi F_\pi^2 M_\pi}\,(t-4M_\pi^2)^{3/2} + \mathcal{O}\Big((t-4M_\pi^2)^{5/2}\Big)\,. \tag{2.39}$$

In the heavy baryon scheme, however, the heavy mass expansion yields the expressions

$$\begin{aligned}
\mathrm{Im}\, F_1^v(t) &= \frac{g_A^2}{96\pi F_\pi^2}\left\{\sqrt{1-\frac{4M_\pi^2}{t}}\Big(5t-8M_\pi^2\Big) - \frac{3\pi}{4m_N}\,\frac{3t^2-12M_\pi^2 t+8M_\pi^4}{t^{1/2}}\right\} \\
&\quad + \frac{1}{96\pi F_\pi^2}\,\frac{(t-4M_\pi^2)^{3/2}}{t^{1/2}} + \mathcal{O}(q^4)\;, \qquad (2.40)\\
\mathrm{Im}\, F_2^v(t) &= \frac{g_A^2\, m_N}{32F_\pi^2}\left\{\frac{t-4M_\pi^2}{t^{1/2}} - \frac{4}{\pi m_N}\sqrt{1-\frac{4M_\pi^2}{t}}\,\Big(t-2M_\pi^2\Big)\right\} \\
&\quad + \frac{m_N\, c_4}{24\pi F_\pi^2}\,\frac{(t-4M_\pi^2)^{3/2}}{t^{1/2}} + \mathcal{O}(q^3)\;, \qquad (2.41)
\end{aligned}$$

which evidently violate the required threshold behaviour $\mathrm{Im}\, F_i^v(t) \sim (t-4M_\pi^2)^{3/2}$ as pointed out in [BKM96c]. As remarked before, this is due to the fact that the two–pion threshold and the singularity on the second Riemann sheet, inherited from the $\pi\pi \to \bar{N}N$ partial waves, coalesce in the heavy–baryon limit. In contrast, the relativistic approach of course yields the correct analytical structures (for a more pedestrian discussion of this point, see e.g. [Me98]).

2.3.4 Results and discussion

First, we must fix the parameters employed in the calculation. We use $F_\pi = 92.4\,\mathrm{MeV}$, $M_\pi = 139.57\,\mathrm{MeV}$, $g_A = 1.26$, and $m_N = (m_p + m_n)/2 = 938.92\,\mathrm{MeV}$. The LECs

c_2 and c_4 are taken from the analysis of pion–nucleon scattering [FMS98, BM00], $c_2 = 3.2\,\mathrm{GeV}^{-1}$ and $c_4 = 3.4\,\mathrm{GeV}^{-1}$. The LECs c_6 and c_7 can be pinned down from the well known magnetic moments of proton and neutron. The remaining two "electric" (d_6, d_7) and two "magnetic" LECs (e_{54}, e_{74}) are determined from the electric and magnetic radii as given by the dispersion theoretical analysis of [MMD96], these values are $r_E^p = 0.847\,\mathrm{fm}$, $(r_E^n)^2 = -0.113\,\mathrm{fm}^2$, $r_M^p = 0.836\,\mathrm{fm}$, and $r_M^n = 0.889\,\mathrm{fm}$. We note that the long standing discrepancy of the proton charge radius determination from electron–proton scattering [Ro00] and Lamb shift measurements [MR00] has been resolved, converging to a value of $r_E^p = (0.88 \pm 0.01)\,\mathrm{fm}$. We do not use this value here because so far no dispersion theoretical analysis exists using this novel information.

As already stated, the Dirac and Pauli form factors are the natural quantities in any relativistic approach like the one used here. However, for easier comparison to existing heavy baryon calculations and to the low energy data, which are often presented in terms of Sachs form factors, we will discuss these in detail.

First we discuss the neutron charge form factor, as shown in Fig. 2.3. The third and fourth order results compare well to the dispersion theoretical analysis and the trend of the novel data up to $Q^2 = 0.4\,\mathrm{GeV}^2$. The latter have been obtained using tensor polarised deuterium, polarised ^{3}He, and polarisation transfer on deuterium [Ed94]. Although it seems that the *third* order curve meets the novel data even better, we observe that the fourth order one is basically identical to the dispersion theoretical fit up to $Q^2 = 0.2\,\mathrm{GeV}^2$. Also given in that figure are the heavy baryon results to third [BFHM98] and fourth [GH] order. These curves can easily be obtained from our analysis by performing the large mass expansion as explained before. Clearly, neither of these two curves is in acceptable agreement with the data, and, what is more, there is no sign of convergence so far. The resummation of the $1/m$ terms in the relativistic approach vastly improves the convergence of the chiral representation. This sensitivity of the neutron charge form factor to such recoil corrections was already anticipated in [KHM99]. We remark however that the only fourth order contributions to the electric form factors in the heavy–baryon approach are $1/m$–corrections to third order diagrams, in other words, the full fourth order heavy–baryon result for these can already be obtained from expanding the *third* order relativistic one. Therefore, the difference that does show up between the relativistic third and fourth order curves is really, in terms of strict chiral power counting, of higher order and hence (comparatively) small.

Consider the proton electric form factor next, shown in Fig. 2.4. As in the neutron case, the third and fourth order curves are very close (where, however, the remarks made about the reasons for the smallness of this difference apply equally here), but here essentially show the linear behaviour from the term proportional to the charge radius. Compared to the dispersion theoretical result (which describes the data very well in this range of momentum transfer), there is clearly not enough curvature. Polynomial terms of order t^2 (and higher) are not included up to fourth order, and

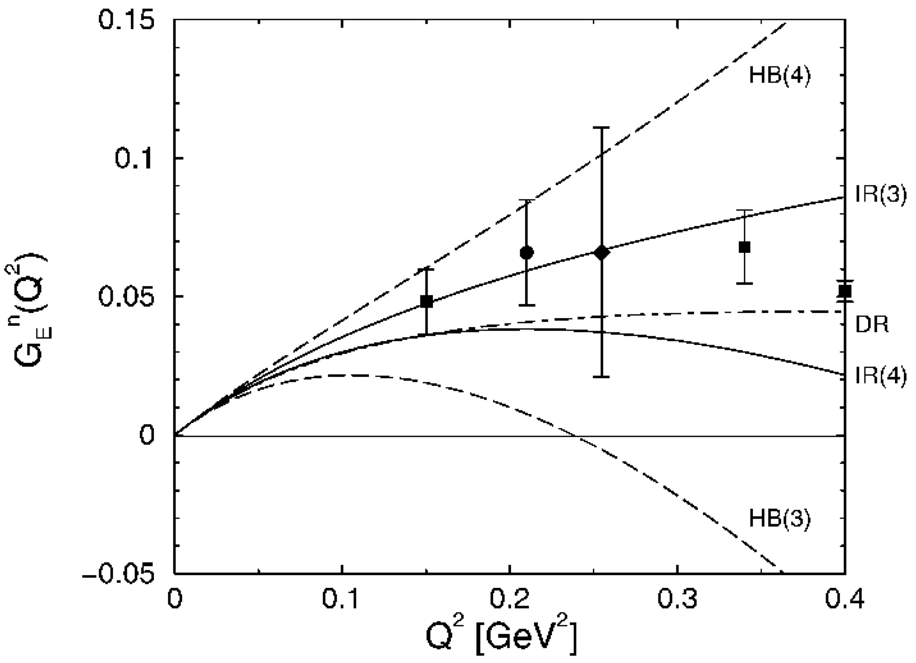

Figure 2.3: The neutron electric form factor in relativistic baryon chiral perturbation theory (solid lines) to third and fourth order, marked as IR(3), IR(4), respectively. For comparison, the results of the heavy baryon approach are also shown (dashed lines, marked as HB(3), HB(4)). All LECs are determined by a fit to the neutron charge radius measured in neutron atom scattering. Also given is the result of the dispersion theoretical analysis (dot dashed line, labelled by DR). The data are from [Ed94], where the Mainz Helium data have been processed in the analysis of [Go01a].

the curvature coming solely from loop functions in the one loop approximation is obviously not sufficient. Fig. 2.4 also displays the results of the third [BKKM92, BFHM98] and fourth [GH] order heavy–baryon calculation. While the general trend of the heavy–baryon results is similar to what is obtained in the relativistic approach (far too small curvature to meet the data), we note that, while there is at least a slight improvement from the third to the fourth order relativistic calculation, the description visibly *worsens* for the fourth order heavy–baryon result, as compared to the third order one.

We now turn to the magnetic form factors of proton and neutron as shown in Fig. 2.5. The qualitative behaviour of the different curves is very similar for both of them: To third order, the momentum dependence is given parameter–free because the LECs at this order only affect the normalisation. We see that the $1/m$ corrections present in our approach visibly worsen the prediction obtained previously in the heavy–baryon limit. That result is based on the leading chiral singularities given in Eq. (2.37) because to

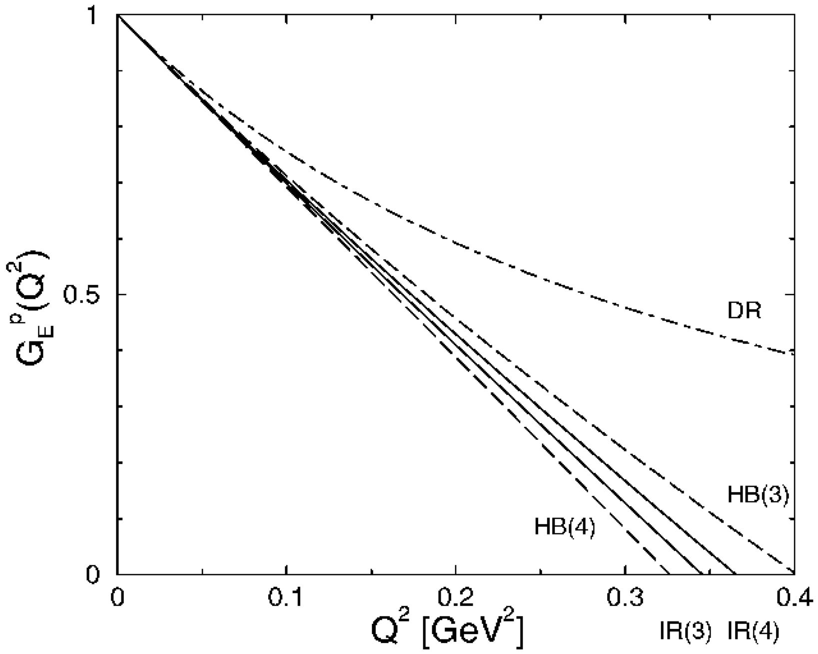

Figure 2.4: The proton electric form factor in relativistic baryon chiral perturbation theory (solid lines) to third and fourth order, marked as IR(3), IR(4), respectively. For comparison, the results of the heavy baryon approach are also shown (dashed lines, marked as HB(3), HB(4)). All LECs are determined by a fit to the proton charge radius as given by the dispersion theoretical result (dot dashed line, labelled by DR).

this order, the corresponding isoscalar form factor is simply constant. We conclude that the recoil corrections are rather large and that the leading chiral limit behaviour is not a good approximation for the Goldstone boson contribution to the magnetic radii in the case of finite pion masses. At fourth order, due to the presence of the counterterms from $\mathcal{L}^{(4)}_{\pi N}$, the radius can be fixed at its empirical value. Consequently, the full relativistic result and its heavy–baryon limit are not very different any more. The absence of curvature terms of order t^2 (and higher) is clearly visible in Fig. 2.5.

The physics underlying this deficiency will be addressed in Section 2.4. Only a uniformly reliable description for all four form factors is acceptable, and hence it is absolutely necessary to understand what is missing in the three dipole–shaped form factors: with large corrections for these, one might expect large corrections also for the neutron charge form factor, such that its very good description presented here might turn out to be only accidental. In the following, we shall show that this is indeed *not* the case.

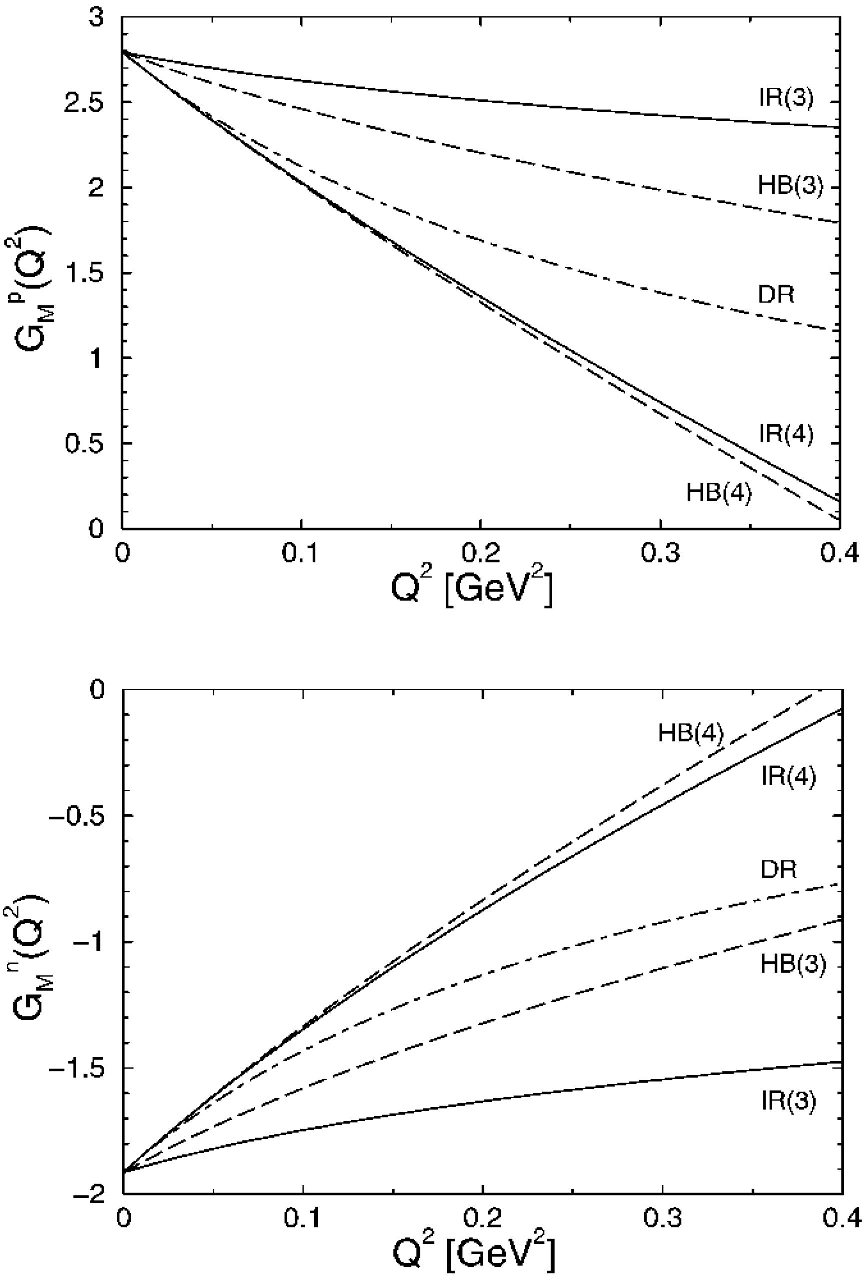

Figure 2.5: The proton and neutron magnetic form factors in relativistic baryon chiral perturbation theory (solid lines) to third and fourth order, marked as IR(3), IR(4), respectively. For comparison, the results of the heavy baryon approach are also shown (dashed lines, marked as HB(3), HB(4)). The third (fourth) order LECs are determined by a fit to the proton/neutron magnetic moments (radii). Also given is the dispersion theoretical result (dot–dashed line, labelled by DR).

2.3.5 Higher–order scale dependence

In Section 2.3.2, we hinted at the fact that infrared regularised loop integrals in general induce a higher order scale dependence in physical observables that cannot be compensated for by the counterterms available at the order one is working. Instead of regarding m_N as the natural scale for baryon ChPT, we restore the scale dependence and replace $\log \mu$ by $\log(M_\pi/\lambda)$. With the counterterms running according to their respective beta functions, one could argue that the remaining variation with the scale is an inherent uncertainty in the calculation of the higher order loop corrections. For the leading moments of the form factors, the higher–order scale dependence in terms of analytical expressions can easily be read off from Eqs. (2.27), (2.28), (2.31), (2.32), (2.34), and (2.35). Here we only wish to quantify these uncertainties numerically. We arrive at the following:

$$\begin{aligned}
\kappa^v(\lambda) &= 3.706 + 0.0062 \log \frac{m_N}{\lambda} \quad , & (2.42)\\
\kappa^s(\lambda) &= -0.120 - 0.0006 \log \frac{m_N}{\lambda} \quad , & (2.43)\\
\left(r_E^v\right)^2(\lambda) &= \left(0.830 + 0.0304 \log \frac{m_N}{\lambda}\right) \mathrm{fm}^2 \quad , & (2.44)\\
\left(r_E^s\right)^2(\lambda) &= \left(0.604 + 0.0088 \log \frac{m_N}{\lambda}\right) \mathrm{fm}^2 \quad , & (2.45)\\
\left(r_M^v\right)^2(\lambda) &= \left(0.736 - 0.0035 \log \frac{m_N}{\lambda}\right) \mathrm{fm}^2 \quad , & (2.46)\\
\left(r_M^s\right)^2(\lambda) &= \left(0.500 + 5 \times 10^{-5} \log \frac{m_N}{\lambda}\right) \mathrm{fm}^2 \quad . & (2.47)
\end{aligned}$$

We conclude that the higher–order variation of the leading moments with the renormalisation scale is very weak, strongest for the electric radii, but even for those only of the order of 1% if λ differs from the "canonical" scale m_N by a factor of 2. In the same range, the magnetic moments and the isovector magnetic radius vary by a few per mille, the isoscalar magnetic radius by a few parts in 10^5. As can be seen from Eq. (2.35), the numerical smallness of the scale dependence in the isoscalar magnetic radius is due to a suppression of the logarithm by two chiral orders as compared to all other moments, while for the magnetic moments and the electric radii, the suppression in the isoscalar quantities as compared to the isovector ones is based on numerical accidents (or, at best, due to the smallness of the isoscalar anomalous magnetic moment).

In order to go beyond the leading moments, we have examined the full Q^2 dependence of the neutron electric form factor under variation of the renormalisation scale. Fig. 2.6 shows the curves for scales between the ρ mass, $\lambda = M_\rho = 769$ MeV, and the mass of the Λ hyperon, $\lambda = m_\Lambda = 1116$ MeV. We emphasise that the low–energy constant entering the radius has *not* been readjusted, the curves clearly show the finding above, namely that the radius is very insensitive to variations of the scale. For increasing Q^2, however, the corrections become significant. This is easily understood from the

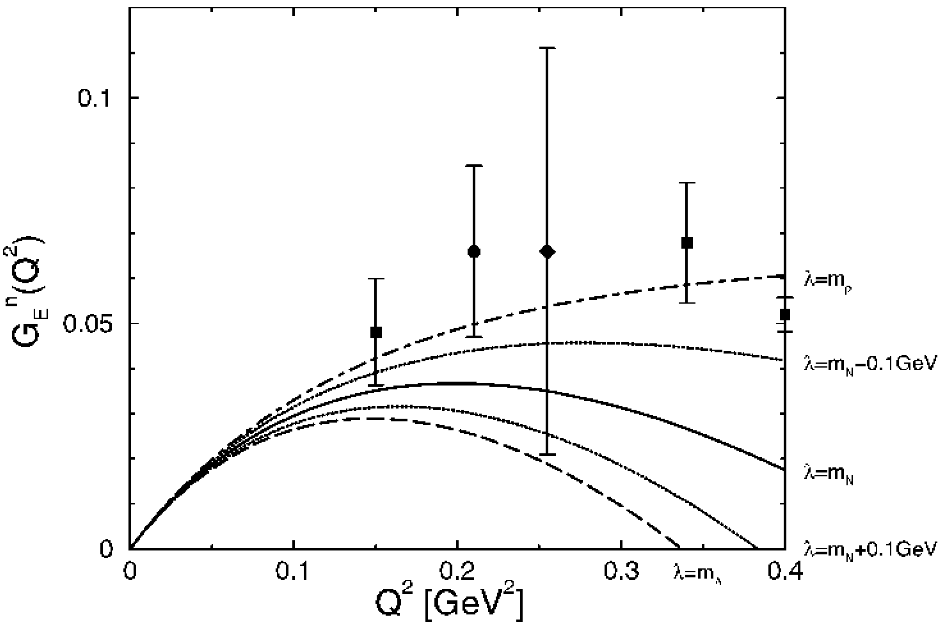

Figure 2.6: The dependence of the neutron electric form factor on variation of the renormalisation scale λ. In addition to the curve for the "canonical" value m_N, we show the fourth order representation for scales $\lambda = m_N \pm 0.1$ GeV, $\lambda = M_\rho$, $\lambda = m_\Lambda$.

precise form of the Q^2–dependent function multiplying the chiral logarithms, which is given explicitly in Appendix A.1.3: it is a function of Q^2/m_N^2, therefore expandable as a finite polynomial to any definite chiral order, but the corrections become significant with Q^2/m_N^2 as large as 0.4. In particular for $\lambda = M_\rho$ one finds much better agreement with the data than for the "canonical" scale $\lambda = m_N$. This should, however, not lead to the conclusion that this scale is a "better choice", but rather indicate (parts of) the uncertainty that is necessarily included in relativistic corrections to heavy baryon loop results.

2.4 Inclusion of vector mesons

It is well established that the vector mesons contribute significantly to the nucleon form factors. For example, extended unitarity allows one to reconstruct the isovector spectral functions [FF60] below $t \simeq 1\,\mathrm{GeV}^2$ from the pion form factor and the analytically continued $\pi\pi \to \bar{N}N$ isovector partial wave amplitudes. Besides the important contribution of the two–pion continuum, the ρ meson clearly shows up. Similarly, in the isoscalar channel, the ω and the ϕ dominate the spectral function at low positive t. All these effects are clearly visible in dispersion theoretical analyses of the nucleon form factors, see [Ho76, MMD96, HMD96]. In the chiral expansion performed in the preceding sections, such effects are included in the low–energy constants. This follows directly from the low momentum expansion of any vector meson propagator (for simplicity, we do not show the explicit Lorentz structures),

$$\frac{1}{1-t/M_V^2} = 1 + \frac{t}{M_V^2} + \frac{t^2}{M_V^4} + \mathcal{O}(t^3) \ . \tag{2.48}$$

In a fourth–order chiral analysis as presented here, one is sensitive up to the terms linear in t, which contribute to the various electromagnetic radii. Stated differently, any vector meson contribution is hidden in the fit values of the various LECs. As we discussed before, the curvature effects on the electric and magnetic form factor of the proton as well as the magnetic neutron form factor are much too small. This can be cured in two ways. One could either attempt a higher order analysis or include vector mesons dynamically. While the first approach would be more systematic, we choose here the second, for various reasons. With explicit vector mesons (VM), we not only account for all terms in the expansion Eq. (2.48) but also do not introduce any new unknown parameter. This can be understood as follows: adding the vector mesons in a chirally symmetric manner and retaining the corresponding dimension two, three, and four counterterms, any LEC α_i takes the form

$$\alpha_i \ \rightarrow \ \hat{\alpha}_i \ + \ \text{vector meson contribution} \ , \tag{2.49}$$

where the remainder $\hat{\alpha}_i$ parameterises the physics not related to the explicitly included vector meson contribution. For such a decomposition to make sense, the scale–dependent LECs should be taken at $\lambda = M_V$. Since in the infrared regularisation procedure, the nucleon mass is taken to be the intrinsic scale for all loop integrals as described in Section 2.3.2, we will neglect scale mismatch due to $M_V \neq m_N$ (which is probably justified because of $\log(m_N/M_\rho) \approx 0.2$). The vector meson propagator generates a whole string of higher order terms, hopefully resumming the most important contributions not included at fourth order. The parameters appearing in the vector meson contributions will be taken from existing dispersive analyses of the nucleon electromagnetic form factors. We therefore only need to refit the low–energy constants $\hat{\alpha}_i$. This also allows to study the concept of resonance saturation. It was already shown in [BKM97] that the numerical values of the dimension two LECs can be understood from s–channel baryon and t–channel meson resonance excitations, in particular from the $\Delta(1232)$ and the ρ. In the case at hand, we can investigate this concept for the LECs c_6, c_7, d_6, d_7, e_{54}, and e_{74}. It was already noted in [BKM97] that c_6 and c_7 are largely saturated by vector meson contributions.

2.4.1 Chiral Lagrangians including vector mesons

We employ the tensor field representation of spin-1 fields as advocated in [GL84], i.e. the vector mesons are written in terms of antisymmetric tensor fields

$$W_{\mu\nu} = -W_{\nu\mu} \tag{2.50}$$

with the three degrees of freedom W_{ij} $(i,j=1,2,3)$ frozen out. This representation is most natural for constructing chirally invariant couplings of vector mesons to pions and photons because no particular dynamical character of the vector mesons is assumed (in contrast e.g. to the massive Yang–Mills or hidden symmetry approaches as reviewed in [Me88, BKY88].) In this section, we temporarily switch to SU(3) chiral Lagrangians, because the ϕ meson contributes to the isoscalar form factors. The free Lagrangian then takes the form

$$\mathcal{L}_V = -\frac{1}{2}\partial^\mu W^a_{\mu\nu}\partial_\rho W^{\rho\nu,a} + \frac{M_V^2}{4} W^a_{\mu\nu}W^{\mu\nu,a} \ , \tag{2.51}$$

where

$$W_{\mu\nu} = \begin{pmatrix} \frac{\rho^0}{\sqrt{2}} + \frac{\omega}{\sqrt{2}} & \rho^+ & K^{*+} \\ \rho^- & -\frac{\rho^0}{\sqrt{2}} + \frac{\omega}{\sqrt{2}} & K^{*0} \\ K^{*-} & \overline{K}^{*0} & -\phi \end{pmatrix}_{\mu\nu} \ . \tag{2.52}$$

Here, we have written the vector meson matrix in terms of physical particles, assuming ideal ϕ–ω mixing. From Eq. (2.51), one easily derives the vector meson propagator as given in [BM96],

$$\begin{aligned} G_{\mu\nu,\rho\sigma}(x,y) &= \langle 0|T\{W_{\mu\nu}(x), W_{\rho\sigma}(y)\}|0\rangle \\ &= \frac{i}{M_V^2}\int \frac{d^4k}{(2\pi)^4}\frac{e^{ik\cdot(x-y)}}{M_V^2-k^2-i\epsilon} \\ &\quad \times\Big[g_{\mu\rho}g_{\nu\sigma}(M_V^2-k^2)+g_{\mu\rho}k_\nu k_\sigma - g_{\mu\sigma}k_\nu k_\rho - (\mu\leftrightarrow\nu)\Big] \ . \end{aligned} \tag{2.53}$$

According to [Ec89], the lowest–order interaction with Goldstone boson fields as well as external vector and axial–vector sources can be written as

$$\mathcal{L}_W = \frac{1}{2\sqrt{2}}\Big(F_V\langle W^{\mu\nu}F^+_{\mu\nu}\rangle + iG_V\langle W^{\mu\nu}[u_\mu,u_\nu]\rangle\Big) \ , \tag{2.54}$$

where the couplings G_V and F_V can e.g. be determined from the decay widths $\rho\to\pi\pi$ and $\rho\to e^+e^-$. Following [BM96], the lowest–order couplings of massive spin–1 fields to baryons can be written in terms of a chirally invariant Lagrangian as

$$\begin{aligned} \mathcal{L}_{\phi BW} =\ & R_{D/F}\,\langle\bar B\sigma^{\mu\nu}(W_{\mu\nu},B)_\pm\rangle \ +\ R_S\,\langle\bar B\sigma^{\mu\nu}B\rangle\,\langle W_{\mu\nu}\rangle \\ & +S_{D/F}\,\langle\bar B\gamma^\mu([D^\nu,W_{\mu\nu}],B)_\pm\rangle \ +\ S_S\,\langle\bar B\gamma^\mu B\rangle\,\langle[D^\nu,W_{\mu\nu}]\rangle \\ & +U_{D/F}\,\langle\bar B\sigma^{\lambda\nu}(W_{\mu\nu},[D_\lambda,[D^\mu,B]])_\pm\rangle \ +\ U_S\,\langle\bar B\sigma^{\lambda\nu}[D_\lambda,[D^\mu,B]]\rangle\langle W_{\mu\nu}\rangle \ , \end{aligned} \tag{2.55}$$

where, as usually in SU(3), the index D refers to the anticommutator $(A,B)_+ = \{A,B\}$, while the index F accompanies the commutator $(A,B)_- = [A,B]$. In addition, we introduced singlet couplings with indices S. These coupling constants are related to the ones used in the Lagrangian of the standard vector representation of the ρ,

$$\mathcal{L}_{\rho N} = \frac{1}{2}g_{\rho NN}\bar\Psi\Big\{\gamma^\mu\boldsymbol{\rho}_\mu\cdot\boldsymbol{\tau} - \frac{\kappa_\rho}{2m_N}\sigma^{\mu\nu}\partial_\nu\boldsymbol{\rho}_\mu\cdot\boldsymbol{\tau}\Big\}\Psi \ , \tag{2.56}$$

by

$$g_{\rho NN} = \frac{M_V}{\sqrt{2}}\Big(m_N(U_D+U_F)-2(S_D+S_F)\Big) \quad , \tag{2.57}$$

$$g_{\rho NN}\,\kappa_\rho = -\frac{4\sqrt{2}m_N}{M_V}(R_D+R_F) \quad . \tag{2.58}$$

In analogy, one finds for the ω and ϕ couplings

$$g_{\omega NN} = \frac{M_V}{\sqrt{2}}\Big(m_N(U_D+U_F+2U_S)-2(S_D+S_F+2S_S)\Big) \quad , \tag{2.59}$$

$$g_{\omega NN}\,\kappa_\omega = -\frac{4\sqrt{2}m_N}{M_V}(R_D+R_F+2R_S) \quad , \tag{2.60}$$

$$g_{\phi NN} = -M_V\Big(m_N(U_D-U_F+U_S)-2(S_D-S_F+S_S)\Big) \quad , \tag{2.61}$$

$$g_{\phi NN}\,\kappa_\phi = \frac{8m_N}{M_V}(R_D-R_F+R_S) \quad . \tag{2.62}$$

In [BM96], one additional term (proportional to new couplings $T_{D/F}$) of higher order in derivatives was introduced,

$$\mathcal{L}'_{\phi BW} = T_{D/F}\,\langle \bar{B}\gamma^\mu([D_\lambda, W_{\mu\nu}],[D^\lambda,[D^\nu,B]])_\mp\rangle + T_S\,\langle \bar{B}\gamma^\mu[D^\lambda,[D^\nu,B]]\rangle\,\langle [D_\lambda, W_{\mu\nu}]\rangle \quad , \tag{2.63}$$

which was subsequently shown to contribute to the electric form factors as a term $\mathcal{O}(q^4)$, therefore beyond the order to which we are working here; the authors of [BM96] however left out a term

$$\mathcal{L}''_{\phi BW} = V_{D/F}\,\langle B\sigma^{\nu\lambda}([D_\lambda,[D^\mu,W_{\mu\nu}]],B)_\pm\rangle + V_S\,\langle B\sigma^{\nu\lambda}B\rangle\,\langle [D_\lambda,[D^\mu,W_{\mu\nu}]]\rangle \tag{2.64}$$

that enters the magnetic radius, i.e. contributes a term $\mathcal{O}(q^2)$ to the magnetic form factors and hence should be considered in a $\mathcal{O}(q^4)$ calculation. However, as nothing is known from elsewhere about such couplings, we shall not introduce these here.[#3] Note that, via the q^2 expansion of the resonance pole, the contributions to the magnetic moments stemming from the $R_{D/F/S}$ terms *do* of course induce additional q^2 dependence in the magnetic form factors.

There is no generalisation of chiral perturbation theory which fully includes the effects of vector mesons as intermediate states to arbitrary loop orders. As the masses of the vector mesons do not vanish in the chiral limit, they introduce a new mass scale which, when appearing inside loop integrals, potentially spoils chiral power counting in a similar manner as the nucleon mass in a "naive" relativistic baryon ChPT approach. In analogy to the heavy–fermion theories, "heavy–meson effective theory" has been used to investigate vector meson properties like masses and decay constants when

[#3] The terms in Eq. (2.63) were allowed for in the analysis [MO00] of πN–scattering and found to be very small. This lends credit to the omission of higher order couplings here.

coupling these to Goldstone bosons in a chirally invariant fashion (see [BGT97] or for some special processes [JMW95]). This approach does not work with the heavy particle number not conserved as in processes where these resonances are virtual intermediate states. However, these difficulties do not arise as long as there is no loop integration over intermediate vector meson momenta. Indeed, to the order we are working here, we can even set up a "power counting scheme" for diagrams including vector mesons which allows to calculate corrections to the simple tree diagrams (where the photon couples to the nucleon via an intermediate vector meson). We count

1. the couplings of vector mesons to the photon and of the ρ to two pions as $\mathcal{O}(q^2)$ (see Eq. (2.54) and the usual power counting for $F^+_{\mu\nu}$ and u_μ);
2. the tensor coupling of vector mesons to nucleons ($R_{D/F/S}$ in our notation) as $\mathcal{O}(q^0)$, the vector coupling ($S_{D/F/S}$, $U_{D/F/S}$) as $\mathcal{O}(q^1)$;
3. the vector meson propagator as $\mathcal{O}(q^0)$ (see Eq. (2.53)).

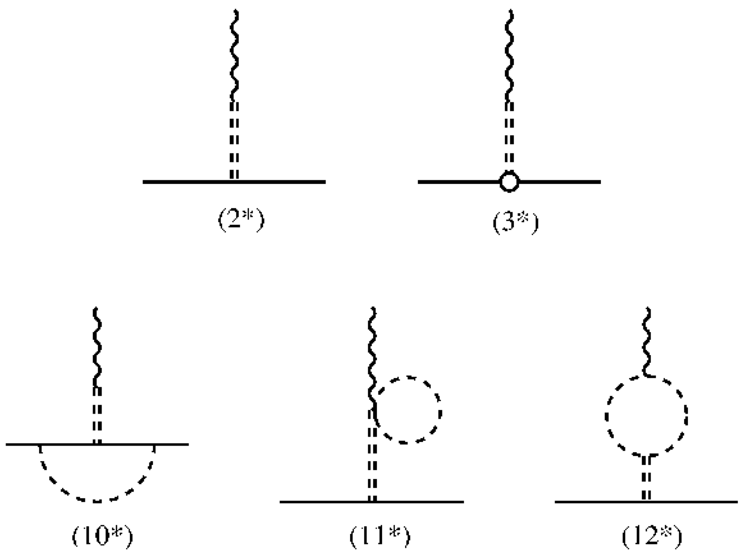

Figure 2.7: Feynman diagrams including explicit vector meson contributions to the electromagnetic form factors up to fourth order. Solid, dashed, double dashed, and wiggly lines refer to nucleons, pions, vector mesons, and the vector source, respectively. The vertex denoted by an open dot refers to the vector coupling of the vector mesons to the nucleon which is of subleading chiral order as compared to the tensor coupling.

Up to $\mathcal{O}(q^4)$, we therefore have to include the diagrams shown in Fig. 2.7. The numbering indicates the correspondence to diagrams with contact terms as shown in Fig. 2.2: the tree level coupling of the vector mesons to the nucleon via the tensor coupling, diagram (2*), enters the magnetic moments as do the LECs c_6, c_7 in diagram

(2), diagrams (10) and (10*) as well as (11) and (11*) yield vertex corrections to these due to pion loops, the vector coupling in diagram (3*) compares to the LECs d_6, d_7 as shown in diagram (3), and finally the ρ exchange in diagram (12*) contributes to the $\pi\pi NN$ coupling $\sim c_4$ in diagram (12).

Explicitly, the analytic results for the form factors including vector mesons can be gained from those with contact terms only by the following replacements:

$$c_6 \;\rightarrow\; \hat{c}_6 + g_{\rho NN}\,\kappa_\rho\,\frac{F_\rho M_\rho}{M_\rho^2 - t}\;, \tag{2.65}$$

$$c_7 \;\rightarrow\; \hat{c}_7 - \frac{g_{\rho NN}\,\kappa_\rho}{2}\,\frac{F_\rho M_\rho}{M_\rho^2 - t} + \frac{g_{\omega NN}\,\kappa_\omega}{2}\,\frac{F_\omega M_\omega}{M_\omega^2 - t} + \frac{g_{\phi NN}\,\kappa_\phi}{2}\,\frac{F_\phi M_\phi}{M_\phi^2 - t}\;, \tag{2.66}$$

$$d_6^r \;\rightarrow\; \hat{d}_6^r - \frac{g_{\rho NN}}{2}\,\frac{F_\rho}{M_\rho}\,\frac{1}{M_\rho^2 - t}\;, \tag{2.67}$$

$$d_7 \;\rightarrow\; \hat{d}_7 - \frac{g_{\omega NN}}{4}\,\frac{F_\omega}{M_\omega}\,\frac{1}{M_\omega^2 - t} - \frac{g_{\phi NN}}{4}\,\frac{F_\phi}{M_\phi}\,\frac{1}{M_\phi^2 - t}\;. \tag{2.68}$$

Especially, these hold for the loop diagrams with pion loops as vertex corrections to photon couplings via c_6, c_7, see diagrams (10), (11) in Fig. 2.2 and (10*), (11*) in Fig. 2.7. At leading order, resonance saturation for c_6, c_7 has already been investigated in [BKM97]. The vector meson contributions to the magnetic moments and the electric radii can be found trivially from Eqs. (2.27)–(2.32) by using Eqs. (2.65)–(2.68) at $t = 0$. The vector meson contributions to the magnetic radii, finally, yield a more complicated replacement law for e_{54}, e_{74} due to the aforementioned loop corrections, which, however, at leading order reads

$$e_{54} \;\rightarrow\; \hat{e}_{54} + \frac{1}{8m_N}\left\{g_{\omega NN}\,\kappa_\omega\,\frac{F_\omega}{M_\omega^3} + g_{\phi NN}\,\kappa_\phi\,\frac{F_\phi}{M_\phi^3}\right\} + \mathcal{O}(\mu^2)\;, \tag{2.69}$$

$$e_{74}^r \;\rightarrow\; \hat{e}_{74}^r + \frac{1}{4m_N}\,g_{\rho NN}\,\kappa_\rho\,\frac{F_\rho}{M_\rho^3} + \mathcal{O}(\mu^2)\;. \tag{2.70}$$

Finally, resonance saturation for the LEC c_4 has also been analysed in [BKM97], where it was found that c_4 is completely saturated by ρ, Δ, and (a very small) Roper contribution. Here, we only want to replace the ρ contribution by its dynamical analogue, therefore setting

$$c_4 \rightarrow \hat{c}_4 + \frac{g_{\rho NN}\,\kappa_\rho}{2m_N}\,\frac{G_\rho M_\rho}{M_\rho^2 - t} \;=\; \hat{c}_4 + \frac{\kappa_\rho}{4m_N}\,\frac{M_\rho^2}{M_\rho^2 - t}\;, \tag{2.71}$$

where, in the second step, a universal ρ–hadron coupling $g = g_{\rho NN} = g_{\rho\pi\pi} \equiv G_\rho M_\rho / F_\pi^2$ and the KSFR relation $M_\rho^2 = 2g^2F_\pi^2$ [KSFR66] were assumed.

2.4.2 Results and discussion

Before presenting results for the four form factors, including the effects of dynamical vector mesons, we have to discuss the values for the miscellaneous coupling constants introduced thereby. First of all, for the vector meson masses we use $M_\rho = 770$ MeV, $M_\omega = 780$ MeV, $M_\phi = 1020$ MeV. The couplings to the photon have been fixed from the partial widths of $V \to e^+e^-$ (in analogy to [MMD96]) to be $F_\rho = 152.5$ MeV, $F_\omega = 45.7$ MeV, $F_\phi = 79.0$ MeV, the ratios being in satisfactory agreement with what one would expect from exact SU(3) symmetry (plus ideal ϕ–ω mixing), $F_V = F_\rho = 3F_\omega = 3/\sqrt{2}F_\phi$.

The couplings of vector mesons to nucleons are taken from the most recent dispersive analysis [MMD96]. The respective values (adjusted to our conventions) are

$$\begin{aligned} g_{\rho NN} &= 4.0 \ , & \kappa_\rho &= 6.1 \ , \\ g_{\omega NN} &= 41.8 \ , & \kappa_\omega &= -0.16 \ , \\ g_{\phi NN} &= -18.3 \ , & \kappa_\phi &= -0.22 \ . \end{aligned} \qquad (2.72)$$

The resulting electric and magnetic form factors of the proton and the neutron are

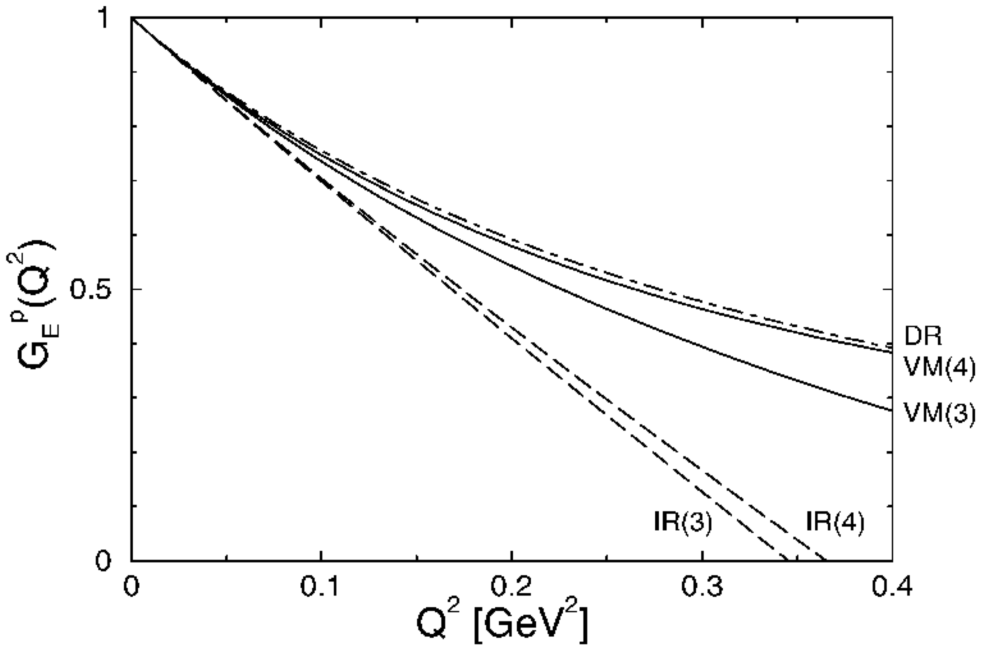

Figure 2.8: The proton electric form factor in relativistic baryon chiral perturbation theory including vector mesons (solid lines) to third and fourth order, marked as VM(3), VM(4), respectively. For comparison, the results without vector mesons are also shown (dashed lines, labelled by IR(3), IR(4)). All LECs are determined by a fit to the proton charge radius as given by the dispersion theoretical result (dot–dashed line, labelled by DR).

shown in Figs. 2.8–2.10. Consider the electric form factors first. The vector meson contribution already supplies sufficient curvature for an adequate description of the

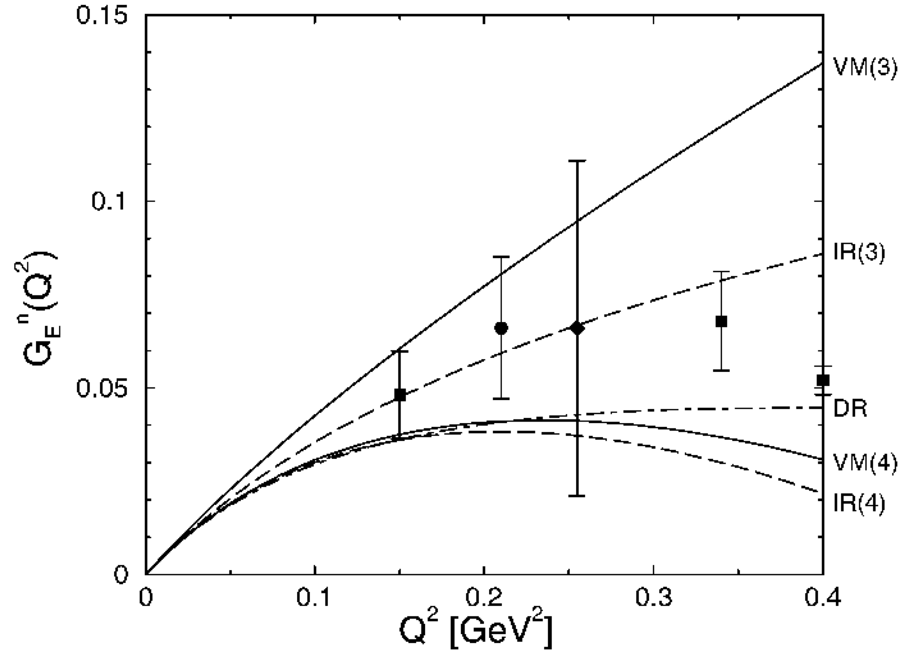

Figure 2.9: The neutron electric form factor in relativistic baryon chiral perturbation theory including vector mesons (solid lines) to third and fourth order, marked as VM(3), VM(4), respectively. For comparison, the results without vector mesons are also shown (dashed lines, labelled by IR(3), IR(4)). All LECs are determined by a fit to the neutron charge radius. Also given is the result of the dispersion theoretical analysis (dot dashed line, labelled by DR). The data are from [Ed94].

proton charge form factor at third order, cf. Fig. 2.8. This is achieved without new adjustable parameters, but simply due to the higher order terms induced by the inclusion of the vector mesons. It is worth noting that at fourth order, the chiral plus vector meson representation is in almost perfect agreement with the result of the dispersive analysis up to momenta of $Q^2 = 0.4\,\mathrm{GeV}^2$, i.e. for much higher momenta than considered so far in chiral perturbation theory approaches. However the already well–described neutron electric form factor, see Fig. 2.9, is, at fourth order, only very mildly affected by the vector meson contribution, but is of course also most sensitive to the precise choice of the vector meson couplings. We only want to state that for a reasonable choice of these parameters, the good result of the chiral one loop representation is not spoiled.[#4]

Turning now to the magnetic form factors, see Fig. 2.10, we find that both the third and the fourth order curves yield reasonable descriptions of the data, in both cases

[#4] We also note that the dispersive analysis of [MMD96] does not include most of the new data [Ed94]. Refitting the vector meson parameters accordingly to the new data base will also lead to an improvement of the fourth order curve in our analysis.

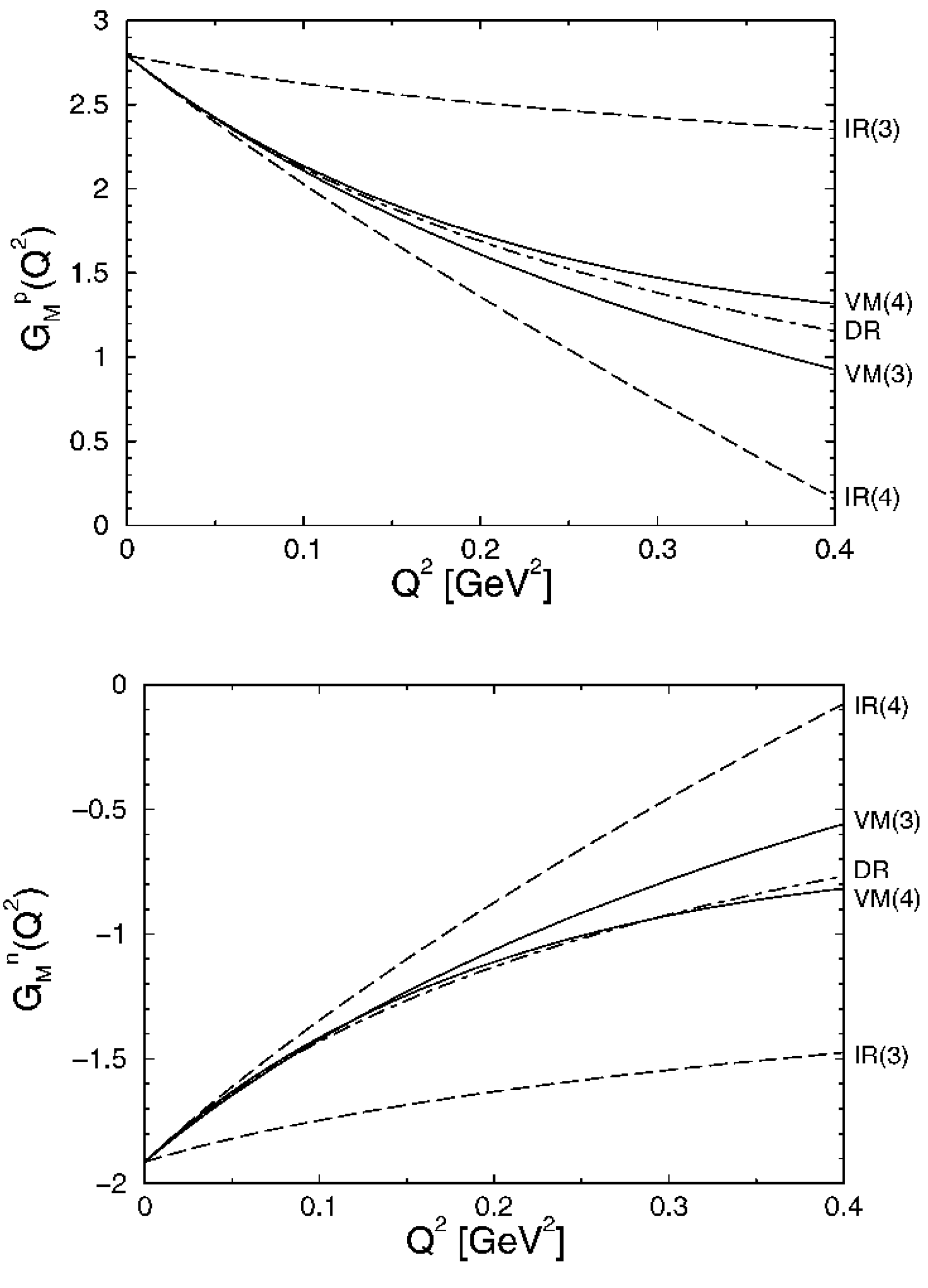

Figure 2.10: The proton and neutron magnetic form factors in relativistic baryon chiral perturbation theory including vector mesons (solid lines) to third and fourth order, marked as VM(3), VM(4). For comparison, the results without vector mesons are also shown (dashed lines, labelled by IR(3), IR(4)). All LECs at third (fourth) order are determined by a fit to the proton/neutron magnetic moments (radii). Also given are the dispersion theoretical results (dot–dashed line, labelled by DR).

the fourth order results being slightly better than the respective third order ones. The latter show the right slope at the origin (which is fitted in the fourth order case), and all curves have approximately the right curvature, which is a bit stronger at fourth order.

We have, in addition, plotted the third and fourth order curves for G_E^p, G_M^p, and G_M^n (including vector mesons), normalised and divided by the dipole form factor

$$G_D(Q^2) = \frac{1}{\left(1 + Q^2/0.71\,\mathrm{GeV}^2\right)^2} \quad , \tag{2.73}$$

see Figs. 2.11, 2.12. Here, again, we see that the fourth order prediction for the proton charge form factor agrees extremely well with the data up to $Q^2 = 0.4\,\mathrm{GeV}^2$. For the neutron magnetic form factor, the fourth order curve, though rising above dipole and dispersion theoretical fit, still is within the error range given by the data, while the fourth order result for the proton magnetic form factor deviates from the data above $Q^2 = 0.3\,\mathrm{GeV}^2$.

It is worth pointing out the following essential conclusions drawn from this discussion:

1. In Section 2.3.4 we saw that the "prediction" of the magnetic radii in a third order calculation worsens considerably when comparing the relativistic and the heavy baryon approach. This observation indicated that the large contribution of the pion cloud to the magnetic radii was an artifact of the $1/m$–expansion to $\mathcal{O}(q^3)$. Inspection of the third order curves including explicit vector meson effects shows that this reduction of the pion cloud effect is indeed consistent with the fairly conventional vector meson parameters, yielding in total excellent results for the magnetic radii which are still "predicted" and not fitted. We here show these "predictions" with the separate contributions of pion–cloud and vector mesons,

$$\begin{aligned} (r_M^p)^2 &= (r_M^p)^2_\pi + (r_M^p)^2_{\mathrm{VM}} = (0.18 + 0.49)\,\mathrm{fm}^2 = (0.82\,\mathrm{fm})^2 \quad , & (2.74)\\ (r_M^n)^2 &= (r_M^n)^2_\pi + (r_M^n)^2_{\mathrm{VM}} = (0.26 + 0.44)\,\mathrm{fm}^2 = (0.84\,\mathrm{fm})^2 \quad , & (2.75)\end{aligned}$$

in good agreement with the values from dispersion analyses, $r_M^p = 0.836\,\mathrm{fm}$ and $r_M^n = 0.889\,\mathrm{fm}$. Note however that, although we did not fit any new parameters to the magnetic radii, additional experimental information enters via the vector meson couplings that in turn have been fitted to the form factors in the dispersive approach.

2. This analysis indicates that a "strict" ChPT calculation to higher–than–fourth order is probably only moderately sensible. Apart from various two–loop contributions which amount only to vertex corrections of diagrams already present in the one–loop case, the major "new" contribution is the three–pion continuum entering the isoscalar form factors, which was already shown to yield a negligibly

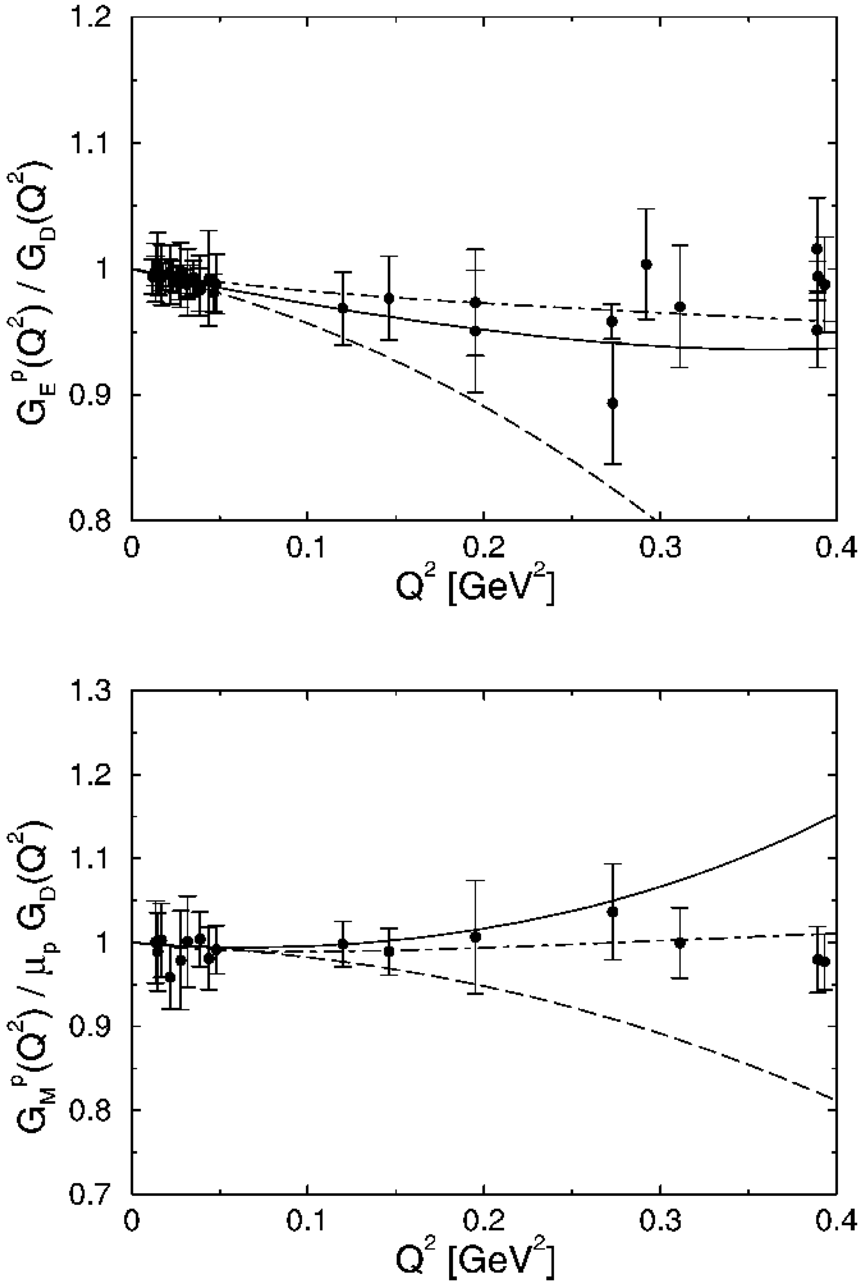

Figure 2.11: The proton electric and magnetic form factors in relativistic baryon chiral perturbation theory including vector mesons to third (dashed line) and fourth (solid line) order, divided by the dipole form factor. For comparison, we show the dispersion theoretical results (dot–dashed line) and the world data available in this energy range.

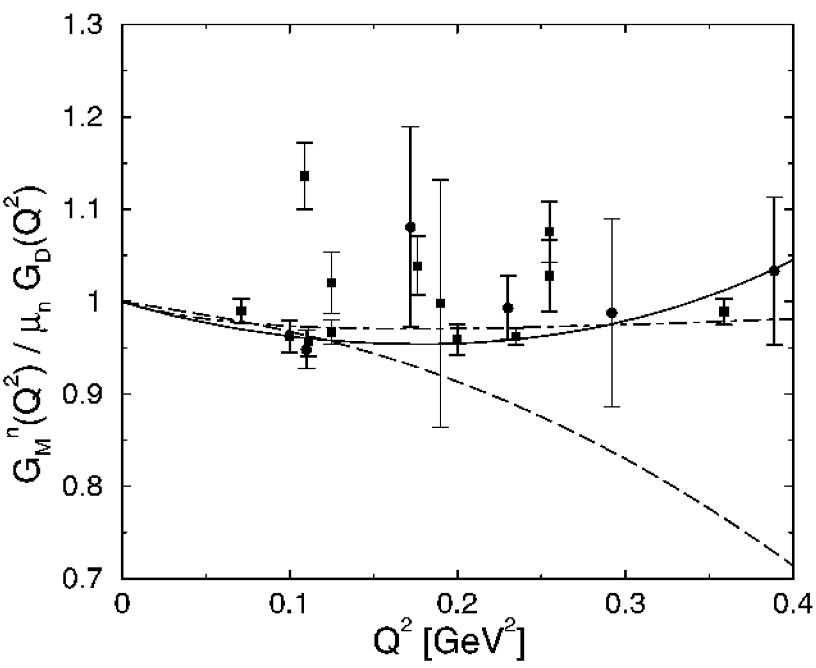

Figure 2.12: The neutron magnetic form factor in relativistic baryon chiral perturbation theory including vector mesons to third (dashed line) and fourth (solid line) order, divided by the dipole form factor. For comparison, we show the dispersion theoretical result (dot dashed line) and the world data available in this energy range, where the data points denoted by squares (instead of circles) refer to the more recent measurements [Ma93]. The older data can be traced back from [MMD96].

small correction to the ω/ϕ–peak in the isoscalar spectral function [BKM96c]. Therefore, an analysis to $\mathcal{O}(q^5)$ or $\mathcal{O}(q^6)$ would basically result in fitting new counterterm parameters in order to reproduce the resonance contributions considered explicitly here.

2.4.3 Resonance saturation

As we have not *assumed* resonance saturation of the various low energy constants, but taken the resonance parameters from elsewhere and refitted the contact terms, we may now check how well resonance saturation by the lowest lying vector mesons actually works. Table 2.1 shows the values for the low energy constants, fitted at third and fourth order, with and without vector meson contributions. The vector meson contribution to the LEC c_4 as given in Eq. (2.71) numerically amounts to 1.6 GeV^{-1} (see also [BKM97]) which reduces the value of $\tilde{c}_4$ by about 50%. This remainder which is due to (mainly) Δ and a small Roper contribution is still represented by a contact term.

	q^3	q^4	q^3+VM	q^4+VM
c_6	5.03	4.77	0.20	-0.06
c_7	-2.72	-2.55	-0.27	-0.09
d_6^r	0.67	0.74	1.34	1.40
d_7	-0.70	-0.69	-0.04	-0.03
e_{54}		0.26		-0.04
e_{74}^r	—	1.65	—	-1.15

Table 2.1: Values for the various low–energy constants, with and without vector meson contributions. Note that the third and the fourth columns, strictly speaking, refer to the LECs $\hat{\alpha}_i$ instead of α_i. c_6, c_7 are dimensionless, the d_i are given in GeV^{-2}, the e_i in GeV^{-3}.

We conclude that the low–energy constants entering the magnetic moments (c_6, c_7) as well as those fitted to the *isoscalar* radii, both electric (d_7) and magnetic (e_{54}), are nearly perfectly saturated by the lowest lying vector meson nonet, while the contact terms entering the *isovector* radii (d_6, e_{74}) are not at all. This can be interpreted to the effect that ω and ϕ are already sufficient to describe the isoscalar channel of the vector form factors to good accuracy, while higher resonances are mandatory for an adequate description of the isovector form factors. This is in agreement with what is found in dispersive analyses. However this does not necessarily invalidate our approach, as these higher resonances have much larger masses (the $\rho(1450)$ being the lowest lying of them) and therefore will hardly contribute to the *curvature* of the form factors (which is the change we are looking for, compared to linear contact terms).

2.5 Summary

We have studied the electromagnetic form factors of the nucleon in a manifestly Lorentz invariant form of baryon chiral perturbation theory to one–loop (fourth) order. As discussed, in this scheme based on the so called infrared regularisation of loop graphs, one is able to set up a systematic power counting scheme in harmony with the strictures from analyticity. The pertinent results of our investigation can be summarised as follows:

(1) To fourth order, the neutron and proton electric form factors each contain one low–energy constant which can be fixed from the empirical information on the corresponding radii. This gives a good description of the neutron charge form factor up to four–momentum transfer squared of $Q^2 = 0.4\,\text{GeV}^2$ and, furthermore, exhibits convergence in that the corrections when going from third to

fourth order are small. This is in contrast to the heavy–baryon expansion and can be traced back to the proper resummation of the recoil terms in the relativistic expansion. For the electric form factor of the proton, the one loop representation gives too little curvature and thus deviates from the data already at $Q^2 \simeq 0.2\,\mathrm{GeV}^2$, similar to the heavy baryon description. However, no large fourth order corrections are found below $Q^2 = 0.4\,\mathrm{GeV}^2$.

(2) To third order, the momentum dependence of the magnetic proton and neutron form factors is given parameter free. The $1/m$ corrections present in our approach worsen the prediction for the magnetic radii based on the leading chiral singularities, like e.g. in the heavy–baryon approach. The leading chiral limit behaviour is not a good approximation for the Goldstone boson contribution to the magnetic radii. At fourth order, the magnetic radii can be fixed. Again, there is not enough curvature in the one–loop representation and one observes large corrections when going from third to fourth order already at $Q^2 \simeq 0.1\,\mathrm{GeV}^2$.

(3) We have demonstrated explicitly that the spectral functions of the isovector form factors have the correct threshold behaviour. The strong momentum–dependence of these spectral functions close to threshold is due to the branch point singularity on the second Riemann sheet inherited from the $\pi\pi \to \bar{N}N$ P wave partial wave amplitudes.

(4) We have included the low lying vector mesons ρ, ω, ϕ in a chirally symmetric manner based on an antisymmetric tensor field representation. This does not introduce any new parameters since these (masses and coupling constants) are taken from the PDG tables and from a dispersion theoretical analysis. Refitting the previously defined low energy constants by subtracting the vector meson contribution, we find a good description of *all four* form factors already at third order, with small fourth order contributions, which further improve the theoretical description. In particular, we demonstrate that the vector meson contributions cancel to a large extent in the neutron charge form factor, thus solidifying the result obtained in the chiral expansion.

(5) The inclusion of vector mesons allows to investigate the resonance saturation hypothesis for these couplings. We find that the couplings related to the magnetic moments and the isoscalar radii are almost completely saturated by the low lying vector mesons. This is, however, not the case for the LECs entering the isovector radii. This can be traced back to the fact that while the ω and the ϕ already give a good description of the isoscalar form factors, for the isovector ones one has to include higher mass states than the ρ, in agreement with findings from dispersion theory.

Chapter 3

Baryon form factors in chiral perturbation theory[#1]

3.1 Introduction

In the last chapter, we have investigated the electromagnetic structure of proton and neutron as characterised by the four form factors that have been measured in electron scattering experiments over decades. As we have seen, in the non–perturbative low–energy region of QCD, baryon chiral perturbation theory can be used to calculate these form factors, and we have shown that relativistic baryon chiral perturbation theory (employing infrared regularisation) supplemented by explicit vector meson contributions allows for a fairly precise description of these fundamental quantities for photon virtualities up to $Q^2 \simeq 0.4$ GeV^2.

This chapter will be devoted to the extension of these considerations to the three–flavour case, i.e. we shall calculate the sizes characteristic for electromagnetic probes of other hadrons than the nucleons, specifically the ground state baryon octet. This is interesting for various reasons: First, the charge radius of the Σ^- has recently been measured [Ad99, Se01] and thus gives a first glimpse of an electric hyperon form factor. Second, chiral SU(3) can be subject to large kaon/eta loop corrections, and the form factors offer another window to study the corresponding convergence properties. They might thus indicate whether or not the strange quark can be considered light and lead to a better understanding of SU(3) flavour breaking. Since the chiral expansion of the form factors is well under control in the two–flavour case, one can hope to encounter a reasonably well–behaved series also in the presence of the strange quark. This expectation is borne out by the results presented in this chapter. Third, one can also address some questions concerning strangeness in the nucleon, more precisely, the role of kaon loops that, in simple models, let one expect sizeable contributions of strange operators. Fourth, the knowledge of certain hyperon form factors is mandatory to

[#1] The contents of this chapter have been published in [KM01b].

gain an understanding of kaon photo– and electroproduction off nucleons and light nuclei as measured at ELSA and TJNAF. We shall come back to most of these topics in the course of this chapter.

In addition, these form factors have already been calculated in the so called heavy baryon approach [KHM99, PRZ01]. A direct comparison of our results obtained in the infrared regularisation formalism to the results of that approach can shed further light on the dynamics underlying the non–perturbative baryon structure, in particular the role of recoil corrections. As a final by–product, we can also readdress the issue of the convergence of the chiral expansion for the magnetic moments, which has been much discussed in the recent literature [Je93, MS97, DH98, DHB99, KM00a, PR00].

This chapter is organised as follows. In Section 3.2 we briefly define the baryon form factors and the corresponding electromagnetic radii, which requires just very little generalisation compared to the last chapter. The formalism to obtain the one–loop representation of the form factors is given in Section 3.3. We heavily borrow from the preceding chapter and defer all lengthy formulae to the appendices. The results are presented and discussed in Section 3.4. Section 3.5 contains a short summary and outlook.

3.2 Baryon form factors

The structure of ground state octet baryons (denoted by 'B') as probed by virtual photons is parameterised in terms of two form factors each,

$$\begin{aligned} \langle B(p')\,|\,\mathcal{J}_\mu\,|\,B(p)\rangle &= e\,\bar{u}(p')\left\{\gamma_\mu F_1^B(t) + \frac{i\sigma_{\mu\nu}q^\nu}{2m_B}F_2^B(t)\right\}u(p)\quad , \qquad (3.1)\\ B &= p,\ n,\ \Lambda,\ \Sigma^+,\ \Sigma^0,\ \Xi^-,\ \Xi^0, \end{aligned}$$

with the quark vector current $\mathcal{J}_\mu = \bar{q}\mathcal{Q}\gamma_\mu q$ now involving the SU(3) quark charge matrix $\mathcal{Q} = e\,\mathrm{diag}(2/3,-1/3,-1,3)$, $q^T = (u,d,s)$, and m_B the respective baryon mass. We shall again frequently employ the positive quantity $Q^2 = -t > 0$. The Dirac and Pauli form factors F_1 and F_2 are subject to the normalisations $F_1^B(0) = Q_B$, $F_2^B(0) = \kappa_B$, where κ_B denotes the anomalous magnetic moment of the baryon B. Eq. (3.1) has to be generalised for the Λ–Σ^0 transition form factors that are defined according to

$$\langle\Sigma^0(p')\,|\,\mathcal{J}_\mu\,|\,\Lambda(p)\rangle = e\,u(p')\left\{\left(\gamma_\mu - \frac{m_{\Sigma^0}-m_\Lambda}{t}\,q_\mu\right)F_1^{\Lambda\Sigma^0}(t) + \frac{i\sigma_{\mu\nu}q^\nu}{m_\Lambda+m_{\Sigma^0}}F_2^{\Lambda\Sigma^0}(t)\right\}u(p) \qquad (3.2)$$

(see also [LWD91]). The form of the generalised Lorentz structure accompanying $F_1^{\Lambda\Sigma^0}(t)$ is required by current conservation (which becomes obvious by contracting Eq. (3.2) with q^μ and applying the Dirac equation). Different definitions which all reduce to Eq. (3.1) for $m_{\Sigma^0} \to m_\Lambda$ are possible, however, the one given here is preferable because it still requires the normalisation $F_1^{\Lambda\Sigma^0}(0) = 0$. One also uses the electric and magnetic Sachs form factors,

$$G_E(t) = F_1(t) + \frac{t}{4m_B^2} F_2(t) \,, \quad G_M(t) = F_1(t) + F_2(t) \,, \tag{3.3}$$

which are again the quantities we shall consider most of the time in the following. The radii characterising the spatial extension of charge and magnetisation distributions are defined as in Eqs. (2.4)–(2.7), in particular the exceptions concerning form factors of vanishing "charge" discussed for the electric neutron form factor in Eq. (2.6) apply of course to all electric form factors of neutral particles.

3.3 Formalism

In this section, we spell out the details necessary to extend the SU(2) calculation of the nucleon form factors in baryon chiral perturbation theory employing infrared regularisation, Chapter 2, to the three–flavour case. The presence of different pseudo–Goldstone bosons and baryons with unequal masses entails more general loop functions than those encountered in the SU(2) calculation, these are tabulated in App. A.1. Here we only spell out the various terms of the effective chiral Lagrangian underlying the calculation. Again we do not give the final formulae for the form factors in the main text since these are rather lengthy, but instead refer to App. A.2.

3.3.1 Effective Lagrangian

The chiral effective Goldstone boson Lagrangian is given by

$$\mathcal{L}_{\phi\phi}^{(2)} = \frac{F^2}{4} \langle u_\mu u^\mu + \chi_+ \rangle \quad , \tag{3.4}$$

where the octet of Goldstone boson fields is collected in the SU(3) valued matrix $U(x) = u^2(x)$ and the chiral vielbein u_μ defined as before. The scalar field χ_+ incorporates the quark mass matrix $\mathcal{M} = \mathrm{diag}(m_u, m_d, m_s)$, where we shall work in the isospin limit, $m_u = m_d = \hat{m}$. The mass term leads to the well known lowest order (isospin symmetric) mass formulae for pions, kaons, and the eta, which enter the description of the baryon form factors via loop contributions. We would like to point out that the mass differences between the Goldstone bosons yield the leading order SU(3) breaking effect for these form factors. For numerical evaluation, we will use $M_\pi = 139.57$ MeV, $M_K = 493.68$ MeV (the *charged* pion and kaon masses), and $M_\eta = 547.45$ MeV. Furthermore, it is legitimate to differentiate between different decay constants F_π, F_K, F_η in the treatment of the chiral loops as these differences are of higher order. We will use $F_\pi = 92.4$ MeV, $F_K/F_\pi = 1.22$, $F_\eta/F_\pi = 1.3$ (see [GL85a] and, for a more recent determination of F_K/F_π, [FKS00]). The main motivation for not using a common decay constant is the comparison to the SU(2) results for the proton and neutron form factors, where we do not want to suggest an SU(3) effect which is only due to a numerically different treatment of the pion loops.

The meson–baryon Lagrangian at leading order reads

$$\mathcal{L}_{\phi B}^{(1)} = \langle \bar{B}\,(i\not{D} - m)\,B\rangle + \frac{D/F}{2}\,\langle \bar{B}\gamma^\mu\gamma_5\,(u_\mu, B)_\pm\rangle \quad , \tag{3.5}$$

where the matrix–valued field B collects the ground state octet baryons, see Eq. (1.65), and D and F are the axial vector coupling constants.[#2] For these, we will use the values $D = 0.80$, $F = 0.46$ extracted from hyperon decays [Ra99], which obey the SU(2) constraint $D + F = g_A = 1.26$. Here, m denotes the baryon mass in the chiral limit. To this order, the photon field only couples to the charge of the baryon. It resides in the chiral covariant derivative, $D_\mu B = \partial_\mu B + [\Gamma_\mu, B]$, with the chiral connection given as before.

Coupling constants from the second–order meson–baryon Lagrangian are needed both at tree level and in one–loop graphs. The following terms are required in our calculation:

$$\begin{aligned}\mathcal{L}_{\phi B}^{(2)} &= b_{D/F}\langle \bar{B}(\chi_+, B)_\pm\rangle + \frac{b_6^{D/F}}{8m}\langle \bar{B}\sigma^{\mu\nu}(F_{\mu\nu}^-, B)_\mp\rangle \\ &\quad + \frac{i}{2}\sigma^{\mu\nu}\Big\{b_9\langle \bar{B}u_\mu\rangle\langle u_\nu B\rangle + b_{10/11}\langle \bar{B}([u_\mu, u_\nu], B)_\pm\rangle\Big\} \quad .\end{aligned} \tag{3.6}$$

We use the same notation for the operators involving the photon field strength tensor as in the SU(2) case. The b_i are low–energy constants that encode information about the more massive states not contained in the effective field theory or other short–distance effects. These parameters have to be pinned down by using some data. In principle there is also a term $\sim b_0\,\langle \bar{B}B\rangle\langle\chi_+\rangle$ which amounts to a quark mass renormalisation of the common octet mass m. This, however, cannot be disentangled from m without further information (like the pion nucleon σ term), and it is sufficient for our purpose to absorb this term in m. The couplings $b_{D/F}$ yield the leading SU(3) breaking effects in the baryon masses. Again, these affect the form factors via various loop contributions. A best fit to the octet masses results in $m_N = 0.942$ GeV, $m_\Lambda = 1.111$ GeV, $m_\Sigma = 1.192$ GeV, $m_\Xi = 1.321$ GeV (for $m = 1.192$ GeV, $b_D = 0.060$ GeV^{-1}, $b_F = -0.190$ GeV^{-1}), compared to the experimental values $m_N = 0.939$ GeV, $m_\Lambda = 1.116$ GeV, $m_\Sigma = 1.193$ GeV, $m_\Xi = 1.318$ GeV (where the average masses within the respective isospin multiplets have been taken). We consider this accurate enough to put all baryon masses to their experimental values in the numerical evaluation. In any third order calculation, however, no mass

[#2]Here and in what follows, we employ a compact notation: the D–type coupling refers to the anticommutator and the F–type coupling to the commutator.

splitting is present, hence the baryon mass parameter will always be put to the average baryon mass $\bar{m} = 1.151$ GeV in this case. It has been discussed in detail in [BL99] as well as in the last chapter how to fix the omnipresent mass scale λ which has to be introduced in loop diagrams treated in dimensional regularisation. It was argued that in an SU(2) calculation, the nucleon mass serves as a natural mass scale. Here we consider it natural to set $\lambda = \bar{m}$. The LECs $b_6^{D/F}$ parameterise the leading magnetic photon couplings to the baryons and will be fitted to the magnetic moments. Finally, the LECs $b_{9/10/11}$ accompany second order couplings of the various pseudo Goldstone bosons to baryons and enter the form factors via (tadpole) loop contributions. Their values have been estimated based on the resonance saturation hypothesis in [MS97], however, the results used there do not satisfy the SU(2) constraint $2(b_{10} + b_{11}) = c_4 \approx 3.4\ \text{GeV}^{-1}$. The latter value is well established, consistently determined from resonance saturation [BKM97] and fits to pion nucleon scattering [FMS98, BM00]. The discrepancy between both determinations can be traced back to different treatments of the Δ contribution in [MS97] and [BKM97]. Adjusting this, we will use the values $b_9 = 1.36\ \text{GeV}^{-1}$, $b_{10} = 1.24\ \text{GeV}^{-1}$, $b_{11} = 0.46\ \text{GeV}^{-1}$. As we would like to specify the uncertainty of our predictions based on these estimates later on, we attribute some errors to these LECs. As an indication we regard the change of a LEC when fitting it within chiral amplitudes of different orders. This change is about $1.0\ \text{GeV}^{-1}$ for c_4 when going from second to third order in πN scattering (see [BKM95c] for a second order fit). We assume that this change should be a factor of 2 smaller when proceeding from third to fourth order such that, due to the different normalisation of the SU(3) couplings, we set $\Delta b_{9/10/11} = 0.25\ \text{GeV}^{-1}$.

The only terms needed from the third order Lagrangian are those entering the electric (charge) radii of the baryons,

$$\mathcal{L}_{\phi B}^{(3)} = \frac{i d_{101/102}}{2m}\Big\{\langle\bar{B}\Big([D^\mu, F_{\mu\nu}^+],[D^\nu, B]\Big)_\mp\rangle + \text{h.c.}\Big\} \ . \tag{3.7}$$

d_{101}, d_{102} have to be fitted to the charge radii of proton and neutron. Both of these contain an infinite part and the corresponding scale dependence, which is given in App. A.5.

At fourth order, two types of coupling constants appear which are of relevance for our calculation: seven couplings proportional to a quark mass insertion contributing to the magnetic moments, and two couplings entering the magnetic radii,

$$\begin{aligned}\mathcal{L}_{\phi B}^{(4)} = {} & \frac{\alpha_{1/2}}{8}\langle\bar{B}\sigma^{\mu\nu}\Big([F_{\mu\nu}^-, B], \chi_+\Big)_\mp\rangle + \frac{\alpha_{3/4}}{8}\langle\bar{B}\sigma^{\mu\nu}\Big(\{F_{\mu\nu}^+, B\}, \chi_+\Big)_\mp\rangle \\ & + \frac{\beta_1}{8}\langle\bar{B}\sigma^{\mu\nu}B\rangle\langle\chi_+ F_{\mu\nu}^+\rangle + \frac{\tilde{b}_6^{D/F}}{8}\langle\chi_+\rangle\langle\bar{B}\sigma^{\mu\nu}(F_{\mu\nu}^-, B)_\pm\rangle \\ & - \frac{\eta_{1/2}}{2}\langle\bar{B}\sigma^{\mu\nu}\Big([D_\lambda,[D^\lambda, F_{\mu\nu}^+]], B\Big)_\mp\rangle \ .\end{aligned} \tag{3.8}$$

As indicated by the notation, the terms $\sim \tilde{b}_6^{D/F}$ only amount to a quark mass renormalisation of the leading magnetic couplings and will therefore be absorbed into $b_6^{D/F}$

according to

$$\bar{b}_6^{D/F} = b_6^{D/F} + 2m\,(2M_K^2 + M_\pi^2)\,\tilde{b}_6^{D/F} \quad . \tag{3.9}$$

The LECs α_{1-4}, β_1, however, incorporate explicit breaking of SU(3) symmetry in the magnetic moments and will be fitted to the octet moments. $\eta_{1/2}$ will be adjusted to the magnetic radii of proton and neutron. All of these absorb certain divergent loop contributions and display logarithmic scale dependence, with the appropriate coefficients as determined in this calculation again displayed in App. A.5.

While there are, all in all, quite some LECs to be fitted in order to describe all electromagnetic form factors, it is important to point out that all these LECs are, on general grounds, expected to be of order 1 (with the appropriate mass dimensions in powers of GeV: as the baryonic scale is of the order of 1 GeV, it is not necessary to normalise the LECs appropriately).#3

3.3.2 Chiral expansion of the baryon form factors

The chiral expansion of a form factor F consists of two contributions, tree and loop graphs. The tree graphs comprise the lowest–order diagram with fixed coupling (the baryon charge) as well as counterterms from the second–, third–, and fourth–order Lagrangians. As one–loop graphs we have both those with just lowest–order couplings and those with exactly one insertion from $\mathcal{L}_{\phi B}^{(2)}$. The pertinent tree and loop graphs are depicted in Fig. 3.1 (we have not shown the diagrams leading to wave function renormalisation). We refrain from giving the rather lengthy expressions in the main text, but concentrate on the phenomenological numerical results and refer to App. A. We mention that in the limit of a heavy strange quark, we recover the SU(2) results of the previous chapter. Also, the heavy baryon (HB) results of [KHM99] can be obtained straightforwardly as detailed in the last chapter.

3.4 Results and discussion

We first discuss the issues concerning the magnetic moments and the electromagnetic radii in some detail. This can be done within the 'pure' chiral expansion. Then we turn to the full momentum dependence of the various form factors for photon virtualities up to $Q^2 = 0.3$ GeV^2. To this end we have to include vector mesons as active degrees of freedom in a chirally symmetric manner.

#3 We would like to point out that we have adopted the natural normalisation for the SU(3) breaking terms in the magnetic moments (by using the field χ_+ proportional to the quark mass matrix as defined above instead of a spurion diag$(0,0,1)$) which is different from e.g. [Je93, MS97]. Numerically, however, this difference amounts to a factor of $4M_K^2 \approx 0.975$ GeV^2, hence apart from a different mass dimension, this does not make any significant difference.

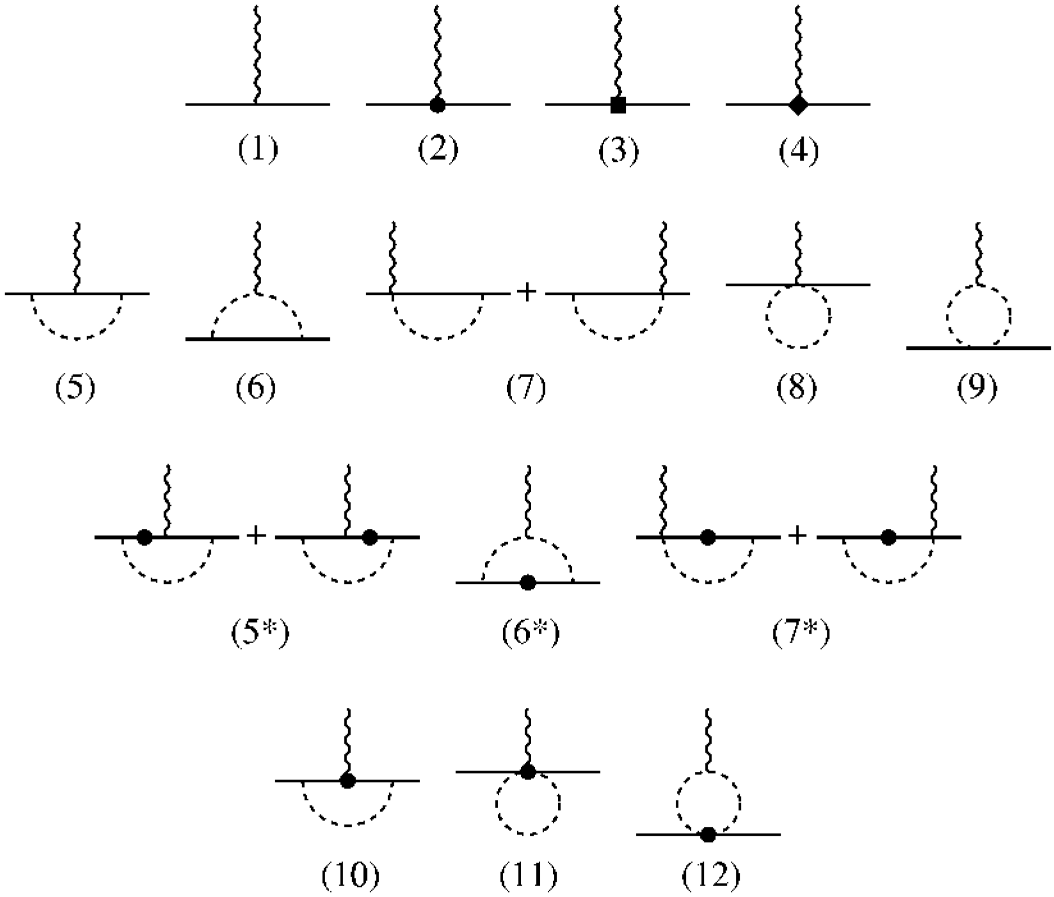

Figure 3.1: Feynman diagrams contributing to the electromagnetic form factors up to fourth order. Solid, dashed, and wiggly lines refer to baryons, Goldstone bosons, and the vector source, respectively. Vertices denoted by a heavy dot/square/diamond refer to insertions from the second/third/fourth order chiral Lagrangian, respectively. Diagrams contributing via wave function renormalisation only are not shown.

3.4.1 Magnetic moments

The issue of convergence of the magnetic moments in chiral perturbation theory has been discussed amply in the literature, with or without inclusion of the decuplet [Je93, MS97, DH98, KM00a, PR00]. We wish to compare the convergence behaviour in the heavy baryon and the infrared regularisation scheme. Table 3.1 shows the best fits to the various orders. The strategy is always to fit the seven experimentally measured static moments (μ_{Σ^0} has not been measured so far, in the theoretical predictions it is always given by $\mu_{\Sigma^0} = (\mu_{\Sigma^+} + \mu_{\Sigma^-})/2$ according to isospin symmetry) and to predict the transition moment $\mu_{\Lambda\Sigma^0}$. At second and third order, only the two leading–order couplings $b_6^{D/F}$ are free parameters, which results in best fits of varying quality, whereas at fourth order the additional five couplings allow for an exact fit of all seven static moments. At second/third order, we have performed an unweighted fit, hence simply minimising $\chi^2 = \sum(\mu_{\rm th} - \mu_{\rm exp})^2$. The χ^2 values given in Table 3.1 thus only serve to indicate the relative quality of the fits.

		HB		IR			
	$\mathcal{O}(q^2)$	$\mathcal{O}(q^3)$	$\mathcal{O}(q^4)$	$\mathcal{O}(q^3)$	$\mathcal{O}(q^3)^*$	$\mathcal{O}(q^4)$	exp.
p	2.56	2.97	2.793	2.61	2.20	2.793	2.793 ± 0.000
n	-1.60	-2.53	-1.913	-1.69	-2.59	-1.913	-1.913 ± 0.000
Λ	-0.80	-0.45	-0.613	-0.76	-0.65	-0.613	-0.613 ± 0.004
Σ^+	2.56	2.21	2.458	2.53	2.41	2.458	2.458 ± 0.010
Σ^0	0.80	0.45	0.649	0.76	0.65	0.649	—
Σ^-	-0.97	-1.32	-1.160	-1.00	-1.12	-1.160	-1.160 ± 0.025
Ξ^0	-1.60	-0.78	-1.250	-1.51	-1.20	-1.250	-1.250 ± 0.014
Ξ^-	-0.97	-0.56	-0.651	-0.93	-1.33	-0.651	-0.651 ± 0.003
$\Lambda\Sigma^0$	1.38	1.65	1.46 ± 0.01	1.41	1.81	1.61 ± 0.01	$\pm 1.61 \pm 0.08$
b_6^D	2.40	5.27	4.56 ± 0.24	3.65	5.18	4.21 ± 0.20	
b_6^F	0.77	2.92	1.65 ± 0.19	1.73	0.56	1.64 ± 0.18	
α_1	—	—	-1.00 ± 0.26	—	—	0.32 ± 0.28	
α_2			1.35 ± 0.29			-0.08 ± 0.18	
α_3			-0.85 ± 0.30			2.14 ± 0.28	
α_4			0.95 ± 0.22			0.05 ± 0.19	
β_1			-2.46 ± 0.33			-3.39 ± 0.34	
χ^2	0.46	0.76	0.00	0.28	1.28	0.00	

Table 3.1: Analysis of the magnetic moments (in units of nuclear magnetons (n.m.)) to different chiral orders. The various best–fit values for the leading order magnetic couplings $b_6^{D/F}$ and the SU(3) breaking couplings α_{1-4}, β_1 are given as well. $b_6^{D/F}$ are dimensionless, α_{1-4}, β_1 are given in units of GeV^{-3}. Errors for fourth–order results display the uncertainty due to $\Delta b_{9/10/11}$. For the definition of χ^2, see text.

It has frequently been noted before that the inclusion of leading loop corrections in the magnetic moments tends to *worsen* the leading order results. This is seen here in the third order heavy baryon results. Within the infrared regularisation scheme, however, it is even disputable which contributions to count as third order: the leading contributions stem from diagram (6) in Fig. 3.1; summing up only the $1/m$ corrections to this graph yields the fit in the column denoted by '$\mathcal{O}(q^3)$' and shows an improvement not only over the heavy–baryon result, but also over the leading order fit. However, defining any one–loop diagram with no higher–order insertions to be of third order, one also has to include diagram (5) in Fig. 3.1 (which only contributes at fourth order in strict chiral power counting). These contributions are large and worsen the fit even over the third–order heavy–baryon one, see the column denoted by '$\mathcal{O}(q^3)^*$'. Especially the magnetic moments of proton, neutron, and Ξ^- are not described to any acceptable accuracy in this case. We note furthermore that the fitted values for the leading order couplings vary considerably among the different fits. Regarding these as indicators for convergence, we again find that the '$\mathcal{O}(q^3)$' result is much closer to the fourth order fit than the '$\mathcal{O}(q^3)^*$' one.

At fourth order, we can compare the two predictions for the transition moment $\mu_{\Lambda\Sigma^0}$. In both cases, we have indicated the uncertainty of these predictions due to the estimated uncertainties of the couplings $b_{9/10/11}$, which turns out to be much smaller than the experimental error of $\Delta\mu^{\rm exp}_{\Lambda\Sigma^0} = 0.08$. It is remarkable that the prediction for this physical quantity is so stable under variation of $b_{9/10/11}$, although the fit values for the individual couplings given in Table 3.1 vary considerably. While the heavy baryon result is about two standard deviations off, the relativistic one ($\mu_{\Lambda\Sigma^0} = 1.606 \pm 0.008$ n.m.) yields exactly the experimental result (to be precise, experimentally only $|\mu_{\Lambda\Sigma^0}|$ is known). Given the errors in $\mu_{\Lambda\Sigma^0}$, a better experimental determination would be desirable. We note furthermore that, while the values for the leading–order magnetic couplings $b_6^{D/F}$ are fairly close in the two different schemes, those for the SU(3) breaking couplings show no similarity at all. This clearly displays the fact that $1/m$ corrections to the various loop diagrams are sizeable even beyond fourth order.

3.4.2 Electric radii

The electric (or charge) radius of any baryon is, according to Eq. (3.3), given by the sum of the Dirac radius and the so–called Foldy term,

$$\langle r_E^2 \rangle = \langle r_1^2 \rangle + \frac{3\,\kappa_B}{2\,m_B^2} \quad . \tag{3.10}$$

Phenomenologically the Foldy term is hence well known *for all ground state octet baryons* from the experimental information on the magnetic moments. What remains to be predicted from any kind of theory or model, as independent quantities, are the Dirac radii. We have therefore always replaced the chiral representation of the Foldy term by the exact value given by experiment. This is legitimate at any chiral order, as the difference is always subleading. Doing otherwise would partly import the well–known problematic convergence properties of the magnetic moments to the description of the electric radii.[#4]

The chiral representations of the electric radii of the baryon octet, both at third and fourth order, involve exactly two low energy constants, d_{101} and d_{102}. These

[#4] This can even entail, in our opinion, misleading conclusions: the huge decuplet effects on the charge radii found in [PRZ01] in some cases stem from the Foldy term, hence have nothing to do with intrinsically *electric* properties of the baryons. It should be noted that in a comparable SU(2) study, only minor effects due to the Δ resonance were found [BFHM98].

	HB		IR		
	$\mathcal{O}(q^3)$	$\mathcal{O}(q^4)$	$\mathcal{O}(q^3)$	$\mathcal{O}(q^4)$	exp.
p	0.717	0.717	0.717	0.717	0.717
n	−0.113	−0.113	−0.113	−0.113	−0.113
Λ	0.14	0.00	0.05	0.11±0.02	
Σ^-	0.59	0.72	0.63	0.60±0.02	—
Σ^0	−0.14	−0.08	−0.05	−0.03±0.01	—
Σ^-	0.87	0.88	0.72	0.67±0.03	0.61±0.12±0.09 [Se01]
					0.91±0.32±0.40 [Ad99]
Ξ^0	0.36	0.08	0.15	0.13±0.03	—
Ξ	0.67	0.75	0.56	0.49±0.05	—
$\Lambda\Sigma^0$	−0.10	−0.09	0.00	0.03±0.01	
d_{101}	−0.84	−0.34	−0.44	−0.15	
d_{102}	1.20	1.64	1.57	1.64	

Table 3.2: Predictions for the electric radii $\langle r_E^2 \rangle$ [fm^2]. The various best–fit values for the pertinent counterterms d_{101}, d_{102} are given as well (in units of GeV^{-2}). The experimental values for the proton and neutron are taken from the dispersion theoretical studies [MMD96, HMD96]. The errors for the relativistic fourth order predictions display the uncertainty due to $\Delta b_6^{D/F}$. The errors for the experimental Σ^- radius values refer to statistical (first) and systematic (second) errors.

can readily be fitted to the charge radii of proton and neutron, such that all others can be predicted. Table 3.2 shows these predictions for third and fourth order calculations, both in the heavy–baryon and the infrared regularisation formalism. The fourth column shows the predictions according to the fourth order relativistic calculation together with errors which reflect some theoretical uncertainty: even with the Foldy term fixed, some uncertainty inherited from the description of the magnetic moments remains. Indeed, though kinematically suppressed (i.e. of higher than fourth order in strict chiral power counting), the loop corrections to the anomalous magnetic couplings, see diagram (10) in Fig. 3.1, contribute to the Dirac radius. We employ the values for $b_6^{D/F}$ obtained from the best fit to the magnetic moments at fourth order, $b_6^D = 4.21$ and $b_6^F = 1.64$, see Table 3.1. In order to get an estimate of the uncertainty due to these LECs, we again assume an error of about half of the change when fitting them at third and fourth order, thus assigning $\Delta b_6^{D/F} = 0.5$. Table 3.2 shows that *this* uncertainty is (relatively) *small*, as would be expected. We would like to stress however that this error only indicates one particular effect. An estimate of the complete uncertainty due to higher order contributions is hardly feasible (or, due to the appearance of new unknown couplings, indeed impossible). Finally, the uncertainties due to the *experimental* errors on the magnetic moments entering the Foldy term are yet one order of magnitude smaller.

With regard to convergence only, i.e. exclusively to the numerical changes when going from third to fourth order, the infrared regularisation scheme yields overall considerable improvement over the heavy–baryon results, especially for Λ, Σ^-, and Ξ^0. This improvement can also be seen in the behaviour of the fitted values of d_{101} and d_{102}, also given in Table 3.2, which are more stable in the relativistic scheme. What is more important though is that both the absolute values and the trends within the two schemes are entirely different for some hyperons. E.g. for the Σ^- radius, the only hyperon radius on which experimental information exists, the heavy–baryon values are very stable at 0.87–0.88 fm^2, but deviate sizeably from the radius given by the SELEX collaboration [Se01], $\langle (r_E^{\Sigma^-})^2\rangle = 0.61 \pm 0.12(\text{stat.}) \pm 0.09(\text{syst.})$ fm^2 (the pioneering WA89 measurement [Ad99] is not precise enough to favor any of the theoretical predictions). In the relativistic scheme however, the third–order value is already within this error range, with the fourth–order one even closer to the central value. Similarly for the other charged hyperons Σ^+ and Ξ^-, the fourth–order corrections *increase* the third–order predictions in the heavy–baryon case, but *reduce* them in the relativistic scheme. We also note that only the relativistic predictions show the hierarchy in the size of the electric radii expected from naive quark model considerations, $\langle (r_E^p)^2\rangle > \langle (r_E^{\Sigma^\pm})^2\rangle > \langle (r_E^{\Xi^-})^2\rangle$. The sizeable difference between the Σ^+ and Σ^- radii at third order in the heavy–baryon scheme is largely reduced in the relativistic results, leaving only a 10% effect at fourth order. For the neutral hyperons, all predictions are consistent as far as the signs of the radii are concerned (with the exception of the radius of the Λ–Σ^0 transition form factor), yielding positive radii for the Λ and Ξ^0 hyperons, and a negative radius for the Σ^0. Quantitatively, the relativistic fourth–order calculation predicts radii of a size very similar to that of the neutron for Λ and Ξ^0, and a Σ^0 radius of about another factor of 3 smaller.

To conclude this section, we would like to comment on the issue of SU(3) breaking in the electric radii. In contrast to the calculation of the magnetic moments to fourth order, the electric radii to this order do not contain any operators which break SU(3) at tree level (compare the LECs α_{1-4}, β_1 in Eq. (3.8) in the magnetic sector), therefore all SU(3) breaking effects are created 'dynamically' via mass splittings in the loop diagrams. The leading (and dominating) effect is the pion–kaon mass difference. We remind the reader that SU(3) symmetry would give the hyperon radii in terms of the proton/neutron radii according to

$$
\begin{aligned}
\langle (r_E^{\Sigma^+})^2\rangle &= \langle (r_E^p)^2\rangle \;, \qquad \langle (r_E^{\Sigma^-})^2\rangle = \langle (r_E^{\Xi^-})^2\rangle = \langle (r_E^p)^2\rangle + \langle (r_E^n)^2\rangle \;, \\
2\,\langle (r_E^{\Lambda})^2\rangle &= -2\,\langle (r_E^{\Sigma^0})^2\rangle = \langle (r_E^{\Xi^0})^2\rangle = -\frac{2}{\sqrt{3}}\,\langle (r_E^{\Lambda\Sigma^0})^2\rangle = \langle (r_E^n)^2\rangle \;. \qquad (3.11)
\end{aligned}
$$

It is obvious that SU(3) breaking due to the large kaon mass changes this pattern considerably: exact SU(3) predicts $\langle (r_E^{\Sigma^-})^2 \rangle > \langle (r_E^{\Sigma^-})^2 \rangle$ which is reversed in all four ChPT results presented above. In addition, it changes the sign of all charge radii for neutral hyperons. The size of the additional SU(3) breaking due to the mass splitting in the baryon octet, see diagrams (5*)–(7*) in Fig. 3.1, can be seen by comparing the predictions at third and fourth order in the relativistic framework, the change being mainly due to these mass differences (in fact, in terms of strict chiral power counting, this is the *only* new effect at fourth order apart from $1/m$ corrections to third order loops). The net effect is a further moderate reduction of the charged hyperon radii. Among the neutral particles, only the Λ radius shows a sizeable correction. Going to fifth order, one would obtain a large amount of additional SU(3) breaking effects (e.g. in the meson–baryon coupling constants or 'explicit' breaking in the charge radii via contact terms) none of which is quantifiable to sufficient accuracy. We thus regard our (fourth order relativistic) predictions as the best one is ever likely to achieve in any ChPT approach.

3.4.3 Magnetic radii

As the electric radii, the magnetic radii at fourth order include two parameters (labeled $\eta_{1/2}$ in Eq. (3.8)) which can be fitted to the respective proton and neutron data (taken here from the dispersive analysis [MMD96, HMD96]) in order to yield predictions for the hyperons. However, in contrast to the electric case, here loops proportional to other rather poorly known LECs ($b_{9/10/11}$) contribute significantly. As there are no further measurements of magnetic radii which would allow to fit these, the most transparent thing to do is to indicate the uncertainty following from this poor knowledge. Table 3.3 shows these uncertainties, based on $\Delta b_{9/10/11} = 0.25\ \text{GeV}^{-1}$ (which are assumed to be uncorrelated errors). Again, this is only one particular effect and does not reflect all possible uncertainties due to higher–order contributions. In addition, errors on these couplings were also only roughly estimated, such that they could even be larger.

Nevertheless, we consider the errors in Table 3.3 indicative enough to state that the magnetic radii can be predicted only to much lower accuracy than the electric ones. Given the sizeable uncertainties, there is no significant discrepancy between the heavy baryon and the relativistic predictions (with the exception of the Σ^0). The general trend is an increase of most magnetic radii in the relativistic scheme compared to the heavy–baryon results, where the central values are surprisingly small for some hyperons (Λ, Σ^0). The values for the LECs $\eta_{1/2}$, however, are completely different. This indicates large SU(3) symmetric loop contributions that have to be canceled by these counterterms. This does not come as a surprise if one remembers what is known about loop contributions to the magnetic moments. Note that with regard to the values for the SU(3) breaking terms in the magnetic moments given in Section 3.4.1, *none* of the fourth–order couplings can be fixed in agreement with *both*

	$\mathcal{O}(q^4)$ HB	$\mathcal{O}(q^4)$ IR	exp.
p	0.699	0.699	0.699
n	0.790	0.790	0.790
Λ	0.30±0.11	0.48±0.09	—
Σ^-	0.74±0.06	0.80±0.05	
Σ^0	0.20±0.10	0.45±0.08	
Σ^-	1.33±0.16	1.20±0.13	—
Ξ^0	0.44±0.15	0.61±0.12	—
Ξ^-	0.44±0.20	0.50±0.16	
$\Lambda\Sigma^0$	0.60±0.10	0.72±0.10	
η_1	0.26±0.10	0.69±0.10	
η_2	−0.02±0.21	0.72±0.21	

Table 3.3: Predictions for the magnetic radii $\langle r_M^2 \rangle$ [fm^2]. The various best–fit values for the pertinent counterterms η_1, η_2 are given as well (in units of GeV^{-3}). The errors display the uncertainty due to $\Delta b_{9/10/11}$.

schemes. SU(3) breaking is large, as a completely SU(3) symmetric treatment of the magnetic form factors (moments *and* radii) would imply

$$\begin{aligned}
\langle (r_M^{\Sigma^+})^2 \rangle &= \langle (r_M^p)^2 \rangle \ , \\
\langle (r_M^{\Sigma^-})^2 \rangle &= \langle (r_M^{\Xi^-})^2 \rangle = \frac{\mu_p \langle (r_M^p)^2 \rangle + \mu_n \langle (r_M^n)^2 \rangle}{\mu_p + \mu_n} \ , \\
\langle (r_M^{\Lambda})^2 \rangle &= \langle (r_M^{\Sigma^0})^2 \rangle = \langle (r_M^{\Xi^0})^2 \rangle = \langle (r_M^{\Lambda\Sigma^0})^2 \rangle = \langle (r_M^n)^2 \rangle \ .
\end{aligned} \tag{3.12}$$

In contrast to these, the values in Table 3.3 show no clear pattern. The magnetic radius of the Σ^- is remarkable in being much larger than all other radii, electric or magnetic. Such an effect, albeit less dramatic, is also found in some lattice studies, see e.g. [LWD91]. (This study also predicts relatively small magnetic radii for Λ and Ξ^- as we do, though not for the Σ^0.) As in the case of the electric radii, improvement of these predictions in the framework of ChPT is hardly feasible as higher order corrections would include numerous unknown SU(3) breaking effects.

3.4.4 Q^2–dependence of the form factors

In the previous chapter it was shown that the complete relativistic chiral one–loop representation fails to describe the Q^2–dependence of the 'large' form factors (i.e. those not vanishing at $Q^2 = 0$) already at rather low Q^2. As a remedy, it was demonstrated that the inclusion of dynamical vector mesons, used in an antisymmetric tensor representation and coupled to nucleons/pions/photons in a chirally invariant fashion, yields a very good description of all electromagnetic nucleon form factors up to about 0.4 GeV^2. Certainly, in order to obtain reasonable predictions for the Q^2 dependence of the hyperon form factors, one has to proceed likewise here. The necessary formalism and the definitions of all pertinent couplings were presented in great detail in Section 2.4 of the previous chapter. Of course one has to assume SU(3) symmetric vector meson couplings to the baryons, which are then fully determined by the values for the vector meson nucleon couplings as given in [MMD96]. As these transform in the same way as the contact terms, replacing part of the latter by explicit vector meson contributions on tree level affects in no way the predictions for the hyperon radii. Note that SU(3) breaking in these couplings is certainly there, but beyond the order we are working at here. Furthermore, nothing is known empirically about such symmetry breaking effects.

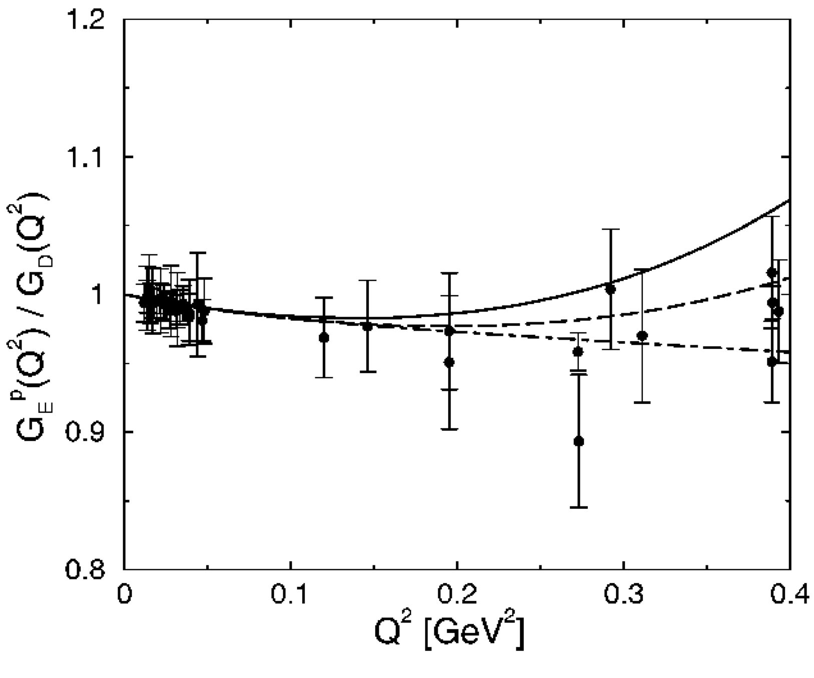

Figure 3.2: The proton electric form factor in SU(3) (solid line) and SU(2) (dashed line) relativistic baryon chiral perturbation theory including vector mesons, divided by the dipole form factor. For comparison, we show the dispersion theoretical result (dot dashed line) and the world data available in this energy range.

The fourth order results for the electric form factors of proton and neutron, including vector meson effects, are shown in Figs. 3.2 and 3.3, respectively, the former divided by the dipole form factor. For comparison we show the equivalent SU(2) results calculated in the previous chapter and the dispersion theoretical fits

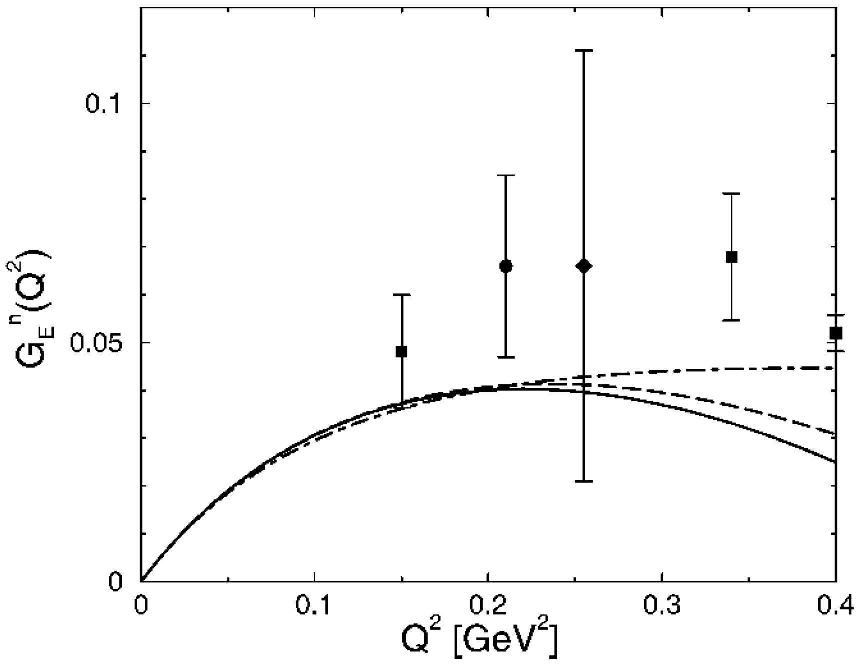

Figure 3.3: The neutron electric form factor in SU(3) (solid line) and SU(2) (dashed line) relativistic baryon chiral perturbation theory including vector mesons. Also given is the result of the dispersion theoretical analysis (dot dashed line). We only show the more recent data as given in [Ed94].

from [MMD96, HMD96]. In both cases the difference between the SU(2) and SU(3) descriptions is very small, though the SU(3) one is slightly worse. From such small differences one concludes that not much room is left for a strangeness contribution via kaon loops, as simple meson cloud models seem to indicate. Strangeness as hidden in the ϕ–meson component or from higher mass states encoded in the value of the LECs $d_{101/102}$ cannot be separated from the analysis presented here. To completely disentangle the strangeness contribution to a given form factor, a full flavour decomposition is necessary. For that, one also has to calculate the singlet form factors since the electromagnetic current is only sensitive to the octet components.

Fig. 3.4 shows the electric form factors of all charged hyperons (those of the negative ones with sign reversed). They all show a Q^2 dependence qualitatively similar to that of the proton charge form factor, the quantitative difference being due to their different sizes as determined by the radii. In all cases, the vector meson effects contribute a large part of the curvature which is far too small for the proton in a purely chiral representation. The neutral hyperon form factors are shown in Fig. 3.5 in comparison to the neutron electric form factor. Similar to what was found for the latter in the previous chapter, the vector meson effects largely cancel for all charge form factors of neutral hyperons. Apart from the neutron, only the Λ–Σ^0 transition form factor

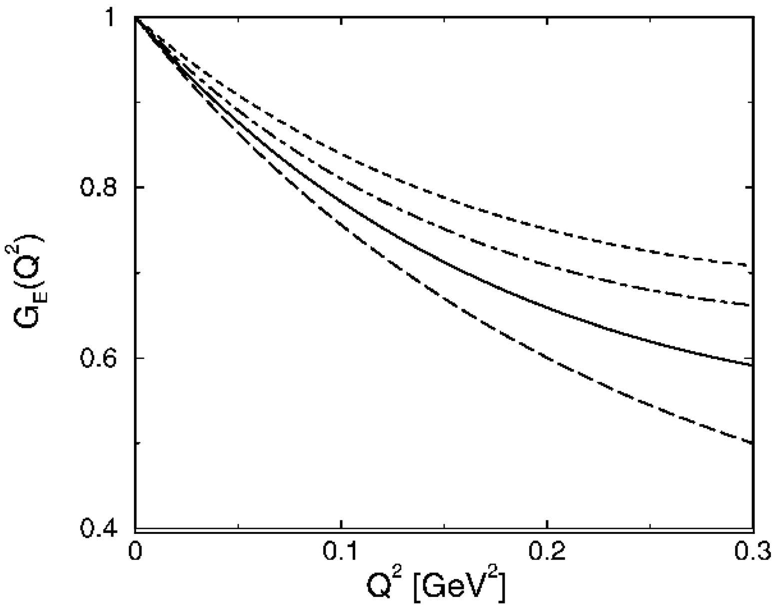

Figure 3.4: Predictions for the electric form factors of the charged hyperons Σ^- (dot–dashed line), Σ^- (solid line), and Ξ^- (dashed line). For the latter two, the absolute value of $G_E(Q^2)$ is shown. For comparison, we also show the proton electric form factor (long dashed line).

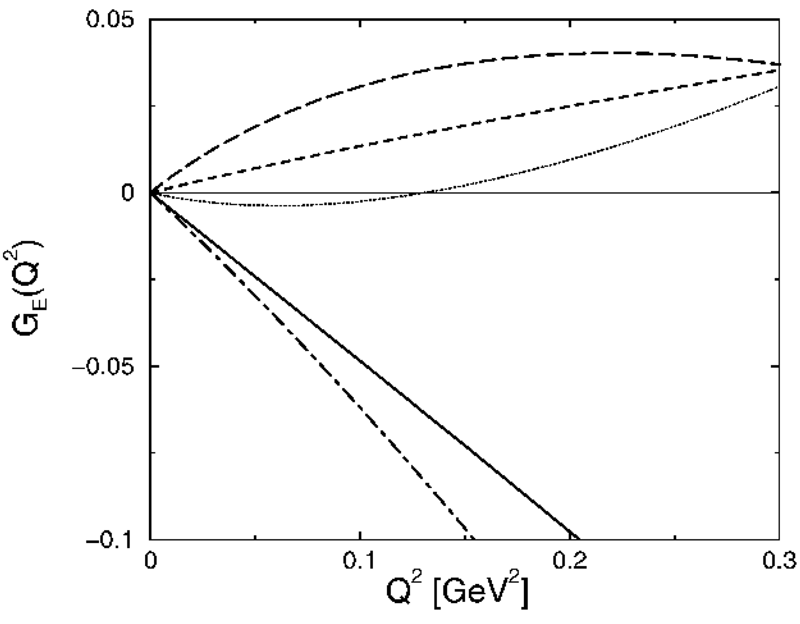

Figure 3.5: Predictions for the electric form factors of the neutral hyperons Λ (solid line), Σ^0 (dashed line), Ξ^0 (dot dashed line), as well as the Λ Σ^0 transition form factor (dotted line). For comparison, we also show the neutron electric form factor (long dashed line).

shows significant curvature, the ones for Λ, Σ^0, and Ξ^0 are dominated by the radius term and display a nearly linear behaviour.

For the magnetic form factors, a problem occurs when trying to transfer the procedure to include vector mesons exactly from the SU(2) to the SU(3) case. In the former, also loop corrections to the tree level diagrams including vector meson exchange were calculated, in strict analogy to loop corrections to the leading order magnetic couplings at fourth order, see diagrams (10)–(12) in Fig. 3.1. However, in contrast to the SU(2) case, these loop corrections are *large* in SU(3), such that there is no reason to identify the bare couplings with the ones determined in a dispersive analysis. What is more, in contrast to the electric form factors, such loops would lead to additional SU(3) breaking effects in the magnetic radii, yielding largely different values compared to a strictly chiral analysis. To avoid these problems, one should use vector mesons on tree level only in an SU(3) analysis, producing predictions for the magnetic form factors in agreement with the chiral predictions for the magnetic radii.

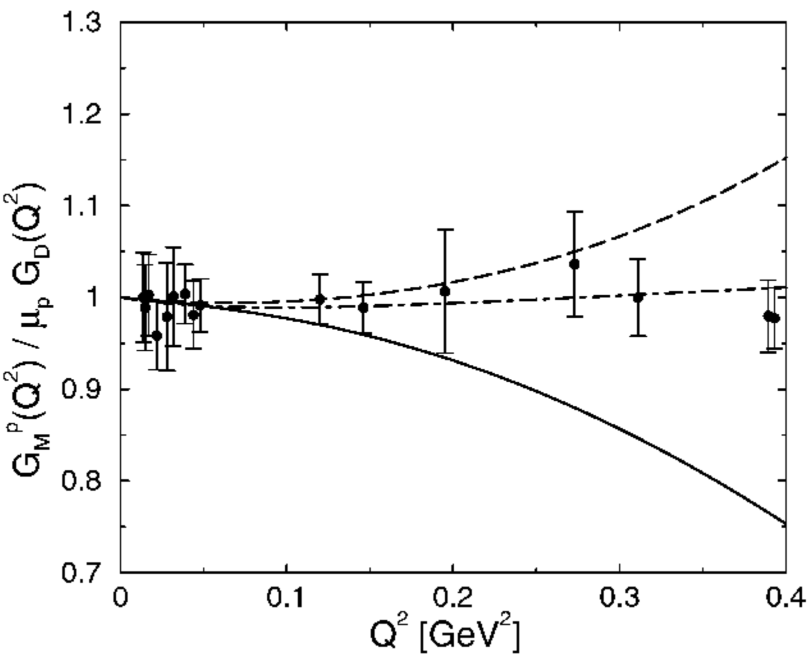

Figure 3.6: The proton magnetic form factor in SU(3) (solid line) and SU(2) (dashed line) relativistic baryon chiral perturbation theory including vector mesons, divided by the dipole form factor. For comparison, we show the dispersion theoretical result (dot–dashed line) and the world data available in this energy range.

We only show the magnetic form factors of proton and neutron divided by the dipole form factor, see Figs. 3.6, 3.7, again compared to the SU(2) analysis in the last chapter. The proton magnetic form factor proves to be worse above 0.2 GeV^2 in the SU(3)

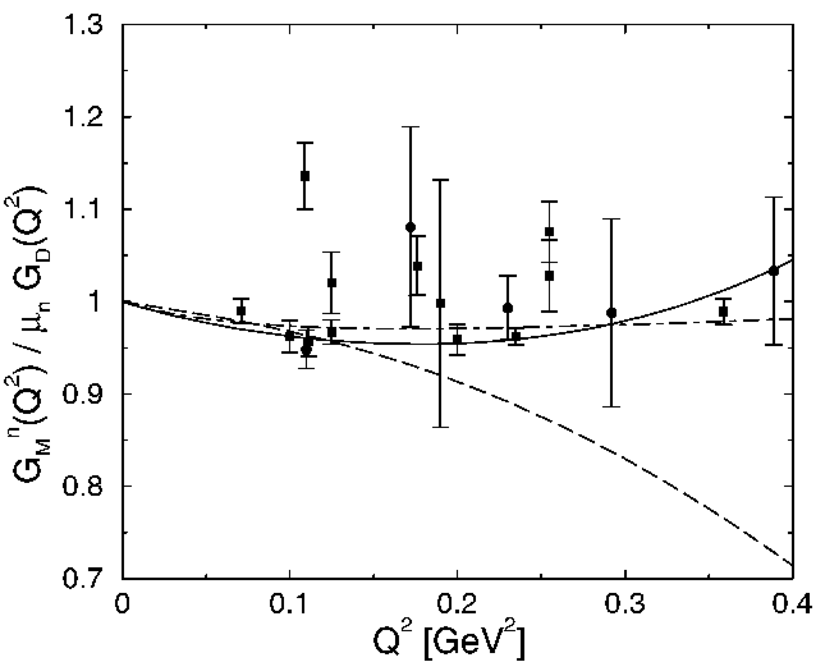

Figure 3.7: The neutron magnetic form factor in SU(3) (solid line) and SU(2) (dashed line) relativistic baryon chiral perturbation theory including vector mesons, divided by the dipole form factor. For comparison, we show the dispersion theoretical result (dot dashed line) and the world data available in this energy range, where the data points denoted by squares (instead of circles) refer to the more recent measurements [Ma93]. The older data can be traced back from [MMD96].

case, much closer to the third order curve given in the SU(2) analysis (which also does not include loop corrections to vector meson couplings). The curvature in the SU(3) calculation is slightly too small to meet the data above 0.2 GeV^2. For the neutron, however, there is hardly any difference between the two descriptions. The general observation for the hyperons (not displayed here) is that the neutral ones, like the neutron, tend to have stronger curvature, while the magnetic form factors of the charged hyperons are closer to a purely chiral description dominated by the radius term, and probably suffer from a similar deficit as the proton magnetic form factor.

3.5 Summary

We have studied the electromagnetic form factors of the baryon octet in a manifestly Lorentz invariant form of baryon chiral perturbation theory to one–loop (fourth) order employing the so–called infrared regularisation of loop graphs. The pertinent results of our investigation can be summarised as follows:

(1) We have argued that the chiral expansion of the magnetic moments in the relativistic scheme is ambiguous at third order, such that no clear statement can be made whether or not convergence is improved in comparison to the heavy baryon scheme. At fourth order, due to the presence of seven low energy constants, one can only predict the Λ Σ^0 transition moment, $\mu_{\Lambda\Sigma^0} = 1.61 \pm 0.01$ n.m., in stunning agreement with the empirical value.

(2) To fourth order, only two LECs affect the electric radii. These can be fixed from the measured neutron and proton radii. Always using the empirical magnetic moments in the Foldy term, we have shown that the fourth order corrections to the electric radii are astonishingly small, and so are the resulting uncertainties. The prediction for the Σ radius agrees with the recent result from the SELEX collaboration [Se01]. The pion–kaon mass difference leads to sizeable deviations from flavour SU(3) symmetry.

(3) The magnetic radii cannot be predicted so precisely. Again, one finds large SU(3) breaking due to loop corrections. In particular, the magnetic radius of the Σ^- is largest.

(4) For the electric form factors of the charged particles, the pure chiral representation provides too little curvature. With vector mesons included as in the corresponding SU(2) analysis of the last chapter, the Q^2–dependence of various charged form factors is given up to virtualities of $Q^2 = 0.3$ GeV^2, see Figs. 3.2, 3.4. For the neutral particles we find in general a large cancellation of these vector meson contributions, and the resulting form factors for the neutral hyperons display less curvature than the neutron one, see Figs. 3.3, 3.5. We do not observe any sizeable effects in the electric proton and neutron form factors when going from SU(2) to SU(3). Again, the corresponding magnetic form factors cannot be predicted so precisely.

Beyond what was achieved in this chapter, it will be of interest to also calculate the singlet form factors. This would allow one to perform a flavour decomposition of the various form factors and in particular to reanalyse the so called strange form factors of the nucleon, which are currently of great interest and have been studied in the heavy baryon limit only [RI97, HMS98, HKM99, Ha02]. This will be attempted in the following chapter.

Chapter 4

Strangeness form factors of the nucleon

4.1 Introduction

One important question yet unsolved about the structure of the nucleon concerns the contribution of strange quarks to various nucleon matrix elements. In simple quark models, the nucleons are exclusively made out of light (*up*– and *down*–) quarks, and many of the nucleon properties can be explained even when neglecting any dynamics of heavier constituents. For example, this is what was done in Chapter 2 where the electromagnetic structure of the nucleon was investigated based on chiral SU(2) dynamics. However, nothing forbids the dynamical creation of (virtual) $s\bar{s}$ pairs in the nucleon (the influence of even heavier quarks with masses exceeding that of the nucleon is probably strongly suppressed), and indeed this was effectively taken into account by generalising our considerations to chiral SU(3) dynamics in Chapter 3. Here, however, we want to investigate strange quark contributions to one specific matrix element even more closely and isolate their effects from possibly dominant light quark physics.

While strange quark contributions in the scalar ($\bar{s}s$, see all discussions about the πN σ term, e.g. [Sa01]) and axialvector ($\bar{s}\gamma_\mu\gamma_5 s$, see e.g. discussion on quark helicities and deep inelastic lepton scattering in [HB01]) sectors are non-negligible, strange contributions to vector current matrix elements ($s\gamma_\mu s$) seem to be particularly elusive. They are experimentally accessible via parity–violating electron scattering, and such investigations are under way at or have even been completed by the SAMPLE collaboration at MIT–Bates [Sa97], the HAPPEX [Ha99] and G0 [G0] experiments at Jefferson Lab (plus other approved experiments using protons and light nuclei as targets), and the MAMI A4 experiment in Mainz [A4].

Model predictions for these quantities vary all over the place (for reviews, see [Mu94, HB01]), such that model–independent predictions from chiral perturbation theory would be highly desirable. However, as pointed out in [RI97], both the strangeness magnetic moment $\mu_s = G_{M,s}(0)$ and the strange electric radius $\langle r^2_{E,s}\rangle = 6\,dG_{E,s}(t)/dt|_{t=0}$ contain new, unknown low energy constants at leading order. This is basically due to the (accidental) fact that the electromagnetic current for the three light quarks is traceless in flavour space and therefore not sensitive to the singlet component of the vector current, while the strange vector current, in terms of an SU(3) decomposition, receives contributions from the 8–component of the octet current and from the singlet (baryon number) current,

$$\bar{s}\gamma_\mu s \;=\; -\frac{1}{3}\left(\bar{u}\gamma_\mu u + \bar{d}\gamma_\mu d - 2\bar{s}\gamma_\mu s\right) + \frac{1}{3}\left(\bar{u}\gamma_\mu u + \bar{d}\gamma_\mu d + \bar{s}\gamma_\mu s\right) \quad . \tag{4.1}$$

In [HMS98], it was shown that this is in principle different for the third leading moment of the strange vector matrix elements, the strange magnetic radius $\langle r^2_{M,s}\rangle = 6\,dG_{M,s}(t)/dt|_{t=0}$ (note the unconventional definition: one does *not* divide by the [unknown] strange magnetic moment), which is at leading order a pure loop effect and can therefore be unambiguously calculated. Besides being an interesting quantity in its own right, the authors of [HMS98] emphasised that the knowledge of the t dependence of the magnetic form factor (and therefore the strange magnetic radius, as long as t is small enough that curvature terms can safely be neglected) is a prerequisite for the extraction of the strange magnetic moment, as $G_{M,s}(t)$ is experimentally accessible in parity–violating electron scattering only for finite t and has to be extrapolated to $t = 0$. Using the result from [HMS98], this was done in [HKM99] in order to obtain μ_s from the SAMPLE result for $G_{M,s}(-0.1\,\mathrm{GeV}^2)$, and the first HAPPEX results were used to (approximately) pin down the low–energy constant in the strange electric radius.

In the light of the results of the previous chapters, one might cast doubts at the numerical validity of the leading–loop result. We found that both $1/m$ corrections and counterterm contributions to the magnetic radii are large, and one should expect a similar behaviour also for the strange magnetic radius. Going to next to leading order, one clearly faces the same problem as for the strange magnetic moment and the strange electric radius, i.e. the result will be non predictive because an unknown new low energy constant associated with the singlet magnetic radius has to be included. Despite its limited experimental significance right now, the investigation of such higher order corrections is however of theoretical interest, if only for an estimate of the reliability of the leading result. Moreover, once many new low–energy data points are available, this improved representation will help to make a consistent and systematic analysis feasible. A study of this kind in the framework of heavy–baryon chiral perturbation theory has very recently been conducted [Ha02], we basically recover those results in the heavy–baryon limit of the infrared regularised loop results.

4.2 Lagrangians for the singlet vector current

In order to study the form factors of the strange vector current matrix element,

$$\langle N(p') \,|\, \bar{s}\gamma_\mu s \,|\, N(p)\rangle \;=\; \bar{u}(p') \left\{ \gamma_\mu F_{1,s}(t) + \frac{i\sigma_{\mu\nu}q^\nu}{2m_N} F_{2,s}(t) \right\} u(p) \quad , \tag{4.2}$$

the Lagrangians Eqs. (3.5)–(3.8) have to be modified and amended in the following sense: we now have to allow for vector fields with a non–vanishing trace, so all field strength tensors in the terms written down so far should be replaced by their traceless parts, $F_{\mu\nu} \to F_{\mu\nu} - \frac{1}{3}\langle F_{\mu\nu}\rangle$, and additional terms have to be introduced involving the trace of vector fields, both in the covariant derivative, $D_\mu B = \partial_\mu B + [\Gamma_\mu, B] - i\langle v_\mu\rangle B$, and

$$\begin{aligned}
\mathcal{L}^{(2)*}_{\phi B} &= \frac{b_6^0}{8m}\langle \bar{B}\sigma^{\mu\nu}B\rangle\langle F^-_{\mu\nu}\rangle \quad , & (4.3)\\
\mathcal{L}^{(3)*}_{\phi B} &= \frac{id^0_{102}}{2m}\Big\{ \langle \bar{B}[D^\nu, B]\rangle\langle [D^\mu, F^+_{\mu\nu}]\rangle + \text{h.c.} \Big\} \quad . & (4.4)\\
\mathcal{L}^{(4)*}_{\phi B} &= \frac{\gamma_{1/2}}{8}\langle \bar{B}\sigma^{\mu\nu}(\chi^+, B)_{=}\rangle\langle F^+_{\mu\nu}\rangle \;+\; \frac{\tilde{b}_6^0}{8}\langle\chi_+\rangle\langle \bar{B}\sigma^{\mu\nu}B\rangle\langle F^-_{\mu\nu}\rangle \\
&\quad -\frac{\eta_0}{2}\langle \bar{B}\sigma^{\mu\nu}B\rangle\langle [D_\lambda, [D^\lambda, F^-_{\mu\nu}]]\rangle \quad . & (4.5)
\end{aligned}$$

Note that $\tilde{b}_6^0$ again corresponds to a quark mass renormalisation of the leading term b_6^0 in complete analogy to Eq. (3.9),

$$\bar{b}_6^0 = b_6^0 + 2\bar{m}\,(2M_K^2 + M_\pi^2)\,\tilde{b}_6^0 \quad . \tag{4.6}$$

In contrast to $d_{101/102}$ and $\eta_{1/2}$, d^0_{102} and η_0 are actually finite and scale independent. Not so the higher order terms for the singlet magnetic moment, however. The β functions for these three counterterms ($\gamma_{1/2}$, $\tilde{b}_6^0$) cannot be disentangled by rendering only the strange magnetic form factor (or, equivalently, the singlet magnetic form factor) of the nucleon finite, such that we have considered the singlet magnetic form factors of all the ground state baryons. The results deduced therefrom are collected in App. A.5.

4.3 Results and discussion

For completeness and reasons of comparison, we here write down the leading terms in the heavy–baryon expansion of the leading strangeness moments. We expand the strange magnetic moment and the strange electric radius consistently up to fourth order,

$$\begin{aligned}
\mu_s &= \mu_s^{(2)} + \mu_s^{(3)} + \mu_s^{(4)} \quad , & (4.7)\\
\langle r^2_{1,s}\rangle &= \langle r^2_{1,s}\rangle^{(3)} + \langle r^2_{1,s}\rangle^{(4)} \quad , & (4.8)
\end{aligned}$$

where of course one has

$$\langle r_{E,s}^2 \rangle^{(i)} = \langle r_{1,s}^2 \rangle^{(i)} + \frac{3}{2m_N^2}\mu_s^{(i-1)} \tag{4.9}$$

(remember $\mu_s = \kappa_s$). Due to the special interest in the quality of the expansion of $\langle r_{M,s}^2 \rangle$, we even write down the partial fifth order result coming from $1/m$ corrections in the infrared regularised calculation,

$$\langle r_{M,s}^2 \rangle = \langle r_{M,s}^2 \rangle^{(3)} + \langle r_{M,s}^2 \rangle^{(4)} + \langle r_{M,s}^2 \rangle^{(5*)} \quad , \tag{4.10}$$

where the index '(5*)' is meant as a reminder that one would of course find additional contributions from two–loop diagrams at that order. The different parts are given as follows:

$$\begin{aligned}
\mu_s^{(2)} &= \frac{b_6^D}{3} - b_6^F + b_6^0 \quad , \qquad (4.11)\\
\mu_s^{(3)} &= \frac{(5D^2 - 6DF + 9F^2) m_N M_K}{24\pi F_K^2} \quad ; \qquad (4.12)\\
\mu_s^{(4)} &= 2m_N\Big(2M_K^2 + M_\pi^2\Big)\Big(\frac{\tilde{b}_6^D}{3} - \tilde{b}_6^F + \tilde{b}_6^0\Big)\\
&- 4m_N\left[(M_K^2 - M_\pi^2)\Big(\alpha_1 - \frac{\alpha_3}{3} - \frac{2\beta_1}{3} + \gamma_2\Big) + M_K^2\Big(\alpha_2 - \frac{\alpha_4}{3} - \gamma_1\Big)\right]\\
&+ \frac{1}{16\pi^2 F_K^2}\left[\frac{1}{3}(D+3F)^2\Big(M_K^2 - m_N \Delta m_\Lambda\Big)\right.\\
&\qquad \left. +3(D-F)^2\Big(M_K^2 - m_N\Delta m_\Sigma\Big)\right]\Big(1 + 2\log\frac{M_K}{\lambda}\Big)\\
&- \frac{1}{8\pi^2}\left[3(D+F)^2\frac{M_\pi^2}{F_\pi^2}\log\frac{M_\pi}{\lambda} + \frac{1}{3}(D-3F)^2\frac{M_\eta^2}{F_\eta^2}\log\frac{M_\eta}{\lambda}\right]\Big(\frac{b_6^D}{3} - b_6^F + b_6^0\Big)\\
&- \frac{M_K^2}{48\pi^2 F_K^2}\left\{\left[\frac{13}{3}D^2 - 10DF + 3F^2 + \Big(\frac{7}{3}D^2 + 2DF + 9F^2\Big)\log\frac{M_K}{\lambda}\right]b_6^D\right.\\
&\qquad \left. -\Big(5D^2 - 6DF + 9F^2\Big)\left[\Big(1 + 3\log\frac{M_K}{\lambda}\Big)b_6^F - 4\log\frac{M_K}{\lambda}b_6^0\right]\right\}\\
&- \frac{M_K^2}{16\pi^2 F_K^2}\Big[b_6^D - 3b_6^F + 4m_N(b_9 - 2b_{10} + 6b_{11})\Big]\log\frac{M_K}{\lambda} \quad . \qquad (4.13)
\end{aligned}$$

While the fourth–order contribution to the magnetic moment obviously contains a large number of terms, the next–to–leading order corrections to the electric radius are relatively simple and entirely given by $1/m$ corrections and effects due to the hyperon–nucleon mass difference:

$$\langle r_{1,s}^2 \rangle^{(3)} = 12\Big(d_{101} - \frac{d_{102}}{3} - d_{102}^0\Big) + \frac{5D^2 - 6DF + 9F^2}{96\pi^2 F_K^2}\Big(7 + 10\log\frac{M_K}{\lambda}\Big)$$

$$+\frac{3}{32\pi^2 F_K^2}\Big(1+2\log\frac{M_K}{\lambda}\Big) \ , \tag{4.14}$$

$$\begin{aligned}\langle r_{1,s}^2\rangle^{(4)} &= -\frac{5}{64\pi^2 F_K^2}\Big\{\frac{1}{3}(D+3F)^2\Big(\frac{7M_K}{2m_N}-\frac{\Delta m_\Lambda}{M_K}\Big) \\ &\qquad +3(D-F)^2\Big(\frac{7M_K}{2m_N}-\frac{\Delta m_\Sigma}{M_K}\Big)\Big\} \ , \end{aligned}\tag{4.15}$$

where we have used the abbreviations $\Delta m_{\Lambda/\Sigma} = m_{\Lambda/\Sigma} - m_N$. Finally, we show the formulae for the strange magnetic radius:

$$\langle r_{M,s}^2\rangle^{(3)} = -\frac{(5D^2-6DF+9F^2)m_N}{48\pi F_K^2 M_K} \ , \tag{4.16}$$

$$\begin{aligned}\langle r_{M,s}^2\rangle^{(4)} &= -24 m_N\Big(\eta_1-\frac{\eta_2}{3}-\eta_0\Big) - \frac{5D^2-6DF+9F^2}{96\pi^2 F_K^2}\Big(9+14\log\frac{M_K}{\lambda}\Big) \\ &\quad +\frac{m_N}{16\pi^2 F_K^2 M_K^2}\Big[\frac{1}{3}(D+3F)^2\Delta m_\Lambda + 3(D-F)^2\Delta m_\Sigma\Big] \\ &\quad +\frac{m_N}{8\pi^2 F_K^2}\Big(1+2\log\frac{M_K}{\lambda}\Big)\Big(b_9-2b_{10}+6b_{11}+\frac{3}{4m_N}\Big) \ , \end{aligned}\tag{4.17}$$

$$\begin{aligned}\langle r_{M,s}^2\rangle^{(5*)} &= \frac{1}{128\pi F_K^2}\Big\{\frac{35}{3}\left(5D^2-6DF+9F^2\right)\frac{M_K}{m_N} \\ &\qquad -\frac{14}{M_K}\Big[\frac{1}{3}(D+3F)^2\Delta m_\Lambda + 3(D-F)^2\Delta m_\Sigma\Big] \\ &\qquad -\frac{2m_N}{M_K^3}\Big[\frac{1}{3}(D+3F)^2\Delta m_\Lambda^2 + 3(D-F)^2\Delta m_\Sigma^2\Big]\Big\} \ . \end{aligned}\tag{4.18}$$

The results of Eqs. (4.13), (4.17) differ in some places from those published in [Ha02], where several polynomial type contributions with fixed coefficients ($1/m$ corrections in the strict sense of the word) have been lumped into counterterms (possibly not always consistently so), and mass splittings in the baryon octet have been neglected altogether. Furthermore, no effort was made to differentiate between the three counterterms yielding quark mass renormalisations of the singlet magnetic moment, $\gamma_{1/2}$ were omitted. For a numerical analysis, we concentrate on the magnetic radius, for the reasons explained above. The leading–loop (third–order) result that has been used to extract the magnetic moment from the magnetic form factor at finite t amounts to

$$\langle r_{M,s}^2\rangle^{(3)} = -0.115 \text{ fm}^2 \ . \tag{4.19}$$

The fourth–order corrections are, at a scale of the average baryon mass $\lambda = m$, possibly dominated by counterterm contributions, we find

$$\langle r_{M,s}^2\rangle^{(4)} = \Big[-0.010 + 0.878\Big(\eta_0-\eta_1+\frac{\eta_2}{3}\Big)/\text{GeV}^3\Big] \text{ fm}^2 \ . \tag{4.20}$$

The loop contribution (which is not unambiguous due to the scale dependence, of course) is composed of $+0.007$ fm^2 from loops with fixed coefficients and the standard axial couplings when neglecting the baryon mass splitting, the latter induces a shift of $+0.027$ fm^2, and the contributions proportional to the couplings $b_{9/10/11}$, with the estimates for these stemming from resonance saturation arguments, amount to -0.044 fm^2. See Table 3.3 for typical values of the couplings $\eta_{1/2}$: it is obvious that for e.g. $\eta_0 = 0$ (there is no good reason to assume this), the magnetic radius would be dominated by the counterterm contributions. What is, though, even more interesting is that the $1/m$–corrections yielding the partial fifth–order part, are found to be

$$\langle r^2_{M,s} \rangle^{(5*)} = 0.053 \text{ fm}^2 \quad . \tag{4.21}$$

These are scale–independent and therefore unambiguous, and constitute nothing more than kinematical corrections to the very same loop diagrams that produce the parameter–free leading–order result. These fifth–order $1/m$ corrections alone, which should be suppressed by two orders in the chiral counting, reduce the leading–order result by nearly 50%. "Neglecting" the baryon mass splitting, one would even find an overcompensation of $+0.137$ fm^2, which demonstrates again that this mass splitting is an important higher order effect. Adding all numbers for the infrared regularised result together, we arrive at

$$\langle r^2_{M,s} \rangle^{\text{IR}} = \left[-0.042 + 0.878 \left(\eta_0 - \eta_1 + \frac{\eta_2}{3} \right) /\text{GeV}^3 + 0.004\, b_6^0 \right] \text{ fm}^2 \quad , \tag{4.22}$$

again for a scale $\lambda = \bar{m}$, and we have used the central values for $b_6^{D/F}$ from Table 3.1.

In Fig. 4.1, we have plotted $G_{M,s}(Q^2)$, once fitting the strange magnetic moment to the SAMPLE data point, once setting it to zero, in both cases comparing the third–order heavy–baryon representation to the fourth–order relativistic one derived above, varying the unknown low–energy constant η_0 from -1 to $+1$. All other constants have been taken from the analysis of the baryon form factors, in particular $\eta_{1/2}$ from the relativistic fit in Table 3.3. The left panel in particular is close in spirit to an equivalent plot in [Ha02]. One notes that the uncertainty due to the singlet magnetic radius constant is larger here, which is due to a factor of 2 difference in the definition of this term (i.e. a variation $\eta_0 = \pm 1/2$ would look closer to their plot). From our analysis, the theoretical uncertainty in extrapolating the SAMPLE measurement from $Q^2 = 0.1$ GeV^2 to vanishing momentum transfer appears to be approximately as large as the experimental error, and no value for the strange magnetic moment between -1 and $+1$ can be excluded. The right panel shows that, assuming a vanishing strange magnetic moment, the whole strange magnetic form factor is consistent with zero (as is of course the SAMPLE data point), but that there is a wide range of potentially allowed values.

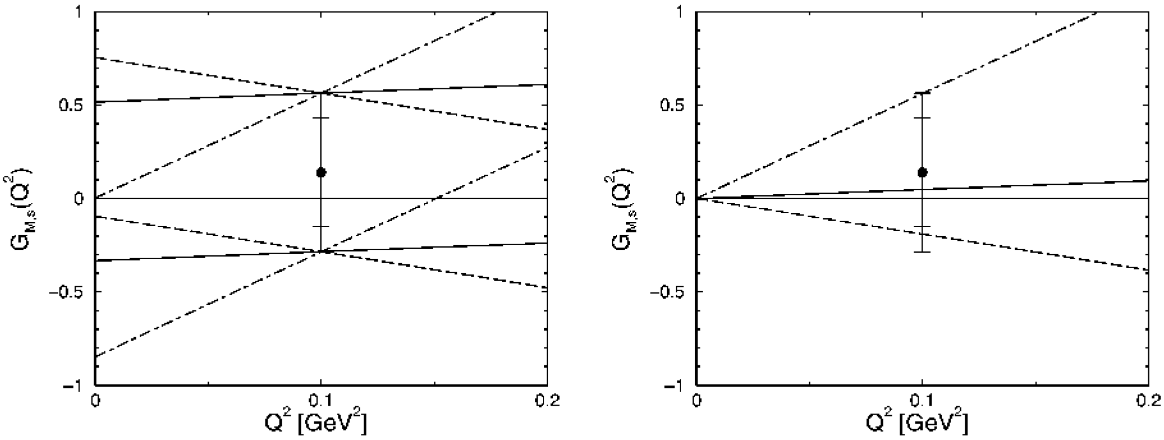

Figure 4.1: The strange magnetic form factor of the nucleon, theoretical predictions versus the SAMPLE data point [Sa97]. The smaller error bars refer to the statistical error only, for the larger error bars, statistical and systematical uncertainties have been added in quadrature. In the left panel, the strange magnetic moment has been fitted such as to reproduce the SAMPLE value, in the right panel, μ_s has been set to zero. The full lines correspond to the parameter–free representation obtained in [HMS98] in the heavy baryon formalism at third order, dashed/dot dashed lines to the fourth order result with infrared regularisation, setting $\eta_0 = -1/1$.

4.4 Conclusions

We have investigated the higher–order corrections to the third–order heavy–baryon results for the strangeness form factors of the nucleon by performing a complete relativistic one–loop calculation. The strange magnetic moment and electric radius contain unknown low–energy constants already at leading order such that higher–order corrections are not of very high phenomenological interest at the moment. In contrast, the leading result for the strange magnetic radius is a parameter free prediction, and we have investigated the stability of this prediction by taking the next corrections into account. The conclusion has to agree with the one by the authors of [Ha02]: the effective field theory result for the strange magnetic radius is only formally dominated by a loop contribution that can be unambiguously calculated, but $1/m$ corrections to this loop result are large, and significant cancellations take place. We find that the numerical value for $\langle r^2_{M,s} \rangle$ is really unknown from this theoretical analysis. Only with the arrival of several very precise low–energy measurements of the strange vector form factors can we hope to better disentangle the different mechanisms contributing to these matrix elements.

Part II

Pion–Kaon Scattering

Chapter 5

Isospin violation in pion–kaon scattering[#1]

5.1 Introduction

The quark masses allow to consider various approximations to Quantum Chromodynamics (QCD). For the c, b, and t quarks, the masses are so large that an expansion in inverse powers of these masses can be performed systematically. This leads to the so–called heavy–quark effective field theory. On the other hand, to a good first approximation, one can consider the light quarks u, d, and s as massless. In that limit, the QCD Lagrangian exhibits a chiral symmetry that is, however, spontaneously broken as witnessed by the appearance of eight almost massless pseudoscalar Goldstone bosons, the pions, the kaons, and the eta. These would–be Goldstone bosons acquire their masses from the explicit symmetry breaking due to the quark mass term. Spontaneous as well as explicit symmetry violation can be explored systematically by means of chiral perturbation theory. At low energies, the generating functional of QCD is characterised by two energy scales: one is the pion (kaon) decay constant in the chiral limit, denoted by F. Its non-vanishing value ($F \simeq 88$ MeV) is a necessary and sufficient condition for spontaneous symmetry breaking, much like the vacuum expectation value of the neutral Higgs boson signals the breaking of the electroweak symmetry. The second scale is given by the quark condensate, $B = |\langle 0|qq|0\rangle|/F^2$, and in the standard scenario of chiral symmetry breaking, $\langle 0|\bar{q}q|0\rangle \simeq (-225 \text{ MeV})^3$ so that $B \simeq 1.5$ GeV $\gg F$. This leads e.g. to a very precise prediction for the S–wave $\pi\pi$ scattering lengths [CGL00]. This scenario seems to be confirmed by recent Brookhaven data on $K_{\ell 4}$ decays [BNL01] and will be further scrutinised when the pionium lifetime measurements performed at CERN [Ad94] have been analysed.

For the three flavour sector, the situation is, however, less clear. Indeed, the observation that $m_s \simeq \Lambda_{\text{QCD}}$ has even led to investigations considering the strange quark as

#1 The contents of this chapter have been published in [KM02a, KM02b].

heavy [CK85, Ro99, Ou01]. One of the cleanest processes to test our understanding of the symmetry breaking pattern in the presence of strange quarks is elastic pion–kaon (πK) scattering near threshold. This reaction is interesting for a variety of reasons. It is similar to $\pi\pi$ scattering in the two flavour sector but also different in that the quark mass difference $m_u - m_d$ can appear at leading order in the πK scattering amplitude. Furthermore it has been pointed out recently that the structure of the QCD vacuum might change dramatically with increasing number of flavours, such that the scenario for chiral symmetry breaking might be different for chiral SU(3) as compared to SU(2) [DGS00]: the quark condensate, which has been shown to be large for two flavours [CGL00], might be sizeably suppressed in the three–flavour case. πK scattering might be used to test different scenarios for the SU(3) condensate in much a similar way as $\pi\pi$ scattering has been used in [CGL00] to show that the large condensate hypothesis indeed holds for two flavours. As was pointed out in [Kn93], one particular combination of the πK S–wave scattering lengths (the isoscalar one) is rather sensitive to deviations from the standard scenario.

There exist abundant data from inelastic processes that allow one to extract low–energy characteristics of the πK scattering amplitude by means of dispersion theory. The existing determinations of the S–wave scattering lengths are, however, plagued by large uncertainties, see e.g. [BKM91a] (for recent work on combining dispersion relations and chiral perturbation theory, see [AB01]), such that hope lies in the extraction of these parameters from πK bound states in the DIRAC experiment at CERN [Ad00]. Measurements of both the partial width for the decay into the neutral channel, $\Gamma_{\pi^0 K^0} \propto |T^{\rm thr}_{\pi^- K^- \to \pi^0 K^0}|^2$, and the strong $2S - 2P$ energy level shift, $\Delta E^{\rm str}_{2S-2P} \propto T^{\rm thr}_{\pi^- K^+ \to \pi^- K^+}$, allow to determine two independent combinations of the scattering lengths. The intended measurement of the lifetime of πK atoms at CERN [Ad00] gives direct access to the isovector S–wave scattering length, while in order to also pin down the isoscalar S–wave scattering length, one would have to measure the $2P - 2S$ level shift, similar to what has been done for the pion–nucleon system at PSI [Sc99]. The precise relation between the πK atom lifetime and the scattering length can be worked out by means of an effective field theory for hadronic bound states (for the pionium case see e.g. [Ga99, JS98]).

To achieve the necessary accuracy in the πK system, it is mandatory to sharpen the existing one–loop predictions for the scattering lengths [BKM91a, BKM91b] by including isospin violation due to strong and electromagnetic effects. Isospin is the quantum number for the unbroken vectorial SU(2) subgroup of the full $SU(3)_L \times SU(3)_R$ chiral symmetry group, transforming the lightest two flavours u and d into each other. Historically know to be a very good approximate symmetry in nuclear physics, isospin symmetry is broken both by the QCD mass term,

$$\mathcal{H}_{\rm QCD} = m_u \bar{u}u + m_d \bar{d}d = \frac{1}{2}(m_u + m_d)\left(\bar{u}u + \bar{d}d\right) + \frac{1}{2}(m_u - m_d)\left(\bar{u}u - \bar{d}d\right) \quad , \tag{5.1}$$

which clearly contains an isovector piece proportional to the light quark mass difference $m_u - m_d$, and by electromagnetism, since the light quark vector current also has an isovector component,

$$\mathcal{J}_\mu = \frac{2}{3}\bar{u}\gamma_\mu u - \frac{1}{3}\bar{d}\gamma_\mu d = \frac{1}{6}\left(\bar{u}\gamma_\mu u + \bar{d}\gamma_\mu d\right) + \frac{1}{2}\left(\bar{u}\gamma_\mu u - \bar{d}\gamma_\mu d\right) \quad . \tag{5.2}$$

Both sources of isospin violation have to be treated consistently and simultaneously.

In order to relate lifetime and strong energy level shift of $\pi^- K^+$ (or $\pi^+ K^-$) atoms to particular combinations of the pion–kaon scattering lengths, one has to make use of modified Deser formulae [De54] that include next–to–leading order effects in isospin breaking,

$$\Gamma_{\pi^0 K^0} \quad \propto \quad \left(a_0^{3/2} - a_0^{1/2} + \epsilon\right)^2 (1+\kappa) \quad , \tag{5.3}$$

$$\Delta E^{\rm str}_{2S-2P} \quad \propto \quad \left(a_0^{3/2} + 2a_0^{1/2} + \epsilon'\right)(1+\kappa') \quad , \tag{5.4}$$

(see [Ga99, LR00] for equivalent formulae for the cases of pionium and pionic hydrogen). Here, $\epsilon(\epsilon')$ represents the isospin violating correction in the regular part of the scattering amplitudes $\pi^- K^+ \to \pi^0 K^0 (\pi^- K^+)$ at threshold, while $\kappa(\kappa')$ is an additional contribution only calculable within the bound state formalism.

This chapter is organised as follows: after a brief presentation of the Lagrangians needed for this calculation in Section 5.2, we introduce and define the necessary formalism for pion–kaon scattering in the isospin limit in Section 5.3 and give a recapitulation of what is known about isovector and isoscalar pion–kaon scattering lengths from analyses in Chiral Perturbation Theory. We afterwards study isospin violation for the S–wave scattering lengths at tree level for all physical channels in Section 5.4. This allows for a first estimate of such effects and is also interesting to compare directly to the $\pi\pi$ case. The correction ϵ to the scattering length relevant for the lifetime measurement will be evaluated up to on–loop order in Section 5.5.1, supplemented by a complete treatment of soft photon radiation for the annihilation channel $\pi^- K^- \to \pi^0 K^0 \gamma$ in Section 5.5.2. In Section 5.6 we complete this analysis by also computing the isospin violating shift ϵ' in the elastic charged channel to one–loop accuracy. Some remarks on isospin breaking in higher threshold parameters are added in Section 5.7, we summarise our findings in Section 5.8.

5.2 Lagrangians

In this section we discuss the strong and electromagnetic effective Lagrangians underlying our calculations. All the pieces have been discussed extensively elsewhere in the literature, so we will just present the terms needed for the following. The effective Lagrangian can be expanded at low energies according to

$$\mathcal{L}_{\rm eff} = \mathcal{L}^{(2)}_{\rm str} + \mathcal{L}^{(2)}_{\rm em} + \mathcal{L}^{(4)}_{\rm str} + \mathcal{L}^{(4)}_{\rm em} + \ldots \quad , \tag{5.5}$$

where the superscripts (2), (4) refer to the chiral dimension and "str" and "em" denote the strong and electromagnetic terms, respectively. Chiral power counting for the strong sector attributes the chiral dimension q to all pseudo Goldstone boson masses (M_π, M_K, M_η) as well as all momenta involved. This scheme is generalised to include electromagnetic terms by counting the electric charge e also as a quantity of order q, which is dictated by the requirement that a unique dimension be assigned to the covariant derivative (that includes the lowest–order photon coupling). Therefore any term of the form $e^{2j}q^{2k}M_\pi^l M_K^m M_\eta^n$ with, e.g., $2j+2k+l+m+n=4$ is counted as fourth order.

The lowest–order Lagrangian is given by

$$\begin{aligned}\mathcal{L}^{(2)} &= -\frac{1}{4}F_{\mu\nu}F^{\mu\nu} - \frac{\lambda}{2}(\partial_\mu A^\mu)^2 \\ &+ \frac{F^2}{4}\langle \nabla_\mu U^\dagger \nabla^\mu U + \chi U^\dagger + \chi^\dagger U\rangle + C\langle QUQU^\dagger\rangle \ , \end{aligned} \tag{5.6}$$

where all the necessary notation was already introduced successively in Chapter 1. We only point out that for all calculations, the gauge fixing parameter λ was set to 1 (Feynman gauge). The Lagrangian $\mathcal{L}^{(2)}$ leads to the well–known lowest–order mass formulae for pions and kaons including leading electromagnetic effects,

$$\begin{aligned} M_{\pi^\pm}^2 &= B(m_u+m_d) + 2Ze^2F^2 \ , \qquad M_{\pi^0}^2 = B(m_u+m_d) + \mathcal{O}\left((m_u-m_d)^2\right) \ , \\ M_{K^\pm}^2 &= B(m_u+m_s) + 2Ze^2F^2 \ , \qquad M_{K^0}^2 = B(m_d+m_s) \ , \end{aligned} \tag{5.7}$$

as well as to the Gell-Mann–Okubo relation valid at this accuracy,

$$3M_\eta^2 = 2M_{K^\pm}^2 + 2M_{K^0}^2 - 2M_{\pi^\pm}^2 + M_{\pi^0}^2 + \mathcal{O}\left((m_u-m_d)^2\right) \ . \tag{5.8}$$

The LEC C accompanying the last term in the Lagrangian Eq. (5.6) can therefore be calculated from the leading order electromagnetic pion mass difference, $M_{\pi^\pm}^2 - M_{\pi^0}^2 = 2Ze^2F^2$ (neglecting a tiny strong mass difference $\sim (m_u-m_d)^2$), where we have defined the convenient dimensionless constant $Z = C/F^4$. Using $F = F_\pi = 92.4$ MeV, one obtains $Z \approx 0.8$.

The fourth order Lagrangian [GL85a] contains the following "strong" terms which are needed for the amplitude describing pion–kaon scattering at one–loop level:

$$\begin{aligned}\mathcal{L}_{\rm str}^{(4)} &= L_1\langle\nabla_\mu U^\dagger\nabla^\mu U\rangle^2 + L_2\langle\nabla_\mu U^\dagger\nabla_\nu U\rangle\langle\nabla^\mu U^\dagger\nabla^\nu U\rangle \\ &+ L_3\langle\nabla_\mu U^\dagger\nabla^\mu U\nabla_\nu U^\dagger\nabla^\nu U\rangle + L_4\langle\nabla_\mu U^\dagger\nabla^\mu U\rangle\langle\chi^\dagger U+\chi U^\dagger\rangle \\ &+ L_5\langle\nabla_\mu U^\dagger\nabla^\mu U\left(\chi^\dagger U+U^\dagger\chi\right)\rangle + L_6\langle\chi^\dagger U+\chi U^\dagger\rangle^2 \\ &+ L_7\langle\chi^\dagger U-\chi U^\dagger\rangle^2 + L_8\langle\chi^\dagger U\chi^\dagger U+\chi U^\dagger\chi U^\dagger\rangle \ . \end{aligned} \tag{5.9}$$

With regard to the analytic formulae given for the S–wave scattering length in App. B.3, we remark that only two of the LECs defined in Eq. (5.9) play a role for the charge exchange scattering length at leading order in isospin violation (when expressed in terms of physical masses and decay constants), though all but L_7 contribute to the isoscalar scattering length.

In addition, the following electromagnetic counterterms given in [Ur95] are needed:

$$
\begin{aligned}
\mathcal{L}_{\rm em}^{(4)} &= K_1\, F^2\langle\nabla_\mu U^\dagger\nabla^\mu U\rangle\langle Q^2\rangle + K_2\, F^2\langle\nabla_\mu U^\dagger\nabla^\mu U\rangle\langle QUQU^\dagger\rangle \\
&+ K_3\, F^2\Big(\langle\nabla_\mu U^\dagger QU\rangle\langle\nabla^\mu U^\dagger QU\rangle + \langle\nabla_\mu U QU^\dagger\rangle\langle\nabla^\mu U QU^\dagger\rangle\Big) \\
&+ K_4\, F^2\langle\nabla_\mu U^\dagger QU\rangle\langle\nabla^\mu U QU^\dagger\rangle + K_5\, F^2\langle\Big(\nabla_\mu U^\dagger\nabla^\mu U + \nabla_\mu U\nabla^\mu U^\dagger\Big)Q^2\rangle \\
&+ K_6\, F^2\langle\nabla_\mu U^\dagger\nabla^\mu U QU^\dagger QU + \nabla_\mu U\nabla^\mu U^\dagger QUQU^\dagger\rangle + K_7\, F^2\langle\chi^\dagger U + \chi U^\dagger\rangle\langle Q^2\rangle \\
&+ K_8\, F^2\langle\chi^\dagger U + \chi U^\dagger\rangle\langle QUQU^\dagger\rangle + K_9\, F^2\langle\Big(\chi^\dagger U + U^\dagger\chi + \chi U^\dagger + U\chi^\dagger\Big)Q^2\rangle \\
&+ K_{10}\, F^2\langle\Big(\chi^\dagger U + U^\dagger\chi\Big)QU^\dagger QU + \Big(\chi U^\dagger + U\chi^\dagger\Big)QUQU^\dagger\rangle \\
&+ K_{11}\, F^2\langle\Big(\chi^\dagger U - U^\dagger\chi\Big)QU^\dagger QU + \Big(\chi U^\dagger - U\chi^\dagger\Big)QUQU^\dagger\rangle \ . \qquad (5.10)
\end{aligned}
$$

Also the dependence on a few of these ($K_{7/8/9}$) cancels in the S–wave scattering length (when expressed in terms of physical observables). One more term (proportional to K_{12} in [Ur95]) that is needed in principle for the renormalisation of the decay constants of charged mesons can be omitted in case one uses physical values for decay constants with electromagnetic effects already subtracted (see section 5.5.1). We have omitted terms of order e^4 that do not contribute at leading order in isospin violation.

For numerical evaluation, we use the central values and error estimates for the hadronic low–energy constants as given in [BEG95]. For the electromagnetic ones, we use the estimates obtained via resonance saturation in [BU97], and add error bars of natural size ($\pm 1/16\pi^2$) uniformly.

5.3 Pion–kaon scattering in the isospin limit

Pion kaon scattering in the isospin limit can be described by two independent amplitudes $T^{1/2}$ and $T^{3/2}$, corresponding to isospin 1/2 and 3/2, respectively. It is sometimes convenient to combine these into isospin even and odd amplitudes $T^\pm$ which are defined by

$$T_{\alpha\beta} = \delta_{\alpha\beta}T^+ + \frac{1}{2}[\tau_\alpha,\tau_\beta]T^- \qquad (5.11)$$

(α, β refer to the isospin indices of the pions) and which can be related to the amplitudes of definite isospin via

$$
\begin{aligned}
3T^- &= T^{1/2} + 2T^{3/2} \ , \qquad (5.12)\\
3T &= T^{1/2} - T^{3/2} \ . \qquad (5.13)
\end{aligned}
$$

All these amplitudes can be expressed in terms of the usual Mandelstam variables s, t, u. They can be decomposed into partial waves $t_l^I(s)$ using

$$T^I(s,t) = 16\pi \sum_l (2l+1) t_l^I(s) P_l(z) \quad , \tag{5.14}$$

where $z = \cos\theta$ denotes the scattering angle in the center–of–mass system, and $P_l(z)$ are the Legendre polynomials. Close to threshold, one can parameterise the real parts of the partial wave amplitudes in terms of scattering lengths (a_l) and effective ranges (b_l),

$$\mathrm{Re}\, t_l^I(s) = \frac{\sqrt{s}}{2} \left(|\mathbf{q}_{\rm in}||\mathbf{q}_{\rm out}|\right)^l \left\{ a_l^I + b_l^I |\mathbf{q}_{\rm in}|^2 + \mathcal{O}\left(|\mathbf{q}_{\rm in}|^4\right)\right\} \quad , \tag{5.15}$$

where we have already accounted for the possibility of different masses of the incoming and outgoing particles and therefore for different incoming and outgoing center–of–mass momenta,

$$|\mathbf{q}_{\rm in}| = \frac{\sqrt{(s-(M_K^{\rm in}-M_\pi^{\rm in})^2)(s-(M_K^{\rm in}+M_\pi^{\rm in})^2)}}{2\sqrt{s}} \quad , \tag{5.16}$$

$$|\mathbf{q}_{\rm out}| = \frac{\sqrt{(s-(M_K^{\rm out}-M_\pi^{\rm out})^2)(s-(M_K^{\rm out}+M_\pi^{\rm out})^2)}}{2\sqrt{s}} \quad , \tag{5.17}$$

where $M_{\pi/K}^{\rm in/out}$ refer to the physical masses of the incoming and outgoing pions and kaons, respectively. In the isospin limit, Eq. (5.15) collapses to the usual definition. We note that the real part of a total amplitude at threshold (i.e. for $|\mathbf{q}_{\rm in}| = 0$) is linked to the S–wave scattering length by

$$\mathrm{Re}\, T_{\rm thr}^I = 8\pi \left(M_K^{\rm in} + M_\pi^{\rm in}\right) a_0^I + \mathcal{O}\left(|\mathbf{q}_{\rm in}|^2, |\mathbf{q}_{\rm in}||\mathbf{q}_{\rm out}|\right) \quad . \tag{5.18}$$

At tree level, the isospin–even and –odd pion–kaon scattering lengths are given by [We66, Gr68]

$$a_0^+ = 0 \quad , \quad a_0^- = \frac{M_\pi M_K}{8\pi F_\pi^2 (M_\pi + M_K)} = 70.8 \times 10^{-3}/M_\pi \quad . \tag{5.19}$$

The pion–kaon scattering lengths in the isospin limit have been evaluated up to one loop order in [BKM91a], and analytic expressions for the complete scattering amplitudes can be found in [BKM91b]. However no analytic formulae for the scattering lengths were written down until recently [Ne02, KM02b]. We therefore quote these for a_0^- here:

$$\begin{aligned} a_0^- =& \frac{M_K M_\pi}{8\pi F_\pi^2 (M_K + M_\pi)} \Bigg\{ 1 + \frac{M_\pi^2}{F_\pi^2} \Bigg[8 L_5^r \\ & - \frac{1}{16\pi^2} \Bigg\{ \frac{8M_K^2 - 5M_\pi^2}{2(M_K^2 - M_\pi^2)} \log\frac{M_\pi}{\lambda} - \frac{23 M_K^2}{9(M_K^2 - M_\pi^2)} \log\frac{M_K}{\lambda} + \frac{28 M_K^2 - 9M_\pi^2}{18(M_K^2 - M_\pi^2)} \log\frac{M_\eta}{\lambda} \end{aligned} \tag{5.20}$$

$$
\begin{aligned}
&+\frac{4M_K}{9M_\pi}\frac{\sqrt{(M_K-M_\pi)(2M_K+M_\pi)}}{M_K+M_\pi}\arctan\left(\frac{2(M_K+M_\pi)}{M_K-2M_\pi}\sqrt{\frac{M_K-M_\pi}{2M_K+M_\pi}}\right)\\
&-\frac{4M_K}{9M_\pi}\frac{\sqrt{(M_K+M_\pi)(2M_K-M_\pi)}}{M_K-M_\pi}\arctan\left(\frac{2(M_K-M_\pi)}{M_K+2M_\pi}\sqrt{\frac{M_K+M_\pi}{2M_K-M_\pi}}\right)\Bigg\}\Bigg]\Bigg\}\,,
\end{aligned}
$$

$$
\begin{aligned}
a_0^- &= \frac{M_K^2M_\pi^2}{8\pi F_\pi^4(M_K+M_\pi)}\Bigg[16\Big(2L_1^r+2L_2^r+L_3-2L_4^r-\frac{L_5^r}{2}+2L_6^r+L_8^r\Big) \qquad (5.21)\\
&+\frac{1}{16\pi^2}\Bigg\{\frac{11M_\pi^2}{2(M_K^2-M_\pi^2)}\log\frac{M_\pi}{\lambda}-\frac{67M_K^2-8M_\pi^2}{9(M_K^2-M_\pi^2)}\log\frac{M_K}{\lambda}+\frac{24M_K^2-5M_\pi^2}{18(M_K^2-M_\pi^2)}\log\frac{M_\eta}{\lambda}\\
&-\frac{4}{9}\frac{\sqrt{(M_K-M_\pi)(2M_K+M_\pi)}}{M_K+M_\pi}\arctan\left(\frac{2(M_K+M_\pi)}{M_K-2M_\pi}\sqrt{\frac{M_K-M_\pi}{2M_K+M_\pi}}\right)\\
&-\frac{4}{9}\frac{\sqrt{(M_K+M_\pi)(2M_K-M_\pi)}}{M_K-M_\pi}\arctan\left(\frac{2(M_K-M_\pi)}{M_K+2M_\pi}\sqrt{\frac{M_K+M_\pi}{2M_K-M_\pi}}\right)+\frac{43}{9}\Bigg\}\Bigg]\,.
\end{aligned}
$$

Here we have used the usual notation L_i^r for the low energy constant L_i with its infinite part removed. (Note that we do note display the scale dependence of the LECs explicitly.) The chiral analysis of these two quantities displays a remarkably different behavior (which only becomes transparent when one discusses $a_0^\pm$ instead of $a_0^{1/2}$, $a_0^{3/2}$): As was pointed out e.g. in [AB01], a_0^- at order $\mathcal{O}(p^4)$ depends only on one single low–energy constant, L_5^r, which is in turn determined by the ratio F_K/F_π, such that a_0^- can be predicted to a very good accuracy, $a_0^- = (0.0793\pm0.0006)M_\pi^{-1}$. On the contrary, no less than seven low–energy constants enter the isoscalar scattering length a_0^+, some of them known to rather poor accuracy, such that the chiral prediction for this quantity at one–loop order is plagued by a very large uncertainty, $a_0^- = (0.025\pm0.017)M_\pi^{-1}$. Furthermore, the tree–level result for a_0^- receives only a 12% correction from one–loop contributions and counterterms (*if*, as done here, one normalises the tree level result to $1/F_\pi^2$; see also the discussion in Sect. 5.5.1), while a_0^+ vanishes at tree level, and the contributions at order $\mathcal{O}(p^4)$ are rather large. In fact, if we regard the kaon as heavy and expand the expressions in Eqs. (5.20), (5.21) in powers of M_π/M_K, a_0^- receives contributions of odd powers of the pion mass only, while a_0^+ scales with even powers of M_π, such that one has symbolically:

$$
\begin{aligned}
a_0^- &= \frac{M_KM_\pi}{8\pi F_\pi^2(M_K+M_\pi)}\left\{1+\frac{M_\pi^2}{\Lambda_\chi^2}\left(c_0^-+c_2^-\frac{M_\pi^2}{M_K^2}+c_4^-\frac{M_\pi^4}{M_K^4}+\ldots\right)+\mathcal{O}(\Lambda_\chi^{-4})\right\}\,, \quad (5.22)\\
a_0^+ &= \frac{M_KM_\pi}{8\pi F_\pi^2(M_K+M_\pi)}\left\{\frac{M_\pi M_K}{\Lambda_\chi^2}\left(c_0^-+c_2^+\frac{M_\pi^2}{M_K^2}+c_4^+\frac{M_\pi^4}{M_K^4}+\ldots\right)+\mathcal{O}(\Lambda_\chi^{-4})\right\}\,, \quad (5.23)
\end{aligned}
$$

where $\Lambda_\chi = 4\pi F_\pi$ is the chiral symmetry breaking scale. This makes it obvious that the one–loop contributions to a_0^- are suppressed by one power of M_π/M_K with respect to those to a_0^+. This behaviour is completely analogous to what one finds for pion–nucleon scattering lengths (see e.g. [BKM95b]). We note that the scattering length of the charge exchange process, entering the πK atom lifetime formula Eq. (5.3), is given by $a_0(\pi^- K^- \to \pi^0 K^0) = -\sqrt{2}a_0$, while the sum of isoscalar and isovector scattering length enter the strong energy level shift Eq. (5.4), $a_0(\pi^- K^+ \to \pi^- K^+) = a_0^- + a_0^+$. We therefore expect a rather different accuracy in the predictions for these two quantities already from the purely strong contributions.

5.4 Isospin violation at tree level

The different physical pion–kaon channels receive corrections to their isospin symmetric scattering lengths when taking into account the mass differences as well as insertions stemming from the electromagnetic term in Eq. (5.6). We collect the isospin breaking parameters as $\delta \in \{m_u - m_d, e^2\}$ and expand the corrections to the scattering lengths up to order δ for all physical channels, based on the tree level amplitudes. The following conventions were used:

- The isospin symmetry limit is defined according to e.g. [Ga99], i.e. we express everything in terms of the *charged* meson masses $M_{\pi^\pm}$, $M_{K^\pm}$. Note that these are not exactly the natural choices from the point of view of a chiral analysis of the meson masses, in which case one would prefer to take the neutral pion mass as a reference (which is indeed done in [MMS97]), as one has $M_{\pi^0}^2 = 2B\hat{m}$ (with $\hat{m} = \frac{1}{2}(m_u + m_d)$) to good accuracy, neglecting only tiny corrections of order $(m_u - m_d)^2$. However, one would consequently have to resolve to using a "non physical" kaon mass $M_K^2 = B(\hat{m} + m_s) \approx 495$ MeV. Arguments *for* the use of the charged pion and kaon masses are the correct kinematics for the experimentally accessible channels (which use incoming charged particles), and the fact that the existing study of pion–kaon scattering in ChPT (in the isospin symmetry limit) [BKM91b] also employs these choices for numerical evaluation.

- As finally we want to evaluate isospin violating effects up to order e^2 and $m_u - m_d$, we can neglect the strong pion mass difference (of order $(m_u - m_d)^2$). Quark mass insertions can then, at leading order, be expressed by physical meson masses according to

$$\begin{aligned} \hat{m} &\to \frac{M_{\pi^0}^2}{2B} \;, & m_d - m_u &\to \frac{\Delta M_\pi^2 - \Delta M_K^2}{B} \;, \\ m_s &\to \frac{M_{K^+}^2 + M_{K^0}^2 - M_{\pi^+}^2}{2B} \;, & Z &\to \frac{\Delta M_\pi^2}{2e^2 F_\pi^2} \;, \end{aligned} \tag{5.24}$$

  where we have used the charged to neutral meson mass differences $\Delta M_\pi^2 = M_{\pi^\pm}^2 - M_{\pi^0}^2$, $\Delta M_K^2 = M_{K^\pm}^2 - M_{K^0}^2$.

- One important isospin breaking effect due to the light quark mass difference is $\pi^0\eta$–mixing: the π^0 and η fields are given in terms of the SU(3) eigenstates ϕ_3,

ϕ_8 according to

$$\begin{pmatrix} \pi^0 \\ \eta \end{pmatrix} = \begin{pmatrix} \cos\epsilon & \sin\epsilon \\ -\sin\epsilon & \cos\epsilon \end{pmatrix} \begin{pmatrix} \phi_3 \\ \phi_8 \end{pmatrix} \quad , \tag{5.25}$$

where the $\pi^0\eta$ mixing angle ϵ is given by

$$\epsilon = \frac{1}{2}\arctan\left(\frac{\sqrt{3}}{2}\frac{m_d - m_u}{m_s - \hat{m}}\right) \quad . \tag{5.26}$$

Replacing the quark masses by meson masses according to Eq. (5.24), one finds the numerical value $\epsilon = 1.00 \times 10^{-2}$. We find it convenient to express all corrections due to the light quark mass difference in terms of this mixing angle ϵ, which is of course of order $m_u - m_d$.

Note finally that we only display scattering lengths for processes involving kaons of positive strangeness (K^+, K^0) as the strong and electromagnetic interactions obey charge conjugation invariance, such that scattering lengths for all channels involving scattering of K^- or $\bar{K}^0$ can be obtained from those given below. We find:

$$\begin{aligned}
a_0\Big(\pi^+K^+ \to \pi^+K^+\Big) &= a_0^{3/2}\left\{1 - \frac{\Delta M_\pi^2}{M_\pi M_K}\right\} + \mathcal{O}(\delta^2) \\
&= a_0^{3/2}\Big\{1 - 0.018\Big\} + \mathcal{O}(\delta^2) \quad , &(5.27)\\
a_0\Big(\pi^-K^0 \to \pi^+K^0\Big) &= \Big(a_0^+ + a_0^-\Big)\left\{1 + \frac{2(M_K - M_\pi)M_\pi}{M_K^2}\frac{\epsilon}{\sqrt{3}} - \frac{M_\pi\,\Delta M_\pi^2}{2M_K^2(M_K + M_\pi)}\right\} \\
&\qquad + \mathcal{O}(\delta^2) \\
&= \Big(a_0^+ + a_0^-\Big)\Big\{1 + 0.002 - 0.001\Big\} + \mathcal{O}(\delta^2) \quad , &(5.28)\\
a_0\Big(\pi^-K^0 \to \pi^0K^-\Big) &= \sqrt{2}\,a_0^-\left\{1 - \frac{M_K^2 - 2M_KM_\pi + 2M_\pi^2}{M_K^2}\frac{\epsilon}{\sqrt{3}}\right. \\
&\qquad \left. - \frac{(M_K^2 + M_\pi^2)\Delta M_\pi^2}{2M_K^2M_\pi(M_K + M_\pi)}\right\} + \mathcal{O}(\delta^2) \\
&= \sqrt{2}\,a_0^-\Big\{1 - 0.003 - 0.008\Big\} + \mathcal{O}(\delta^2) \quad , &(5.29)\\
a_0\Big(\pi^0K^+ \to \pi^0K^-\Big) &= a_0^- - \frac{M_K^2}{4\pi F_\pi^2(M_K + M_\pi)}\frac{\epsilon}{\sqrt{3}} + \mathcal{O}(\delta^2) \\
&= a_0^- - 2.9 \times 10^{-3}/M_\pi + \mathcal{O}(\delta^2) \quad , &(5.30)\\
a_0\Big(\pi^-K^+ \to \pi^-K^-\Big) &= \Big(a_0^+ + a_0^-\Big)\left\{1 + \frac{\Delta M_\pi^2}{M_\pi M_K}\right\} + \mathcal{O}(\delta^2) \\
&= \Big(a_0^+ + a_0^-\Big)\Big\{1 + 0.018\Big\} + \mathcal{O}(\delta^2) \quad , &(5.31)\\
a_0\Big(\pi^-K^+ \to \pi^0K^0\Big) &= -\sqrt{2}\,a_0\left\{1 + \frac{\epsilon}{\sqrt{3}} + \frac{\Delta M_\pi^2}{2M_\pi M_K}\right\} + \mathcal{O}(\delta^2) \\
&= -\sqrt{2}\,a_0\Big\{1 + 0.006 + 0.009\Big\} + \mathcal{O}(\delta^2) \quad , &(5.32)
\end{aligned}$$

$$
\begin{aligned}
a_0\Big(\pi^0 K^0 \to \pi^0 K^0\Big) &= a_0^+ + \frac{M_K^2}{4\pi F_\pi^2 (M_K + M_\pi)} \frac{\epsilon}{\sqrt{3}} + \mathcal{O}(\delta^2) \\
&= a_0^+ + 2.9 \times 10^{-3}/M_\pi + \mathcal{O}(\delta^2) \;, \qquad (5.33) \\
a_0\Big(\pi^- K^0 \to \pi^- K^0\Big) &= a_0^{3/2} \left\{ 1 + \frac{2(M_K - M_\pi)M_\pi}{M_K^2} \frac{\epsilon}{\sqrt{3}} - \frac{M_\pi \Delta M_\pi^2}{2M_K^2 (M_K + M_\pi)} \right\} + \mathcal{O}(\delta^2) \\
&= a_0^{3/2} \Big\{ 1 + 0.002 - 0.001 \Big\} + \mathcal{O}(\delta^2) \;. \qquad (5.34)
\end{aligned}
$$

For the elastic charged channels, Eqs. (5.27), (5.31), subtraction of the one photon exchange Born term is required in order to arrive at the above results (see [KU98] for the comparable $\pi\pi$ case). These charged particle Coulomb interactions in principle require a separate treatment tailored to scattering or bound state problems. Further discussion of this point is found in Sect. 5.6. (For the $\pi\pi$ scattering problem, this is discussed e.g. in [RS76, KN02].) We remark that isospin violation effects can only be given in absolute size for those amplitudes which are (in the isospin limit) proportional to T^-, as a_0^+ vanishes at tree level. The one–loop corrections to a_0^+ are rather large, $a_0^{+(1)} = 31.9 \times 10^{-3}/M_\pi$ [BKM91b], but still then the corrections displayed in Eqs. (5.30), (5.33) amount to 10% effects. (The caveat is, of course, that isospin violating contributions at one–loop level might reduce the leading–order terms considerably.) In fact, this is neatly comparable to pion–nucleon scattering: as pointed out by Weinberg, the isoscalar πN amplitude vanishes at leading chiral order [We66] and is therefore prone to display large isospin violation effects [We77], which have indeed been confirmed in [MS98].

It is instructive to compare the results above also to the corresponding corrections calculated in [KU98] for $\pi\pi$ scattering. First of all, $m_u - m_d$ effects are suppressed in SU(2), such that the only isospin breaking corrections of interest in the $\pi\pi$ case are of electromagnetic origin. In contrast, strong isospin breaking appears at leading order in πK scattering and, as shown above, is potentially of equal significance as the electromagnetic effects. On the other hand, the authors of [KU98] find corrections at tree level of the order of 6%, while the largest corrections given above are 1.8% (for the elastic charged meson channels). This is not due to a particular "smallness" of e.g. the electromagnetic contribution for πK scattering, but due to the fact that the (isospin conserving) S wave scattering length is larger, $a_0(\pi K) \sim M_\pi M_K$ in contrast to $a_0(\pi\pi) \sim M_\pi^2$. As already hinted at in the introduction, processes with a conserved number of strange quarks (such as πK scattering) can also be studied in a chiral SU(2) theory in which Green's functions are only expanded around the limit $m_u = m_d = 0$, while m_s is held fixed at its physical value. Consequently, only the pion is considered to be "light", while the kaon is now a heavy particle and has to be treated in analogy to e.g. nucleons in ChPT, resulting in what one might call "heavy–kaon" ChPT [Ro99, Ou01, FKM02]. The πK Lagrangian then starts out at order q, as does the (isovector) πK scattering length (see again the analogy to πN scattering). In such a counting scheme, electromagnetic corrections to πK scattering lengths are therefore necessarily suppressed by one chiral order (as they scale like

ϵ^2), which sheds some light on why these corrections are smaller here than for $\pi\pi$ scattering.

We want to emphasise that it is in general impossible to arrive at the results above by assuming the dominance of certain "effects" for the violation of isospin symmetry, e.g. studying the implications of meson mass splittings or $\pi^0\eta$ mixing alone. From the point of view of ChPT, such a partial analysis is not very useful and can lead to strongly misleading results. In order to demonstrate this, we show such a decomposition (artificial though this really is) for the specific channel studied in more detail in the following chapter, $\pi^- K^+ \to \pi^0 K^0$. We distinguish "kinematical" effects (due to meson mass splittings, entering essentially via corrections to the values of u and t at threshold), "$\pi^0\eta$ mixing" effects that modify the isospin symmetric amplitude by factors of $\sin\epsilon$ or $\cos\epsilon$, "quark mass insertions" for the four meson vertex (which vanish in the isospin limit for the channel in question), and "electromagnetic (em) insertions" ($\sim Z$) for the four–meson vertex[#2]. The relative corrections can then be decomposed as follows:

$$\text{strong}: \quad \frac{\epsilon}{\sqrt{3}} = \frac{\epsilon}{\sqrt{3}}\left\{\underbrace{1 - \frac{M_K}{M_\pi}}_{\text{kinematical}} + \underbrace{\frac{2M_K^2 + M_\pi^2}{3M_K M_\pi}}_{\pi^0\eta-\text{mixing}} + \underbrace{\frac{M_K^2 - M_\pi^2}{3M_K M_\pi}}_{\text{quark mass}}\right\}, \tag{5.35}$$

$$\text{electromagnetic}: \quad \frac{Ze^2F_\pi^2}{M_K M_\pi} = \underbrace{\frac{Ze^2F_\pi^2}{2M_K M_\pi}}_{\text{kinematical}} + \underbrace{\frac{Ze^2F_\pi^2}{2M_K M_\pi}}_{\text{em insertions}} . \tag{5.36}$$

It is obvious from the above that for the strong isospin violating contributions, individual "effects" are much larger than the total sum.

5.5 $\pi^- K^+ \to \pi^0 K^0$ at one–loop level

5.5.1 S–wave scattering length up to fourth order

In this section, we work out the complete one loop corrections including isospin breaking for the pion kaon channel that is relevant for the lifetime of πK atoms, $\pi^- K^+ \to \pi^0 K^0$. At this level, virtual photon loops play a role and enter the amplitude both via wave function renormalisation and electromagnetic corrections to the (lowest–order) strong vertex, see Fig. 5.1. As is well known, the photon exchange diagram (a) in Fig. 5.1 induces a pole at threshold, the so-called Coulomb pole, which resides in the loop function $G^{\pi K\gamma}(s)$ discussed in detail in Chapter 6. This Coulomb pole, however, can be calculated and subtracted from the amplitude unambiguously. The threshold expansion Eq. (5.18) therefore has to be modified for $\pi^- K^- \to \pi^0 K^0$

[#2]Note that this separation is even representation dependent, as can be seen in the example of pion–pion scattering: in the σ–model gauge, there are no electromagnetic insertions $\sim Z$ in the four pion vertex, while these are present in the exponential gauge.

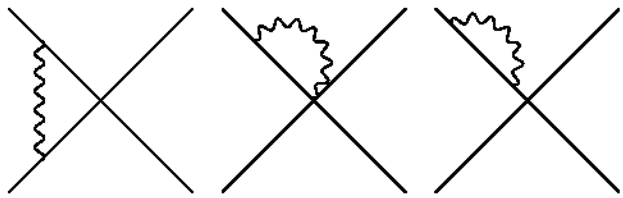

(a) (b) (c)

Figure 5.1: Virtual photon loop diagrams for $\pi^- K^- \to \pi^0 K^0$. Crossed diagrams are not shown. Diagram (c) denotes effects entering the scattering amplitude via wave function renormalisation of the incoming charged mesons.

in the presence of virtual photons in order to sensibly define corrections to the S–wave scattering length:

$$\mathrm{Re}\, T = \frac{e^2 \pi M_{K^+} M_{\pi^+} a_0^{(2)}}{|\mathbf{q}_{\mathrm{in}}|} + 8\pi \left(M_{K^\pm} + M_{\pi^\pm} \right) a_0 + \mathcal{O}(|\mathbf{q}_{\mathrm{in}}|) \quad , \tag{5.37}$$

where $a_0^{(2)}$ denotes the S–wave scattering length in its tree level approximation (given explicitly up to order δ in Eq. (5.32)), and a_0 is the S–wave scattering length to be defined here, including all corrections.

A further problem occurs when including virtual photon loops: the amplitude becomes infrared divergent. We will give details on how to deal with these infrared divergences in the following section. For the moment we only note that these vanish at threshold and therefore do not affect the definition of the S–wave scattering length as given in Eq. (5.37).

The various pieces of the full scattering amplitude are spelled out explicitly in App. B.1. Analytic formulae for the S–wave scattering length at one loop accuracy are given in App. B.3. In order to arrive at these, the following effects were taken into account, as well as the following conventions were used in addition to those already mentioned in the previous section:

- In order to have a strong check on the scattering amplitude, we have checked the cancellation of divergences in the *exact* expressions, i.e. without any expansion in ϵ and e^2. For this purpose, we have used the β–functions for the various counterterms as given in [GL85a, Ur95].

- For quark mass insertions at tree level replaced by meson masses according to Eq. (5.24), the renormalisation of these meson masses has to be taken into account properly.

- The mass of the η is always taken as given by the Gell-Mann–Okubo relation when taking into account isospin violation up to order e^2 and $m_u - m_d$, see

Eq. (5.8). Deviations from this relation are beyond the accuracy considered here, as the η mass only enters via loop diagrams.

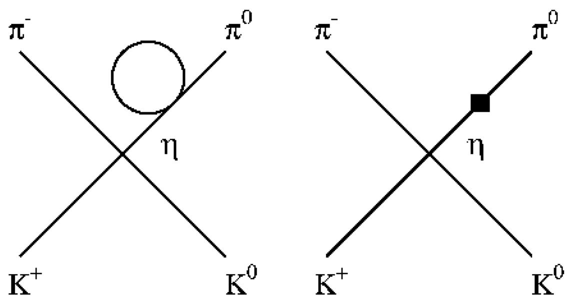

Figure 5.2: Diagrams contributing to $\pi^0\eta$ mixing at next to leading order. The labels "π^0" and "η" refer to the tree level mass eigenstates. The black square denotes a fourth order insertion (strong or electromagnetic).

- $\pi^0\eta$–mixing has to be taken into account at next–to–leading order. Details on how this is to be done can be found e.g. in [GL85c, NR95, Ec00, ABT01]. It is probably easiest to calculate the diagrams in Fig. 5.2 directly in order to account for mixing beyond leading order. We have done the calculations using tree level mass eigenfields for π^0 and η throughout. The off diagonal element of the self energy matrix (in the basis of tree level eigenfields) may be written as $\Sigma_{\pi^0\eta}(q^2) = Z_{\pi^0\eta}q^2 + Y_{\pi^0\eta}$, such that $Z_{\pi^0\eta} = \partial\Sigma_{\pi^0\eta}/\partial q^2$ can be thought of as the off–diagonal analogy to the field renormalisation factors. Denoting the tree–level amplitude for $\pi^- K^+ \to \eta K^0$ by T_η, we can write the additional mixing diagrams as

$$\begin{aligned} & T_\eta \times \frac{1}{M_{\pi^0}^2 - M_\eta^2} \times \Sigma_{\pi^0\eta}\left(q^2 = M_{\pi^0}^2\right) \\ = \;& T_\eta \times \left\{ \frac{Z_{\pi^0\eta}}{2} + \underbrace{\frac{1}{M_{\pi^0}^2 - M_\eta^2} \times \Sigma_{\pi^0\eta}\left(q^2 = \frac{1}{2}\left(M_{\pi^0}^2 + M_\eta^2\right)\right)}_{\epsilon^{(4)}} \right\} \;. \end{aligned} \tag{5.38}$$

  $\epsilon^{(4)}$ thus defined is the correction to the tree level $\pi^0\eta$ mixing angle up to order $\mathcal{O}(q^4)$, as given e.g. in [Ec00]. In contrast to the wave function renormalisation factor $Z_{\pi^0\eta}$, $\epsilon^{(4)}$ is finite. All these quantities are written down explicitly in App. B.1.5.

- When expressing the low–energy constant F in terms of physically observable decay constants, we always renormalise it such as to obtain F_π (as opposed to F_K, say). At tree level, the difference between using a normalisation of the amplitude equal to $1/F_\pi^2$ and $1/F_\pi F_K$ amounts to nothing more but shifting certain contributions from tree to one–loop level, which makes no difference in the sum. However, it turns out that the one–loop corrections e.g. for the scattering lengths are much smaller when normalising the tree level expression to $1/F_\pi^2$, which means that in the seemingly more "symmetric" case of using $1/F_\pi F_K$, the bulk of the (large) corrections at $\mathcal{O}(q^4)$ have nothing to do with corrections to the scattering dynamics, but only with the renormalisation of F_K.

For the one loop contributions, the difference between F_π and F_K is of higher order, whereas the numerical difference is potentially significant (noting that these scale as $1/F^4$). If one regards the meson decay constant in the chiral limit, $F \simeq 88$ MeV [GL83, GL84], as the "natural" constant when writing down a scattering amplitude, F_π seems more appropriate than F_K.

Finally heavy–kaon ChPT, which we alluded to before already, also provides some insight on F_π versus F_K: there is of course no kaon decay constant in a kaon–number conserving theory, hence F_π is the only meson decay constant available. As heavy–kaon ChPT is supposed to have a better convergence behaviour than SU(3) ChPT, but ultimately is equivalent up to matching of the different sets of LECs, it seems reasonable also from this perspective to only use F_π in the πK amplitudes.

- We use the charged pion decay constant in the absence of electromagnetism, as the value commonly used for the physical pion decay constant, $F_\pi = 92.4$ MeV [Ho90], was extracted from *charged* pion decays with electromagnetic corrections already taken care of. The relation to the bare decay constant F is therefore as given in [GL85a], and independent of photon loop effects or electromagnetic counterterms. See however the discussion on the "correct" isospin limit for F_π below.

The scattering length for the process $\pi^- K^+ \to \pi^0 K^0$ up to one loop order, including leading order effects in the isospin breaking parameters ϵ and e^2, can be brought into the following form:

$$a_0(\pi^- K^+ \to \pi^0 K^0) = -\frac{M_\pi M_K}{4\sqrt{2}F^2(M_\pi + M_K)} \left\{ C_0 + \frac{\epsilon}{\sqrt{3}} C_\epsilon + \frac{Z e^2 F^2}{M_\pi M_K} C_{e^2} \right\} \quad , \tag{5.39}$$

where we shall first of all use the meson decay constant in the chiral limit, F. The three parameters C_0, C_ϵ, C_{e^2} take the tree level values $C_0 = C_\epsilon = C_{e^2} = 1$ as can be seen in Eq. (5.32). The expressions up to one loop accuracy are very lengthy and are therefore relegated to App. B.3, we only show the numerical results here, obtained with the values and error estimates for the various low–energy constants according to the sources cited in Section 5.2. We find

$$C_0 \;=\; 0.95 \pm 0.24 \;\;, \quad C_\epsilon \;=\; 2.49 \pm 0.69 \;\;, \quad C_{e^2} \;=\; 0.86 \pm 1.60 \;\; . \tag{5.40}$$

In order to express ϵ and Z by physical quantities, i.e. physical meson masses, we have to correct for the next to leading order corrections to the tree level results

$$\frac{4\epsilon}{\sqrt{3}} = \frac{\Delta M_\pi^2 - \Delta M_K^2}{M_K^2 - M_\pi^2} + \mathcal{O}(\delta^2) \quad , \tag{5.41}$$

$$2Ze^2F^2 = \Delta M_\pi^2 + \mathcal{O}(\delta^2) \quad . \tag{5.42}$$

This can be achieved by putting together the different pieces from the existing literature,

$$\begin{aligned} -\frac{(\Delta M_K^2)_{\mathrm{QCD}}}{M_K^2 - M_\pi^2} &= \frac{4\epsilon}{\sqrt{3}}\left\{1 + \frac{1}{F^2}\left[8(2L_8^r - L_5^r)\left(M_K^2 - M_\pi^2\right) - \frac{1}{2}\Delta_\pi + \frac{1}{2}\Delta_\eta\right]\right\} \\ &\equiv \frac{4\epsilon}{\sqrt{3}}\left\{1 + \delta_M\right\} \quad , \end{aligned} \tag{5.43}$$

for the strong kaon mass difference [GL85a], where we have used the familiar abbreviation for the tadpole loop function

$$\Delta_\phi = \frac{M_\phi^2}{8\pi^2}\log\frac{M_\phi}{\lambda} \quad , \tag{5.44}$$

furthermore

$$\begin{aligned} \left(\Delta M_\pi^2 - \Delta M_K^2\right)_{\mathrm{em}} &= \frac{\Delta M_\pi^2}{F^2}\Bigg\{8L_5^r\left(M_K^2 - M_\pi^2\right) - 2\Delta_\pi + \Delta_K - \frac{M_\pi^2}{16\pi^2} \\ &\quad - \frac{2}{Z}\Bigg[\left(K_3^r - \frac{1}{2}K_4^r + \frac{1}{3}(K_9^r + K_{10}^r)\right)M_\pi^2 \\ &\quad - \frac{1}{3}(K_5^r + K_6^r)M_K^2 + 2(K_{10}^r + K_{11}^r)\left(M_K^2 - M_\pi^2\right) \\ &\quad - \frac{3}{4}\left(\Delta_K - \Delta_\pi\right) + \frac{M_K^2 - M_\pi^2}{16\pi^2}\Bigg]\Bigg\} \\ &\equiv \Delta M_\pi^2\ \delta_D \end{aligned} \tag{5.45}$$

as given in [Ur95], and

$$\begin{aligned} \Delta M_\pi^2 &= 2Ze^2F^2\Bigg\{1 - \frac{1}{F^2}\left[8\left(L_4^r\left(2M_K^2 + M_\pi^2\right) + L_5^r M_\pi^2\right) + 3\Delta_\pi + \Delta_K + \frac{M_\pi^2}{16\pi^2}\right] \\ &\quad - \frac{2}{ZF^2}\Bigg[\left(K_3^r - \frac{1}{2}K_4^r - 2(K_{10}^r + K_{11}^r)\right)M_\pi^2 - K_8^r\left(2M_K^2 + M_\pi^2\right) \\ &\quad + \frac{3}{4}\Delta_\pi - \frac{M_\pi^2}{16\pi^2}\Bigg]\Bigg\} \\ &\equiv 2Ze^2F^2\left\{1 + \delta_{\Delta\pi}\right\} \quad . \end{aligned} \tag{5.46}$$

In addition, there is a difficulty in linking the pion decay constant F_π to F: using the isospin symmetric relation between the two quantities as formulated in terms of quark masses, one obtains additional isospin violating contributions due to our definition of the isospin limes in terms of charged meson masses:

$$\begin{aligned}
F_\pi &= F\left\{1+\frac{8B}{F^2}\Big((2\hat{m}+m_s)L_4^r+mL_5^r\Big)\right. \\
&\qquad \left.-\frac{B\hat{m}}{8\pi^2F^2}\log\frac{2B\hat{m}}{\lambda^2}-\frac{B(\hat{m}+m_s)}{32\pi^2F^2}\log\frac{B(\hat{m}+m_s)}{\lambda^2}\right\} \\
&\equiv F\left\{1+\delta_F+\frac{\epsilon}{\sqrt{3}}\delta_F^\epsilon+\frac{\Delta M_\pi^2}{2M_\pi M_K}\delta_F^{e^2}\right\} \quad , \qquad (5.47)
\end{aligned}$$

where

$$\begin{aligned}
\delta_F &= \frac{1}{F^2}\left\{4\Big((2M_K^2+M_\pi^2)L_4^r+M_\pi^2L_5^r\Big)-\Delta_\pi-\frac{1}{2}\Delta_K\right\} \quad , \qquad (5.48)\\
\delta_F^\epsilon &= \frac{M_K^2-M_\pi^2}{F^2}\left\{16L_4^r-\frac{1}{16\pi^2}\left(1+2\log\frac{M_K}{\lambda}\right)\right\} \quad , \qquad (5.49)\\
\delta_F^{e^2} &= -\frac{M_\pi M_K}{F^2}\left\{8(3L_4^r+L_5^r)-\frac{1}{16\pi^2}\left(3+4\log\frac{M_\pi}{\lambda}+2\log\frac{M_K}{\lambda}\right)\right\} \quad . \qquad (5.50)
\end{aligned}$$

This is what was done in [KM02a, KM02b, NT02, Ne02]. One can argue that this is the "wrong" isospin limit for the pion decay constant, and that in the above expressions, δ_F^ϵ and $\delta_F^{e^2}$ should be set to zero. One reason for still proceeding as suggested is that in this scheme, the low–energy constant L_4 drops out completely, which is what also would happen in a different isospin limit defined with respect to the quark masses.

Putting all pieces together, we can write the scattering length at one–loop order in terms of physical quantities (as far as possible) as

$$\begin{aligned}
a_0(\pi^-K^+\to\pi^0K^0) &= -\frac{M_\pi M_K}{4\sqrt{2}F_\pi^2(M_\pi+M_K)} \\
&\quad\times\left\{\tilde{C}_0+\frac{\Delta M_\pi^2-\Delta M_K^2}{4(M_K^2-M_\pi^2)}\tilde{C}_\epsilon+\frac{\Delta M_\pi^2}{2M_\pi M_K}\tilde{C}_{e^2}\right\} \quad , \qquad (5.51)
\end{aligned}$$

with the relations

$$\begin{aligned}
\tilde{C}_0 &= C_0+2\delta_F \quad , \qquad (5.52)\\
\tilde{C}_\epsilon &= C_\epsilon-\delta_M+2\Big(\delta_F+\delta_F^\epsilon\Big) \quad , \qquad (5.53)\\
\tilde{C}_{e^2} &= C_{e^2}-\delta_{\Delta\pi}-\frac{M_\pi M_K}{2(M_K^2-M_\pi^2)}\delta_D+2\left(\delta_F+\delta_F^{e^2}\right) \quad , \qquad (5.54)
\end{aligned}$$

where we have made use of the fact that $C_0=C_\epsilon=C_{e^2}=1$ at tree level and omitted explicit mentioning of the higher orders neglected here. We note that $\tilde{C}_0$

has already been written out in Eq. (5.20), the coefficients $\tilde{C}_\epsilon$, $\tilde{C}_{e^2}$ are also collected in App. B.3. We point out that, despite the nomenclature, this last decomposition is no strict separation of electromagnetic and strong isospin breaking effects, as $\tilde{C}_\epsilon$ contains contributions from the corrections to Dashen's theorem, $(\Delta M_\pi^2 - \Delta M_K^2)_{\rm em}$.[#3] Numerically, we find for these coefficients

$$\tilde{C}_0 = 1.121 \pm 0.009 \ , \quad \tilde{C}_\epsilon = 2.40 \pm 0.10 \ , \quad \tilde{C}_{e^2} = -0.00 \pm 1.36 \ . \qquad (5.55)$$

With these numbers, we are in the position to summarise the isospin violating shifts in the scattering length $a_0 = a_0(\pi^-K^+ \to \pi^0K^0)$ at one–loop level, comparing them to the tree–level result

$$a_0(\pi \quad K \quad \to \pi^0K^0) = -\sqrt{2}a_0^{-(2)} \Big\{ 1 + \underbrace{0.6\%}_{\mathcal{O}(\epsilon)} + \underbrace{0.9\%}_{\mathcal{O}(e^2)} \Big\} \qquad (5.56)$$

as cited in Eq. (5.32):

$$\begin{aligned} a_0 &= -\sqrt{2}a_0^{-(2)} \Big\{ (1.121 \pm 0.9\%) + \underbrace{(1.4 \pm 0.1)\%}_{\mathcal{O}(\epsilon)} - \underbrace{(0.0 \pm 1.2)\%}_{\mathcal{O}(e^2)} \Big\} \\ &= -\sqrt{2}a_0^- \Big\{ (1 \pm 0.8\%) + \underbrace{(1.3 \pm 0.1)\%}_{\mathcal{O}(\epsilon)} - \underbrace{(0.0 \pm 1.1)\%}_{\mathcal{O}(e^2)} \Big\} \ . \end{aligned} \qquad (5.57)$$

Here, $a_0^{-(2)}$ symbolises the isovector scattering length in its tree level approximation, while a_0^- in the second line really represents this quantity completely in the isospin limit, to the accuracy we are working here. All errors quoted for the different contributions above are due to uncertainties in the respective strong and electromagnetic LECs as given in [BEG95, BU97]. Regarding these numbers, and comparing Eq. (5.55) to Eq. (5.40), we note the following:

- The isospin symmetric corrections at one–loop order as given by $\tilde{C}_0$ are moderate, given the expected slow convergence of chiral SU(3). As detailed above, this depends heavily on our choice to normalise the tree amplitude by $1/F_\pi^2$ and not $1/F_\pi F_K$: this way, one finds $\tilde{C}_0 = 1 + \mathcal{O}(M_\pi^2)$ (see Eq. (5.22)), which is what one would expect from an SU(2) expansion and which accounts for the smallness of the one–loop corrections. The isospin symmetric coefficient $\tilde{C}_0$ is much more precise when using the physical pion decay constant F_π, the large error in C_0 is dominated by the uncertainty of L_4 parameterising the ratio F_π/F. We also note that for C_0, one rather finds $C_0 = 1 + \mathcal{O}(M_K^2)$, as witnessed by the large uncertainty (if not by a large shift in the central value).

- Although they are very small corrections to the scattering length, one might worry about the fact that tree and one–loop level isospin breaking corrections

[#3] This was misleadingly not made clear in [KM02a].

(strong and electromagnetic effects taken separately) are of equal size. In order to understand the relative largeness of these effects, it is again instructive to expand the terms for C_ϵ, C_{e^2} given in App. B.3 in powers of M_π/M_K, where we find $C_\epsilon = 1 + \mathcal{O}(M_K^2)$, $C_{e^2} = 1 + \mathcal{O}(M_K^2)$ (the same holds for $\tilde{C}_{e^2}$, while $\tilde{C}_\epsilon = 1 + \mathcal{O}(M_K M_\pi)$). Another way of seeing this is to remember that isospin violating terms are suppressed in comparison to isospin conserving ones at the same chiral order by factors which happen to be small, but are of chiral order 1. At tree level, these suppression factors for $\pi^- K^+ \to \pi^0 K^0$ are ϵ, $e^2F^2/M_\pi M_K \sim 0.01$, respectively, see Eq. (5.32). On one–loop level, however, where the isospin symmetric loop corrections are particularly small, the isospin violating ones are suppressed with respect to these only by factors of $\epsilon\, M_K^2/M_\pi^2$, $e^2F^2M_K/M_\pi^3 \sim 0.1$ (at leading order in M_π).

- On the other hand, combining strong and electromagnetic isospin breaking effects, the corrections at one–loop level cancel to a large extent, leaving mainly an uncertainty due to a lack of sufficiently precise knowledge of the relevant counterterms. This cancellation does not take place at tree level. We have checked numerically that no significant errors arise from truncating the "exact" expressions at leading orders in the isospin breaking parameters ϵ, e^2. In fact, the corrections arising thereof are at least one order of magnitude smaller than the accuracy displayed in Eq. (5.57).

- With the large number of electromagnetic counterterms, one might have suspected that one cannot make any sensible prediction about electromagnetic effects at all. While the uncertainty quoted above is as large as the absolute size of the electromagnetic correction at tree or one–loop level (individually), it is, on the other hand, still of the same magnitude as the uncertainty stemming from our lack of knowledge of the values for the hadronic low–energy constants.

- The reduction of the uncertainty in $\tilde{C}_\epsilon$ as compared to C_ϵ is also due to the cancellation of L_4 in the corresponding expression, see App. B.3. The inclusion of the shift δ_F^ϵ is of course essential for this to happen.

- Numerically, the shift of the contribution $\propto \delta_D$ from C_{e^2} effectively into $\tilde{C}_\epsilon$ does not affect either constant much. The seemingly large change from C_{e^2} to $\tilde{C}_{e^2}$ are mostly due to the renormalisation factors $\delta_{\Delta\pi}$ and $\delta_F^{e^2}$.

The last two points signify that the central values of $\tilde{C}_{e^2}$ (in particular) and $\tilde{C}_\epsilon$ are non-negligibly affected by the treatment of the pion decay constant, as described above. Setting $\delta_F^\epsilon = \delta_F^{e^2} = 0$, we find

$$\tilde{C}_\epsilon = 2.64 \pm 0.54 \ , \quad \tilde{C}_{e^2} = 0.57 \pm 1.36 \ . \tag{5.58}$$

Note, however, that these changes are not really significant as compared to the estimated uncertainties.

5.5.2 Infrared divergences and $\pi^- K^+ \to \pi^0 K^0 \gamma$

As mentioned in the previous section, photon loop corrections induce infrared divergences in the scattering amplitude. It is well known how to handle this problem, namely by introducing a small photon mass m_γ which brings the infrared divergences into a form $\sim \log m_\gamma$. Such terms enter both via wave function renormalisation of charged mesons and via the loop function $G^{\pi K \gamma}(s)$, as discussed in App. B.5. One then has to include the corresponding radiative process ($\pi^- K^+ \to \pi^0 K^0 \gamma$ for the case in question) up to some maximal photon energy, given either by the maximal energy available due to kinematics, or by some experimental detector resolution ΔE below which soft photon radiation cannot be discriminated from the non–radiative process. We are interested in the threshold region, where the kinematical limit for the photon energy,

$$E_\gamma^{\max} = \frac{s - (M_{K^0} + M_{\pi^0})^2}{2\sqrt{s}} \quad , \tag{5.59}$$

numerically amounts to 0.6 MeV, such that it seems reasonable to integrate the full cross section without making additional cuts on the photon energy. The infrared divergences cancel upon adding up the cross sections for both non–radiative and radiative processes. This is demonstrated in some detail in App. B.6.1.

We have emphasised in the previous chapter that the infrared divergences induced by photon loops vanish at threshold, such that one might even omit all these considerations when one is exclusively interested in the S–wave scattering length. The authors of [KU98] have argued, however, that one should rather *define* the S–wave scattering length from an infrared–finite quantity, which would be the combined total cross section. For an amplitude that can be expanded according to Eq. (5.18), the total cross section at threshold is given in terms of the S–wave scattering length as

$$\sigma_{\text{thr}} = \frac{|\mathbf{q}_{\text{out}}|}{|\mathbf{q}_{\text{in}}|} 4\pi (a_0)^2 \quad . \tag{5.60}$$

One may now replace the cross section on the left–hand side of Eq. (5.60) by the combined total cross section $\sigma + \sigma^\gamma$ and define a_0 via Eq. (5.60).

This is what was suggested in [KU98] for the similar case of the scattering process $\pi^-\pi^- \to \pi^0\pi^0(\gamma)$, where the authors claim to find a shift in the (redefined) scattering length induced by the (infrared finite) remainder of the radiative cross section at threshold. We have however recalculated the cross section for $\pi^-\pi^- \to \pi^0\pi^0\gamma$ at threshold and find that it vanishes. This is in our opinion rather obvious for the isospin symmetric case, where the neutral pions in the final state are of the same mass as the charged incoming ones. One would therefore expect the corrections to the scattering length due to soft photon radiation to be small compared to other isospin breaking effects, as they should be suppressed by at least two powers in isospin breaking parameters (a factor e^2 in the cross section due to the photon coupling, and at least one power of the pion mass difference). The fact that this cross section vanishes exactly at threshold in the $\pi\pi$ case is due to the enhanced symmetry of this reaction, see App. B.6.2.

We do not find the cross section for $\pi^- K^+ \to \pi^0 K^0 \gamma$ to vanish exactly at threshold, but to be highly suppressed: the leading contribution is of order δ^4 in isospin breaking parameters, which is clearly way beyond the level of accuracy we achieve in our calculation of isospin breaking effects in the non–radiative amplitude. Details for the calculation can be found in App. B.6.2, the result found there is

$$\sigma^{\gamma}_{\text{thr}} = \frac{e^2}{105(2\pi)^3 F_\pi^4} \frac{|\mathbf{q}_{\text{out}}|}{|\mathbf{q}_{\text{in}}|} \frac{M_{K^\pm} M_{\pi^\pm}}{(M_{K^\pm} + M_{\pi^\pm})^3} \Big(M_{K^\pm} - M_{K^0} + M_{\pi^\pm} - M_{\pi^0} \Big)^3 + \mathcal{O}(\delta^5) \quad . \tag{5.61}$$

In addition to the high power in δ, there is even an unnatural suppression in the mass difference $(M_{K^\pm} - M_{K^0} + M_{\pi^\pm} - M_{\pi^0})$ which is due to a numerical cancellation of strong and electromagnetic isospin breaking effects. If one calculates a shift in the scattering length defined via Eq. (5.60) which is due to the inclusion of the radiative cross section, $a_0 \to a_0 + a_0^\gamma$, the quantity a_0^γ is found to be

$$\begin{aligned} a_0^\gamma &= -\frac{e^2}{840\sqrt{2}\pi^3 F_\pi^2} \frac{(M_{K^+} - M_{K^0} + M_{\pi^+} - M_{\pi^0})^3}{(M_{K^+} + M_{\pi^+})^2} + \mathcal{O}(\delta^5) \\ &= -2.2 \times 10^{-14} / M_{\pi^\pm} \; = \; 2.2 \times 10^{-13} \times a_0^{(2)} \quad , \end{aligned} \tag{5.62}$$

which is a suppression of about eleven orders of magnitude compared to the shifts in the scattering length calculated before. We therefore conclude that bremsstrahlung corrections are totally negligible for any analysis of $\pi\pi$ or πK bound state experiments.

5.6 $\pi^- K^+ \to \pi^- K^+$ at one–loop level

In the presence of isospin violation and in particular of virtual photon effects, the threshold expansion Eq. (5.18) has to be modified already at tree level: the one photon exchange contributing to $\pi^- K^+ \to \pi^- K^+$ cannot be decomposed into partial waves and diverges at threshold. In order to allow for a direct matching to the description of the energy–level shift in the bound state formalism, we follow the prescription given in [LR00] (for the analogous case of $\pi^- p$ atoms) to circumvent these problems, valid to leading order in the fine structure constant: the amplitude $T_{\pi^- K^+ \to \pi^- K^+}$ can be uniquely decomposed into the piece containing all diagrams that can be made disconnected by cutting one photon line, and the remainder that contains at least one strong pion–kaon interaction vertex: $T_{\pi^- K^+ \to \pi^- K^+} = T_{ex} + T_s$, where

$$T_{ex} = e^2 \left(\frac{u - s}{t} \right) F_\pi^V(t) F_K^V(t) \quad . \tag{5.63}$$

T_{ex} is represented diagrammatically in Fig. 5.3. To the accuracy we are working, the pion and kaon vector form factors are only needed in their isospin symmetric

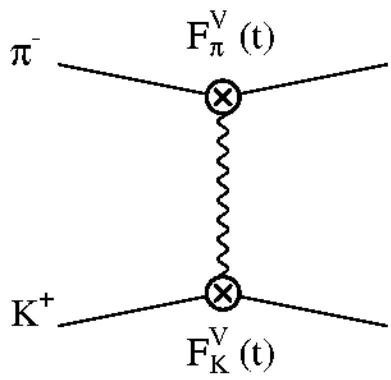

Figure 5.3: One–photon exchange contributions to $\pi^- K^+ \to \pi^- K^+$.

representation to one–loop order as given in [GL85b]. Subtraction of the one–photon exchange diagram suffices to define the modified scattering length for $\pi^- K^+ \to \pi^- K^+$ in the presence of photons at tree level, which is now taken to be T_s at threshold instead of the full scattering amplitude.

We note that in [Ne02], a different convention was used to subtract the long–range photon exchange: only the *tree–level* exchange was disregarded. The difference of the two approaches in the amplitude at threshold can be easily expressed in terms of the radii of the pion and kaon vector form factors,

$$T^{\rm thr}_{\rm Nehme} = T^{\rm thr}_{\rm KM} - \frac{2}{3} e^2 M_\pi M_K \left(\langle r^2 \rangle^V_\pi + \langle r^2 \rangle^V_K \right) \quad .$$

However, even the scattering amplitude with the one–photon exchange diagrams subtracted cannot be expanded at threshold according to Eq. (5.18) once photon loop corrections are included, as the vertex correction diagrams, see Fig. 5.4, induce a

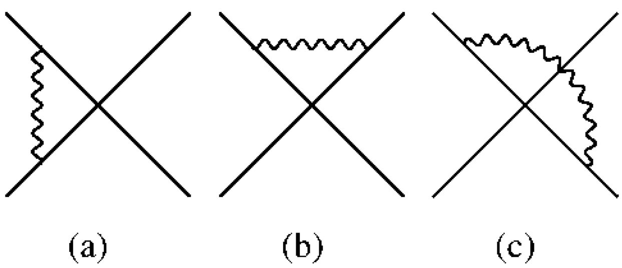

Figure 5.4: Vertex corrections by photon loops contributing to $\pi^- K^+ \to \pi^- K^+$.

kinematical divergence, the Coulomb pole. The real part of the corresponding scalar loop function

$$G^{ab\gamma}(P^2) = -i\int \frac{d^4k}{(2\pi)^4}\frac{1}{\Big((q_a+k)^2-M_a^2\Big)\Big((q_b-k)^2-M_b^2\Big)\Big(k^2-m_\gamma^2\Big)} \tag{5.64}$$

(with $P = q_a + q_b$, and a and b referring to the particles involved), has the following threshold behaviour in the s channel (Fig. 5.4(a)) for $s \approx (M_K + M_\pi)^2$:

$$\begin{aligned}\text{Re}\; G^{\pi K\gamma}(s) \;&=\; -\frac{1}{32(M_K+M_\pi)\,q} \\ &+\; \frac{1}{32\pi^2 M_K M_\pi}\left\{2-\frac{M_K-M_\pi}{M_K+M_\pi}\log\frac{M_K}{M_\pi}-\log\frac{m_\gamma^2}{M_K M_\pi}\right\}+\mathcal{O}(q)\;,\end{aligned} \tag{5.65}$$

while the corresponding loop functions in the t– and u–channels (Fig. 5.4(b) and (c), respectively) are regular at threshold,

$$\begin{aligned}G^{\pi K\gamma}(u) \;&=\; \frac{1}{32\pi^2 M_K M_\pi}\left\{\frac{M_K+M_\pi}{M_K-M_\pi}\log\frac{M_K}{M_\pi}-2+\log\frac{m_\gamma^2}{M_K M_\pi}\right\}+\mathcal{O}(q)\;\;, \quad (5.66)\\ G^{\pi\pi\gamma}(t) \;&=\; \frac{1}{16\pi^2 M_\pi^2}\log\frac{m_\gamma}{M_\pi}+\mathcal{O}(q)\;\;, \quad (5.67)\end{aligned}$$

for $u = (M_K - M_\pi)^2$ and $t = 0$, respectively. The infrared divergences, collected here as terms involving $\log m_\gamma$, again cancel at threshold. We therefore define the scattering length a_0 as the regular part of the amplitude T_s at threshold,

$$\text{Re}\; T_s \;=\; \frac{2\pi e^2 M_K M_\pi\, a_0^{(2)}}{q} \;+\; 8\pi(M_K+M_\pi)\,a_0 \;+\; \mathcal{O}(q)\;\;, \tag{5.68}$$

where $a_0^{(2)}$ again denotes the corresponding scattering length in its tree level approximation, given to order δ in Eq. (5.31).

Again, we have collected the pieces of the complete scattering amplitude for the physical channel $\pi^-K^+ \to \pi^-K^+$ in App. B.2. We now give the results for the isospin violating effects in the scattering length, which are expanded up to order ϵ and e^2. We employ a similar form as in Eq. (5.39), writing

$$a_0(\pi^-K^+\to\pi^-K^+) = \frac{M_\pi M_K}{8F^2(M_\pi+M_K)}\left\{D_0+\frac{\epsilon}{\sqrt{3}}\,D_\epsilon+\frac{2Ze^2F^2}{M_\pi M_K}\,D_{e^2}\right\}\;\;, \tag{5.69}$$

where Eq. (5.31) shows $D_0 = D_{e^2} = 1$, $D_\epsilon = 0$ at tree level. Furthermore, we shall also use a form in terms of physical mass differences in analogy to Eq. (5.51),

$$a_0(\pi^-K^+\to\pi^-K^-) = \frac{M_\pi M_K}{8F_\pi^2(M_\pi+M_K)}\left\{\tilde{D}_0+\frac{\Delta M_\pi^2-\Delta M_K^2}{4(M_K^2-M_\pi^2)}\,\tilde{D}_\epsilon+\frac{\Delta M_\pi^2}{M_\pi M_K}\,\tilde{D}_{e^2}\right\}\;\;, \tag{5.70}$$

where the coefficients D and $\tilde{D}$ are linked to each other by

$$
\begin{aligned}
\tilde{D}_0 &= D_0 + 2\delta_F \quad , && (5.71)\\
\tilde{D}_\epsilon &= D_\epsilon + 2\delta_F^\epsilon \quad , && (5.72)\\
\tilde{D}_{e^2} &= D_{e^2} - \delta_{\Delta\pi} + 2\delta_F + \delta_F^{e^2} \quad . && (5.73)
\end{aligned}
$$

Note that, due to the fact that the isoscalar scattering length a_0^- vanishes at tree level, the coefficients D_0 and $\tilde{D}_0$ can be expressed just in terms of a_0^+ and the corresponding coefficients C_0, $\tilde{C}_0$,

$$
D_0 = C_0 + a_0^+/a_0{}^{(2)} \quad , \qquad \tilde{D}_0 = \tilde{C}_0 + a_0^+/a_0{}^{(2)} \quad . \tag{5.74}
$$

The remaining coefficients are collected in App. B.4. Numerically, we find

$$
D_0 = 1.31 \pm 0.42 \quad , \quad D_\epsilon = 0.78 \pm 0.42 \quad , \quad D_{e^2} = 1.32 \pm 3.11 \quad , \tag{5.75}
$$

for the first set of coefficients, and

$$
\tilde{D}_0 = 1.48 \pm 0.24 \quad , \quad \tilde{D}_\epsilon = 0.53 \quad , \quad \tilde{D}_{e^2} = 0.76 \pm 2.58 \quad , \tag{5.76}
$$

for the second, inserting the values for the low–energy constants as given in [BEG95, BU97]. Although the effect is not quite as dramatic, we again find, as for the charge exchange channel, that the uncertainty for the one–loop isospin symmetric prediction is much enhanced if expressed in terms of the pion decay constant in the chiral limit. We remark that the *strong* isospin breaking is a pure loop effect and free of any counterterms for our choice of renormalising F_π, while a normalisation to F again produces a sizeable uncertainty. The coefficients D_{e^2}, $\tilde{D}_{e^2}$ are only moderately shifted from the tree–level results for the central values of the electromagnetic low–energy constants, but are largely dominated by the uncertainty in these.

For the isospin breaking shifts in the scattering length as compared to the tree level result cited in Eq. (5.31),

$$
a_0(\pi^- K^+ \to \pi^- K^+) = -\sqrt{2} a_0^{-(2)} \left\{ 1 + \underbrace{1.8\%}_{\mathcal{O}(e^2)} \right\} \quad , \tag{5.77}
$$

we find the following corrections to the one–loop isospin symmetric prediction:

$$
\begin{aligned}
a_0 &= \left(a_0^{-(2)} + a_0^{+(2)} \right) \left\{ (1.48 \pm 24\%) + \underbrace{0.3\%}_{\mathcal{O}(\epsilon)} + \underbrace{(1.4 \pm 4.7)\%}_{\mathcal{O}(e^2)} \right\} \\
&= \left(a_0^- + a_0^+ \right) \left\{ (1 \pm 16.1\%) + \underbrace{0.2\%}_{\mathcal{O}(\epsilon)} + \underbrace{(0.9 \pm 3.2)\%}_{\mathcal{O}(e^2)} \right\} \quad . && (5.78)
\end{aligned}
$$

Again, in the first line, we show the relative corrections to the sum of the current algebra isospin symmetric predictions $a_0^{\pm(2)}$, while in the second line the full one–loop result is taken as the normalisation. Due to the appearance of the isoscalar scattering length, the one–loop representation for the isospin symmetric amplitude at threshold is afflicted by a rather large uncertainty (of about 16%). Even if one includes isospin breaking corrections, this uncertainty still dominates the combined error for a chiral *prediction* of this quantity by far. If, however, the aim is to *extract* the sum of isovector and isoscalar scattering lengths from the experimental measurement of the strong energy level shift, the corresponding uncertainty in the electromagnetic corrections amounts to only 3.2% and is therefore reasonable with respect to the experimental accuracy that is expected. The central values for the various electromagnetic low–energy constants lead to a total isospin breaking shift of 0.9%.

Comparing the results Eq. (5.57), (5.78), we note that in contrast to the latter, Eq. (5.57) allows for a precise *prediction* of the charge exchange amplitude at threshold: compared to the isospin symmetric result, it is increased by 1.3% (for the central values of the low–energy constants involved), while the combined uncertainty is enlarged only from 0.8% to 1.4%. We note that, in contrast to what was found for the one–loop representations of a_0^+, there is no *systematic* reason for the difference in sizes of the electromagnetic uncertainties in the two channels at hand. As we attribute error bars $\pm 1/16\pi^2$ uniformly to all electromagnetic constants K_i, the total uncertainty is dominated by those counterterms which happen to appear with the largest numerical prefactors. For the process $\pi^- K^+ \to \pi^0 K^0$, the dominant of such terms turns out to be $4e^2(M_K/M_\pi)(K_{10}+K_{11})$ (for the relative corrections to the scattering length, at leading order in M_π/M_K), while the very same combination dominates in $\pi^- K^- \to \pi^- K^+$, just with a larger coefficient, $12e^2(M_K/M_\pi)(K_{10}+K_{11})$.

5.7 Higher threshold parameters

Although a precise knowledge of the S–wave scattering lengths is of highest interest for πK atom studies, one can of course also study isospin breaking corrections to other threshold parameters, particularly to the S–wave effective range b_0 and the P–wave scattering length a_1. We will not show results for these in as much detail as for a_0, but concentrate on the two channels of relevance to these atoms. We remark that, as indicated in Eq. (5.37), photon loops also induce a term *linear* in $|\mathbf{q}_{\rm in}|$ in the threshold expansion of the scattering amplitude, which we disregard here (as it can also be calculated and subtracted unambiguously).

The isospin symmetric tree level results for these two quantities are given by

$$b_0^{-(2)} = \frac{M_K^2 + M_\pi^2}{16\pi F_\pi^2 M_\pi M_K (M_K + M_\pi)} , \tag{5.79}$$

$$b_0^{+(2)} = -\frac{1}{16\pi F_\pi^2 (M_K + M_\pi)} , \tag{5.80}$$

$$a_1^{-(2)} = a_1^{+(2)} = \frac{1}{48\pi F_\pi^2 (M_K + M_\pi)} . \tag{5.81}$$

The isospin violating effects at tree level for the two physical channels can be expressed as

$$\begin{aligned}
b_0\Big(\pi^- K^- \to \pi^0 K^0\Big) &= -\sqrt{2}\, b_0^- \left\{1 + \frac{\epsilon}{\sqrt{3}} - \frac{\Delta M_\pi^2}{2(M_K^2 + M_\pi^2)}\right\} + \mathcal{O}(\delta^2) \\
&= -\sqrt{2}\, b_0^- \left\{1 + \underbrace{0.6\%}_{\mathcal{O}(\epsilon)} - \underbrace{0.2\%}_{\mathcal{O}(\epsilon^2)}\right\} + \mathcal{O}(\delta^2) \quad , \qquad (5.82)
\end{aligned}$$

$$\begin{aligned}
b_0\Big(\pi^- K^- \to \pi^- K^+\Big) &= \Big(b_0^- + b_0^-\Big)\left\{1 - \frac{\Delta M_\pi^2}{M_K^2 - M_K M_\pi + M_\pi^2}\right\} + \mathcal{O}(\delta^2) \\
&= \Big(b_0^- + b_0^-\Big)\left\{1 - \underbrace{0.6\%}_{\mathcal{O}(\epsilon^2)}\right\} + \mathcal{O}(\delta^2) \quad , \qquad (5.83)
\end{aligned}$$

$$\begin{aligned}
a_1\Big(\pi^- K^- \to \pi^0 K^0\Big) &= -\sqrt{2}\, a_1^- \left\{1 - \sqrt{3}\,\epsilon\right\} + \mathcal{O}(\delta^2) \\
&= -\sqrt{2}\, a_1^- \left\{1 - \underbrace{2\%}_{\mathcal{O}(\epsilon)}\right\} + \mathcal{O}(\delta^2) \quad , \qquad (5.84)
\end{aligned}$$

$$a_1\Big(\pi^- K^- \to \pi^- K^+\Big) = \Big(a_1^- + a_1^-\Big)\left\{1 + \mathcal{O}(\delta^2)\right\} \quad . \qquad (5.85)$$

Again, no strong isospin violating effects enter the charged–to–charged channel, and no electromagnetic effects affect the P–wave scattering lengths at this order, such that there is no isospin breaking at tree level at all for the charged–to–charged P–wave scattering length.

We evaluate the fourth–order contributions to these threshold parameters numerically only, and only for the charge exchange channel. We therefore do not differentiate between strong and electromagnetic isospin violation at this level. Again, all corrections are given relative to the isospin symmetric tree–level result:

$$\begin{aligned}
b_0\Big(\pi^- K^+ \to \pi^0 K^0\Big) &= -\sqrt{2} b_0^{-(2)} \left\{ (1.012 \pm 3.8\%) - \underbrace{(0.9 \pm 0.5)\%}_{\mathcal{O}(\delta)} \right\} \\
&= -\sqrt{2} b_0^- \left\{ (1 \pm 3.8\%) - \underbrace{(0.9 \pm 0.5)\%}_{\mathcal{O}(\delta)} \right\} \quad , \qquad (5.86)
\end{aligned}$$

$$\begin{aligned}
a_1\Big(\pi^- K^+ \to \pi^0 K^0\Big) &= -\sqrt{2} a_1^{-(2)} \left\{ (1.53 \pm 0.14) - \underbrace{(5 \pm 1)\%}_{\mathcal{O}(\delta)} \right\} \\
&= -\sqrt{2} a_1^- \left\{ (1 \pm 9\%) - \underbrace{(3 \pm 1)\%}_{\mathcal{O}(\delta)} \right\} \quad . \qquad (5.87)
\end{aligned}$$

We note that the isospin symmetric one–loop corrections to the P–wave scattering length are rather large compared to the leading term. The isospin breaking corrections for both quantities are of similar size as for a_0, only slightly enhanced for a_1. The main difference is that the cancellation between electromagnetic and $m_u - m_d$ effects at fourth order observed for a_0 does not occur here, such that isospin breaking at fourth chiral order is equally important as on tree level. If we compare the one–loop contributions only, the isospin breaking effects on the S–wave effective range appear to be very large, equally large even as the isospin symmetric one loop corrections. However, as already hinted at by the error range for the latter, this does not result from an unnatural enhancement of isospin violation effects, but from an accidental suppression of the isospin conserving part. Individual contributions to the latter (from separate loop diagrams, counterterms) are much larger.

In contrast to both the S–wave and the P–wave scattering lengths, the S–wave effective range as defined naively from the scattering amplitude alone is infrared divergent. The above results were achieved by setting m_γ equal to the maximal energy of a bremsstrahlung photon, which at threshold is roughly 0.6 MeV. This is what effectively happens when rendering infrared divergent expressions finite by including the appropriate radiative process, while we neglect here any finite contributions from the latter, see the discussion in the previous section. We also note that a redefinition of these higher–order threshold parameters from the infrared–finite total cross section (as done in the previous section for the S–wave scattering length) cannot be done unambiguously.

5.8 Summary

In this chapter, we have considered isospin violation in pion–kaon scattering near threshold. To systematically account for such effects due to the light quark mass difference as well as electromagnetic interactions, we have made use of SU(3) chiral perturbation theory in the presence of virtual photons. The pertinent results of this investigation can be summarised as follows:

(1) Already at tree level, one has strong as well as electromagnetic isospin violation. We have considered all physical channels and found that these effects are in general small (at most two percent). In particular, the relative corrections are smaller than in the comparable case of $\pi\pi$ scattering where isospin violation at tree level is a purely electromagnetic effect. We have also stressed that considering one particular source of isospin violation only can ensue very misleading results.

(2) Because of its relevance to the lifetime of πK atoms, we have considered the one loop corrections to the S–wave scattering length for the process $\pi^- K^- \to \pi^0 K^0$. The fourth order isospin symmetric corrections are moderate and the isospin violation effects at this order cancel to a large extent (for the central values of the low–energy constants used here). The uncertainty in these isospin violating contributions is mainly due to the poor knowledge of the electromagnetic LECs K_i, and is comparable to the one in the isospin symmetric amplitude induced by the variations in the strong LECs L_i. These results allow for a rather precise prediction of the lifetime of πK atoms with isospin breaking corrections and the

combined uncertainty of a size of the order of 1% (modulo the additional bound states corrections that still have to be calculated).

(3) We have also considered the radiative process $\pi^- K^+ \to \pi^0 K^0 \gamma$. We have explicitly demonstrated the cancellation of the infrared divergences. The remaining radiative cross section is strongly suppressed at threshold so that the properly redefined (finite) scattering length acquires no significant correction.

(4) We have completed the analysis of leading order isospin breaking corrections to the pion kaon threshold amplitudes that enter the description of pion kaon bound state properties by also considering the elastic charged channel $\pi^- K^+ \to \pi^- K^+$. A prediction for the strong contribution to the $2S - 2P$ energy level shift is hampered by the poor knowledge of the (strong) isoscalar scattering length. The uncertainty for the *extraction* of the linear combination $a_0^- + a_0^+$ as induced by electromagnetic corrections, however, is only about 3% and therefore sufficiently well under control. The isospin breaking shift for the central values of the low–energy constants involved is again about 1%.

(5) We have also evaluated the leading isospin violating corrections for the effective range b_0 and the P–wave scattering length a_1, numerically to one–loop order in the charge–exchange channel. They are somewhat more pronounced than for the S–wave scattering length.

In order to complete an effective field theory analysis of pion kaon atoms, these results now have to be incorporated into a study along the lines of [Ga99] (for pionium) and [LR00] (for pionic hydrogen). Such work is under way [GS02].

Chapter 6

Infrared regularisation for photon loops

In our study of isospin–breaking corrections in pion–kaon scattering, the main phenomenological motivation has been to provide the necessary input for the bound–state analysis of pion kaon atoms. In the formalism for these electromagnetically bound states, both pion and kaon are regarded as heavy particles, with all energies involved well below these mass scales. It might therefore have appeared natural to at least perform the intermediate step and do the analyses of the previous chapter in the newly developed heavy kaon scheme [Ro99, Ou01, FKM02]. This was avoided for rather practical reasons: in order to establish numerical values for the various new low–energy constants in that scheme, one has to resort to matching them to the three–flavour ChPT results anyway, as there are simply not enough low–energy data for kaon number conserving processes to fit all of them independently. Furthermore, the appropriate electromagnetic Lagrangian would have to be constructed entirely, with again no independent information on the corresponding constants available.

We therefore wish to discuss here only one very specific aspect of such a calculation: the appropriate regularisation of the photon loop integrals in schemes with heavy particles, both for heavy kaons and for heavy pions *and* kaons, using the infrared regularisation scheme. This investigation is also interesting for other calculations since the resulting loop integrals are of course the same as for specific radiative corrections in πN and NN scattering, say. Furthermore, such an investigation may deepen the understanding of the specific properties of photon loop diagrams such as infrared divergences and the Coulomb pole.

The main focus is on the triangle diagram that is the only "non trivial" diagram in pion–kaon scattering, see diagram (a) in Fig. 5.1. We also concentrate on the s–channel exchange that produces the pole in the center-of-mass momentum at threshold. We shall employ the following suggestive notation: "light" particles that produce low–energy singularities are written as superscripts, "heavy" particles as subscripts. Therefore, the infrared regularised loop integral for heavy kaons, corresponding to the full relativistic integral $G^{\pi K\gamma}(s)$, will be written as $G_K^{\pi\gamma}(s)$, the loop integral for heavy kaons and pions as $G_{\pi K}^{\gamma}(s)$. We shall furthermore write the regular parts as $RG_K^{\pi\gamma}(s)$, $RG_{\pi K}^{\gamma}(s)$.

6.1 The relativistic loop integral $G^{\pi K\gamma}(s)$

We briefly repeat the straightforward calculation of the scalar loop integral for the triangle diagram with one vanishing mass and on-shell external particles ($q_K^2 = M_K^2$, $q_\pi^2 = M_\pi^2$),

$$G^{\pi K\gamma}(s) = -i \int \frac{d^d k}{(2\pi)^4} \frac{1}{\Big((q_\pi+k)^2 - M_\pi^2\Big)\Big((q_K-k)^2 - M_K^2\Big)\Big(k^2 - m_\gamma^2\Big)} \quad . \tag{6.1}$$

We use a Feynman parameterisation according to

$$\frac{1}{ABC} = \int_0^1 dx \int_0^1 dy \int_0^1 dz\, \delta(x+y+z-1) \frac{2}{[xA + yB + zC]^3} \quad , \tag{6.2}$$

and the dimensional regularisation formula

$$-i \int \frac{d^d k}{(2\pi)^d} \frac{1}{(k^2-\Delta)^n} = \frac{(-1)^n}{(4\pi)^{d/2}} \frac{\Gamma(n-\frac{d}{2})}{\Gamma(n)} \left(\frac{1}{\Delta}\right)^{n-\frac{d}{2}} \quad , \tag{6.3}$$

to arrive at

$$\begin{aligned} G^{\pi K\gamma}(s) &= -\frac{\lambda^{4-d}}{(4\pi)^{d/2}} \Gamma\Big(3 - \frac{d}{2}\Big) \\ &\quad \times \int_0^1 dy \int_0^{1-y} dx \frac{1}{\Big[(x+y)(xM_K^2 + yM_\pi^2) - xys + (1-x-y)m_\gamma^2\Big]^{3-\frac{d}{2}}} \quad , \end{aligned}$$

with the regularisation scale λ. We keep d general here for later purposes. With the substitutions $w = x+y$, $z = x/w$ and the abbreviation $f(z) = zM_K^2 + (1-z)M_\pi^2 - z(1-z)s$, one finds

$$\begin{aligned} G^{\pi K\gamma}(s) &= -\frac{\lambda^{4-d}}{(4\pi)^{d/2}} \Gamma\Big(3-\frac{d}{2}\Big) \int_0^1 dz \int_0^1 dw \frac{w}{\Big[w^2 f(z) + (1-w)m_\gamma^2\Big]^{3-\frac{d}{2}}} \\ &= -\frac{\lambda^{4-d}}{(4\pi)^{d/2}} \frac{\Gamma(3-\frac{d}{2})}{d-4} \int_0^1 \frac{dz}{f(z)} \int_0^1 dw \frac{d}{dw} \Big[w^2 f(z) + (1-w)m_\gamma^2\Big]^{\frac{d}{2}-2} \\ &\quad + \mathcal{O}(m_\gamma^2) \quad . \end{aligned} \tag{6.4}$$

The general integration domain both in (x,y) and (w,z) is depicted in Fig. 6.1, with the doubly hatched area representing the specific integration domain of the formula

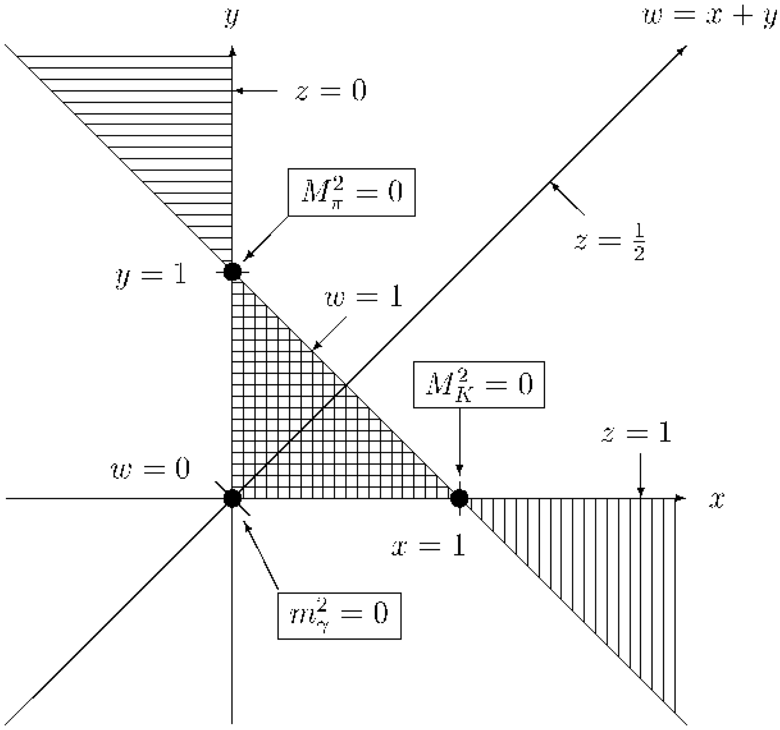

Figure 6.1: Integration variables and limits for the triangle diagram. The region hatched both vertically and horizontally is the original integration domain for the full relativistic integral. Its corners correspond to sub-subleading singularities for $M_K^2 = 0$, $M_\pi^2 = 0$, $m_\gamma^2 = 0$, respectively. Subtraction of the vertically and/or horizontally hatched regions subtracts the singularities corresponding to $M_K^2 = 0$ and/or $M_\pi^2 = 0$.

above, $0 \leq w, z \leq 1$. In this domain, the integral is (ultraviolet) finite, and we can take the limit $d = 4$ without running into divergences in $d - 4$. With the following further definitions:

$$F(a,b) = \frac{1}{32\pi^2} \int_a^b \frac{dz}{f(z)} \quad , \tag{6.5}$$

$$H(a,b) = \frac{1}{32\pi^2} \int_a^b dz \frac{\log \frac{f(z)}{s}}{f(z)} \quad , \tag{6.6}$$

we can write the result as

$$G^{\pi K\gamma}(s) = \log \frac{m_\gamma^2}{s} F(0,1) - H(0,1) \quad , \tag{6.7}$$

where the explicit forms for $F(0,1)$ and $H(0,1)$ can be written as

$$
\begin{aligned}
F(0,1) &= -\frac{1}{32\pi^2\sigma s}\left\{\log\frac{1-z_1}{1-z_2}+\log\frac{z_2}{z_1}-2\pi i\right\} \;, && (6.8)\\
H(0,1) &= -\frac{1}{32\pi^2\sigma s}\left\{\log^2(1-z_1)-\log^2(1-z_2)+\log^2 z_2-\log^2 z_1+\mathrm{Li}\left(\frac{z_1}{z_2}\right)\right.\\
&\quad\left.-\mathrm{Li}\left(\frac{z_2}{z_1}\right)+\mathrm{Li}\left(\frac{1-z_2}{1-z_1}\right)-\mathrm{Li}\left(\frac{1-z_1}{1-z_2}\right)-2\pi^2-4\pi i\log\sigma\right\} \;, && (6.9)
\end{aligned}
$$

where

$$
\begin{aligned}
z_{1/2} &= \frac{1}{2}\left(1-\frac{\Delta}{s}\right)\mp\frac{\sigma}{2} \;, \quad \sigma = \sqrt{1-\frac{2\Sigma}{s}+\frac{\Delta^2}{s^2}} \;,\\
\Sigma &= M_K^2+M_\pi^2 \;, \quad \Delta = M_K^2-M_\pi^2 \;, && (6.10)
\end{aligned}
$$

and

$$
\mathrm{Li}(z) = \int_1^z \frac{\log t}{1-t}dt \qquad (6.11)
$$

is the dilogarithm or Spence function. This is an unambiguous expression in the physical region for πK scattering, i.e. for $s > (M_K + M_\pi)^2$. We have checked that this loop function coincides with the analogous one needed for $\pi\pi$ scattering as given in [Wi96, KU98] when going to the limit of equal pion and kaon masses. We remark that in this representation, the Coulomb pole term, i.e. the kinematical divergence at threshold (in the real part), resides exclusively in the term $\propto -2\pi^2$ in the above expression for $H(0,1)$, all the logarithms and dilogarithms turn out to be regular at threshold.

What we want to investigate in the following is how this calculation has to be modified in order to isolate the infrared divergent parts of this loop integral in the case where either the kaon or both pion and kaon are no longer considered to be "light". In the case of heavy kaon ChPT, the prescription given in [BL99] is in principle straightforward, but turns out to be slightly unpractical when it comes to the analytical evaluation of the integrals involved. The reason is that we cannot use Eq. (6.2) straight away, but have to resort to a parameterisation

$$
\frac{1}{ABC} = 2\int_0^1 dx\int_0^1 dy\frac{1-x}{[(1-x)(yA+(1-y)C)+xB]^3} \;, \qquad (6.12)
$$

which, when appropriately collected, yields a representation for $G^{\pi K\gamma}(s)$ of the form

$$
\begin{aligned}
G^{\pi K\gamma}(s) &= -\frac{\lambda^{4-d}}{(4\pi)^{d/2}}\Gamma\left(3-\frac{d}{2}\right)\int_0^1 dx\int_0^1 dy && (6.13)\\
&\times\frac{1-y}{\left[(x+(1-x)y)(xM_K^2+(1-x)yM_\pi^2)-x(1-x)ys+(1-x)(1-y)m_\gamma^2\right]^{3-\frac{d}{2}}} \;.
\end{aligned}
$$

In order to obtain the infrared part, the x integration has to be extended to infinity, or, equivalently, the regular part is given by changing the x integration limits to $1 \leq x < \infty$. Analytic integration however seems only possible if one transforms the integration variables to the same set used for the full relativistic expression above, and one carefully has to keep track of the integration boundaries. (This can be achieved by setting $y' = (1-x)y$ and $w = x + y'$, $z = x/w$ similar to the above.)

6.2 Singularities in Feynman parameter space

An elegant way to visualise this problem and to arrive at the solution more quickly is given in [LP01], and is based on representing the singularity structure of Feynman diagrams according to its occurrence in Feynman parameter space. The tools to examine singularities in Feynman diagrams are the Landau equations. For an introduction, see [Ed66, IZ80], this short outline follows essentially the presentation in [LP01].

For a one loop Feynman diagram with I propagators $i/(q_i^2 - m_i^2 + i\epsilon)$, with momenta q_i flowing around the loop, combined by I Feynman parameters α_i subject to the constraint $\sum_{i=1}^{I} \alpha_i = 1$, the Landau equations read

$$\alpha_i \left(q_i^2 - m_i^2\right) = 0 \qquad \text{for each } i \ , \tag{6.14}$$

$$\sum_{i=1}^{I} \alpha_i q_i^\mu = 0 \qquad \text{for each } i \text{ with } \alpha_i \neq 0 \ . \tag{6.15}$$

The *leading singularity* is a solution of Eqs. (6.14), (6.15) with none of the α_i equal to zero. A solution with one, two... of the Feynman parameters vanishing is called *sub-leading, sub-subleading... singularity*. Subleading singularities correspond to leading singularities of the diagram with the propagator of the vanishing Feynman parameter contracted to a point. Multiplying Eq. (6.15) with $q_{j\mu}$ for all j indexing uncontracted propagators, one arrives at the eigenvalue problem

$$\sum_{i=1}^{I} (q_j \cdot q_i)\alpha_j = 0 \tag{6.16}$$

for the matrix

$$\Omega_{ji} = (q_j \cdot q_i) = \frac{1}{2}\left(m_j^2 + m_i^2 - (q_j - q_i)^2\right) \ , \tag{6.17}$$

where the on-shell condition derived from Eq. (6.14) has been used. For the pion kaon photon triangle, the maximal matrix Ω_{ji} corresponding to the leading singularity is

$$\begin{pmatrix} M_K^2 & \frac{1}{2}\left(M_K^2 + M_\pi^2 - s\right) & \frac{1}{2}\left(M_K^2 + m_\gamma^2 - q_K^2\right) \\ \frac{1}{2}\left(M_K^2 + M_\pi^2 - s\right) & M_\pi^2 & \frac{1}{2}\left(M_\pi^2 + m_\gamma^2 - q_\pi^2\right) \\ \frac{1}{2}\left(M_K^2 + m_\gamma^2 - q_K\right) & \frac{1}{2}\left(M_\pi^2 + m_\gamma^2 - q_\pi^2\right) & m_\gamma^2 \end{pmatrix} \ , \tag{6.18}$$

for external pion/kaon momenta $q_{\pi/K}$. Subleading singularities can be calculated from submatrices with one or two lines and rows erased. Specifically, one finds the following by solving for zero eigenvalues:

1. The leading singularity is given as a complicated manifold lying (partly) within the integration domain. We only mention one particular case for the kinematical conditions we are interested in, namely that for on-shell external particles, $q^2_{\pi/K} = M^2_{\pi/K}$, the determinant of Ω_{ji} vanishes for

$$s = M_K^2 + M_\pi^2 + 2\sqrt{M_K^2 - \frac{m_\gamma^2}{4}}\sqrt{M_\pi^2 - \frac{m_\gamma^2}{4}} - \frac{m_\gamma^2}{2} \ , \qquad (6.19)$$

   which is below, but very close to threshold (and coincides with the threshold for $m_\gamma \to 0$). It is unphysical as it occurs approximately for the Feynman parameter values

$$\alpha_K = \frac{2M_K}{M_K + M_\pi} + \mathcal{O}(m_\gamma^2) \ , \quad \alpha_\pi = \frac{2M_\pi}{M_K + M_\pi} + \mathcal{O}(m_\gamma^2) \ , \quad \alpha_\gamma = -1 \ , \qquad (6.20)$$

   with the suggestive notation $\alpha_{K/\pi/\gamma}$ for the parameters multiplying the kaon/pion/photon propagators, i.e. outside the integration domain.

2. Subleading singularities lie at the borders of the domain (i.e. one of the Feynman parameters equals zero), as one of the Feynman parameters vanishes. They correspond to the well–known two–particle cuts and are given as follows:

$$\begin{aligned}
\alpha_K = 0: &\quad q_\pi^2 = (M_\pi \pm m_\gamma)^2 \quad \text{for} \quad \alpha_\pi = \pm\frac{m_\gamma}{M_\pi \pm m_\gamma} \ , \quad \alpha_\gamma = \frac{M_\pi}{M_\pi \pm m_\gamma} \ ; \\
\alpha_\pi = 0: &\quad q_K^2 = (M_K \pm m_\gamma)^2 \quad \text{for} \quad \alpha_K = \pm\frac{m_\gamma}{M_K \pm m_\gamma} \ , \quad \alpha_\gamma = \frac{M_K}{M_K \pm m_\gamma} \ ; \\
\alpha_\gamma = 0: &\quad s = (M_K \pm M_\pi)^2 \quad \text{for} \quad \alpha_K = \pm\frac{M_\pi}{M_K \pm M_\pi} \ , \quad \alpha_\pi = \frac{M_K}{M_K \pm M_\pi} \ .
\end{aligned} \qquad (6.21)$$

   All the singularities for the respective "−" signs are pseudo–thresholds, they lie outside the integration domain in Feynman parameter space.

3. Sub-subleading singularities are associated with the corners of the Feynman parameter space (two parameters equal to zero), and correspond to

$$M_K^2 = 0 \ , \qquad M_\pi^2 = 0 \ , \qquad m_\gamma^2 = 0 \ . \qquad (6.22)$$

These sub-subleading singularities are depicted explicitly in Fig. 6.1. As they occur in the limits of one of the masses involved going to zero, they seize to be low–energy singularities as soon as these masses are heavy. The regular part of the loop integral that incorporates only the singularities of the heavy mass going to zero therefore has to be given by an integration domain that overlaps with the original domain in exactly these corner points. For the heavy kaon case, one can directly read off from Fig. 6.1 that the regular part, containing no singularities for $M_\pi \to 0$ or $m_\gamma \to 0$, can be obtained by integrating over the vertically hatched domain in Feynman parameter space. If, as in the non relativistic theory for πK bound states, the pion is also taken as a heavy particle, the horizontally hatched area is added to the regular part, as this contains the divergent pieces for $M_\pi \to 0$. Neither the infrared singularities for $m_\gamma \to 0$ nor the πK cut for $s > (M_K + M_\pi)^2$ are modified when subtracting these regular pieces.

6.3 The regular parts $RG_K^{\pi\gamma}(s)$ and $RG_\pi^{K\gamma}(s)$

We only show the calculation in detail for the regular part containing the $M_K^2 = 0$ singularities. Starting from Eq. (6.4), Fig. 6.1 makes it obvious that the integration has to be performed for $1 \leq w < \infty$, $1 \leq z < \infty$, leading to

$$\begin{aligned} RG_K^{\pi\gamma}(s) &= -\frac{\lambda^{4-d}}{(4\pi)^{d/2}} \frac{\Gamma(3-\frac{d}{2})}{d-4} \int_1^\infty \frac{dz}{f(z)} \left[w^2 f(z) + (1-w)m_\gamma^2\right]^{\frac{d}{2}-2}\Big|_1^\infty \\ &= \frac{\lambda^{4-d}}{(4\pi)^{d/2}} \frac{\Gamma(3-\frac{d}{2})}{d-4} \int_1^\infty f(z)^{\frac{d}{2}-3} \quad , \end{aligned} \tag{6.23}$$

which, after expanding all pieces in $d-4$, is found to be

$$\begin{aligned} RG_K^{\pi\gamma}(s) &= \frac{1}{16\pi^2}\left\{\frac{1}{d-4} + \frac{1}{2}\left(\gamma_E - \log 4\pi\right)\right\} \int_1^\infty \frac{dz}{f(z)} + \frac{1}{32\pi^2} \int_1^\infty dz \frac{\log \frac{f(z)}{\lambda^2}}{f(z)} \\ &= \left(\tilde{L} + \log \frac{s}{\lambda^2}\right) F(1,\infty) + H(1,\infty) \quad , \end{aligned} \tag{6.24}$$

where $\tilde{L}$ collects the divergent plus some finite pieces and is related to the "standard" L by $\tilde{L} = 32\pi^2 L + 1$. Of course, the expression associated with the regular part in $M_\pi^2 = 0$ singularities is obtained in a completely analogous fashion and can be written as

$$RG_\pi^{K\gamma}(s) = \left(\tilde{L} + \log \frac{s}{\lambda^2}\right) F(-\infty, 0) + H(-\infty, 0) \quad . \tag{6.25}$$

This is meant to imply $RG_{\pi K}^{\gamma}(s) = RG_K^{\pi\gamma}(s) + RG_\pi^{K\gamma}(s)$, of course. We also write down the explicit formulae for all functions $F(a,b)$ and $H(a,b)$, and expand them in appropriate variables for the heavy–kaon regime:

$$\mu = \frac{M_\pi}{M_K} \quad , \qquad \Omega = \frac{s - M_K^2 - M_\pi^2}{2M_\pi M_K} \quad , \tag{6.26}$$

where Ω is of order 1 in the heavy–kaon expansion. Besides, a threshold expansion corresponds to an expansion in powers of $(\Omega - 1)$. We then find:

$$F(-\infty, 0) = \frac{1}{32\pi^2 \sigma s} \log \frac{z_2}{z_1} \tag{6.27}$$

$$
\begin{aligned}
&= \frac{1}{32\pi^2 M_K^2}\left\{\frac{1}{2\mu\sqrt{\Omega^2-1}}\log\left(\frac{\Omega+\sqrt{\Omega^2-1}}{\Omega-\sqrt{\Omega^2-1}}\right) - 1 + \Omega\mu + \mathcal{O}(\mu^2)\right\} \;, \\
F(1,\infty) &= \frac{1}{32\pi^2\sigma s}\log\frac{1-z_1}{1-z_2} = \frac{1}{32\pi^2 M_K^2}\left\{1 - \Omega\mu + \mathcal{O}(\mu^2)\right\} \;, \qquad (6.28) \\
H(-\infty,0) &= \frac{1}{32\pi^2\sigma s}\left\{\log^2 z_2 - \log^2 z_1 + \mathrm{Li}\left(\frac{z_1}{z_2}\right) - \mathrm{Li}\left(\frac{z_2}{z_1}\right)\right\} \\
&= \frac{1}{32\pi^2 M_K^2}\left\{-\frac{1}{2\mu\sqrt{\Omega^2-1}}\left[\mathrm{Li}\left(\frac{\Omega+\sqrt{\Omega^2-1}}{\Omega-\sqrt{\Omega^2-1}}\right) - \mathrm{Li}\left(\frac{\Omega-\sqrt{\Omega^2-1}}{\Omega+\sqrt{\Omega^2-1}}\right)\right]\right. \\
&\quad + \left[\frac{\log\mu}{\mu} - 2\Omega + \left(2\Omega^2-1\right)\mu\right]\frac{1}{\sqrt{\Omega^2-1}}\log\left(\frac{\Omega+\sqrt{\Omega^2-1}}{\Omega-\sqrt{\Omega^2-1}}\right) \\
&\quad \left. -2\log\mu + (3 + 2\log\mu)\,\Omega\mu + \mathcal{O}(\mu^2)\right\} \;, \qquad (6.29) \\
H(1,\infty) &= \frac{1}{32\pi^2\sigma s}\left\{\log^2(1-z_1) - \log^2(1-z_2) + \mathrm{Li}\left(\frac{1-z_2}{1-z_1}\right) - \mathrm{Li}\left(\frac{1-z_1}{1-z_2}\right)\right\} \\
&= \frac{1}{16\pi^2 M_K^2}\left\{1 - 2\Omega\mu + \mathcal{O}(\mu^2)\right\} \;. \qquad (6.30)
\end{aligned}
$$

We summarise the following properties of the various pieces:

1. Both functions associated with the heavy–kaon singularities, $F(1,\infty)$ and $H(1,\infty)$, can be expanded as simple polynomials in μ and Ω in the low energy regime, they are indeed regular.

2. The integration domain associated with the $M_\pi^2 = 0$ singularities, in contrast, includes terms diverging like $1/\mu$ and $\log\mu$ as well as complicated non analytic functions of Ω.

These two points lead to one important conclusion: if our main goal had been to isolate only the *leading* term in the M_π/M_K expansion of the infrared singular part of the integral, i.e. the loop integral in strict heavy–kaon counting, one could have abbreviated the procedure and directly expand the full relativistic integral in μ. Power counting immediately shows that the leading term has to be of order $1/\mu$, while the difference between the relativistic and the infrared singular part is regular in μ.

3. Neither of these two domains displays any of the special features associated with the masslessness of the exchanged photon: $\log m_\gamma$ singularities and the Coulomb pole (i.e. the threshold expansion is regular). These reside entirely in the functions $F(0,1)$ and $H(0,1)$.

4. Neither domain includes an imaginary part (for the kinematical region considered), the πK cut is unaffected.

In order to illustrate the last two points, we give the explicit and rather compact expression for the triangle diagram with both the M_π^2 and the M_K^2 divergences subtracted:

$$\begin{aligned} G^\gamma_{\pi K}(s) &= -\frac{1}{32\pi^2\sigma s}\left\{\log\frac{z_2}{z_1}+\log\frac{1-z_1}{1-z_2}\right\}\left(\tilde{L}+\log\frac{m_\gamma^2}{\lambda^2}\right) \\ &\quad -\frac{1}{16\sigma s}+\frac{i}{16\pi\sigma s}\left(\log\frac{m_\gamma^2}{s}-2\log\sigma\right) \ , \end{aligned} \tag{6.31}$$

which is the "minimal" low energy representation of this diagram, retaining nothing but the (photon) infrared divergence, the Coulomb pole, and the πK cut structure.

6.4 Other domains of integration; infrared divergences, Coulomb pole

We have calculated the triangle loop integral in all possible domains and collected the results in terms of functions $F(a,b)$ and $H(a,b)$, as displayed in Fig. 6.2. All the infinite domains contain pieces that diverge in four space–time dimensions, we collect these in terms of $\tilde{L}$ as defined above. Furthermore, when summing different integration domains, it is useful to note

$$F(-\infty,\infty) = \frac{i}{16\pi\sigma s} = \frac{i}{32\pi M_K^2\,\mu\sqrt{\Omega^2-1}} \ , \tag{6.32}$$

$$\begin{aligned} H(-\infty,\infty) &= \frac{1}{16\sigma s}+\frac{i\log\sigma}{8\pi\sigma s} = \frac{1}{32M_K^2}\left\{\frac{1}{\mu\sqrt{\Omega^2-1}}\right. \\ &\quad \left. +\frac{2i}{\pi\sqrt{\Omega^2-1}}\left[\frac{1}{\mu}\log\left(2\mu\sqrt{\Omega^2-1}\right)-2\Omega+\left(2\Omega^2-1\right)\mu+\mathcal{O}(\mu^2)\right]\right\} \ . \end{aligned} \tag{6.33}$$

These isolate exclusively the pieces with irregular threshold behaviour from the expressions appearing in the relativistic loop integral. We note that adding up *all* integration domains yields the sum zero.

Fig. 6.2 shows how one can quickly recover the $\log m_\gamma$ terms alone, throwing away even the πK cuts and the Coulomb pole, by extending the w integration to infinity as compared to the original domain for the fully relativistic expression, Eq. (6.4) (or, equivalently, integrate the domain $-\infty < w \leq 0$). The infrared divergence of the photon loop is therefore a sub-subleading divergence associated with the $m_\gamma^2 = 0$ corner of the integration domain.

The origin of the Coulomb pole, in contrast, is slightly more difficult to locate: in terms of the functions defined above, it is included in $H(-\infty,\infty)$ and still persists if all the sub-subleading singularities are subtracted. As we mentioned before and as

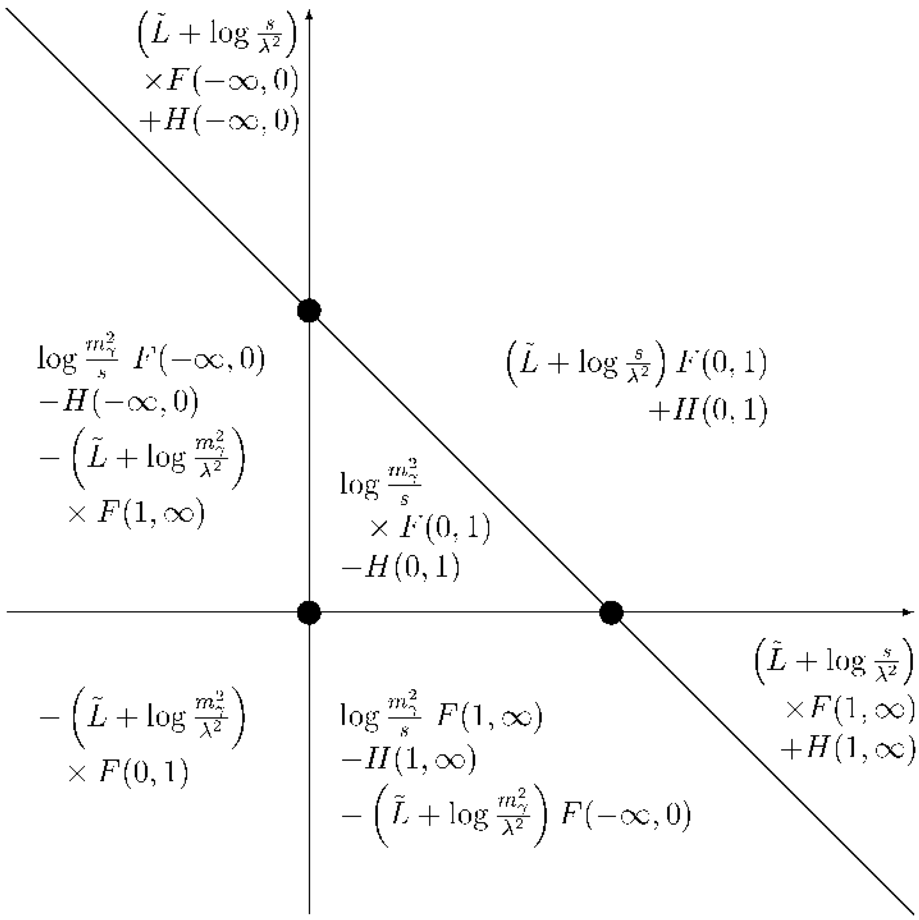

Figure 6.2: Different domains of integration for the triangle diagram. All entries have to be multiplied by $1/32\pi^2$.

can be seen by solving the Landau equation for the leading (pinch) singularity, there is a singularity near threshold for

$$\begin{aligned} s &= M_K^2 + M_\pi^2 + 2\sqrt{M_K^2 - \frac{m_\gamma^2}{4}}\sqrt{M_\pi^2 - \frac{m_\gamma^2}{4}} - \frac{m_\gamma^2}{2} \\ &= (M_K + M_\pi)^2\left(1 - \frac{m_\gamma^2}{4M_K M_\pi}\right) + \mathcal{O}\left(m_\gamma^4\right) \quad , \end{aligned} \tag{6.34}$$

which, however, is located on an unphysical Riemann sheet [Ed66, IZ80]. For finite m_γ, therefore, both real and imaginary parts of the amplitude are regular near threshold (as is, say, the nucleon–nucleon scattering amplitude with pion exchange plus point interaction). However, in the physical case of $m_\gamma = 0$, the singularity coincides with the physical threshold and thereby causes the disturbance as given by the pole in center-of-mass momentum. This is actually very similar to what happens to the isovector nucleon form factor spectral function in heavy baryon ChPT as discussed in Chapter 2.3.2, 2.3.3: the anomalous threshold in the triangle diagram (under different kinematical conditions, at $t = 4M_\pi^2 - M_\pi^4/m_N^2$) coincides with the physical threshold to leading order in the chiral expansion, resulting in a wrong analytic threshold behaviour. Here, however, the "distorted" analytic behaviour *is* physical and is caused by the exchange of a massless particle, not by an "artificial" expansion around the limit of vanishing pion mass.

6.5 $u-$ and $t-$channel

We only briefly comment on the photon triangle loop integral in the $u-$ and $t-$channels, as it is needed for the radiative corrections in the charged–to–charged channel $\pi^- K^+ \to \pi^- K^-$, see Fig. 5.4. We discuss this issue for heavy kaons and light pions first. The representation given by Eqs. (6.7), (6.24) for the $s-$channel holds equally for the u–channel, with the appropriate analytical continuations for the kinematical region $u < (M_K - M_\pi)^2$,

$$G_K^{\pi\gamma}(u) = \log\frac{m_\gamma^2}{u} F(0,1) - \left(\tilde{L} + \log\frac{u}{\lambda^2}\right) F(1,\infty) - H(0,\infty) \quad , \tag{6.35}$$

where

$$\begin{aligned} F(0,1) &= -\frac{1}{32\pi^2\sigma u}\left\{\log\frac{1-z_1}{1-z_2} + \log\frac{z_2}{z_1}\right\} \quad , & (6.36)\\ H(0,\infty) &= -\frac{1}{32\pi^2\sigma u}\left\{\log^2(-z_2) - \log^2(-z_1) + \mathrm{Li}\Big(\frac{z_1}{z_2}\Big) - \mathrm{Li}\Big(\frac{z_2}{z_1}\Big)\right\} \quad , & (6.37) \end{aligned}$$

and $F(1,\infty)$ can be taken directly from Eq. (6.28). The threshold expansion Eq. (5.66) then changes to

$$\begin{aligned} G_K^{\pi\gamma}(u) &= -\frac{1}{32\pi^2(M_K - M_\pi)}\left\{\frac{1}{M_K}\left(\tilde{L} + 2\log\frac{m_\gamma}{\lambda}\right) + \frac{2}{M_\pi}\left(1 - \log\frac{m_\gamma}{M_\pi}\right)\right\} + \mathcal{O}(q) \\ &= G^{\pi K\gamma}(u) - \frac{1}{32\pi^2 M_K(M_K - M_\pi)}\left\{\tilde{L} + 2\log\frac{M_K}{\lambda} + 2\right\} + \mathcal{O}(q) \quad . \end{aligned} \tag{6.38}$$

If the pion is still considered a light particle, $G^{\pi\pi\gamma}(t)$ and its threshold expansion Eq. (5.67) of course do not change, but the analogous $G^{KK\gamma}(t)$ does. Here it does not suffice to subtract the sub-subleading singularities, but rather we have to subtract the KK cut, too ($t - 4M_K^2$ for $t \leq 0$ is not a small variable any more), as described in the previous paragraph in order to isolate the $\log m_\gamma$ terms alone. We find the representation and threshold behaviour

$$G_{KK}^{\gamma}(t) = -\frac{1}{16\pi^2\sigma t}\log\frac{\sigma+1}{\sigma-1}\left(\tilde{L} + \log\frac{m_\gamma^2}{\lambda^2}\right)$$

$$= \frac{1}{32\pi^2 M_K^2}\left(\tilde{L} + \log\frac{m_\gamma^2}{\lambda^2}\right) + \mathcal{O}(q) \quad , \tag{6.39}$$

where now $\sigma = \sqrt{1 - 4M_K^2/t}$. We once more note that the infrared behaviour is unchanged, only ultraviolet divergences are newly introduced.

In order to find the appropriate low energy representation with heavy kaons *and* pions, no additional work has to be done for the t–channel: the representation Eq. (6.39) only has to be used for $G^\gamma_{\pi\pi}(t)$, too. For the u–channel, however, the distance to the two–particle cut near threshold is not small any longer, $u-(M_K+M_\pi)^2 \overset{\text{thr}}{\approx} -4M_K M_\pi$, such that we cannot use a crossing–symmetric form to Eq. (6.31)[#1]. We therefore have to subtract the cut, too, and use a similar representation as for the t–channel in Eq. (6.39),

$$\begin{aligned}
G^\gamma_{\pi K}(u) &= -\frac{1}{32\pi^2\sigma u}\left\{\log\frac{1-z_1}{1-z_2} + \log\frac{z_2}{z_1}\right\}\left(\tilde{L} + \log\frac{m_\gamma^2}{\lambda^2}\right) \\
&= \frac{1}{32\pi^2 M_K M_\pi}\left(\tilde{L} + \log\frac{m_\gamma^2}{\lambda^2}\right) + \mathcal{O}(q) \quad . \qquad (6.40)
\end{aligned}$$

This completes our study of low energy representations of the pion kaon photon triangle diagram.

6.6 Other photon loops

The other two types of photon loop diagrams displayed in Fig. 5.1 are dealt with very easily in infrared regularisation. Both can be discussed in terms of the self–energy diagram consisting of a photon loop around a meson (pion or kaon), which we shall briefly consider here. We write M for either pion or kaon mass, and use the abbreviations

$$\alpha = \frac{m_\gamma}{M} \quad , \qquad \Omega = \frac{s - M^2 - m_\gamma^2}{2m_\gamma M} \quad .$$

We write both the scalar loop function for two propagators involving different masses $J(s)$ and its infrared part $I(s)$ in terms of these variables (dropping infinite pieces $\propto L$):

$$\begin{aligned}
J(s) &= -\frac{1}{8\pi^2}\left\{\log\frac{M}{\lambda} - \frac{1}{2}\right. \\
&\left. + \frac{\alpha}{1+2\alpha\Omega+\alpha^2}\left[(\Omega+\alpha)\log\alpha + \sqrt{1-\Omega^2}\arccos(-\Omega)\right]\right\} \quad , \qquad (6.41)
\end{aligned}$$

[#1]In fact, that representation has an unphysical imaginary part for $s < (M_K - M_\pi)^2$, which however does not have to bother us: the *low energy* structure is unadulterated.

$$
\begin{aligned}
I(s) &= -\frac{1}{8\pi^2}\frac{\alpha}{1+2\alpha\Omega+\alpha^2}\Bigg[(\Omega+\alpha)\Big(\log\frac{m_\gamma}{\lambda}-\frac{1}{2}\Big) \\
&\qquad +\sqrt{1-\Omega^2}\arccos\Big(-\frac{\Omega+\alpha}{\sqrt{1+2\alpha\Omega+\alpha^2}}\Big)\Bigg] \quad , \qquad (6.42)
\end{aligned}
$$

(in appropriate representations near the on-shell point $s = M^2$). The self-energy diagrams are given by

$$
\begin{aligned}
\Sigma(s) &= e^2\left\{4s\left(J(s)-J^{(1)}(s)\right)-\Delta\right\} \quad , \qquad (6.43)\\
\Sigma_I(s) &= e^2\left\{4s\left(I(s)-I^{(1)}(s)\right)\right\} \quad , \qquad (6.44)
\end{aligned}
$$

where

$$
\begin{aligned}
J^{(1)}(s) &= \frac{1}{2s}\left\{\left(s-M^2+m_\gamma^2\right)J(s)+\Delta_\gamma-\Delta\right\} \quad , \qquad (6.45)\\
I^{(1)}(s) &= \frac{1}{2s}\left\{\left(s-M^2+m_\gamma^2\right)I(s)+\Delta_\gamma\right\} \quad , \qquad (6.46)
\end{aligned}
$$

and

$$
\Delta = \frac{M^2}{8\pi^2}\log\frac{M}{\lambda} \quad , \qquad \Delta_\gamma = \frac{m_\gamma^2}{8\pi^2}\log\frac{m_\gamma}{\lambda} \quad . \qquad (6.47)
$$

(The difference here is that the heavy tadpoles Δ vanish in the infrared part.) In addition, we define the regular part of the self energy $\Sigma_R(s) = \Sigma(s) - \Sigma_I(s)$. Putting pieces together and expanding the resulting expressions for the self energy around the on-shell point $\Omega = -\alpha/2$ and in powers of α, we find

$$
\begin{aligned}
\frac{\Sigma(s)}{e^2M^2} &= \left\{\frac{1}{8\pi^2}\left(2-3\log\frac{M}{\lambda}\right)-\frac{\alpha}{4\pi}+\mathcal{O}(\alpha^2)\right\} \qquad (6.48)\\
&+ \left\{-\frac{1}{8\pi^2}\left(1+2\log\frac{m_\gamma}{\lambda}\right)+\frac{\alpha}{16\pi}+\mathcal{O}(\alpha^2)\right\}2\alpha\left(\Omega+\frac{\alpha}{2}\right)+\mathcal{O}\Big(\Omega+\frac{\alpha}{2}\Big)^2 \quad ,\\
\frac{\Sigma_I(s)}{e^2M^2} &= \left\{-\frac{\alpha}{4\pi}+\mathcal{O}(\alpha^2)\right\}+\left\{-\frac{1}{8\pi^2}\left(1+2\log\frac{m_\gamma}{\lambda}\right)+\frac{\alpha}{16\pi}+\mathcal{O}(\alpha^2)\right\}2\alpha\left(\Omega+\frac{\alpha}{2}\right)\\
&\qquad +\mathcal{O}\Big(\Omega+\frac{\alpha}{2}\Big)^2 \quad , \qquad (6.49)\\
\frac{\Sigma_R(s)}{e^2M^2} &= \left\{\frac{1}{8\pi^2}\left(2-3\log\frac{M}{\lambda}\right)+\mathcal{O}(\alpha^2)\right\}+\mathcal{O}(\alpha^2)\,2\alpha\left(\Omega+\frac{\alpha}{2}\right)+\mathcal{O}\Big(\Omega+\frac{\alpha}{2}\Big)^2 \quad .\\
&\qquad (6.50)
\end{aligned}
$$

As the physical limit corresponds to $\alpha \to 0$, we have written down terms of higher order in α than actually needed, just to demonstrate further cancellations of non–analytic terms in the regular part. We note the following:

1. The on-shell value of the self energy that leads to electromagnetic mass renormalisation vanishes for $m_\gamma \to 0$ in the infrared part: for heavy mesons, the electromagnetic mass shift is given, to one-loop order, by counterterms, in contrast to the fully relativistic result.

2. On the contrary, the derivative of the self energy at the on-shell point, leading to the wave function renormalisation factor, is fully maintained in the infrared part (or, equivalently, the derivative of the regular part vanishes). In particular, the infrared divergence $\propto \log m_\gamma$ is preserved. This could of course have been anticipated as the cancellation of these infrared divergences via inclusion of bremsstrahlung cannot depend on a regularisation prescription of loop diagrams.

We conclude that diagram (c) in Fig. 5.1 remains unchanged, no matter what regularisation prescription is used, while diagram (b) as well as mass shifts due to photon loops vanish for heavy mesons.

Outlook

In the end of each chapter, we have summarised the various results, such that we refrain from repeating our findings again here and instead rather point towards more general extensions and possibilities of future research related to both main parts of this work. The common ground for these different applications is that the theoretical tools used throughout this work have been demonstrated to finally allow for a model independent analysis of the many precision data in low–energy hadron physics that are already available or about to come. We only briefly discuss three particular examples.

Pion photo– and electroproduction on the nucleon.

Much experimental effort is devoted to measuring pion photo– and electroproduction close to threshold. Very precise data from MAMI, SAL, and NIKHEF are already available, further runs at MAMI are planned for the near future. While the description of these processes has been one of the key successes of chiral perturbation theory involving nucleons in the past ten years [BKM96a, BKM01, BKLM94, BKM96b], several further extensions are still desirable.

First of all, a calculation in the infrared regularisation scheme would be a natural extension of the analyses done for the electromagnetic form factors in Chapter 2, allowing for another important comparison of the relativistic and heavy–baryon approaches. Recent data for electroproduction at MAMI [A102] show a seemingly strong discrepancy between the data taken at photon virtualities $Q^2 = 0.1$ GeV^2 and $Q^2 = 0.05$ GeV^2, such that a renewed analysis in the framework of relativistic chiral perturbation theory is very interesting not only from a purely theoretical, but also from a phenomenological point of view.

There is a second strong incentive to perform such a relativistic calculation: in order to obtain experimental information on electroproduction amplitudes on the neutron, actual measurements always have to be performed with a nuclear target, preferably deuterium or ^{3}He. ChPT investigations of photo– [Be97] and electroproduction [KBM00] on the deuteron exist and will soon be extended to higher order such that the single–nucleon amplitude becomes the limiting factor in the accuracy of such a calculation. Moreover, as the inclusion of this single–nucleon amplitude involves a Lorentz boost of the same, also having a manifestly invariant representation of this amplitude would largely facilitate such an analysis.

Third, due to the high quality of data near threshold, pion production might be an even more suitable process than pion nucleon scattering for the extraction of isospin violating effects in the single nucleon sector. One of these effects, the cusp due to the $\pi^- n$ to $\pi^0 p$ mass difference, is already included in the existing calculations. Once a complete one loop analysis of all isospin channels and all relevant partial waves will have been achieved, one should go beyond that and systematically include all isospin breaking effects up to a certain order in the chiral power counting. Moreover, this reaction also permits conclusions about isospin violation again in pion–nucleon scattering, as it allows for the direct determination of the imaginary part of the S–wave amplitude and thus the neutral pion–proton scattering length, through a measurement of the polarised target asymmetries.

Isospin violation and electromagnetic corrections in the pion form factor.

Several experiments in the regime of low energy Goldstone boson interactions have reached a level of accuracy that requires to take isospin violating effects and electromagnetic corrections into account. Chiral perturbation theory, as we have seen, is the preferred tool to investigate such effects, as it allows for a consistent treatment of isospin violation due to both the light quark mass difference and electromagnetism. One particularly important topic are the electromagnetic corrections to the pion vector form factor, which are of great interest for the hadronic corrections to the anomalous magnetic moment of the muon that we have already discussed in the introduction (see [Me01]). While these have been evaluated to one loop order both in chiral power counting and in the fine structure constant [KM00b], one should certainly go beyond this level of accuracy. An isospin symmetric calculation to two loop order exists [GM91, BCT98], such that it is a feasible goal to add leading–order electromagnetic corrections to this representation.

Hadronic Atoms.

As we have emphasised in Chapter 5, much of the relevance of the isospin violation studies on meson meson scattering lies in the extraction of the hadronic scattering lengths from bound state experiments. Isospin breaking effects however do not only enter via corrections to the scattering amplitude at threshold, there are additional effects that can only be calculated within the bound state formalism. Much work in this area has been done over the past few years, ongoing efforts include the generalisation of the pionium results to pion–kaon bound states [GS02]. Remaining problems that are objects of current experimental efforts include πd (see [Be02] for an effective field theory analysis) and KN bound states, and while it is obvious that these do not lend themselves so easily to chiral perturbation theory and effective field theory analyses, it might still be worthwhile to gain an understanding of these processes as far as possible, and to at least estimate the isospin breaking corrections involved.

Appendix A

Explicit representations for baryon form factors

A.1 Loop integrals

In this appendix, we define the loop integrals needed in this paper and evaluate them in the infrared regularisation scheme.

A.1.1 Definition of the loop integrals

We use the following notation:

$$p'_\mu + p_\mu = Q_\mu \ , \qquad p'_\mu - p_\mu = q_\mu \ , \qquad t = q^2 \ .$$

Define the following loop integrals:

$$\frac{1}{i}\int_I \frac{d^dk}{(2\pi)^d}\frac{1}{M^2-k^2} \;=\; \Delta \ , \tag{A.1}$$

$$\frac{1}{i}\int_I \frac{d^dk}{(2\pi)^d}\frac{1}{[M^2-k^2][M^2-(k+q)^2]} \;=\; J(t) \ , \tag{A.2}$$

$$\frac{1}{i}\int_I \frac{d^dk}{(2\pi)^d}\frac{k_\mu}{[M^2-k^2][M^2-(k+q)^2]} \;=\; -\frac{1}{2}q_\mu J(t) \ , \tag{A.3}$$

$$\frac{1}{i}\int_I \frac{d^dk}{(2\pi)^d}\frac{k_\mu k_\nu}{[M^2-k^2][M^2-(k+q)^2]} \;=\; \Big(q_\mu q_\nu - g_{\mu\nu}t\Big)\, J^{(1)}(t) + q_\mu q_\nu\, J^{(2)}(t) \ , \tag{A.4}$$

$$\frac{1}{i}\int_I \frac{d^dk}{(2\pi)^d}\frac{1}{[M^2-k^2][m^2-(p-k)^2]} \;=\; I(p^2) \ , \tag{A.5}$$

$$\frac{1}{i}\int_I \frac{d^dk}{(2\pi)^d}\frac{k_\mu}{[M^2-k^2][m^2-(p-k)^2]} \;=\; p_\mu\, I^{(1)}(p^2) \ , \tag{A.6}$$

$$\frac{1}{i}\int_I \frac{d^dk}{(2\pi)^d}\frac{1}{[M^2-k^2][m^2-(p-k)^2][m^2-(p'-k)^2]} = I_{12}(t,p^2,p'^2) \ , \tag{A.7}$$

$$\frac{1}{i}\int_I \frac{d^dk}{(2\pi)^d}\frac{k_\mu}{[M^2-k^2][m^2-(p-k)^2][m^2-(p'-k)^2]} = Q_\mu I_{12}^{(1)}(t,p^2,p'^2) + q_\mu I_{12}^{(2)}(t,p^2,p'^2) \ , \tag{A.8}$$

$$\frac{1}{i}\int_I \frac{d^dk}{(2\pi)^d}\frac{k_\mu k_\nu}{[M^2-k^2][m^2-(p-k)^2][m^2-(p'-k)^2]} = g_{\mu\nu} I_{12}^{(3)}(t,p^2,p'^2) \tag{A.9}$$
$$+Q_\mu Q_\nu I_{12}^{(4)}(t,p^2,p'^2) + q_\mu q_\nu I_{12}^{(5)}(t,p^2,p'^2) + \left(q_\mu Q_\nu + q_\nu Q_\mu\right) I_{12}^{(6)}(t,p^2,p'^2) \ ,$$

$$\frac{1}{i}\int_I \frac{d^dk}{(2\pi)^d}\frac{1}{[M^2-k^2][M^2-(k+q)^2][m^2-(p-k)^2]} = I_{21}(t,p^2,p'^2) \ , \tag{A.10}$$

$$\frac{1}{i}\int_I \frac{d^dk}{(2\pi)^d}\frac{k_\mu}{[M^2-k^2][M^2-(k+q)^2][m^2-(p-k)^2]} = Q_\mu I_{21}^{Q}(t,p^2,p'^2) + q_\mu I_{21}^{q}(t,p^2,p'^2) \ , \tag{A.11}$$

$$\frac{1}{i}\int_I \frac{d^dk}{(2\pi)^d}\frac{k_\mu k_\nu}{[M^2-k^2][M^2-(k+q)^2][m^2-(p-k)^2]} = g_{\mu\nu} I_{21}^{00}(t,p^2,p'^2) \tag{A.12}$$
$$+Q_\mu Q_\nu I_{21}^{QQ}(t,p^2,p'^2) + q_\mu q_\nu I_{21}^{qq}(t,p^2,p'^2) + \left(q_\mu Q_\nu + q_\nu Q_\mu\right) I_{21}^{qQ}(t,p^2,p'^2) \ ,$$

where $\int_I$ symbolises loop integration according to the infrared regularisation scheme. In the case of equal external on-shell momenta $p^2 = p'^2$, we shall sometimes use the simplified notation $I_{12}^{(i)}(t,p^2) \equiv I_{12}^{(i)}(t,p^2,p^2)$.

A.1.2 Reduction of the tensorial loop integrals

The reduction of the tensorial loop integrals to the corresponding scalar ones can be performed in the standard way. For all form factors except for the $\Lambda - \Sigma^0$ transition we have the simplification $p^2 = p'^2$. In this case, the tensor loop functions $I_{12}^{(2)}(t,p^2)$ and $I_{12}^{(6)}(t,p^2)$ vanish on symmetry reasons alone. When applying power counting arguments, many of the terms proportional to (powers of) $p^2 - p'^2$, $p^2 - m^2$ etc. are, strictly speaking, of higher order and could be neglected, we prefer, however, to give the kinematically exact forms here. As useful abbreviations, we shall employ

$$\tilde{M}^2 = \frac{1}{2}\left(M^2 + \bar{p}^2 - m^2\right) \ , \qquad \bar{p}^2 = \frac{1}{2}\left(p^2 + p'^2\right) \ , \qquad \Delta p^2 = p^2 - p'^2 \ ,$$
$$p = \sqrt{p^2} \ , \qquad p' = \sqrt{p'^2} \ .$$

p/p', in our case, are really the masses of the (incoming/outgoing) external baryons, whereas m is the mass of the intermediate baryon state. Note that we use the sloppy notation Δp^4 for $(\Delta p^2)^2$. We find

$$J^{(1)}(t) = \frac{1}{4(d-1)\,t}\Big\{(t-4M^2)J(t) + 2\Delta\Big\} \ , \tag{A.13}$$

$$
\begin{aligned}
J^{(2)}(t) &= \frac{1}{4}J(t) - \frac{1}{2t}\Delta \quad , && \text{(A.14)}\\
I^{(1)}(p^2) &= \frac{1}{2p^2}\Big\{2\tilde{M}^2\, I(p^2) + \Delta\Big\} \quad , && \text{(A.15)}\\
I^{(1)}_{12}(t,p^2,p'^2) &= \frac{1}{2\left(4\bar{p}^2 - t - \frac{\Delta p^4}{t}\right)}\Bigg\{\Big(1+\frac{\Delta p^2}{t}\Big)I(p^2) + \Big(1-\frac{\Delta p^2}{t}\Big)I(p'^2) \\
&\quad +\Big(4\tilde{M}^2 - \frac{\Delta p^4}{t}\Big)\, I_{12}(t,p^2,p'^2)\Bigg\} \quad , && \text{(A.16)}\\
I^{(2)}_{12}(t,p^2,p'^2) &= \frac{1}{2t\left(4p^2 - t - \frac{\Delta p^4}{t}\right)}\Bigg\{\Big(4\bar{p}^2 - t\Big)\Big(I(p^2) - I(p'^2)\Big) && \text{(A.17)}\\
&\quad +\Delta p^2\Big[I(p^2) + I(p'^2) - \Big(4(\bar{p}^2 - \tilde{M}^2) - t\Big)\, I_{12}(t,p^2,p'^2)\Big]\Bigg\} \quad ; \\
I^{(3)}_{12}(t,p^2,p'^2) &= \frac{1}{d-2}\Bigg\{M^2 I_{12}(t,p^2,p'^2) - 2\tilde{M}^2 I^{(1)}_{12}(t,p^2,p'^2) + \frac{\Delta p^2}{2} I^{(2)}_{12}(t,p^2,p'^2)\Bigg\}, \\
& && \text{(A.18)}\\
I^{(4)}_{12}(t,p^2,p'^2) &= -\frac{1}{4\bar{p}^2 - t - \frac{\Delta p^4}{t}}\Bigg\{\frac{1}{d-2}\Big[M^2 I_{12}(t,p^2,p'^2) \\
&\qquad -2(d-1)\tilde{M}^2 I^{(1)}_{12}(t,p^2,p'^2) + \frac{\Delta p^2}{2} I^{(2)}_{12}(t,p^2,p'^2)\Big] \\
&\quad -\frac{1}{4}\Big(1 - \frac{\Delta p^4}{2\bar{p}^2 t}\Big)\Big(I^{(1)}(p^2) + I^{(1)}(p'^2)\Big) && \text{(A.19)}\\
&\quad +\frac{\Delta p^2}{8\bar{p}^2}\Big[\frac{\Delta p^2}{t}\Big(4\tilde{M}^2 + t\Big) I^{(1)}_{12}(t,p^2,p'^2) \\
&\qquad -\Big(4\tilde{M}^2 - \frac{\Delta p^4}{t}\Big) I^{(2)}_{12}(t,p^2,p'^2)\Big]\Bigg\} \quad , \\
I^{(5)}_{12}(t,p^2,p'^2) &= -\frac{1}{t\left(4\bar{p}^2 - t - \frac{\Delta p^4}{t}\right)}\Bigg\{\frac{4\bar{p}^2 - t}{d-2}\Big[M^2 I_{12}(t,p^2,p'^2) - 2\tilde{M}^2 I^{(1)}_{12}(t,p^2,p'^2) \\
&\qquad +\frac{\Delta p^2}{2}(d-1) I^{(2)}_{12}(t,p^2,p'^2)\Big] \\
&\quad +\frac{1}{4}\Big(4\bar{p}^2 - t - \frac{\Delta p^4}{2\bar{p}^2}\Big)\Big(I^{(1)}(p^2) + I^{(1)}(p'^2)\Big) \\
&\quad +\frac{\Delta p^4}{8p^2}\Big(4(p^2 - \tilde{M}^2) - t\Big) I^{(1)}_{12}(t,p^2,p'^2) \\
&\quad -\frac{\Delta p^2}{2p^2}\Big((4\bar{p}^2 - t)\tilde{M}^2 + \frac{\Delta p^4}{4}\Big) I^{(2)}_{12}(t,p^2,p'^2) \quad , && \text{(A.20)}\\
I^{(6)}_{12}(t,p^2,p'^2) &= \frac{1}{4\bar{p}^2 - t - \frac{\Delta p^4}{t}}\Bigg\{\frac{\tilde{M}^2}{2\bar{p}^2}\Big(4\bar{p}^2 - t + \frac{\Delta p^4}{4\tilde{M}^2}\Big) I^{(2)}_{12}(t,p^2,p'^2)
\end{aligned}
$$

$$
\begin{aligned}
&-\frac{\Delta p^2}{t(d-2)}\Big[M^2 I_{12}(t,p^2,p'^2) - 2\tilde{M}^2 I_{12}^{(1)}(t,p^2,p'^2) \\
&+\frac{d-1}{2}\Delta p^2 I_{12}^{(2)}(t,p^2,p'^2)\Big] - \frac{\Delta p^2}{8\bar{p}^2}\Big[\Big(4(\bar{p}^2-\tilde{M}^2)-t\Big) I_{12}^{(1)}(t,p^2,p'^2) \\
&+\frac{2p^2-t}{t}\left(I^{(1)}(p^2)+I^{(1)}(p'^2)\right)\Big]\Big\} \quad , \qquad \text{(A.21)}
\end{aligned}
$$

$$
\begin{aligned}
I_{21}^{Q}(t,p^2,p'^2) &= \frac{1}{2\left(4p^2 - t - \frac{\Delta p^4}{t}\right)}\Big\{2J(t) - \Big(1+\frac{\Delta p^2}{t}\Big)I(p^2) - \Big(1-\frac{\Delta p^2}{t}\Big)I(p'^2) \\
&+\left(4\tilde{M}^2 - t\right) I_{21}(t,p^2,p'^2)\Big\} \quad , \qquad \text{(A.22)}
\end{aligned}
$$

$$
\begin{aligned}
I_{21}^{q}(t,p^2,p'^2) &= -\frac{1}{2}I_{21}(t,p^2,p'^2) + \frac{\Delta p^2}{2t\left(4\bar{p}^2 - t - \frac{\Delta p^4}{t}\right)}\Big\{2J(t) - \Big(I(p^2)+I(p'^2)\Big) \\
&-\frac{4\bar{p}^2-t}{\Delta p^2}\left(I(p^2)-I(p'^2)\right) + \left(4\tilde{M}^2 - t\right) I_{21}(t,p^2,p'^2)\Big\} \quad , \qquad \text{(A.23)}
\end{aligned}
$$

$$
\begin{aligned}
I_{21}^{00}(t,p^2,p'^2) &= -\frac{1}{2(d-2)}\Big\{I(p'^2) - 2M^2 I_{21}(t,p^2,p'^2) - t\, I_{21}^{q}(t,p^2,p'^2) \\
&+\left(4\tilde{M}^2 - t + \Delta p^2\right) I_{21}^{Q}(t,p^2,p'^2)\Big\} \quad , \qquad \text{(A.24)}
\end{aligned}
$$

$$
\begin{aligned}
I_{21}^{QQ}(t,p^2,p'^2) &= \frac{1}{2\left(4\bar{p}^2 - t - \frac{\Delta p^4}{t}\right)}\Big\{\frac{1}{d-2}\Big[I(p'^2) - 2M^2 I_{21}(t,p^2,p'^2) \\
&\quad -t\, I_{21}^{q}(t,p^2,p'^2) + (d-1)\left(4\tilde{M}^2 - t + \Delta p^2\right) H_{21}^{Q}(t,p^2,p'^2)\Big] \\
&-\frac{1}{2}\left(I^{(1)}(p^2)+I^{(1)}(p'^2)\right) \\
&-\frac{\Delta p^2}{4p^2}\Big[J(t) - \Big(1-\frac{\Delta p^2}{t}\Big)I(p'^2) - \frac{\Delta p^2}{t}\left(I^{(1)}(p^2)+I^{(1)}(p'^2)\right) \\
&\quad -\left(4\tilde{M}^2 - t\right) I_{21}^{q}(t,p^2,p'^2) \\
&\quad +\Big(t+\frac{\Delta p^2}{t}\Big(4\tilde{M}^2 - t + \Delta p^2\Big)\Big) I_{21}^{Q}(t,p^2,p'^2)\Big]\Big\} \quad , \qquad \text{(A.25)}
\end{aligned}
$$

$$
\begin{aligned}
I_{21}^{qq}(t,p^2,p'^2) &= -\frac{1}{4t\left(4\bar{p}^2 - t - \frac{\Delta p^4}{t}\right)}\Big\{\frac{4\bar{p}^2-t}{d-2}\Big[2(d-3)I(p'^2) + 4M^2 I_{21}(t,p^2,p'^2) \\
&\quad -(d-2)\left(I^{(1)}(p^2)+I^{(1)}(p'^2)\right) + 2(d-1)\,t\, I_{21}^{q}(t,p^2,p'^2) \\
&\quad -2\Big(4\tilde{M}^2 - t + \Delta p^2\Big) I_{21}^{Q}(t,p^2,p'^2)\Big] + \frac{\Delta p^2}{2\bar{p}^2}\Big[(4\bar{p}^2-t)J(t) \\
&\quad -\Big(4\bar{p}^2 - t + \Delta p^2\Big)I(p'^2) + \Delta p^2\left(I^{(1)}(p^2)+I^{(1)}(p'^2)\right) \\
&\quad -\left((4p^2-t)(4\tilde{M}^2-t) + 4p^2\Delta p^2\right) I_{21}^{q}(t,p^2,p'^2) \qquad \text{(A.26)}
\end{aligned}
$$

$$+\left(t(4\bar{p}^2-t)-\Delta p^2\left(4\tilde{M}^2-t+\Delta p^2\right)\right)I_{21}^{Q}(t,p^2,p'^2)\Big]\Bigg\}\ ,$$

$$\begin{aligned}
I_{21}^{qQ}(t,p^2,p'^2) &= -\frac{1}{2\left(4p^2-t-\frac{\Delta p^4}{t}\right)}\Bigg\{\frac{1}{4\bar{p}^2}\Big[(4\bar{p}^2-t)J(t)-\left(4\bar{p}^2-t+\Delta p^2\right)I(p'^2) \\
&\quad -\left((4\bar{p}^2-t)(4\tilde{M}^2-t)+4\bar{p}^2\Delta p^2\right)I_{21}^{q}(t,p^2,p'^2) \\
&\quad +\left(t(4\bar{p}^2-t)-\Delta p^2\left(4\tilde{M}^2-t+\Delta p^2\right)\right)I_{21}^{Q}(t,p^2,p'^2) \\
&\quad -\frac{\Delta p^2}{t}(2\bar{p}^2-t)\left(I^{(1)}(p^2)+I^{(1)}(p'^2)\right)\Big] \\
&\quad +\frac{\Delta p^2}{(d-2)t}\Big[(d-3)I(p'^2)+2M^2I_{21}(t,p^2,p'^2)+(d-1)t\,I_{21}^{q}(t,p^2,p'^2) \\
&\quad -\left(4\tilde{M}^2-t+\Delta p^2\right)I_{21}^{Q}(t,p^2,p'^2)\Big]\Bigg\}\ . \qquad \text{(A.27)}
\end{aligned}$$

As the expressions for the tensorial loop integrals simplify drastically for the SU(2) form factors, i.e. one has only one heavy mass scale $p^2=p'^2=m_N^2$, we write out these simplified forms explicitly. As mentioned above, the loop functions $I_{12}^{(2)}(t,p^2)$ and $I_{12}^{(6)}(t,p^2)$ already vanish for equal external on-shell masses $p^2=p'^2$. We specify the notation $M\to M_\pi$, $\Delta\to\Delta_\pi$ here.

$$I^{(1)}(m_N^2) = \frac{1}{2m_N^2}\Big\{M_\pi^2\,I(m_N^2)+\Delta_\pi\Big\}\ , \qquad \text{(A.28)}$$

$$I_{12}^{(1)}(t,m_N^2) = \frac{1}{4m_N^2-t}\Big\{I(m_N^2)+M_\pi^2\,I_{12}(t,m_N^2)\Big\}\ , \qquad \text{(A.29)}$$

$$I_{12}^{(3)}(t,m_N^2) = \frac{1}{d-2}\Big\{I_{12}(t,m_N^2)-I_{12}^{(1)}(t,m_N^2)\Big\}M_\pi^2\ , \qquad \text{(A.30)}$$

$$\begin{aligned}
I_{12}^{(4)}(t,m_N^2) &= \frac{1}{(d-2)(4m_N^2-t)}\Big\{\Big((d-1)I_{12}^{(1)}(t,m_N^2)-I_{12}(t,m_N^2)\Big)M_\pi^2 \\
&\quad +\frac{d-2}{2}I^{(1)}(m_N^2)\Big\}\ , \qquad \text{(A.31)}
\end{aligned}$$

$$I_{12}^{(5)}(t,m_N^2) = \frac{1}{(d-2)\,t}\Big\{\Big(I_{12}^{(1)}(t,m_N^2)-I_{12}(t,m_N^2)\Big)M_\pi^2-\frac{d-2}{2}I^{(1)}(m_N^2)\Big\}\ , \qquad \text{(A.32)}$$

$$I_{21}^{Q}(t,m_N^2) = \frac{1}{2(4m_N^2-t)}\Big\{(2M_\pi^2-t)I_{21}(t,m_N^2)-2I(m_N^2)+2J(t)\Big\}\ , \qquad \text{(A.33)}$$

$$I_{21}^{q}(t,m_N^2) = -\frac{1}{2}I_{21}(t,m_N^2)\ , \qquad \text{(A.34)}$$

$$I_{21}^{00}(t,m_N^2) = \frac{1}{4(2-d)}\Big\{2I(m_N^2)-(4M_\pi^2-t)I_{21}(t,m_N^2)+2(2M_\pi^2-t)I_{21}^{Q}(t,m_N^2)\Big\}\ , \qquad \text{(A.35)}$$

$$I_{21}^{QQ}(t,m_N^2) = \frac{1}{4(d-2)(4m_N^2-t)}\Big\{2I(m_N^2)-2(d-2)I^{(1)}(m_N^2) \qquad \text{(A.36)}$$

$$
\begin{aligned}
& \qquad -(4M_\pi^2 - t)I_{21}(t, m_N^2) + 2(d-1)(2M_\pi^2 - t)I_{21}^Q(t, m_N^2)\Big\} \ , \\
I_{21}^{qq}(t, m_N^2) &= \frac{1}{4(d-2)t}\Big\{-2(d-3)I(m_N^2) + 2(d-2)I^{(1)}(m_N^2) \qquad \text{(A.37)} \\
& \qquad -\Big(4M_\pi^2 - (d-1)\,t\Big)I_{21}(t, m_N^2) + 2(2M_\pi^2 - t)I_{21}^Q(t, m_N^2)\Big\} \ , \\
I_{21}^{qQ}(t, m_N^2) &= -\frac{1}{2}I_{21}^Q(t, m_N^2) \ . \qquad \text{(A.38)}
\end{aligned}
$$

A.1.3 Scalar loop integrals

The scalar loop integrals, for $p^2 = p'^2$, are found to be

$$
\begin{aligned}
\Delta &= 2M^2\Big\{L + \frac{1}{16\pi^2}\log\frac{M}{\lambda}\Big\} \ , \qquad \text{(A.39)} \\
J(t) &= -2\Big\{L + \frac{1}{16\pi^2}\log\frac{M}{\lambda}\Big\} - \frac{1}{16\pi^2}\Big(1 + k(t)\Big) \ , \qquad \text{(A.40)} \\
I(p^2) &= -\frac{2\tilde{M}^2}{p^2}\Big\{L + \frac{1}{16\pi^2}\Big(\log\frac{M}{\lambda} - \frac{1}{2}\Big)\Big\} - \frac{\sqrt{p^2M^2 - \tilde{M}^4}}{8\pi^2 p^2}\arccos\Big(-\frac{\tilde{M}^2}{p\,M}\Big) \ , \qquad \text{(A.41)} \\
I_{12}(t, p^2) &= -f(t, p^2)\Big\{L + \frac{1}{16\pi^2}\Big(\log\frac{M}{\lambda} + \frac{1}{2}\Big)\Big\} + \frac{1}{16\pi^2}g(t, p^2) \ , \qquad \text{(A.42)} \\
I_{21}(t, p^2) &= f(t, p^2)\Big\{L + \frac{1}{16\pi^2}\Big(\log\frac{M}{\lambda} + \frac{1}{2}\Big)\Big\} \\
& \quad + \frac{1}{32\pi^2}\Big(h_1(t, p^2) + 2\,\Big(p^2 - \tilde{M}^2\Big)\,h_2(t, p^2)\Big) \ , \qquad \text{(A.43)}
\end{aligned}
$$

where L contains the infinite part according to

$$
L = \frac{\lambda^{d-4}}{16\pi^2}\Big\{\frac{1}{d-4} + \frac{1}{2}\Big(\gamma_E - 1 - \log 4\pi\Big)\Big\} \ , \qquad \text{(A.44)}
$$

and the following loop functions have been reduced to at most integrals over one Feynman parameter:

$$
\begin{aligned}
k(t) &= \int_0^1 \log\Big(1 - x(1-x)\frac{t}{M^2}\Big) = \sigma\log\frac{\sigma+1}{\sigma-1} - 2 \ , \quad \sigma = \sqrt{1 - \frac{4M^2}{t}} \ , \qquad \text{(A.45)} \\
f(t, p^2) &= \int_0^1 \frac{dx}{p^2 - x(1-x)t} = -\frac{2}{\tilde{\sigma}\,t}\log\frac{\tilde{\sigma}+1}{\tilde{\sigma}-1} \ , \qquad \tilde{\sigma} = \sqrt{1 - \frac{4p^2}{t}} \ , \qquad \text{(A.46)} \\
g(t, p^2) &= \int_0^1 dx \frac{\tilde{M}^2\arccos\Big(-\frac{\tilde{M}^2}{M\sqrt{p^2 - x(1-x)\,t}}\Big)}{\Big(p^2 - x(1-x)\,t\Big)\sqrt{M^2(p^2 - x(1-x)\,t) - \tilde{M}^4}} \ , \qquad \text{(A.47)}
\end{aligned}
$$

$$h_1(t,p^2) \;=\; \int_0^1 dx \frac{\log\Big(1-x(1-x)\,t/M^2\Big)}{p^2-x(1-x)\,t} \quad , \tag{A.48}$$

$$h_2(t,p^2) \;=\; \int_0^1 dx \frac{\arccos\Big(-\frac{\tilde M^2 - x(1-x)\,t}{\sqrt{(p^2-x(1-x)\,t)\,(M^2-x(1-x)\,t)}}\Big)}{\Big(p^2-x(1-x)\,t\Big)\sqrt{m^2(M^2-x(1-x)\,t)-(M^2-\tilde M^2)^2}} \quad . \tag{A.49}$$

The generalisation to $p^2 \neq p'^2$ is simple in principle and can be achieved by replacing p^2 by $xp^2+(1-x)p'^2$ everywhere in the above (which is understood to be done under the x integral).

For the SU(2) calculation, the scalar loop integrals (involving nucleon propagators) can be slightly simplified in terms of the parameter $\mu = M_\pi/m_N$ to read

$$I(m_N^2) \;=\; -\mu^2\Big\{L+\frac{1}{16\pi^2}\Big(\log\mu-\frac{1}{2}\Big)\Big\} - \frac{\mu\sqrt{4-\mu^2}}{16\pi^2}\arccos\Big(-\frac{\mu}{2}\Big) \quad , \tag{A.50}$$

$$I_{12}(t,m_N^2) \;=\; -f(t,m_N^2)\Big\{L+\frac{1}{16\pi^2}\Big(\log\mu+\frac{1}{2}\Big)\Big\} + \frac{1}{16\pi^2}g(t,m_N^2) \quad , \tag{A.51}$$

$$\begin{aligned} I_{21}(t,m_N^2) \;=\;& f(t,m_N^2)\Big\{L+\frac{1}{16\pi^2}\Big(\log\mu+\frac{1}{2}\Big)\Big\} \\ &+\frac{1}{32\pi^2}\Big(h_1(t,m_N^2)+m_N^2(2-\mu^2)h_2(t,m_N^2)\Big) \quad , \end{aligned} \tag{A.52}$$

and the loop functions $g(t,m_N^2)$, $h_{1/2}(t,m_N^2)$ can be written in terms of dimensionless parameters $\tau = t/m_N^2$, $\theta = t/M_\pi^2$ as

$$g(t,m_N^2) \;=\; \frac{\mu}{2m_N^2}\int_0^1 dx \frac{\arccos\Big(-\frac{\mu}{2\sqrt{1-x(1-x)\tau}}\Big)}{\Big(1-x(1-x)\,\tau\Big)\sqrt{1-\frac{\mu^2}{4}-x(1-x)\,\tau}} \quad , \tag{A.53}$$

$$h_1(t,m_N^2) \;=\; \frac{1}{m_N^2}\int_0^1 dx \frac{\log\Big(1-x(1-x)\,\theta\Big)}{1-x(1-x)\,\tau} \quad , \tag{A.54}$$

$$h_2(t,m_N^2) \;=\; \frac{1}{\mu m_N^4}\int_0^1 dx \frac{\arccos\Big(-\frac{\mu\left(\frac{1}{2}-x(1-x)\,\theta\right)}{\sqrt{(1-x(1-x)\,\tau)\,(1-x(1-x)\,\theta)}}\Big)}{\Big(1-x(1-x)\,\tau\Big)\sqrt{1-\frac{\mu^2}{4}-x(1-x)\,\theta}} \quad . \tag{A.55}$$

A.2 Form factor contributions from separate diagrams

In this section, we give the contributions to the Dirac and Pauli form factors $F_1(t)$, $F_2(t)$, respectively, coming from the various diagrams shown in Fig. 2.2.

A.2.1 Kinematic structures of loop diagrams

First, we show the basic kinematic structures of the different loop diagrams, which have to be weighted with various coefficients for different particles and different intermediate states. Here again, we display the more general case that allows for $p^2 \neq p'^2$. The following expressions contribute to the Dirac form factors $F_1(s)$, where the subscripts "i" in E_i refer to the diagram numbers in Fig. 3.1:

$$\begin{aligned}
E_5 &= \frac{1}{4F^2}\Big\{\Delta + (p+m)\left[(p-m)\,I(p^2) - p\,I^{(1)}(p^2)\right] \\
&\quad +(p'+m)\left[(p'-m)\,I(p'^2) - p'\,I^{(1)}(p'^2)\right] \\
&\quad +(p+m)(p'+m)\Big[\Big((p-m)(p'-m) - M^2\Big)I_{12}(t,p^2,p'^2) \\
&\qquad -2\,(2pp' - (p+p')m)\,I_{12}^{(1)}(t,p^2,p'^2) + 2I_{12}^{(3)}(t,p^2,p'^2) \\
&\qquad +2(p+p')^2 I_{12}^{(4)}(t,p^2,p'^2) - 2(p^2-p'^2)I_{12}^{(6)}(t,p^2,p'^2)\Big]\Big\} \ , \qquad (A.56)
\end{aligned}$$

$$\begin{aligned}
E_6 &= \frac{1}{2F^2}\Big\{tJ^{(1)}(t) - (p+m)(p'+m)\Big[(p+p')(p-m)I_{21}^{Q}(t,p^2,p'^2) \qquad (A.57) \\
&\quad -I_{21}^{00}(t,p^2,p'^2) - (p+p')^2 I_{21}^{QQ}(t,p^2,p'^2) + (p^2-p'^2)I_{21}^{qQ}(t,p^2,p'^2)\Big]\Big\} \ ,
\end{aligned}$$

$$\begin{aligned}
E_7 &= -\frac{1}{4F^2}\Big\{2\Delta + (p+m)\left[(p-m)\,I(p^2) - p\,I^{(1)}(p^2)\right] \\
&\quad +(p'+m)\left[(p'-m)\,I(p'^2) - p'\,I^{(1)}(p'^2)\right]\Big\} \ , \qquad (A.58)
\end{aligned}$$

$$E_8 = -\frac{1}{2F^2}\Delta \ , \qquad (A.59)$$

$$E_9 = \frac{t}{F^2}J^{(1)}(t) \ , \qquad (A.60)$$

$$\begin{aligned}
E_{10} &= -\frac{t(p+m)(p'+m)}{8\bar{m}F^2}\Big\{(p+p'-2m)I_{12}^{(1)}(t,p^2,p'^2) - 2(p+p')I_{12}^{(4)}(t,p^2,p'^2) \\
&\quad -(p-p')\left[I_{12}^{(2)}(t,p^2,p'^2) - 2I_{12}^{(6)}(t,p^2,p'^2)\right]\Big\} \ . \qquad (A.61)
\end{aligned}$$

The kinematic structures of the various loop diagrams contributing to the Pauli form factors $F_2(t)$ are given as follows, again referring to the numbering in Fig. 3.1:

$$M_5 = \frac{(p+p')(p+m)(p'+m)}{4F^2}\Big\{(p+p'-2m)I_{12}^{(1)}(t,p^2,p'^2) - 2(p+p')I_{12}^{(4)}(t,p^2,p'^2)$$

$$-(p-p')\left[I_{12}^{(2)}(t,p^2,p'^2)-2I_{12}^{(6)}(t,p^2,p'^2)\right]\Big\} \ , \quad \text{(A.62)}$$

$$\begin{aligned} M_6 &= \frac{(p+p')(p+m)(p'+m)}{2F^2}\Big\{(p-m)I_{21}^{Q}(t,p^2,p'^2)-(p+p')\,I_{21}^{QQ}(t,p^2,p'^2) \\ &\quad +(p-p')\,I_{21}^{qQ}(t,p^2,p'^2)\Big\} \ , \end{aligned} \quad \text{(A.63)}$$

$$\begin{aligned} M_{10} &= -\frac{p+p'}{8\bar{m}F^2}\Big\{\Delta+(p+m)\left[(p-m)\,I(p^2)-p\,I^{(1)}(p^2)\right] \\ &\quad +(p'+m)\left[(p'-m)\,I(p'^2)-p'\,I^{(1)}(p'^2)\right] \\ &\quad +(p+m)(p'+m)\Big[\Big((p-m)(p'-m)+M^2\Big)I_{12}(t,p^2,p'^2) \\ &\qquad -2\Big(2pp'-(p+p')m\Big)I_{12}^{(1)}(t,p^2,p'^2)-4I_{12}^{(3)}(t,p^2,p'^2) \\ &\qquad -2\left((p-p')^2-t\right)I_{12}^{(4)}(t,p^2,p'^2)-2tI_{12}^{(5)}(t,p^2,p'^2) \\ &\qquad +2(p^2-p'^2)I_{12}^{(6)}(t,p^2,p'^2)\Big]\Big\} \ , \end{aligned} \quad \text{(A.64)}$$

$$M_{11} = -\frac{p+p'}{4\bar{m}F^2}\,\Delta \ , \quad \text{(A.65)}$$

$$M_{12} = \frac{2(p+p')t}{F^2}\,J^{(1)}(t) \ . \quad \text{(A.66)}$$

We finally spell out the loop contribution to the baryon Z factor needed for wave function renormalisation up to fourth order:

$$\begin{aligned} Z &= \frac{1}{4F^2}\Big\{\frac{p^2-m^2}{p^2}\,\Delta+\left[M_\pi^2-\frac{p^2-m^2}{p^2}(m^2-M^2)\right]I(p^2)-(3p^2-m^2)I^{(1)}(p^2) \\ &\quad -(p+m)^2\left((p-m)^2-M^2\right)\left[I_{12}(0,p^2)-2I_{12}^{(1)}(0,p^2)\right]\Big\} \ . \end{aligned} \quad \text{(A.67)}$$

A.2.2 Heavy–baryon expansion of loop diagrams

In this section, we give some more explicit results for the diagram contributions shown in the previous section, namely expand them according to the heavy–baryon scheme and up to linear order in t. It is obvious from the formulae what higher terms are neglected, so we allow our notation to be a bit sloppy about these: all diagrams are given up to orders M^4 and tM^2, both higher orders in M and t are dropped. Also, we drop the infinite parts, and only show results for the simplified case $p^2 = p'^2$. We will use the abbreviation $\delta = p(m-p)/M^2$ as a quantity of chiral order 1 that characterises the baryon mass splitting in the loops.

$$\begin{aligned} E_5 &= \frac{M^2}{32\pi^2F^2}\Big\{1+3\log\frac{M}{\lambda}-\frac{3\pi M}{p}\Big(\frac{1}{2}-\delta\Big)-\frac{M^2}{p^2}\Big[\frac{3}{2}-6\delta+5\delta^2 \quad \text{(A.68)} \\ &\quad +\left(2-9\delta+6\delta^2\right)\log\frac{M}{\lambda}\Big]+\frac{t}{6p^2}\Big(1+8\log\frac{M}{\lambda}\Big)\Big\}+\ldots \ , \end{aligned}$$

$$
\begin{aligned}
E_6 &= -\frac{M^2}{32\pi^2F^2}\Big\{1+3\log\frac{M}{\lambda}-\frac{\pi M}{2p}(5-6\delta) \\
&\qquad -\frac{M^2}{p^2}\Big[2-7\delta+5\delta^2+3\left(1-4\delta+2\delta^2\right)\log\frac{M}{\lambda}\Big]\Big\} \\
&\quad +\frac{t}{384\pi^2F^2}\Big\{7+10\log\frac{M}{\lambda}-\frac{5\pi M}{2p}(7-2\delta) \\
&\qquad -\frac{2M^2}{p^2}\Big[13-26\delta+5\delta^2+6(4-5\delta)\log\frac{M}{\lambda}\Big]\Big\}+\ldots\ , && \text{(A.69)} \\
E_7 &= -\frac{M^3}{32\pi^2F^2p}\Big\{\pi+\frac{M}{2p}\Big[1-2\delta+2(1-3\delta)\log\frac{M}{\lambda}\Big]\Big\}+\ldots\ , && \text{(A.70)} \\
E_8 &= -\frac{M^2}{16\pi^2F^2}\log\frac{M}{\lambda}\ , && \text{(A.71)} \\
E_9 &= \frac{M^2}{16\pi^2F^2}\log\frac{M}{\lambda}-\frac{t}{192\pi^2F^2}\left(1+2\log\frac{M}{\lambda}\right)+\ldots\ , && \text{(A.72)} \\
E_{10} &= \frac{M^2t}{32\pi^2F^2p^2}\log\frac{M}{\lambda}+\ldots\ , && \text{(A.73)} \\
M_5 &= -\frac{M^2}{8\pi^2F^2}\Big\{\log\frac{M}{\lambda}-\frac{\pi M}{4p}(3-4\delta)-\frac{M^2}{2p^2}\Big[1-3\delta+2\delta^2 \\
&\qquad +2\left(1-4\delta+2\delta^2\right)\log\frac{M}{\lambda}\Big]+\frac{t}{3p^2}\log\frac{M}{\lambda}\Big\}+\ldots\ , && \text{(A.74)} \\
M_6 &= \frac{M^2}{16\pi^2F^2}\Big\{\frac{\pi p}{M}+1-\delta+2(2-\delta)\log\frac{M}{\lambda}-\frac{\pi M}{2p}\left(\frac{15}{4}-8\delta+\delta^2\right) \\
&\qquad -\frac{M^2}{6p^2}\Big[(1-2\delta)^2(8-\delta)+12\left(1-5\delta+4\delta^2\right)\log\frac{M}{\lambda}\Big]\Big\} \\
&\quad -\frac{t}{192\pi^2F^2}\Big\{\frac{\pi p}{M}+2\left(4-\delta+6\log\frac{M}{\lambda}\right)-\frac{\pi M}{2p}\left(\frac{105}{4}-12\delta-\delta^2\right) && \text{(A.75)} \\
&\qquad -\frac{4M^2}{3p^2}\Big[13-\frac{123}{4}\delta+9\delta^2+\delta^3+12(2-3\delta)\log\frac{M}{\lambda}\Big]\Big\}+\ldots\ , \\
M_{10} &= \frac{M^2}{32\pi^2F^2}\Big\{1-\log\frac{M}{\lambda}+\frac{\pi M}{2p}(1-2\delta)+\frac{M^2}{p^2}\Big[(2-\delta)\delta && \text{(A.76)} \\
&\qquad +\left(1-3\delta+2\delta^2\right)\log\frac{M}{\lambda}\Big]+\frac{t}{6p^2}\left(1-6\log\frac{M}{\lambda}\right)\Big\}+\ldots\ , \\
M_{11} &= -\frac{M^2}{16\pi^2F^2}\log\frac{M}{\lambda}\ , && \text{(A.77)} \\
M_{12} &= \frac{M^2}{4\pi^2F^2}\log\frac{M}{\lambda}-\frac{t}{48\pi^2F^2}\left(1+2\log\frac{M}{\lambda}\right)+\ldots\ . && \text{(A.78)}
\end{aligned}
$$

In these expressions, the increasingly high powers of δ might seem worrisome for the following reason: As will be written out explicitly below, the form factors of $\Sigma^\pm$

contain $\pi^-\Lambda$ intermediate states, for which δ becomes

$$\delta = \frac{m_\Sigma(m_\Lambda - m_\Sigma)}{M_\pi^2} \propto \frac{m_s - \hat{m}}{\hat{m}} \tag{A.79}$$

in terms of quark masses, i.e. there seem to be chiral $SU(2)$ singularities (for $\hat{m} \to 0$, but m_s fixed) of higher and higher orders. This puzzle is easy to resolve in this relativistic framework, where one finds that these "critical" powers in δ stem from expressions that have an ill–defined limit $M \ll |p-m|$, of the form

$$\frac{\arccos\left(-\frac{\tilde{M}^2}{Mp}\right)}{\sqrt{M^2 - \tilde{M}^4/p^2}} \quad \stackrel{M \ll |p-m|}{\longrightarrow} \quad \frac{\arccos\left(\frac{m-p}{M}\right)}{\sqrt{M^2-(m-p)^2}} \quad .$$

It is obvious that the arccos cannot be sensibly expanded in $(m-p)/M$ (which is formally of order $\sqrt{m_q}$) if $M < m-p$, such that one has to make an analytical continuation first,

$$\frac{\arccos\left(\frac{m-p}{M}\right)}{\sqrt{M^2-(m-p)^2}} \longrightarrow \frac{1}{\sqrt{(m-p)^2-M^2}}\left\{\log\left|\frac{m-p}{M}+\sqrt{\left(\frac{m-p}{M}\right)^2-1}\right| - i\pi\,\theta(p-m)\right\} ,$$

which approaches

$$\frac{1}{p-m}\left\{\log\frac{M}{2|m-p|} - i\pi\theta(p-m)\right\}$$

for $M \ll |m-p|$, showing that this loop contribution really diverges logarithmically only and can be seen to be subleading everywhere, e.g. yielding a $\log M_\pi$ divergence in the magnetic radius (compared to the leading $1/M_\pi$ chiral divergence), and reducing the $\log M_\pi$ divergence in the electric radius to a non–divergent term,

$$\log\frac{M}{\lambda} \longrightarrow \log\frac{2(m-p)}{\lambda} \quad .$$

We wish to emphasise, though, that in the real world, the ratio $(m_\Sigma - m_\Lambda)/M_\pi \approx 0.55$ is *not* large (due to the particular smallness of the low–energy constant controlling the $\Sigma - \Lambda$ mass splitting, $b_D = 0.06$ GeV^{-1}), and an expansion of the arccos, though not particularly fast converging, can be done.

A.2.3 The octet form factors

In order to write down the contributions of these diagrams to the various form factors, we use the following notational form: $E_i(\phi, B)$ denotes the diagram E_i with the meson ϕ and the baryon B in the (virtual) intermediate state, i.e. in the above formulae for the kinematic structures of the diagrams E_i, one has to set $M \to M_\phi$ and $m \to m_B$. The equal notation applies to magnetic contributions $M_i(\phi, B)$. For the tadpole–type diagrams $E_{8/9}$, only a meson state has to be specified. p/p' are of course given by the mass(es) of the particle(s) whose form factor is considered. One peculiarity concerns diagram E_{10} (M_{10}), where the magnetic coupling of the vector current allows for a $\Lambda - \Sigma^0$ transition in the virtual intermediate state. Basic symmetry considerations show that, for all form factors with identical in and out states, a $\Lambda - \Sigma^0$ and a $\Sigma^0 - \Lambda$ transition yield the same kinematical structure, such that contributions of the form $E_{10}(\phi, \Lambda\Sigma)$ comprise the sum of both such diagrams. However, this is not the case for the $\Lambda - \Sigma^0$ transition form factor, such that in this case we have distinguished between the different orders in the intermediate state and written $E_{10}(\pi, \Sigma\Lambda)$ and $E_{10}(\eta, \Lambda\Sigma)$, even though the baryon mass difference in this (fourth–order) diagram is in principle beyond the order we are working at here.

The Dirac form factors $F_1(t)$ are given as follows:

$$\begin{aligned}
F_1^p(t) &= Z_N - 2\Big(d_{101} + \frac{d_{102}}{3}\Big)\, t \\
&+ (D+F)^2(E_5 - 2E_6 - 2E_7)(\pi, N) - \frac{1}{3}(D+3F)^2(E_6 + E_7)(K, \Lambda) \\
&\quad + (D-F)^2(2E_5 - E_6 - E_7)(K, \Sigma) + \frac{1}{3}(D-3F)^2 E_5(\eta, N) \\
&+ (E_8 + E_9)(\pi) + 2(E_8 + E_9)(K) \\
&- (D+F)^2(b_6^D - b_6^F)E_{10}(\pi, N) - \frac{1}{9}(D+3F)^2 b_6^D E_{10}(K, \Lambda) \\
&\quad + (D-F)^2(b_6^D + 2b_6^F)E_{10}(K, \Sigma) - \frac{2}{3}(D-F)(D+3F)b_6^D E_{10}(K, \Lambda\Sigma) \\
&\quad + \frac{1}{9}(D-3F)^2(b_6^D + 3b_6^F)E_{10}(\eta, N) \quad , \qquad\qquad (A.80) \\
F_1^n(t) &= \frac{4d_{102}}{3}\, t \\
&+ 2(D+F)^2(E_5 + E_6 + E_7)(\pi, N) - 2(D-F)^2(E_5 + E_6 + E_7)(K, \Sigma) \\
&- (E_8 + E_9)(\pi) + (E_8 + E_9)(K) \\
&+ 2(D+F)^2 b_6^F E_{10}(\pi, N) - \frac{1}{9}(D+3F)^2 b_6^D E_{10}(K, \Lambda) \\
&\quad + (D-F)^2(b_6^D - 2b_6^F)E_{10}(K, \Sigma) + \frac{2}{3}(D-F)(D+3F)b_6^D E_{10}(K, \Lambda\Sigma) \\
&\quad - \frac{2}{9}(D-3F)^2 b_6^D E_{10}(\eta, N) \quad , \qquad\qquad (A.81) \\
F_1^\Lambda(t) &= \frac{2d_{102}}{3}\, t \\
&+ \frac{1}{3}(D+3F)^2(E_5 + E_6 + E_7)(K, N) \\
&\quad - \frac{1}{3}(D-3F)^2(E_5 + E_6 + E_7)(K, \Xi) \\
&+ \frac{4}{3}D^2 b_6^D E_{10}(\pi, \Sigma) - \frac{1}{9}(D+3F)^2(b_6^D - 3b_6^F)E_{10}(K, N)
\end{aligned}$$

$$
\begin{aligned}
& -\frac{1}{9}(D-3F)^2(b_6^D+3b_6^F)E_{10}(K,\Xi)-\frac{4}{9}D^2b_6^DE_{10}(\eta,\Lambda) \quad , && \text{(A.82)}\\
F_1^{\Sigma^-}(t) \;=\; & Z_\Sigma - 2\Big(d_{101}+\frac{d_{102}}{3}\Big)\,t \\
+\; & 4F^2(E_5-E_6-E_7)(\pi,\Sigma)-\frac{4}{3}D^2(E_6+E_7)(\pi,\Lambda) \\
& +2(D-F)^2E_5(K,N)-2(D+F)^2(E_6+E_7)(K,\Xi)+\frac{4}{3}D^2E_5(\eta,\Sigma) \\
+\; & 2(E_8+E_9)(\pi)+(E_8+E_9)(K) \\
+\; & \frac{4}{3}F^2(2b_6^D+3b_6^F)E_{10}(\pi,\Sigma)-\frac{4}{9}D^2b_6^DE_{10}(\pi,\Lambda)-\frac{8}{3}DFb_6^DE_{10}(\pi,\Lambda\Sigma) \\
& +\frac{2}{3}(D-F)^2(b_6^D+3b_6^F)E_{10}(K,N)-\frac{4}{3}(D+F)^2b_6^DE_{10}(K,\Xi) \\
& +\frac{4}{9}D^2(b_6^D+3b_6^F)E_{10}(\eta,\Sigma) \quad , && \text{(A.83)}\\
F_1^{\Sigma^0}(t) \;=\; & -\frac{2d_{102}}{3}\,t \\
+\; & (D-F)^2(E_5+E_6+E_7)(K,N)-(D+F)^2(E_5+E_6+E_7)(K,\Xi) \\
+\; & \frac{8}{3}F^2b_6^DE_{10}(\pi,\Sigma)-\frac{4}{9}D^2b_6^DE_{10}(\pi,\Lambda) \\
& -\frac{1}{3}(D-F)^2(b_6^D-3b_6^F)E_{10}(K,N) \\
& -\frac{1}{3}(D+F)^2(b_6^D+3b_6^F)E_{10}(K,\Xi)+\frac{4}{9}D^2b_6^DE_{10}(\eta,\Sigma) \quad , && \text{(A.84)}\\
F_1^{\Sigma^-}(t) \;=\; & -Z_\Sigma + 2\Big(d_{101}-\frac{d_{102}}{3}\Big)\,t \\
-\; & 4F^2(E_5-E_6-E_7)(\pi,\Sigma)+\frac{4}{3}D^2(E_6+E_7)(\pi,\Lambda) \\
& +2(D-F)^2(E_6+E_7)(K,N)-2(D+F)^2E_5(K,\Xi)-\frac{4}{3}D^2E_5(\eta,\Sigma) \\
-\; & 2(E_8+E_9)(\pi)-(E_8+E_9)(K) \\
+\; & \frac{4}{3}F^2(2b_6^D-3b_6^F)E_{10}(\pi,\Sigma)-\frac{4}{9}D^2b_6^DE_{10}(\pi,\Lambda)+\frac{8}{3}DFb_6^DE_{10}(\pi,\Lambda\Sigma) \\
& -\frac{4}{3}(D-F)^2b_6^DE_{10}(K,N)+\frac{2}{3}(D+F)^2(b_6^D-3b_6^F)E_{10}(K,\Xi) \\
& +\frac{4}{9}D^2(b_6^D-3b_6^F)E_{10}(\eta,\Sigma) \quad , && \text{(A.85)}\\
F_1^{\Xi^0}(t) \;=\; & \frac{4d_{102}}{3}\,t \\
-\; & 2(D-F)^2(E_5+E_6+E_7)(\pi,\Xi)+2(D+F)^2(E_5+E_6+E_7)(K,\Sigma) \\
+\; & (E_8+E_9)(\pi)-(E_8+E_9)(K) \\
-\; & 2(D-F)^2b_6^FE_{10}(\pi,\Xi)-\frac{1}{9}(D-3F)^2b_6^DE_{10}(K,\Lambda)
\end{aligned}
$$

$$
\begin{aligned}
& +(D+F)^2(b_6^D+2b_6^F)E_{10}(K,\Sigma)+\frac{2}{3}(D+F)(D-3F)b_6^D E_{10}(K,\Lambda\Sigma) \\
& -\frac{2}{9}(D+3F)^2 b_6^D E_{10}(\eta,\Xi) \quad , \qquad \text{(A.86)}
\end{aligned}
$$

$$
\begin{aligned}
F_1^{\Xi^-}(t) &= -Z_\Xi+2\Big(d_{101}-\frac{d_{102}}{3}\Big)\,t \\
&- (D-F)^2(E_5-2E_6-2E_7)(\pi,\Xi)+\frac{1}{3}(D-3F)^2(E_6+E_7)(K,\Lambda) \\
& -(D+F)^2(2E_5-E_6-E_7)(K,\Sigma)-\frac{1}{3}(D+3F)^2E_5(\eta,\Xi) \\
&- (E_8+E_9)(\pi)-2(E_8+E_9)(K) \\
&- (D-F)^2(b_6^D+b_6^F)E_{10}(\pi,\Xi)-\frac{1}{9}(D-3F)^2b_6^D E_{10}(K,\Lambda) \\
& +(D+F)^2(b_6^D-2b_6^F)E_{10}(K,\Sigma)-\frac{2}{3}(D+F)(D-3F)b_6^D E_{10}(K,\Lambda\Sigma) \\
& +\frac{1}{9}(D+3F)^2(b_6^D-3b_6^F)E_{10}(\eta,\Xi) \quad , \qquad \text{(A.87)}
\end{aligned}
$$

$$
\begin{aligned}
\sqrt{3}F_1^{\Lambda\Sigma^0}(t) &= -2d_{102}\,t \\
&- 8DF(E_5+E_6+E_7)(\pi,\Sigma) \\
& -(D-F)(D+3F)(E_5+E_6+E_7)(K,N) \\
& +(D+F)(D-3F)(E_5+E_6+E_7)(K,\Xi) \\
&- 8DFb_6^F E_{10}(\pi,\Sigma)+\frac{4}{3}D^2b_6^D E_{10}(\pi,\Sigma\Lambda) \\
& -(D-F)(D+3F)(b_6^D+b_6^F)E_{10}(K,N) \\
& -(D-3F)(D+F)(b_6^D-b_6^F)E_{10}(K,\Xi)-\frac{4}{3}D^2b_6^D E_{10}(\eta,\Lambda\Sigma) \ . \qquad \text{(A.88)}
\end{aligned}
$$

In the same way, we show the results for the Pauli form factors $F_2(t)$. We noted that the lowest order coupling constants for the anomalous magnetic moments, $b_6^{D/F}$, receive quark mass renormalisations by the fourth–order couplings $\tilde{b}_6^{D/F}$, such that we shall employ the abbreviations $\bar{b}_6^{D/F}=b_6^{D/F}+2m\,(2M_K^2+M_\pi^2)\,\tilde{b}_6^{D/F}$ as in Eq. (3.9). Note, however, that it is fully justified to set $b_6^{D/F}\to b_6^{D/F}$ for the fourth order loop contributions.

$$
\begin{aligned}
F_2^p(t) &= \frac{m_N}{\bar{m}}\Big(\frac{\bar{b}_6^D}{3}+b_6^F\Big)Z_N \\
&+ 4m_N\Big[(M_K^2-M_\pi^2)\Big(\alpha_1+\frac{\alpha_3}{3}-\frac{\beta_1}{3}\Big)+M_K^2\Big(\alpha_2+\frac{\alpha_4}{3}\Big)\Big] \\
&+ 2\Big[d_{101}+\frac{d_{102}}{3}+2m_N\Big(\eta_1+\frac{\eta_2}{3}\Big)\Big]\,t \\
&+ (D+F)^2(M_5-2M_6)(\pi,N)-\frac{1}{3}(D+3F)^2M_6(K,\Lambda)
\end{aligned}
$$

$$
\begin{aligned}
& +(D-F)^2(2M_5-M_6)(K,\Sigma)+\frac{1}{3}(D-3F)^2M_5(\eta,N) \\
- & \quad (D+F)^2(b_6^D-b_6^F)M_{10}(\pi,N)-\frac{1}{9}(D+3F)^2b_6^DM_{10}(K,\Lambda) \\
& +(D-F)^2(b_6^D+2b_6^F)M_{10}(K,\Sigma) \\
& -\frac{2}{3}(D-F)(D+3F)b_6^DM_{10}(K,\Lambda\Sigma) \\
& +\frac{1}{9}(D-3F)^2(b_6^D+3b_6^F)M_{10}(\eta,N) \\
+ & \quad (b_6^D+b_6^F)M_{11}(\pi)+2b_6^FM_{11}(K) \\
+ & \quad 2(b_{10}+b_{11})M_{12}(\pi)+(b_9+4b_{11})M_{12}(K) \quad , \qquad \text{(A.89)}
\end{aligned}
$$

$$
\begin{aligned}
F_2^n(t) \; = & \; -\frac{m_N}{\bar{m}}\frac{2\bar{b}_6^D}{3}Z_N-\frac{4}{3}m_N\left[(M_K^2-M_\pi^2)(2\alpha_3+\beta_1)+2M_K^2\alpha_4\right] \\
- & \quad \frac{4}{3}\Big[d_{102}+2m_N\eta_2\Big]\,t \\
+ & \quad 2(D+F)^2(M_5+M_6)(\pi,N)-2(D-F)^2(M_5+M_6)(K,\Sigma) \\
+ & \quad 2(D+F)^2b_6^FM_{10}(\pi,N)-\frac{1}{9}(D+3F)^2b_6^DM_{10}(K,\Lambda) \\
& +(D-F)^2(b_6^D-2b_6^F)M_{10}(K,\Sigma) \\
& +\frac{2}{3}(D-F)(D+3F)b_6^DM_{10}(K,\Lambda\Sigma)-\frac{2}{9}(D-3F)^2b_6^DM_{10}(\eta,N) \\
- & \quad (b_6^D+b_6^F)M_{11}(\pi)-(b_6^D-b_6^F)M_{11}(K) \\
- & \quad 2(b_{10}+b_{11})M_{12}(\pi)-2(b_{10}-b_{11})M_{12}(K) \quad , \qquad \text{(A.90)}
\end{aligned}
$$

$$
\begin{aligned}
F_2^\Lambda(t) \; = & \; -\frac{m_\Lambda}{\bar{m}}\frac{\bar{b}_6^D}{3}Z_\Lambda-\frac{4}{3}m_\Lambda\left[(8M_K^2-5M_\pi^2)\frac{\alpha_4}{3}+(M_K^2-M_\pi^2)\beta_1\right] \\
- & \quad \frac{2}{3}\Big[d_{102}+2m_\Lambda\eta_2\Big]\,t \\
+ & \quad \frac{1}{3}(D+3F)^2(M_5+M_6)(K,N)-\frac{1}{3}(D-3F)^2(M_5+M_6)(K,\Xi) \\
+ & \quad \frac{4}{3}D^2b_6^DM_{10}(\pi,\Sigma)-\frac{1}{9}(D+3F)^2(b_6^D-3b_6^F)M_{10}(K,N) \\
& -\frac{1}{9}(D-3F)^2(b_6^D+3b_6^F)M_{10}(K,\Xi)-\frac{4}{9}D^2b_6^DM_{10}(\eta,\Lambda) \\
- & \quad b_6^DM_{11}(K)-2b_{10}M_{12}(K) \quad , \qquad \text{(A.91)}
\end{aligned}
$$

$$
\begin{aligned}
F_2^{\Sigma^+}(t) \; = & \; \frac{m_\Sigma}{\bar{m}}\left(\frac{b_6^D}{3}+\bar{b}_6^F\right)Z_\Sigma+4m_\Sigma\left[M_\pi^2\left(\alpha_2+\frac{\alpha_4}{3}\right)-\frac{1}{3}(M_K^2-M_\pi^2)\beta_1\right] \\
+ & \quad 2\left[d_{101}+\frac{d_{102}}{3}+2m_\Sigma\left(\eta_1+\frac{\eta_2}{3}\right)\right]\,t \\
+ & \quad 4F^2(M_5-M_6)(\pi,\Sigma)-\frac{4}{3}D^2M_6(\pi,\Lambda)+2(D-F)^2M_5(K,N) \\
& -2(D+F)^2M_6(K,\Xi)+\frac{4}{3}D^2M_5(\eta,\Sigma)
\end{aligned}
$$

$$
\begin{aligned}
&+ && \frac{4}{3}F^2(2b_6^D+3b_6^F)M_{10}(\pi,\Sigma)-\frac{4}{9}D^2b_6^DM_{10}(\pi,\Lambda)-\frac{8}{3}DFb_6^DM_{10}(\pi,\Lambda\Sigma)\\
& && +\frac{2}{3}(D-F)^2(b_6^D+3b_6^F)M_{10}(K,N)-\frac{4}{3}(D+F)^2b_6^DM_{10}(K,\Xi)\\
& && +\frac{4}{9}D^2(b_6^D+3b_6^F)M_{10}(\eta,\Sigma)\\
&+ && 2b_6^FM_{11}(\pi)+(b_6^D+b_6^F)M_{11}(K)\\
&+ && (b_9+4b_{11})M_{12}(\pi)+2(b_{10}+b_{11})M_{12}(K)\quad , \qquad\qquad (A.92)\\
F_2^{\Sigma^0}(t) &= && \frac{m_\Sigma}{\bar m}\frac{\bar b_6^D}{3}Z_\Sigma+\frac{4}{3}m_\Sigma\Big[M_\pi^2\alpha_4-(M_K^2-M_\pi^2)\beta_1\Big]+\frac{2}{3}\Big[d_{102}+2m_\Sigma\eta_2\Big]\,t\\
&+ && (D-F)^2(M_5+M_6)(K,N)-(D+F)^2(M_5+M_6)(K,\Xi)\\
&+ && \frac{8}{3}F^2b_6^DM_{10}(\pi,\Sigma)-\frac{4}{9}D^2b_6^DM_{10}(\pi,\Lambda)\\
& && -\frac{1}{3}(D-F)^2(b_6^D-3b_6^F)M_{10}(K,N)\\
& && -\frac{1}{3}(D+F)^2(b_6^D+3b_6^F)M_{10}(K,\Xi)+\frac{4}{9}D^2b_6^DM_{10}(\eta,\Sigma)\\
&+ && b_6^DM_{11}(K)+2b_{10}M_{12}(K)\quad , \qquad\qquad (A.93)\\
F_2^{\Sigma^-}(t) &= && \frac{m_\Sigma}{\bar m}\Big(\frac{\bar b_6^D}{3}-b_6^F\Big)Z_\Sigma-4m_\Sigma\Big[M_\pi^2\Big(\alpha_2-\frac{\alpha_4}{3}\Big)+\frac{1}{3}(M_K^2-M_\pi^2)\beta_1\Big]\\
&- && 2\Big[d_{101}-\frac{d_{102}}{3}+2m_\Sigma\Big(\eta_1-\frac{\eta_2}{3}\Big)\Big]\,t\\
&- && 4F^2(M_5-M_6)(\pi,\Sigma)+\frac{4}{3}D^2M_6(\pi,\Lambda)+2(D-F)^2M_6(K,N)\\
& && -2(D+F)^2M_5(K,\Xi)-\frac{4}{3}D^2M_5(\eta,\Sigma)\\
&+ && \frac{4}{3}F^2(2b_6^D-3b_6^F)M_{10}(\pi,\Sigma)-\frac{4}{9}D^2b_6^DM_{10}(\pi,\Lambda)+\frac{8}{3}DFb_6^DM_{10}(\pi,\Lambda\Sigma)\\
& && -\frac{4}{3}(D-F)^2b_6^DM_{10}(K,N)+\frac{2}{3}(D+F)^2(b_6^D-3b_6^F)M_{10}(K,\Xi)\\
& && +\frac{4}{9}D^2(b_6^D-3b_6^F)M_{10}(\eta,\Sigma)\\
&- && 2b_6^FM_{11}(\pi)+(b_6^D-b_6^F)M_{11}(K)\\
&- && (b_9+4b_{11})M_{12}(\pi)+2(b_{10}-b_{11})M_{12}(K)\quad , \qquad\qquad (A.94)\\
F_2^{\Xi^0}(t) &= && -\frac{m_\Xi}{\bar m}\frac{2\bar b_6^D}{3}Z_\Xi+\frac{4}{3}m_\Xi\Big[(M_K^2-M_\pi^2)(2\alpha_3-\beta_1)-2M_K^2\alpha_4\Big]\\
&- && \frac{4}{3}\Big[d_{102}+2m_\Xi\eta_2\Big]\,t\\
&- && 2(D-F)^2(M_5+M_6)(\pi,\Xi)+2(D+F)^2(M_5+M_6)(K,\Sigma)\\
&- && 2(D-F)^2b_6^FM_{10}(\pi,\Xi)-\frac{1}{9}(D-3F)^2b_6^DM_{10}(K,\Lambda)\\
& && +(D+F)^2(b_6^D+2b_6^F)M_{10}(K,\Sigma)
\end{aligned}
$$

$$
\begin{aligned}
&\quad +\frac{2}{3}(D+F)(D-3F)b_6^D M_{10}(K,\Lambda\Sigma) - \frac{2}{9}(D+3F)^2 b_6^D M_{10}(\eta,\Xi) \\
&- \quad (b_6^D - b_6^F)M_{11}(\pi) - (b_6^D + b_6^F)M_{11}(K) \\
&- \quad 2(b_{10}-b_{11})M_{12}(\pi) - 2(b_{10}+b_{11})M_{12}(K) \quad , \qquad \text{(A.95)} \\
F_2^{\Xi^-}(t) \quad &= \quad \frac{m_\Xi}{\bar{m}}\left(\frac{\bar{b}_6^D}{3} - b_6^F\right)Z_\Xi \\
&+ \quad 4m_\Xi\left[(M_K^2 - M_\pi^2)\left(\alpha_1 - \frac{\alpha_3}{3} - \frac{\beta_1}{3}\right) - M_K^2\left(\alpha_2 - \frac{\alpha_4}{3}\right)\right] \\
&- \quad 2\left[d_{101} - \frac{d_{102}}{3} + 2m_\Xi\left(\eta_1 - \frac{\eta_2}{3}\right)\right] t \\
&- \quad (D-F)^2(M_5 - 2M_6)(\pi,\Xi) + \frac{1}{3}(D-3F)^2 M_6(K,\Lambda) \\
&\quad -(D+F)^2(2M_5 - M_6)(K,\Sigma) - \frac{1}{3}(D+3F)^2 M_5(\eta,\Xi) \\
&- \quad (D-F)^2(b_6^D + b_6^F)M_{10}(\pi,\Xi) - \frac{1}{9}(D-3F)^2 b_6^D M_{10}(K,\Lambda) \\
&\quad +(D+F)^2(b_6^D - 2b_6^F)M_{10}(K,\Sigma) \\
&\quad -\frac{2}{3}(D+F)(D-3F)b_6^D M_{10}(K,\Lambda\Sigma) \\
&\quad +\frac{1}{9}(D+3F)^2(b_6^D - 3b_6^F)M_{10}(\eta,\Xi) \\
&+ \quad (b_6^D - b_6^F)M_{11}(\pi) - 2b_6^F M_{11}(K) \\
&+ \quad 2(b_{10}-b_{11})M_{12}(\pi) - (b_9 + 4b_{11})M_{12}(K)) \quad , \qquad \text{(A.96)} \\
\sqrt{3}F_2^{\Lambda\Sigma^0}(t) \quad &= \quad \frac{m_\Lambda + m_\Sigma}{2m}\bar{b}_6^D\sqrt{Z_\Lambda Z_\Sigma} + 2(m_\Lambda + m_\Sigma)M_\pi^2\alpha_4 + 2\left[d_{102} + (m_\Lambda + m_\Sigma)\eta_2\right] t \\
&- \quad 8DF(M_5 + M_6)(\pi,\Sigma) - (D-F)(D+3F)(M_5+M_6)(K,N) \\
&\quad +(D+F)(D-3F)(M_5+M_6)(K,\Xi) \\
&- \quad 8DFb_6^F M_{10}(\pi,\Sigma) + \frac{4}{3}D^2 b_6^D M_{10}(\pi,\Sigma\Lambda) \\
&\quad -(D-F)(D+3F)(b_6^D + b_6^F)M_{10}(K,N) \\
&\quad -(D-3F)(D+F)(b_6^D - b_6^F)M_{10}(K,\Xi) - \frac{4}{3}D^2 b_6^D M_{10}(\eta,\Lambda\Sigma) \\
&+ \quad 2b_6^D M_{11}(\pi) + b_6^D M_{11}(K) + 4b_{10}M_{12}(\pi) + 2b_{10}M_{12}(K) \quad . \qquad \text{(A.97)}
\end{aligned}
$$

Finally, the four Z factors of relevance are given by

$$
\begin{aligned}
Z_N \quad &= \quad 1 + 3(D+F)^2\, Z(\pi,N) + \frac{1}{3}(D+3F)^2\, Z(K,\Lambda) \\
&\qquad + 3(D-F)^2\, Z(K,\Sigma) + \frac{1}{3}(D-3F)^2\, Z(\eta,N) \quad , \qquad \text{(A.98)} \\
Z_\Lambda \quad &= \quad 1 + 4D^2\, Z(\pi,\Sigma) + \frac{2}{3}(D+3F)^2\, Z(K,N)
\end{aligned}
$$

$$
\begin{aligned}
& + \frac{2}{3}(D-3F)^2\, Z(K,\Xi) \;+\; \frac{4}{3}D^2\, Z(\eta,\Lambda) \quad , && \text{(A.99)}\\
Z_\Sigma \;=\;& 1 \;+\; 8F^2\, Z(\pi,\Sigma) \;+\; \frac{4}{3}D^2\, Z(\pi,\Lambda) \;+\; 2(D-F)^2\, Z(K,N) \\
& + 2(D+F)^2\, Z(K,\Xi) \;+\; \frac{4}{3}D^2\, Z(\eta,\Sigma) \quad , && \text{(A.100)}\\
Z_\Xi \;=\;& 1 \;+\; 3(D-F)^2\, Z(\pi,\Xi) \;+\; \frac{1}{3}(D-3F)^2\, Z(K,\Lambda) \\
& + 3(D+F)^2\, Z(K,\Sigma) \;+\; \frac{1}{3}(D+3F)^2\, Z(\eta,\Xi) \quad , && \text{(A.101)}
\end{aligned}
$$

employing again the same notation for different intermediate states as for the form factor diagrams.

A.3 The nucleon form factors in SU(2)

Again due to vast simplifications for the kinematics in the SU(2) calculation, and also for the sake of the more elegant combined representation of proton and neutron form factors in terms of isovector and isoscalar contributions, we also summarise the forms of the different Feynman diagrams in terms of loop functions for this particular case, although all of the below can in principle be isolated from the pion loop contributions to the SU(3) form factors in the previous sections. For the contributions to the form factors $F_1^{p/n}(t)$, we find

$$
\begin{aligned}
E_{1+3} &= \frac{1}{2}(1+\tau_3) - \left(\tau^3\, d_6 + 2\, d_7\right) t \quad , && \text{(A.102)}\\
E_5 &= \frac{g_A^2}{8F_\pi^2}\,(3-\tau^3)\left\{\Delta_\pi - 4m_N^2 I^{(1)}(m_N^2) - 4m_N^2 M_\pi^2 I_{12}(t)\right.\\
&\qquad\qquad \left. + 8m_N^2 I_{12}^{(3)}(t) + 32m_N^4 I_{12}^{(4)}(t)\right\} \quad , && \text{(A.103)}\\
E_6 &= -\frac{g_A^2}{F_\pi^2}\,\tau^3\left\{t J^{(1)}(t) + 4m_N^2 I_{21}^{00}(t) + 16m_N^4 I_{21}^{QQ}(t)\right\} \quad , && \text{(A.104)}\\
E_7 &= \frac{g_A^2}{F_\pi^2}\,\tau^3\left\{\Delta_\pi - 2m_N^2 I^{(1)}(m_N^2)\right\} \quad , && \text{(A.105)}\\
E_8 &= -\frac{\tau^3}{2F_\pi^2}\,\Delta_\pi \quad , && \text{(A.106)}\\
E_9 &= \frac{\tau^3}{F_\pi^2}\, t\, J^{(1)}(t) \quad , && \text{(A.107)}\\
E_{10} &= \frac{m_N^2 g_A^2}{F_\pi^2}\Big((3-\tau^3)c_6 + 6c_7\Big)\, t\, I_{12}^{(4)}(t) \quad , && \text{(A.108)}\\
E_{11} &= \frac{3M_\pi^2}{4m_N F_\pi^2}\,(1+\tau^3)\, c_2\left\{\Delta_\pi - \frac{M_\pi^2}{32\pi^2}\right\} \quad . && \text{(A.109)}
\end{aligned}
$$

Similarly, one obtains for the $F_2^{p/n}(t)$ contributions

$$
\begin{aligned}
M_{2-3+4} &= \frac{1}{2}(1+\tau^3)\,c_6 + c_7 + \Big(\tau^3\,d_6 + 2\,d_7\Big)\,t + 2m_N\Big(2\,e_{54} + \tau^3\,e_{74}\Big)\,t \\
&\quad -8m_N M_\pi^2\Big(2\,e_{105} + \tau^3\,e_{106}\Big) \;, \qquad \text{(A.110)} \\
M_5 &= -\frac{g_A^2}{F_\pi^2}\,(3-\tau^3)\,4m_N^1\,I_{12}^{(4)}(t) \;, \qquad \text{(A.111)} \\
M_6 &= \frac{g_A^2}{F_\pi^2}\,\tau^3\,16m_N^4\,I_{21}^{QQ}(t) \;, \qquad \text{(A.112)} \\
M_{10} &= -\frac{g_A^2}{8F_\pi^2}\Big((3-\tau^3)\,c_6 + 6c_7\Big)\Big\{\Delta_\pi - 4m_N^2 I^{(1)}(m_N^2) + 4m_N^2 M_\pi^2 I_{12}(t) \\
&\qquad -16m_N^2 I_{12}^{(3)}(t) + 8m_N^2 t\Big(I_{12}^{(4)}(t) - I_{12}^{(5)}(t)\Big)\Big\} \;, \qquad \text{(A.113)} \\
M_{11} &= -\frac{3M_\pi^2}{4m_N F_\pi^2}\,(1+\tau^3)\,c_2\left\{\Delta_\pi - \frac{M_\pi^2}{32\pi^2}\right\} - \frac{\tau^3}{2F_\pi^2}\,c_6\,\Delta_\pi \;, \qquad \text{(A.114)} \\
M_{12} &= \frac{4m_N}{F_\pi^2}\,\tau^3\,c_4\,t\,J^{(1)}(t) \;. \qquad \text{(A.115)}
\end{aligned}
$$

Observe the one inconsistency in our treatment of certain higher order contributions in SU(2) compared to SU(3): the diagram E_{11}, see Fig. 2.2 for reference, was omitted in the previous section, as well as c_2–like contributions to M_{11}. These c_2 contributions are of higher order than would be allowed for in a fourth–order heavy–baryon calculation, so one might argue whether or not to include these terms at all. For the sake of completeness, we have included them in the SU(2) calculation. They have been omitted in the SU(3) calculation mainly because the corresponding low energy constants would again have been unknown. We emphasise that these terms, as tadpole type contributions, only enter indirectly via small renormalisation effects and have no significant impact on the phenomenological description of the form factors at all.

We here spell out the Z factor needed for wave function renormalisation up to fourth order. Of course, we now also have to take care of c_2 contributions here, which cancel the direct ones in the electric form factors. The other terms can also be taken directly from the SU(3) representation of the wave function renormalisation given above. For the evaluation of the form factor F_1, the nucleon charge has to be multiplied by Z_N, while for F_2, the anomalous magnetic moment (a second order contribution) only has to be renormalised by the Z–factor up to third order, i.e. the term $\sim c_2$ can be dropped.

$$
\begin{aligned}
Z_N &= 1 + \frac{3g_A^2}{4F_\pi^2}\Big\{M_\pi^2 I(m_N^2) - 2m_N^2 I^{(1)}(m_N^2) + 4m_N^2 M_\pi^2\Big(I_{12}(0) - 2I_{12}^{(1)}(0)\Big)\Big\} \\
&\quad - c_2\,\frac{3M_\pi^2}{2m_N F_\pi^2}\left(\Delta_\pi - \frac{M_\pi^2}{32\pi^2}\right) \;. \qquad \text{(A.116)}
\end{aligned}
$$

A.4 Strangeness form factors of the nucleon

As for the electromagnetic form factors of the baryon ground state octet, we show the strange vector form factors of the nucleon in terms of basic Feynman diagram structures. In analogy to what was done before, we shall use the abbreviation $\bar{b}_6^0 = b_6^0 + 2\bar{m}\,(2M_K^2 + M_\pi^2)\,\tilde{b}_6^0$ as in Eq. (4.6). Again, one can use $\bar{b}_6^0$ instead of b_6^0 in the loop contributions to the accuracy given here.

$$
\begin{aligned}
F_{1,s}(t) &= 2\Big(d_{101} - \frac{d_{102}}{3} - d_{102}^0\Big)\,t \\
&+ \frac{1}{3}(D+3F)^2(E_5+E_6+E_7)(K,\Lambda) + 3(D-F)^2(E_5+E_6+E_7)(K,\Sigma) \\
&- 3(E_8+E_9)(K) \\
&+ (D+F)^2(b_6^D - 3b_6^F + 3b_6^0)E_{10}(\pi,N) + \frac{1}{9}(D+3F)^2(2b_6^D + 3b_6^0)E_{10}(K,\Lambda) \\
&\quad -(D-F)^2(2b_6^D - 3b_6^0)E_{10}(K,\Sigma) \\
&\quad +\frac{1}{9}(D-3F)^2(b_6^D - 3b_6^F + 3b_6^0)E_{10}(\eta,N) \quad , \qquad \text{(A.117)} \\
F_{2,s}(t) &= \frac{m_N}{m}\Big(\frac{\bar{b}_6^D}{3} - \bar{b}_6^F + \bar{b}_6^0\Big)Z_N \\
&- 4m_N\Big[(M_K^2 - M_\pi^2)\Big(\alpha_1 - \frac{\alpha_3}{3} - \frac{2\beta_1}{3} + \gamma_2\Big) + M_K^2\Big(\alpha_2 - \frac{\alpha_4}{3} - \gamma_1\Big)\Big] \\
&- 2\Big[d_{101} - \frac{d_{102}}{3} - d_{102}^0 + 2m_N\Big(\eta_1 - \frac{\eta_2}{3} - \eta_0\Big)\Big]\,t \\
&+ \frac{1}{3}(D+3F)^2(M_5+M_6)(K,\Lambda) + 3(D-F)^2(M_5+M_6)(K,\Sigma) \\
&+ (D+F)^2(b_6^D - 3b_6^F + 3b_6^0)M_{10}(\pi,N) + \frac{1}{9}(D+3F)^2(2b_6^D + 3b_6^0)M_{10}(K,\Lambda) \\
&\quad -(D-F)^2(2b_6^D - 3b_6^0)M_{10}(K,\Sigma) \\
&\quad +\frac{1}{9}(D-3F)^2(b_6^D - 3b_6^F + 3b_6^0)M_{10}(\eta,N) \\
&+ (b_6^D - 3b_6^F)M_{11}(K) - (b_9 - 2b_{10} + 6b_{11})M_{12}(K) \quad . \qquad \text{(A.118)}
\end{aligned}
$$

A.5 Counterterm scale dependences

In this appendix, we collect the scale dependence of the various third– and fourth–order counterterms that enter the description of the baryon form factors.

There are two infinite counterterms at third order entering the electric radii, d_{101} and d_{102} (see Eq. (3.7), the scale dependence of which is determined by the appropriate β–functions [MM97]

$$\beta_{d_{101}} = -\frac{9 + 25D^2 + 45F^2}{36} \quad , \qquad \text{(A.119)}$$

$$\beta_{d_{102}} = -\frac{5DF}{2} \quad . \tag{A.120}$$

Remember the the low energy constant for the singlet radius, d^0_{102}, is finite.

At fourth order, another two low–energy constants ($\eta_{1/2}$ as defined in Eq. (3.8)) enter the magnetic radii. There infinite parts are given by

$$\beta_{\eta_1} = \frac{1}{8m}\left[1 - \frac{7}{9}\left(5D^2 + 9F^2\right)\right] + \frac{b_9}{6} + b_{11} \quad , \tag{A.121}$$

$$\beta_{\eta_2} = -\frac{7DF}{4m} + b_{10} \quad . \tag{A.122}$$

Again, the corresponding constant for the singlet magnetic radius, η_0, is finite.

No less than seven infinite counterterms have to be included in the description of the magnetic moments at fourth order. These are also defined in Eq. (3.8). We have disentangled also the scale dependence of these and found:

$$\begin{aligned}\beta_{\alpha_1} &= -\frac{1}{3m}\left[19DF + \frac{1}{24}\left(27 + 25D^2 - 99F^2\right)b_6^D + \frac{31}{4}DFb_6^F\right] \\ &\quad -\frac{5}{3}\left[2DFb_D + \left(D^2 - 3F^2\right)b_F\right] + 3b_{10} \quad , \end{aligned}\tag{A.123}$$

$$\begin{aligned}\beta_{\alpha_2} &= -\frac{1}{2m}\left[\frac{5}{3}D^2 - 9F^2 + \frac{1}{6}DFb_6^D - \frac{1}{12}\left(9 - 25D^2 + 63F^2\right)b_6^F\right] \\ &\quad -\frac{1}{3}\left(17D^2 + 9F^2\right)b_D - 6DFb_F - b_9 - 3b_{11} \quad , \end{aligned}\tag{A.124}$$

$$\begin{aligned}\beta_{\alpha_3} &= -\frac{1}{2m}\left[3\left(D^2 + F^2\right) + \frac{31}{6}DFb_6^D + \frac{3}{4}\left(1 - D^2 - F^2\right)b_6^F\right] \\ &\quad +3\left(D^2 + F^2\right)b_D + 6DFb_F + 3b_{11} \quad , \end{aligned}\tag{A.125}$$

$$\begin{aligned}\beta_{\alpha_4} &= \frac{1}{m}\left[3DF + \frac{1}{24}\left(9 + 11D^2 - 9F^2\right)b_6^D - \frac{3}{4}DFb_6^F\right] \\ &\quad +6DFb_D + 3\left(D^2 - 3F^2\right)b_F - 3b_{10} \quad , \end{aligned}\tag{A.126}$$

$$\begin{aligned}\beta_{\beta_1} &= -\frac{1}{m}\left[4DF + \frac{1}{18}\left(9 + 17D^2 - 45F^2\right)b_6^D - DFb_6^F\right] \\ &\quad -16DFb_D - 8D^2b_F + 4b_{10} \quad , \end{aligned}\tag{A.127}$$

$$\begin{aligned}\beta_{b_6^D} &= \frac{1}{2m}\left[4DF + \frac{1}{18}\left(9 + 43D^2 + 135F^2\right)b_6^D - DFb_6^F\right] \\ &\quad -4DFb_D - 2\left(D^2 - 3F^2\right)b_F - 2b_{10} \quad , \end{aligned}\tag{A.128}$$

$$\begin{aligned}\beta_{b_6^F} &= \frac{1}{2m}\left[\frac{70}{9}D^2 + 6F^2 - DFb_6^D + \frac{1}{18}\left(9 + 95D^2 + 63F^2\right)b_6^F\right] \\ &\quad +\frac{2}{9}\left(17D^2 + 9F^2\right)b_D + 4DFb_F - 2b_{11} \quad . \end{aligned}\tag{A.129}$$

Finally, we also show the beta–functions for the three new magnetic moment counterterms that have to be included for the singlet current, see Eq. (4.5):

$$\beta_{\gamma_1} = -\frac{1}{m}\left(D^2 - 3F^2\right)\left(1 + b_6^0\right) , \tag{A.130}$$

$$\beta_{\gamma_2} = \frac{10}{3m} DF\left(1 + b_6^0\right) , \tag{A.131}$$

$$\beta_{\tilde{b}_6^0} = \frac{2}{9m}\left(13D^2 + 9F^2\right)\left(1 + b_6^0\right) . \tag{A.132}$$

A.6 Imaginary parts and spectral functions

Out of the diagrams depicted in Fig. 2.2, only graphs (6), (9), and (12) contribute to the spectral functions of the isovector form factors in the low–energy region, i.e. starting at the threshold $t = 4M_\pi^2$. The separate contributions can be calculated either from the imaginary parts of the two basic loop functions involved (see also [GSS88]),

$$\mathrm{Im}\, J(t) = \frac{1}{16\pi}\sqrt{1 - \frac{4M_\pi^2}{t}} , \tag{A.133}$$

$$\mathrm{Im}\, I_{21}(t) = \frac{1}{8\pi}\frac{1}{\sqrt{t(4m_N^2 - t)}} \arctan\frac{\sqrt{(4m_N^2 - t)(t - 4M_\pi^2)}}{t - 2M_\pi^2} , \tag{A.134}$$

or directly by using Cutkosky rules. This leads to the following expressions:

$$\begin{aligned}
\mathrm{Im}\, E_6 &= \frac{\tau^3 g_A^2}{192\pi F_\pi^2 (4m_N^2 - t)^2}\sqrt{1 - \frac{4M_\pi^2}{t}} \\
&\times \left\{16m_N^4\left(5t - 8M_\pi^2\right) + 4m_N^2\, t\left(5t - 14M_\pi^2\right) - t^2\left(t - 4M_\pi^2\right)\right. &\quad (\mathrm{A}.135)\\
&- \left. 48m_N^2\, \frac{m_N^2\left(3t^2 - 12M_\pi^2 t + 8M_\pi^4\right) + M_\pi^4 t}{\sqrt{(4m_N^2 - t)(t - 4M_\pi^2)}} \arctan\frac{\sqrt{(4m_N^2 - t)(t - 4M_\pi^2)}}{t - 2M_\pi^2}\right\} ,
\end{aligned}$$

$$\begin{aligned}
\mathrm{Im}\, M_6 &= \frac{\tau^3 g_A^2 m_N^4}{4\pi F_\pi^2 (4m_N^2 - t)^2}\sqrt{1 - \frac{4M_\pi^2}{t}}\left\{-3\left(t - 2M_\pi^2\right)\right. &\quad (\mathrm{A}.136)\\
&\left. + 2\,\frac{\left(2m_N^2 + t\right)\left(t - 4M_\pi^2\right) + 6M_\pi^4}{\sqrt{(4m_N^2 - t)(t - 4M_\pi^2)}} \arctan\frac{\sqrt{(4m_N^2 - t)(t - 4M_\pi^2)}}{t - 2M_\pi^2}\right\} ,
\end{aligned}$$

$$\mathrm{Im}\, E_9 = \frac{\tau^3}{192\pi F_\pi^2}\frac{(t - 4M_\pi^2)^{3/2}}{t^{1/2}} , \tag{A.137}$$

$$\mathrm{Im}\, M_{12} = \frac{m_N\, c_4\, \tau^3}{48\pi F_\pi^2}\frac{(t - 4M_\pi^2)^{3/2}}{t^{1/2}} . \tag{A.138}$$

For these results, see also [GSS88, BKM96c].

Appendix B

Pion–kaon amplitudes, scattering lengths, and infrared divergences

B.1 The scattering amplitude $\pi^- K^+ \to \pi^0 K^0$

In this appendix, we collect the various pieces of the scattering amplitude for the process $\pi^- K^+ \to \pi^0 K^0$ up to one–loop order, including isospin–breaking corrections up to order $\delta \in \{\epsilon,\, e^2\}$.

B.1.1 Loop functions

First, we write down the loop functions needed for this section. We define

$$\frac{1}{i}\int \frac{d^d k}{(2\pi)^d}\frac{1}{M_a^2 - k^2} \;=\; \Delta_a \quad , \tag{B.1}$$

$$\begin{aligned}\frac{1}{i}\int \frac{d^d k}{(2\pi)^d}&\frac{\{\,1\,;\,k_\mu\,;\,k_\mu k_\nu\,\}}{(M_a^2 - k^2)(M_b^2 - (k-q)^2)} \\ &= \left\{J_{ab}(q^2)\,;\,q_\mu J_{ab}^{(1)}(q^2)\,;\,q_\mu q_\nu J_{ab}^{(2)}(q^2) + g_{\mu\nu} J_{ab}^{(3)}(q^2)\right\} \quad ,\end{aligned} \tag{B.2}$$

$$\begin{aligned}\frac{1}{i}\int \frac{d^d k}{(2\pi)^d}&\frac{\{\,1\,;\,k_\mu\,\}}{(M_a^2 - (k+q_a)^2)(M_b^2 - (k-q_b)^2)(k^2 - m_\gamma^2)} \\ &= \left\{G_{ab\gamma}(q^2)\,;\,(q_a+q_b)_\mu\, G^+_{ab\gamma}(q^2) + (q_a-q_b)_\mu\, G^-_{ab\gamma}(q^2)\right\} \quad ,\end{aligned} \tag{B.3}$$

where, for Eq. (B.3), we have used $q^2 = (q_a+q_b)^2$. The tadpole loop function Δ_a has been given before in App. A.1, and $G_{ab\gamma}(q^2)$ is discussed extensively in Chapter 6. In addition, we have

$$J_{ab}(q^2) \;=\; -2L - \frac{1}{16\pi^2}\left\{\frac{2}{M_a^2 - M_b^2}\left(M_a^2 \log\frac{M_a}{\lambda} - M_b^2 \log\frac{M_a}{\lambda}\right)\right. \tag{B.4}$$

$$+\left(\frac{M_a^2-M_b^2}{q^2}-\frac{M_a^2+M_b^2}{M_a^2-M_b^2}\right)\log\frac{M_a}{M_b}-1$$
$$+\frac{\nu}{2q^2}\left[\log\left(\frac{q^2-M_a^2-M_b^2+\nu}{q^2-M_a^2-M_b^2-\nu}\right)-2\pi i\,\theta\left(q^2-(M_a+M_b)^2\right)\right]\theta\left(\nu^2\right)$$
$$+\frac{\sqrt{-\nu^2}}{q^2}\left[\arctan\left(\frac{M_a^2-M_b^2+q^2}{\sqrt{-\nu^2}}\right)-\arctan\left(\frac{M_a^2-M_b^2-q^2}{\sqrt{-\nu^2}}\right)\right]\theta\left(-\nu^2\right)\Bigg\}\ ,$$

where we have made use of the usual Heavyside function $\theta(x)$ and the definition

$$\nu^2 = \left(q^2-(M_a-M_b)^2\right)\left(q^2-(M_a+M_b)^2\right)\ . \tag{B.5}$$

The constant L containing the divergent part in $d-4$ is given in Eq. (A.44). The tensor loop integrals $J_{ab}^{(i)}(q^2)$ can be reduced according to [GL85a]: we define the auxiliary functions

$$I_1(q^2) = M_a^2\,J_{ab}(q^2)-\Delta_b\ , \tag{B.6}$$
$$I_2(q^2) = \frac{1}{4}\left\{(\Delta_a-\Delta_b)\left(q^2+M_a^2-M_b^2\right)-2q^2\Delta_b+\left(q^2+M_a^2-M_b^2\right)^2 J_{ab}(q^2)\right\}\ , \tag{B.7}$$

and find

$$J_{ab}^{(1)}(q^2) = \frac{1}{2q^2}\left\{\Delta_a-\Delta_b+\left(q^2+M_a^2-M_b^2\right)J_{ab}(q^2)\right\}\ , \tag{B.8}$$
$$J_{ab}^{(2)}(q^2) = -\frac{1}{(d-1)\,q^4}\left\{q^2I_1(q^2)-d\,I_2(q^2)\right\}\ , \tag{B.9}$$
$$J_{ab}^{(3)}(q^2) = \frac{1}{(d-1)\,q^4}\left\{q^2I_1(q^2)-I_2(q^2)\right\}\ . \tag{B.10}$$

Finally, the loop functions $G_{ab\gamma}^{\pm}(q^2)$ are found to be

$$G_{ab\gamma}^{+}(q^2) = \frac{1}{\nu^2}\Bigg\{\left(M_b^2-M_a^2\right)\left(J_{ab}(q^2)-\frac{1}{16\pi^2}\right)$$
$$+\frac{q^2-3M_a^2-M_b^2}{2M_a^2}\,\Delta_a-\frac{q^2-M_a^2-3M_b^2}{2M_b^2}\,\Delta_b\Bigg\}\ , \tag{B.11}$$
$$G_{ab\gamma}^{-}(q^2) = \frac{1}{\nu^2}\left\{q^2\left(J_{ab}(q^2)-\frac{1}{16\pi^2}\right)+\frac{q^2+M_a^2-M_b^2}{2M_a^2}\,\Delta_a+\frac{q^2-M_a^2+M_b^2}{2M_b^2}\,\Delta_b\right\}\ . \tag{B.12}$$

Note that, as in Chapter 6, we have only considered the simplified case $q_{a/b}^2 = M_{a/b}^2$ that is needed for the calculation at hand. We mention that for equal masses $M_a = M_b$, $G_{ab\gamma}^{+}(q^2)$ vanishes on symmetry reasons.

B.1.2 Hadronic loop diagrams

Here we display the analytic formulae for the various $s-$, $t-$, $u-$channel loops in terms of the loop functions defined in the previous section. We reemphasise that the masses M_K, M_π refer to our choice of the isospin limit, the *charged* meson masses. Isospin breaking effects are usually expressed in terms of the lowest–order $\pi^0\eta$ mixing angle ϵ and the charged–to–neutral pion mass difference $\Delta M_\pi^2 = M_{\pi^\pm}^2 - M_{\pi^0}^2$, just occasionally $\Delta M_K^2 = M_{K^-}^2 - M_{K^0}^2$ or just neutral meson masses are used when this simplifies expressions significantly. The superscripts s, t, u of the various amplitudes T specify the channel, the subscripts the virtual mesons in the intermediate state. In cases where loop functions are already multiplied by isospin breaking parameters, the charge of the virtual mesons is not specified (as the difference is of higher order).

$$
\begin{aligned}
T^s_{\pi^-K^+} &= -\frac{1}{12\sqrt{2}F^4}\Big(1+\frac{\epsilon}{\sqrt{3}}\Big)\bigg\{\Big[3(s-M_\pi^2)+M_K^2+8\Delta M_\pi^2\Big]\Delta_{K^+} \\
&\quad+\Big[(s-M_K^2)^2-M_\pi^4+4\left(2(s-M_K^2)-M_\pi^2\right)\Delta M_\pi^2\Big]J_{\pi^-K^+}(s) \\
&\quad+2\Big[(s-M_\pi^2)^2+M_K^2(s+M_\pi^2)-2M_K^4 \\
&\qquad+2\left(2s+3(M_K^2-M_\pi^2)\right)\Delta M_\pi^2\Big]J^{(1)}_{\pi^-K^+}(s) \\
&\quad+\left(s+3(M_K^2-M_\pi^2)\right)\left(s+M_K^2-M_\pi^2\right)J^{(2)}_{\pi^-K^+}(s) \\
&\quad+2s\Big[u-2t+3M_K^2-M_\pi^2 \\
&\qquad+\left(3(t-u)+M_K^2-M_\pi^2\right)\frac{2\epsilon}{\sqrt{3}}-\Delta M_\pi^2\Big]J^{(3)}_{\pi^-K^+}(s)\bigg\}\ ,
\end{aligned}
\tag{B.13}
$$

$$
\begin{aligned}
T^s_{\pi^0K^0} &= \frac{1}{24\sqrt{2}F^4}\Big(1-\frac{5\epsilon}{\sqrt{3}}\Big)\bigg\{\bigg[\left(s-M_K^2-3M_\pi^2\right)^2-4M_\pi^4+8\left(s-M_K^2-2M_\pi^2\right)\Delta M_\pi^2 \\
&\qquad-\left(3(s-M_K^2)M_K^2-(M_K^2+2M_\pi^2)M_\pi^2\right)\frac{8\epsilon}{\sqrt{3}}\bigg]J_{\pi^0K^0}(s) \\
&\quad+2\bigg[s^2-2s(M_K^2+M_\pi^2)+(M_K^2-M_\pi^2)^2+4s\,\Delta M_\pi^2 \\
&\qquad-\left(s\,(5M_K^2-2M_\pi^2)+3\left(M_K^4-3M_K^2M_\pi^2+2M_\pi^4\right)\right)\frac{4\epsilon}{\sqrt{3}}\bigg]J^{(1)}_{\pi^0K^0}(s) \\
&\quad+\bigg[\left(s+M_K^2-M_\pi^2\right)\left(s-3(M_K^2-M_\pi^2)\right)-s\,(M_K^2-M_\pi^2)\frac{16\epsilon}{\sqrt{3}}\bigg]J^{(2)}_{\pi^0K^0}(s) \\
&\quad-2s\Big[2u-t-2M_\pi^2+\Delta M_\pi^2+\left(t-u+M_K^2-M_\pi^2\right)2\sqrt{3}\epsilon\Big]J^{(3)}_{\pi^0K^0}(s) \\
&\quad+\bigg[3s-5M_K^2-3M_\pi^2+8\Delta M_\pi^2-\left(11M_K^2-5M_\pi^2\right)\frac{4\epsilon}{\sqrt{3}}\bigg]\Delta_{K^0}\bigg\}\ ,
\end{aligned}
\tag{B.14}
$$

$$
\begin{aligned}
T^s_{\eta K^0} \;=\; & -\frac{1}{24\sqrt{2}F^4}\Big(1-\frac{5\epsilon}{\sqrt{3}}\Big)\bigg\{\frac{1}{9}\bigg[\Big(3s+M_K^2-7M_\pi^2\Big)\Big(3s+M_K^2-7M_\pi^2+12\Delta M_\pi^2\Big) \\
& \qquad + \Big(3s(M_K^2-M_\pi^2)+M_K^4-8M_K^2M_\pi^2+7M_\pi^4\Big)\frac{10\epsilon}{\sqrt{3}}\bigg]J_{\eta K^0}(s) \qquad \text{(B.15)} \\
& +2\bigg[s\Big(s-\frac{8}{3}M_K^2+\frac{2}{3}M_\pi^2\Big)-(M_K^2-7M_\pi^2)(M_K^2-M_\pi^2) \\
& \qquad -\Big(2s+9(M_K^2-2M_\pi^2)\Big)(M_K^2-M_\pi^2)\frac{8\epsilon}{3\sqrt{3}} \\
& \qquad +2\Big(s-3(M_K^2-M_\pi^2)\Big)\Delta M_\pi^2\bigg]J^{(1)}_{\eta K^0}(s) \\
& +\Big(s-3(M_K^2-M_\pi^2)\Big)\bigg[s-3(M_K^2-M_\pi^2)\Big(1+\frac{8\epsilon}{\sqrt{3}}\Big)\bigg]J^{(2)}_{\eta K^0}(s) \\
& +2s\bigg[4u-5t-2M_K^2+4M_\pi^2-\Delta M_\pi^2-\Big(9(t-u)+5(M_K^2-M_\pi^2)\Big)\frac{2\epsilon}{\sqrt{3}}\bigg]J^{(3)}_{\eta K^0}(s) \\
& +\bigg[3s-5M_K^2+M_\pi^2+4\Delta M_\pi^2-(M_K^2-M_\pi^2)4\sqrt{3}\epsilon\bigg]\Delta_{K^0}\bigg\} \quad , \\
T^t_{\pi^-\pi^0} \;=\; & \frac{1}{\sqrt{2}F^4}\bigg\{t(s-u)J^{(3)}_{\pi^-\pi^0}(t)-\frac{1}{4}\Big(t-2M_\pi^2\Big)\bigg[\Big(3t-4M_K^2\Big)\frac{\epsilon}{\sqrt{3}}-\Delta M_\pi^2\bigg]J_{\pi\pi}(t) \\
& \qquad -\frac{1}{6}\bigg[\Big(5t-4M_K^2-6M_\pi^2\Big)\frac{\epsilon}{\sqrt{3}}-\Delta M_\pi^2\bigg]\Delta_\pi\bigg\} \quad , \qquad \text{(B.16)} \\
T^t_{K^-K^0} \;=\; & \frac{1}{2\sqrt{2}F^4}\bigg\{t(s-u)J^{(3)}_{K^-K^0}(t)+\frac{t}{4}\bigg[\Big(3t-4M_K^2\Big)\frac{\epsilon}{\sqrt{3}}-\Delta M_\pi^2\bigg]J_{KK}(t) \\
& \qquad +\frac{1}{6}\bigg[\Big(5t-4M_K^2\Big)\frac{\epsilon}{\sqrt{3}}-\Delta M_\pi^2\bigg]\Delta_K\bigg\} \quad , \qquad \text{(B.17)} \\
T^t_{\pi^-\eta} \;=\; & \frac{\epsilon}{12\sqrt{6}F^4}\bigg\{\Big(3(t-M_\eta^2)-M_\pi^2\Big)^2J_{\pi\eta}(t)+\Big(5(t-M_\eta^2)-3M_\pi^2\Big)\Delta_\pi \\
& \qquad +\Big(5t-7M_\eta^2-M_\pi^2\Big)\Delta_\eta\bigg\} \quad , \qquad \text{(B.18)} \\
T^u_{K^-\pi^0} \;=\; & -\frac{1}{24\sqrt{2}F^4}\Big(1+\frac{5\epsilon}{\sqrt{3}}\Big)\bigg\{\bigg[\Big(u-3M_K^2-M_\pi^2\Big)^2-4M_K^2(M_K^2-\Delta M_\pi^2) \qquad \text{(B.19)} \\
& \qquad +M_K^2\Big(u-M_K^2-M_\pi^2\Big)8\sqrt{3}\epsilon\bigg]J_{K^-\pi^0}(u) \\
& +2\bigg[\Big(u-M_K^2-M_\pi^2\Big)^2-4M_K^2M_\pi^2+2\Big(u-3M_K^2\Big)\Delta M_\pi^2 \\
& \qquad +\Big(u+M_K^2-M_\pi^2\Big)(2M_K^2+M_\pi^2)\frac{4\epsilon}{\sqrt{3}}\bigg]J^{(1)}_{K^-\pi^0}(u)
\end{aligned}
$$

$$
\begin{aligned}
&+\Big[\Big(u+3(M_K^2-M_\pi^2)\Big)\Big(u-(M_K^2-M_\pi^2)\Big(1+\frac{8\epsilon}{\sqrt{3}}\Big)\Big)+4u\,\Delta M_\pi^2\Big]J^{(2)}_{K^-\pi^0}(u)\\
&-2u\Big[2s-t-2M_K^2-\Delta M_\pi^2+\Big(3(s-t)+M_K^2-M_\pi^2\Big)\frac{2\epsilon}{\sqrt{3}}\Big]J^{(3)}_{K^-\pi^0}(u)\\
&+\Big[3(u-M_K^2)-5\Big(M_\pi^2-\Delta M_\pi^2\Big)+(2M_K^2+M_\pi^2)\frac{8\epsilon}{\sqrt{3}}\Big]\Delta_{\pi^0}\quad ,
\end{aligned}
$$

$$
\begin{aligned}
T^u_{\pi^- K^0} \;=\;& \frac{1}{12\sqrt{2}F^4}\Big(1-\frac{\epsilon}{\sqrt{3}}\Big)\Big\{\Big[(u-M_K^2)^2-M_\pi^2(M_\pi^2+2\Delta M_\pi^2) \qquad \text{(B.20)}\\
&\quad -(u-M_K^2)(M_K^2-M_\pi^2)\frac{8\epsilon}{\sqrt{3}}\Big]J_{\pi^-K^0}(u)\\
&+2\Big[(u-M_\pi^2)^2+M_K^2(u+M_\pi^2)-2M_K^4-\Big(u-3M_\pi^2\Big)\Delta M_\pi^2\\
&\quad +\Big(u-4M_K^2+M_\pi^2\Big)(M_K^2-M_\pi^2)\frac{4\epsilon}{\sqrt{3}}\Big]J^{(1)}_{\pi^-K^0}(u)\\
&+\Big[\Big(u+3(M_K^2-M_\pi^2)\Big)\Big(u+M_K^2-M_\pi^2\Big)-2u\,\Delta M_\pi^2\\
&\quad +\Big(2u+3(M_K^2-M_\pi^2)\Big)(M_K^2-M_\pi^2)\frac{8\epsilon}{\sqrt{3}}\Big]J^{(2)}_{\pi^-K^0}(u)\\
&+2u\Big[s-2t+3M_K^2-M_\pi^2-2\Delta M_\pi^2+\Big(3(s-t)+5(M_K^2-M_\pi^2)\Big)\frac{2\epsilon}{\sqrt{3}}\Big]J^{(3)}_{\pi^-K^0}(u)\\
&+\Big[3(u-M_\pi^2)+M_K^2-\Delta M_\pi^2+(M_K^2-M_\pi^2)\frac{4\epsilon}{\sqrt{3}}\Big]\Delta_{K^0}\Big\}\quad ,
\end{aligned}
$$

$$
\begin{aligned}
T^u_{K^-\eta} \;=\;& \frac{1}{24\sqrt{2}F^4}\Big(1+\frac{5\epsilon}{\sqrt{3}}\Big)\Big\{\frac{1}{9}\Big[\Big(3u-7M_K^2+M_\pi^2\Big)^2 \qquad \text{(B.21)}\\
&\quad -\Big(3u(M_K^2-M_\pi^2)-7M_K^4+8M_K^2M_\pi^2-M_\pi^4\Big)\frac{16\epsilon}{\sqrt{3}}\Big]J_{K^-\eta}(u)\\
&+2\Big[u^2+\frac{2}{3}u(M_K^2-4M_\pi^2)-7M_K^4+8M_K^2M_\pi^2-M_\pi^4\\
&\quad -\Big(u+3(M_K^2-M_\pi^2)\Big)(M_K^2-M_\pi^2)\frac{8\epsilon}{3\sqrt{3}}\Big]J^{(1)}_{K^-\eta}(u)\\
&+\Big(u+3(M_K^2-M_\pi^2)\Big)^2J^{(2)}_{K^-\eta}(u)\\
&+2u\Big[4s-5t+4M_K^2-2M_\pi^2-\Delta M_\pi^2-\Big(9(s-t)-M_K^2+M_\pi^2\Big)\frac{2\epsilon}{\sqrt{3}}\Big]J^{(3)}_{K^-\eta}(u)\\
&+\Big[3u+M_K^2-5M_\pi^2+\Delta M_\pi^2-(M_K^2-M_\pi^2)\frac{8\epsilon}{\sqrt{3}}\Big]\Delta_\eta\Big\}\quad . \qquad \text{(B.22)}
\end{aligned}
$$

Next, the tadpole contributions can be written as

$$
\begin{aligned}
T^{\rm tad} = &\ \frac{1}{12\sqrt{2}F^4}\Bigg\{3\left[s-u+\frac{1}{9}\Big(4(M_K^2+2M_\pi^2)-15t\Big)\frac{\epsilon}{\sqrt{3}}+\frac{5}{3}\Delta M_\pi^2\right]\Delta_{\pi^\pm} \qquad \text{(B.23)}\\
&+2\left[s-u+\Big(4M_K^2-3(t+M_\pi^2)\Big)\frac{\epsilon}{\sqrt{3}}+\Delta M_\pi^2\right]\Delta_{\pi^0}\\
&+\left[4s+t-\frac{8}{3}(2M_K^2+M_\pi^2)+\Big(2s-7t-\frac{10}{3}M_K^2+\frac{34}{3}M_\pi^2\Big)\frac{\epsilon}{\sqrt{3}}+13\,\Delta M_\pi^2\right]\Delta_{K^\pm}\\
&+\left[s-3u+\frac{10}{3}M_K^2+\frac{2}{3}M_\pi^2+\Big(7s+9u-20M_\pi^2\Big)\frac{\epsilon}{\sqrt{3}}-\Delta M_\pi^2\right]\Delta_{K^0}\\
&+\left[s-u+\Big(12M_K^2-2M_\pi^2-3t\Big)\frac{\epsilon}{\sqrt{3}}+\Delta M_\pi^2\right]\Delta_\eta\Bigg\}\ .
\end{aligned}
$$

B.1.3 Photon loop diagrams

Here we write down the amplitudes corresponding to the photon loop diagrams (a) and (b) in Fig. 5.1. The subscripts again specify the virtual intermediate states and therefore also distinguish between the triangle diagram ($\pi K\gamma$) and the two self–energy type loops ($\pi\gamma$, $K\gamma$).

$$
\begin{aligned}
T_{\pi K\gamma} = &\ \frac{e^2}{\sqrt{2}F^2}\Bigg\{\Big(s-M_K^2-M_\pi^2\Big)\Big[(s-u)G_{\pi K\gamma}(s) \qquad \text{(B.24)}\\
&\qquad +(M_K^2-M_\pi^2)\,G^1_{\pi K\gamma}(s)+(t-u)\,G_{\pi K\gamma}(s)\Big]\\
&+\frac{1}{4sM_K^2}\Big[s\Big(2(s-u)-t\Big)+(s-M_K^2)\Big(s+M_K^2-M_\pi^2\Big)\Big]\Delta_K\\
&+\frac{1}{4sM_\pi^2}\Big[s\Big(2(s-u)-t\Big)+(s-M_\pi^2)\Big(s-M_K^2+M_\pi^2\Big)\Big]\Delta_\pi\\
&+\frac{1}{4s}\Big[3s^2-2s(M_K^2+M_\pi^2)-(M_K^2-M_\pi^2)^2\Big]J_{\pi K}(s)-\frac{2s-u-M_K^2-M_\pi^2}{16\pi^2}\Bigg\}\ ,\\
T_{\pi\gamma} = &\ \frac{3e^2}{4\sqrt{2}F^2}\Big(u-M_K^2+M_\pi^2\Big)\left\{\frac{\Delta_\pi}{M_\pi^2}-\frac{1}{12\pi^2}\right\}\ , \qquad \text{(B.25)}\\
T_{K\gamma} = &\ \frac{3e^2}{4\sqrt{2}F^2}\Big(u+M_K^2-M_\pi^2\Big)\left\{\frac{\Delta_K}{M_K^2}-\frac{1}{12\pi^2}\right\}\ . \qquad \text{(B.26)}
\end{aligned}
$$

B.1.4 Tree graphs

The lowest order tree graph for the scattering process $\pi^- K^+ \to \pi^0 K^0$ is given, up to order δ, by

$$T^{\rm tree} = -\frac{1}{2\sqrt{2}F^2}\left\{s-u+\frac{\epsilon}{\sqrt{3}}\Big(s-2t+u+2B(m_s-\hat{m})\Big)+2Ze^2F^2\right\}\ . \qquad \text{(B.27)}$$

We do not express the quark mass insertions and the low–energy constant Z in terms of meson masses. The Lagrangians Eqs. (5.9), (5.10) contribute to the scattering amplitude via tree graphs as well as indirectly through various renormalisation effects (as discussed throughout Chapter 5). Here we list the tree graph contributions. The purely strong Lagrangian yields an amplitude

$$
\begin{aligned}
T^{\text{ct}} = & -\frac{\sqrt{2}}{F^4}\Bigg\{L_3\Bigg[\left(1+\frac{\epsilon}{\sqrt{3}}\right)\left(s-M_K^2-M_\pi^2\right)\left(s-M_{K^0}^2-M_{\pi^0}^2\right) \qquad \text{(B.28)}\\
& -\frac{2\epsilon}{\sqrt{3}}\left(t-2M_\pi^2\right)\left(t-2M_K^2\right)\\
& -\left(1-\frac{\epsilon}{\sqrt{3}}\right)\left(u-M_\pi^2-M_{K^0}^2\right)\left(u-M_{\pi^0}^2-M_K^2\right)\Bigg]\\
& +2L_4\left[2M_K^2+M_\pi^2+\frac{4\epsilon}{\sqrt{3}}(M_K^2-M_\pi^2)-3\Delta M_\pi^2\right]\left(s-u+\frac{\epsilon}{\sqrt{3}}(s-2t+u)\right)\\
& +2L_5\Bigg[s\left((M_K^2+M_\pi^2)\left(1+\frac{\epsilon}{\sqrt{3}}\right)-2\Delta M_\pi^2\right)\\
& -u\left((M_K^2+M_\pi^2)+\frac{\epsilon}{\sqrt{3}}(3M_K^2-5M_\pi^2)-2\Delta M_\pi^2\right)\\
& -\frac{4\epsilon}{\sqrt{3}}\left(M_K^2(t-M_\pi^2)+M_\pi^4\right)\Bigg]\\
& +\frac{8\epsilon}{\sqrt{3}}\left(L_6+4L_7\right)(2M_K^2+M_\pi^2)(M_K^2-M_\pi^2)\\
& +\frac{8\epsilon}{3\sqrt{3}}L_8\left(17M_K^4-10M_K^2M_\pi^2-7M_\pi^4\right)\Bigg\} \ . \qquad \text{(B.29)}
\end{aligned}
$$

In addition, the electromagnetic counterterms of the Lagrangian Eq. (5.10) give an amplitude

$$
\begin{aligned}
T^{\text{ct, em}} = & -\frac{\sqrt{2}\,e^2}{9F^2}\Bigg\{6(K_1+K_2)(s-u)-3(2K_3-K_4)\left(3(s-M_K^2)-M_\pi^2\right) \qquad \text{(B.30)}\\
& +K_5\left(2(s+2M_\pi^2)-5u\right)+K_6\left(11s-5u-9M_K^2-5M_\pi^2\right)\\
& +9K_8\left(2M_K^2+M_\pi^2\right)-(K_9+K_{10})M_\pi^2+18(K_{10}+K_{11})\left(M_K^2+M_\pi^2\right)\Bigg\} \ .
\end{aligned}
$$

B.1.5 Z–factors, mixing

In order to account for wave function renormalisation and $\pi^0\eta$ mixing beyond leading order, we have to write down the various Z factors as well as the quantities defined in Eq. (5.38). These are given as follows:

$$
Z_{\pi^\pm} = 1+\frac{1}{6F^2}\left\{2\Delta_{\pi^\pm}+2\Delta_{\pi^0}+\Delta_{K^\pm}+\Delta_{K^0}\right\} \qquad \text{(B.31)}
$$

$$
\begin{aligned}
& -\frac{8}{F^2}\left\{L_4\Big(2M_K^2+M_\pi^2+(M_K^2-M_\pi^2)\frac{4\epsilon}{\sqrt{3}}-3\Delta M_\pi^2\Big)+L_5\left(M_\pi^2-\Delta M_\pi^2\right)\right\} \\
& -e^2\left\{\frac{2\Delta_\pi}{M_\pi^2}+\frac{1}{4\pi^2}\log\frac{m_\gamma}{M_\pi}+\frac{1}{8\pi}+\frac{8}{3}(K_1+K_2)+\frac{20}{9}(K_5+K_6)\right\} \quad ,
\end{aligned}
$$

$$
\begin{aligned}
Z_{\pi^0} \;=\;& 1+\frac{1}{6F^2}\Big\{4\Delta_{\pi^-}+\Delta_{K^+}+\Delta_{K^0}\Big\} \qquad \text{(B.32)}\\
& -\frac{8}{F^2}\left\{L_4\Big(2M_K^2+M_\pi^2+(M_K^2-M_\pi^2)\frac{4\epsilon}{\sqrt{3}}-3\Delta M_\pi^2\Big)+L_5\left(M_\pi^2-\Delta M_\pi^2\right)\right\} \\
& -e^2\left\{\frac{8}{3}(K_1+K_2)-2(2K_3-K_4)+\frac{20}{9}(K_5+K_6)\right\} \quad ,
\end{aligned}
$$

$$
\begin{aligned}
Z_{K^\pm} \;=\;& 1+\frac{1}{6F^2}\left\{\Delta_{\pi^\pm}+\frac{1}{2}\left(1+2\sqrt{3}\epsilon\right)\Delta_{\pi^0}+2\Delta_{K^\pm}+\Delta_{K^0}+\frac{3}{2}\Big(1-\frac{2\epsilon}{\sqrt{3}}\Big)\Delta_\eta\right\} \\
& -\frac{8}{F^2}\left\{L_4\Big(2M_K^2+M_\pi^2+(M_K^2-M_\pi^2)\frac{4\epsilon}{\sqrt{3}}-3\Delta M_\pi^2\Big)+L_5\left(M_K^2-\Delta M_\pi^2\right)\right\} \\
& -e^2\left\{\frac{2\Delta_K}{M_K^2}+\frac{1}{4\pi^2}\log\frac{m_\gamma}{M_K}+\frac{1}{8\pi}+\frac{8}{3}(K_1+K_2)+\frac{20}{9}(K_5+K_6)\right\} \quad , \qquad \text{(B.33)}
\end{aligned}
$$

$$
\begin{aligned}
Z_{K^0} \;=\;& 1+\frac{1}{6F^2}\left\{\Delta_{\pi^+}+\frac{1}{2}\left(1-2\sqrt{3}\epsilon\right)\Delta_{\pi^0}+\Delta_{K^-}+2\Delta_{K^0}+\frac{3}{2}\Big(1+\frac{2\epsilon}{\sqrt{3}}\Big)\Delta_\eta\right\} \\
& -\frac{8}{F^2}\bigg\{L_4\Big(2M_K^2+M_\pi^2+(M_K^2-M_\pi^2)\frac{4\epsilon}{\sqrt{3}}-3\Delta M_\pi^2\Big) \\
& \qquad +L_5\Big(M_K^2+(M_K^2-M_\pi^2)\frac{4\epsilon}{\sqrt{3}}-\Delta M_\pi^2\Big)\bigg\} \\
& -e^2\left\{\frac{8}{3}(K_1+K_2)+\frac{8}{9}(K_5+K_6)\right\} \quad , \qquad \text{(B.34)}
\end{aligned}
$$

$$
Z_{\pi^0\eta} \;=\; \frac{2\epsilon}{3F^2}\Big(\Delta_K-\Delta_\pi\Big)+\frac{1}{2\sqrt{3}F^2}\Big(\Delta_{K^\pm}-\Delta_{K^0}\Big)+\frac{2e^2}{\sqrt{3}}\left\{2K_3-K_4-\frac{2}{3}(K_5+K_6)\right\} \; ; \qquad \text{(B.35)}
$$

$$
\begin{aligned}
\epsilon^{(4)} \;=\;& -\frac{\epsilon}{F^2}\bigg\{\frac{M_K^2-3M_\pi^2}{2(M_K^2-M_\pi^2)}\Delta_\pi-\frac{M_K^2-2M_\pi^2}{M_K^2-M_\pi^2}\Delta_K-\frac{1}{2}\Delta_\eta-\frac{M_K^2}{16\pi^2} \qquad \text{(B.36)}\\
& \qquad +32(3L_7+L_8)(M_K^2-M_\pi^2)\bigg\} \\
& -\frac{e^2}{\sqrt{3}(M_K^2-M_\pi^2)}\bigg\{\frac{3Z}{2}\Big(\Delta_K+\frac{M_K^2}{16\pi^2}\Big) \\
& \qquad +\Big(K_3-\frac{K_4}{2}-\frac{1}{3}(K_5+K_6)\Big)(2M_K^2+M_\pi^2)+(K_9+K_{10})M_\pi^2\bigg\} \quad .
\end{aligned}
$$

The last two quantities multiply the tree–level amplitude for $\pi^- K^+ \to \eta K^0$, which is given by

$$T_\eta = -\frac{1}{2\sqrt{6}F^2}\left(s - 2t + u + \frac{2}{3}\left(M_K^2 - M_\pi^2\right)\right) \quad . \tag{B.37}$$

As $Z_{\pi^0\eta}$ and $\epsilon^{(4)}$ are both of one–loop order and of order δ, it suffices to use T_η in the isospin–symmetric limit and with quark mass insertions replaced by meson masses.

B.2 The scattering amplitude $\pi^- K^+ \to \pi^- K^+$

In this appendix, we collect the various pieces of the scattering amplitude for the process $\pi^- K^+ \to \pi^- K^-$ up to one loop order, including isospin breaking corrections up to order $\delta \in \{\epsilon, e^2\}$.

B.2.1 Hadronic loop diagrams

We again write down analytic formulae for the various s , t , u channel loops. The notation is exactly as before.

$$\begin{aligned}
T^s_{\pi^- K^+} \;=\;& \frac{1}{36F^4}\Big\{\left(s - M_K^2 + M_\pi^2\right)\left(s - M_K^2 + M_\pi^2 + 12\Delta M_\pi^2\right) J_{\pi^- K^+}(s) \\
&+2\Big[s^2 + 2s(M_K^2 - M_\pi^2) - 3(M_K^2 - M_\pi^2)^2 \\
&\qquad +6\left(s + 3(M_K^2 - M_\pi^2)\right)\Delta M_\pi^2\Big] J^{(1)}_{\pi^- K^+}(s) \\
&+\left(s + 3(M_K^2 - M_\pi^2)\right)^2 J^{(2)}_{\pi^- K^+}(s) - 2s\left(5t - 4u - 4M_K^2 + 2M_\pi^2\right) J^{(3)}_{\pi^- K^-}(s) \\
&+3\left(s + M_K^2 - M_\pi^2 + 4\Delta M_\pi^2\right)\Delta_{K^-}\Big\} \quad ,
\end{aligned} \tag{B.38}$$

$$\begin{aligned}
T^s_{\pi^0 K^0} \;=\;& \frac{1}{8F^4}\left(1 + \frac{2\epsilon}{\sqrt{3}}\right)\Big\{\Big[s - M_K^2 - M_\pi^2 + (M_K^2 - M_\pi^2)\frac{8\epsilon}{\sqrt{3}} + 4\Delta M_\pi^2\Big] \\
&\qquad\qquad \times\left(s - M_K^2 - M_\pi^2\right) J_{\pi^0 K^0}(s) \\
&+2\Big[(s - M_\pi^2)^2 - M_K^4 + M_K^2(M_K^2 - M_\pi^2)\frac{8\epsilon}{\sqrt{3}} \\
&\qquad +2\left(s + M_K^2 - M_\pi^2\right)\Delta M_\pi^2\Big] J^{(1)}_{\pi^0 K^0}(s) \\
&+\Big[s + (M_K^2 - M_\pi^2)\Big(1 - \frac{8\epsilon}{\sqrt{3}}\Big)\Big]\left(s + M_K^2 - M_\pi^2\right) J^{(2)}_{\pi^0 K^0}(s) \\
&+2s\Big[2M_K^2 - t + \left(t - u - M_K^2 + M_\pi^2\right)\frac{4\epsilon}{\sqrt{3}}\Big] J^{(3)}_{\pi^0 K^0}(s) \\
&+\Big[3(s - M_\pi^2) - M_K^2 - (M_K^2 - M_\pi^2)\frac{4\epsilon}{\sqrt{3}} + 4\Delta M_\pi^2\Big]\Delta_{K^0}\Big\} \quad ,
\end{aligned}$$

$$
\begin{aligned}
T^s_{\eta K^0} &= \frac{1}{24F^2}\Big(1-2\sqrt{3}\epsilon\Big)\Bigg\{\frac{1}{9}\left[3s+M_K^2-7M_\pi^2+(M_K^2-M_\pi^2)\frac{40\epsilon}{\sqrt{3}}+12\Delta M_\pi^2\right] \\
&\qquad\qquad \times\left(3s+M_K^2-7M_\pi^2\right)J_{\eta K^0}(s) \qquad\qquad (\mathrm{B.39})\\
&\quad +2\Big[s^2-\frac{2}{3}s(4M_K^2-M_\pi^2)-M_K^4+8M_K^2M_\pi^2-7M_\pi^4 \\
&\qquad -(M_K^2-M_\pi^2)\left(2s+9(M_K^2-2M_\pi^2)\right)\frac{8\epsilon}{3\sqrt{3}} \\
&\qquad +2\left(s-3(M_K^2-M_\pi^2)\right)\Delta M_\pi^2\Big]J^{(1)}_{\eta K^0}(s) \\
&\quad +\left(s-3(M_K^2-M_\pi^2)\right)\left[s-3(M_K^2-M_\pi^2)\Big(1+\frac{8\epsilon}{\sqrt{3}}\Big)\right]J^{(2)}_{\eta K^0}(s) \\
&\quad -2s\Big[5t-4u+2M_K^2-4M_\pi^2+\left(3(t-u)+M_K^2-M_\pi^2\right)4\sqrt{3}\epsilon\Big]J^{(3)}_{\eta K^0}(s) \\
&\quad +\Big[3s-5M_K^2+M_\pi^2-(M_K^2-M_\pi^2)4\sqrt{3}\epsilon+4\Delta M_\pi^2\Big]\Delta_{K^0}\Bigg\}\ ,
\end{aligned}
$$

$$
\begin{aligned}
T^t_{\pi^-\pi^-} &= \frac{1}{12F^4}\Bigg\{\Big[s(t-4M_\pi^2)+2t^2-t\left(M_K^2+3M_\pi^2-12\Delta M_\pi^2\right) \qquad (\mathrm{B.40})\\
&\qquad +4M_\pi^2(M_K^2+M_\pi^2)\Big]J_{\pi^+\pi^-}(t) \\
&\quad +2\Big[s+\frac{4}{3}t-M_K^2-M_\pi^2+4\Delta M_\pi^2\Big]\Delta_{\pi^\pm}+\frac{(s-u)(t-6M_\pi^2)}{48\pi^2}\Bigg\}\ ,
\end{aligned}
$$

$$
\begin{aligned}
T^t_{\pi^0\pi^0} &= \frac{1}{36F^2}\Bigg\{\frac{9}{2}\left(t-M_{\pi^0}^2\right)\left[t+\left(3t-4M_K^2\right)\frac{2\epsilon}{\sqrt{3}}\right]J_{\pi^0\pi^0}(t) \qquad (\mathrm{B.41})\\
&\quad +\Big[\left(5t-3M_{\pi^0}^2\right)\left(1+2\sqrt{3}\epsilon\right)-8\sqrt{3}\epsilon M_K^2\Big]\Delta_{\pi^0}\Bigg\}\ ,
\end{aligned}
$$

$$
\begin{aligned}
T^t_{\pi^0\eta} &= -\frac{\epsilon}{12\sqrt{3}F^4}\Bigg\{\left(3t-4M_K^2\right)\left(3t-4M_\pi^2\right)J_{\pi^0\eta}(t) \qquad (\mathrm{B.42})\\
&\quad +\Big[5t-\frac{8}{3}(M_K^2+2M_\pi^2)\Big]\Delta_{\pi^0}+\Big[5t-\frac{8}{3}(2M_K^2+M_\pi^2)\Big]\Delta_\eta\Bigg\}\ ,
\end{aligned}
$$

$$
T^t_{\eta\eta} = \frac{M_{\pi^0}^2}{12F^4}\Big(1-\frac{2\epsilon}{\sqrt{3}}\Big)\Bigg\{\Bigg[\frac{3}{2}t-\frac{4}{3}\Bigg(M_K^2\Big(1-\frac{\epsilon}{\sqrt{3}}\Big)-\Delta M_\pi^2\Bigg)\Bigg]J_{\eta\eta}(t)+\Delta_\eta\Bigg\}\ , \qquad (\mathrm{B.43})
$$

$$
\begin{aligned}
T^t_{K^+K^-} &= \frac{1}{12F^4}\Bigg\{\Big[s(t-4M_K^2)+2t^2-t(3M_K^2+M_\pi^2)+4M_K^2(M_K^2+M_\pi^2) \qquad (\mathrm{B.44})\\
&\qquad +12t\,\Delta M_\pi^2\Big]J_{K^+K^-}(t) \\
&\quad +2\Big[s+\frac{4}{3}t-M_K^2-M_\pi^2+4\Delta M_\pi^2\Big]\Delta_{K^-}+\frac{(s-u)(t-6M_K^2)}{48\pi^2}\Bigg\}\ ,
\end{aligned}
$$

$$
\begin{aligned}
T^t_{K^0 K^0} &= \frac{1}{24F^4}\Big\{\Big[t(t+2M_K^2) - (t-4M_K^2)\left(s - M_K^2 - M_\pi^2\right) - 2(s-u)\Delta_K\Big] J_{K^0\bar{K}^0}(t) \\
&\quad -\left(s - \frac{5}{3}t - u\right)\Delta_{K^0} - \frac{(s-u)(t-6M_{K^0}^2)}{48\pi^2}\Big\} \ , \\
T^u_{\pi^+ K^+} &= \frac{1}{36F^4}\Big\{9\left(u - M_K^2 - M_\pi^2\right)\left(u - M_K^2 - M_\pi^2 - 4\Delta M_\pi^2\right) J_{\pi^+K^+}(u) \qquad \text{(B.45)} \\
&\quad + \left(5u - 6\left(M_K^2 + M_\pi^2 + 2\Delta M_\pi^2\right)\right)\left(\Delta_{K^+} + \Delta_{\pi^+}\right) \\
&\quad - \left(M_K^2 - M_\pi^2\right)\left(\Delta_{K^+} - \Delta_{\pi^+}\right)\Big\} \ .
\end{aligned}
$$

Furthermore, we find the tadpole contributions to be

$$
\begin{aligned}
T^{\text{tad}} &= -\frac{1}{3F^4}\Big\{\Big[s + \frac{3}{4}t - M_K^2 - \frac{4}{3}M_\pi^2 + 6\Delta M_\pi^2\Big]\Delta_{\pi^-} \qquad \text{(B.46)} \\
&\quad + \frac{1}{4}\Big[s + \frac{7}{6}t - M_K^2 - 3M_\pi^2 - \left(t + \frac{2}{3}(2M_K^2 + M_\pi^2)\right)\frac{\epsilon}{\sqrt{3}} + 4\Delta M_\pi^2\Big]\Delta_{\pi^0} \\
&\quad + \Big[s + \frac{3}{4}t - \frac{4}{3}M_K^2 - M_\pi^2 + 6\Delta M_\pi^2\Big]\Delta_{K^+} \\
&\quad + \frac{1}{3}\Big[t - M_K^2 - \frac{1}{2}M_\pi^2 - (M_K^2 - M_\pi^2)\frac{2\epsilon}{\sqrt{3}} + \frac{3}{2}\Delta M_\pi^2\Big]\Delta_{K^0} \\
&\quad + \frac{1}{4}\Big[s + \frac{3}{2}t - \frac{7}{3}M_K^2 - M_\pi^2 + \left(t + 2(2M_K^2 - M_\pi^2)\right)\frac{\epsilon}{\sqrt{3}} + \frac{10}{3}\Delta M_\pi^2\Big]\Delta_\eta\Big\} \ .
\end{aligned}
$$

B.2.2 Photon loop diagrams

Here we write down the amplitudes corresponding to the photon loop diagrams (a), (b), (c) in Fig. 5.4 (as well as those depicted in diagram (b) of Fig. 5.1). As there are different photon triangle diagrams, we also specify the channel of these with superscripts s, t, u. Note that both the s- and u-channel amplitudes as well as the two self-energy type diagrams occur *twice* in the full amplitude.

$$
\begin{aligned}
T^s_{\pi K\gamma} &= \frac{e^2}{F^2}\Big\{\left(s - M_K^2 - M_\pi^2\right)\Big[\left(u - M_K^2 - M_\pi^2\right) G_{\pi K\gamma}(s) \qquad \text{(B.47)} \\
&\qquad - (M_K^2 - M_\pi^2)\, G^1_{\pi K\gamma}(s) - (t-u)\, G_{\pi K\gamma}(s)\Big] \\
&\quad - \frac{1}{4}\left[\frac{2(s-M_\pi^2)+t}{M_K^2} - \frac{s + M_K^2 - M_\pi^2}{s}\right]\Delta_K \\
&\quad - \frac{1}{4}\left[\frac{2(s-M_K^2)+t}{M_\pi^2} - \frac{s - M_K^2 + M_\pi^2}{s}\right]\Delta_\pi \\
&\quad - \frac{1}{4s}\left(s - M_K^2 + M_\pi^2\right)\left(s + M_K^2 - M_\pi^2\right) J_{\pi K}(s) + \frac{2(s-u)+t}{48\pi^2}\Big\} \ ,
\end{aligned}
$$

$$\begin{aligned}
T^t_{\pi\pi\gamma} &= \frac{e^2}{F^2}\Big\{\left(t-2M_\pi^2\right)\Big[\left(u-M_K^2-M_\pi^2\right)G_{\pi\pi\gamma}(t)-(s-u)G^-_{\pi\pi\gamma}(t)\Big] \qquad \text{(B.48)}\\
&\qquad -\frac{t}{4}J_{\pi\pi}(t)+\frac{u-t-M_K^2}{2M_\pi^2}\Delta_\pi-\frac{2(u-t)-s-M_K^2+M_\pi^2}{48\pi^2}\Big\} \ ,\\
T^t_{KK\gamma} &= \frac{e^2}{F^2}\Big\{\left(t-2M_K^2\right)\Big[\left(u-M_K^2-M_\pi^2\right)G_{KK\gamma}(t)-(s-u)G^-_{KK\gamma}(t)\Big] \qquad \text{(B.49)}\\
&\qquad -\frac{t}{4}J_{KK}(t)+\frac{u-t-M_\pi^2}{2M_K^2}\Delta_K-\frac{2(u-t)-s+M_K^2-M_\pi^2}{48\pi^2}\Big\} \ ,\\
T^u_{\pi K\gamma} &= -\frac{e^2}{F^2}\left(u-M_K^2-M_\pi^2\right)\Big\{\left(u-M_K^2-M_\pi^2\right)G_{\pi K\gamma}(u)+\frac{1}{2}J_{\pi K}(u) \qquad \text{(B.50)}\\
&\qquad +\frac{3}{4}\left(\frac{\Delta_K}{M_K^2}+\frac{\Delta_\pi}{M_\pi^2}\right)-\frac{5}{48\pi^2}\Big\} \ ,\\
T_{\pi\gamma} &= -\frac{e^2}{F^2}\left(u-M_K^2+M_\pi^2\right)\left\{\frac{\Delta_\pi}{M_\pi^2}-\frac{1}{12\pi^2}\right\} \ ; \qquad \text{(B.51)}\\
T_{K\gamma} &= -\frac{e^2}{F^2}\left(u+M_K^2-M_\pi^2\right)\left\{\frac{\Delta_K}{M_K^2}-\frac{1}{12\pi^2}\right\} \ . \qquad \text{(B.52)}
\end{aligned}$$

B.2.3 Tree graphs

The lowest order tree graph for the scattering process $\pi^- K^+ \to \pi^- K^+$ is given by

$$T^{\text{tree}} = \frac{1}{6F^2}\left\{s+t-2u+B(2m_u+m_d+m_s)+16Ze^2F^2\right\} \ , \qquad \text{(B.53)}$$

where, again, we refrain from expressing the quark masses and Z in terms of meson masses. Also for this process, we list the tree graph contributions of the various counterterms of the Lagrangians Eqs. (5.9), (5.10). The purely strong Lagrangian results in an amplitude

$$\begin{aligned}
T^{\text{ct}} = \frac{2}{F^4}\Big\{ & 4L_1\left(t-2M_\pi^2\right)\left(t-2M_K^2\right)+2L_2\Big[\left(s-M_K^2-M_\pi^2\right)^2+\left(u-M_K^2-M_\pi^2\right)^2\Big]\\
& +L_3\Big[\left(s-M_K^2-M_\pi^2\right)^2+\left(t-2M_\pi^2\right)\left(t-2M_K^2\right)\Big] \qquad \text{(B.54)}\\
& -2L_4\Big[\Big(2M_K^2+M_\pi^2+\frac{4\epsilon}{\sqrt{3}}(M_K^2-M_\pi^2)\Big)\Big(u-\frac{2}{3}(M_K^2+M_\pi^2)\Big)\\
& \qquad -2t(M_K^2+M_\pi^2)+8M_K^2M_\pi^2-(s-3t+4u)\Delta M_\pi^2\Big]\\
& -2L_5\Big[\Big(u+\frac{2}{3}\Delta M_\pi^2\Big)\left(M_K^2+M_\pi^2-2\Delta M_\pi^2\right)-\frac{2}{3}(M_K^4+M_\pi^4)\Big]\\
& +\frac{4}{3}L_6\Big[2M_K^4+15M_K^2M_\pi^2+M_\pi^4+\frac{4\epsilon}{\sqrt{3}}(M_K^4-M_\pi^4)-\left(19M_K^2+17M_\pi^2\right)\Delta M_\pi^2\Big]
\end{aligned}$$

$$+\frac{4}{3}L_8\left[M_K^4+6M_K^2M_\pi^2+M_\pi^4-8(M_K^2+M_\pi^2)\Delta M_\pi^2\right]\Bigg\} \ .$$

Furthermore, the electromagnetic counterterms contribute on tree level according to

$$\begin{aligned}
T^{\mathrm{ct,em}} &= \frac{4\,e^2}{9F^2}\Bigg\{(K_1+K_2)(s+t-2u)+18K_2\left(t-M_K^2-M_\pi^2\right)+9\Big(K_3+\frac{K_4}{2}\Big)(s-u)\\
&\quad -\frac{1}{3}(K_5+K_6)(2s-7t+5u)-9K_6u+K_8\left(43M_K^2+31M_\pi^2\right) \qquad \text{(B.55)}\\
&\quad +\frac{1}{3}(K_9+K_{10})\left(M_K^2+4M_\pi^2\right)+\Big(K_7+30(K_{10}+K_{11})\Big)\left(M_K^2+M_\pi^2\right)\Bigg\} \ .
\end{aligned}$$

B.3 $a_0(\pi^- K^+ \to \pi^0 K^0)$

In this appendix, we show the analytic expressions for the one–loop corrections to the scattering length a_0 for $\pi^- K^+ \to \pi^0 K^0$. The isospin violating effects are expanded up to order ϵ and e^2. The low–energy constants with the infinite part subtracted are denoted by L_i^r, K_i^r, as done conventionally. Note however that we do not display the dependence of these various constants on the renormalisation scale λ explicitly. All corrections given below are of course scale independent.

First, we show the coefficients C_0, C_ϵ, C_{e^2} as defined in Eq. (5.39) for corrections strictly in terms of ϵ, e^2:

$$\begin{aligned}
C_0 &= 1-\frac{1}{F^2}\Bigg\{8L_4^r\left(2M_K^2+M_\pi^2\right) \qquad \text{(B.56)}\\
&+ \frac{1}{16\pi^2}\Bigg[\frac{1}{M_K^2-M_\pi^2}\Bigg(\frac{3}{2}M_\pi^4\log\frac{M_\pi}{\lambda}-\Big(2M_K^2+\frac{5}{9}M_\pi^2\Big)M_K^2\log\frac{M_K}{\lambda}\\
&\qquad +\Big(\frac{14}{9}M_K^2-\frac{M_\pi^2}{2}\Big)M_\pi^2\log\frac{M_\eta}{\lambda}\Bigg)\\
&+ \frac{4M_\pi M_K}{9}\Bigg(\frac{\sqrt{(M_K-M_\pi)(2M_K+M_\pi)}}{M_K+M_\pi}\arctan\Bigg(\frac{2(M_K+M_\pi)}{M_K-2M_\pi}\sqrt{\frac{M_K-M_\pi}{2M_K+M_\pi}}\Bigg)\\
&\quad -\frac{\sqrt{(M_K+M_\pi)(2M_K-M_\pi)}}{M_K-M_\pi}\arctan\Bigg(\frac{2(M_K-M_\pi)}{M_K+2M_\pi}\sqrt{\frac{M_K+M_\pi}{2M_K-M_\pi}}\Bigg)\Bigg)\Bigg]\Bigg\} \ ,
\end{aligned}$$

$$\begin{aligned}
C_\epsilon &= 1-\frac{1}{F^2}\Bigg\{8\Big[2L_3M_\pi\left(M_K-M_\pi\right)+3L_4^r\left(2M_K^2-M_\pi^2\right) \qquad \text{(B.57)}\\
&\qquad -(2L_8^r-L_5^r)\left(M_K^2-M_\pi^2\right)\Big]\\
&+ \frac{1}{48\pi^2(M_K-M_\pi)^2(M_K+M_\pi)}
\end{aligned}$$

$$
\begin{aligned}
&\times\Bigg[\left(34M_K^4 - 35M_K^3 M_\pi - 90M_K^2 M_\pi^2 + \frac{37}{2}M_K M_\pi^3 - \frac{35}{2}M_\pi^4\right) M_\pi \log\frac{M_\pi}{\lambda} \\
&-\frac{1}{9}\left(162M_K^5 - 68M_K^4 M_\pi - 455M_K^3 M_\pi^2 - 645M_K^2 M_\pi^3 + 154M_K M_\pi^4 - 128M_\pi^5\right) \\
&\qquad\qquad\qquad\qquad\qquad\qquad\qquad\qquad\qquad\qquad \times \log\frac{M_K}{\lambda} \\
&-\frac{1}{18}\left(72M_K^5 + 352M_K^4 M_\pi - 350M_K^3 M_\pi^2 + 300M_K^2 M_\pi^3 + 259M_K M_\pi^4 - 293M_\pi^5\right) \\
&\qquad\qquad\qquad\qquad\qquad\qquad\qquad\qquad\qquad\qquad \times \log\frac{M_\eta}{\lambda} \\
&-\frac{2}{9}\left(116M_K^4 - 79M_K^3 M_\pi - 156M_K^2 M_\pi^2 + 74M_K M_\pi^3 + 8M_\pi^4\right) M_\pi \\
&\qquad\qquad \times\sqrt{\frac{M_K + M_\pi}{2M_K - M_\pi}}\arctan\left(\frac{2(M_K - M_\pi)}{M_K + 2M_\pi}\sqrt{\frac{M_K + M_\pi}{2M_K - M_\pi}}\right)\Bigg] \\
-\ & \frac{1}{24\pi^2}\Bigg[\frac{M_K M_\pi(4M_K + M_\pi)}{M_K + M_\pi}\sqrt{\frac{M_K - M_\pi}{2M_K + M_\pi}}\arctan\left(\frac{2(M_K + M_\pi)}{M_K - 2M_\pi}\sqrt{\frac{M_K - M_\pi}{2M_K + M_\pi}}\right) \\
&\quad + \frac{9M_K^3 - 25M_K^2 M_\pi + 31M_K M_\pi^2 + 56M_\pi^3}{3(M_K - M_\pi)}\Bigg]\Bigg\},
\end{aligned}
$$

$$
\begin{aligned}
C_{e^2} \;=\; & 1 + \frac{1}{F^2}\Bigg\{8\Bigg[L_3 M_K M_\pi - 2L_4^r(2M_K - M_\pi)(M_K - M_\pi) \\
&\qquad\qquad - \frac{L_5^r}{2}\left(2M_K^2 - M_K M_\pi + 2M_\pi^2\right)\Bigg] \\
-\ & \frac{1}{48\pi^2(M_K - M_\pi)^3(M_K + M_\pi)} \\
&\times\Bigg[\left(4M_K^5 + 13M_K^4 M_\pi - 9M_K^3 M_\pi^2 + 17M_K^2 M_\pi^3 + \frac{67}{2}M_K M_\pi^4 - \frac{27}{2}M_\pi^5\right) \\
&\qquad\qquad\qquad\qquad\qquad\qquad\qquad\qquad\qquad \times M_\pi \log\frac{M_\pi}{\lambda} \\
&+\frac{1}{9}\left(54M_K^5 - 52M_K^4 M_\pi - 346M_K^3 M_\pi^2 + 81M_K^2 M_\pi^3 - 175M_K M_\pi^4 - 52M_\pi^5\right) \\
&\qquad\qquad\qquad\qquad\qquad\qquad\qquad\qquad\qquad \times M_K \log\frac{M_K}{\lambda} \\
&+\frac{1}{18}\left(32M_K^5 + 296M_K^4 M_\pi - 270M_K^3 M_\pi^2 + 260M_K^2 M_\pi^3 - 121M_K M_\pi^4 - 27M_\pi^5\right) \\
&\qquad\qquad\qquad\qquad\qquad\qquad\qquad\qquad\qquad \times M_\pi \log\frac{M_\eta}{\lambda} \\
&-\frac{1}{6}\left(5M_K^4 - 42M_K^3 M_\pi - 138M_K^2 M_\pi^2 - 91M_K M_\pi^3 - 18M_\pi^4\right)(M_K - M_\pi)M_\pi\Bigg] \\
&-\frac{M_K M_\pi}{144\pi^2}\Bigg[\frac{16M_K^2 - 17M_K M_\pi - 8M_\pi^2}{(M_K + M_\pi)\sqrt{(2M_K + M_\pi)(M_K - M_\pi)}}
\end{aligned}
\tag{B.58}
$$

$$
\begin{aligned}
&\qquad\qquad\qquad\qquad \times \arctan\left(\frac{2(M_K+M_\pi)}{M_K-2M_\pi}\sqrt{\frac{M_K-M_\pi}{2M_K+M_\pi}}\right) \\
&\qquad + \frac{32M_K^4+35M_K^3M_\pi-108M_K^2M_\pi^2-40M_KM_\pi^3+44M_\pi^4}{3(M_K-M_\pi)^3\sqrt{(2M_K-M_\pi)(M_K+M_\pi)}} \\
&\qquad\qquad\qquad\qquad \times \arctan\left(\frac{2(M_K-M_\pi)}{M_K+2M_\pi}\sqrt{\frac{M_K+M_\pi}{2M_K-M_\pi}}\right)\Bigg]\Bigg\} \\
- & \frac{1}{ZF^2}\Bigg\{\frac{8}{3}(K_1^r+K_2^r)M_KM_\pi \\
&\quad + (2K_3^r-K_4^r)\frac{M_\pi(2M_K^3+2M_K^2M_\pi-M_KM_\pi^2-2M_\pi^3)}{2(M_K^2-M_\pi^2)} \\
&\quad + (K_5^r+K_6^r)\frac{M_K^2(2M_K^2-M_KM_\pi-2M_\pi^2)}{3(M_K^2-M_\pi^2)} + \frac{2}{9}(10K_5^r+K_6^r)M_KM_\pi \\
&\quad - 2K_8^r\left(2M_K^2+M_\pi^2\right) + K_9^r\,\frac{M_KM_\pi^3}{3(M_K^2-M_\pi^2)} \\
&\quad - K_{10}^r\,\frac{12M_K^4-6M_K^3M_\pi+5M_KM_\pi^3-12M_\pi^4}{3(M_K^2-M_\pi^2)} \\
&\quad - 2K_{11}^r\left(2M_K^2-M_KM_\pi+2M_\pi^2\right) \\
&+ \frac{1}{16\pi^2}\left[\frac{3(M_K^2+2M_\pi^2)}{M_K+M_\pi}M_K\log\frac{M_K}{\lambda} + \frac{3(2M_K^2+M_\pi^2)}{M_K+M_\pi}M_\pi\log\frac{M_\pi}{\lambda}\right. \\
&\qquad\qquad \left. -2M_K^2+7M_KM_\pi-2M_\pi^2\right]\Bigg\}\,.
\end{aligned}
$$

For the coefficients $\tilde{C}_\epsilon$, $\tilde{C}_{\epsilon^2}$ as defined in Eq. (5.51) in order to express isospin breaking corrections as far as possible in terms of physical quantities (meson mass differences), we find:

$$
\begin{aligned}
\tilde{C}_\epsilon \;=\; & 1-\frac{M_\pi}{F^2}\Bigg\{8\Big[2L_3\,(M_K-M_\pi)-L_5^rM_\pi\Big] \qquad\qquad (\mathrm{B.59}) \\
+ \;& \frac{1}{48\pi^2(M_K-M_\pi)^2(M_K+M_\pi)} \\
& \times\Bigg[\left(34M_K^4-26M_K^3M_\pi-99M_K^2M_\pi^2+\frac{19}{2}M_KM_\pi^3-\frac{17}{2}M_\pi^4\right)\log\frac{M_\pi}{\lambda} \\
& -\frac{1}{9}\left(94M_K^4-185M_K^3M_\pi-915M_K^2M_\pi^2+46M_KM_\pi^3-20M_\pi^4\right)\log\frac{M_K}{\lambda} \\
& -\frac{1}{9}\left(212M_K^4-130M_K^3M_\pi+105M_K^2M_\pi^2+\frac{241}{2}M_KM_\pi^3-\frac{275}{2}M_\pi^4\right)\log\frac{M_\eta}{\lambda} \\
& -\frac{2}{9}\left(116M_K^4-79M_K^3M_\pi-156M_K^2M_\pi^2+74M_KM_\pi^3+8M_\pi^4\right)
\end{aligned}
$$

$$
\times\sqrt{\frac{M_K+M_\pi}{2M_K-M_\pi}}\arctan\left(\frac{2(M_K-M_\pi)}{M_K+2M_\pi}\sqrt{\frac{M_K+M_\pi}{2M_K-M_\pi}}\right)\Bigg]
$$

$$
- \frac{1}{24\pi^2}\left[\frac{M_K(4M_K+M_\pi)}{M_K+M_\pi}\sqrt{\frac{M_K-M_\pi}{2M_K+M_\pi}}\arctan\left(\frac{2(M_K+M_\pi)}{M_K-2M_\pi}\sqrt{\frac{M_K-M_\pi}{2M_K+M_\pi}}\right)\right.
$$

$$
\left.-\frac{16M_K^2-40M_KM_\pi-47M_\pi^2}{3(M_K-M_\pi)}\right]\Bigg\}\,,
$$

$$
\begin{aligned}
\tilde{C}_{e^2} &= 1+\frac{1}{F^2}\Bigg\{8\left[L_3 M_K M_\pi - L_5^r\left(M_K^2+2M_KM_\pi-M_\pi^2\right)\right] \qquad\qquad (\mathrm{B}.60)\\
&+ \frac{1}{48\pi^2(M_K-M_\pi)^3(M_K+M_\pi)}\\
&\quad\times\Bigg[\frac{1}{2}\left(40M_K^5-110M_K^4M_\pi+6M_K^3M_\pi^2+38M_K^2M_\pi^3-79M_KM_\pi^4+15M_\pi^5\right)\\
&\qquad\qquad\times M_\pi\log\frac{M_\pi}{\lambda}\\
&\quad-\frac{1}{9}\left(54M_K^5-133M_K^4M_\pi-184M_K^3M_\pi^2+108M_K^2M_\pi^3-391M_KM_\pi^4+56M_\pi^5\right)\\
&\qquad\qquad\times M_K\log\frac{M_K}{\lambda}\\
&\quad-\frac{1}{18}\left(32M_K^5+296M_K^4M_\pi-270M_K^3M_\pi^2+260M_K^2M_\pi^3-121M_KM_\pi^4-27M_\pi^5\right)\\
&\qquad\qquad\times M_\pi\log\frac{M_\eta}{\lambda}\\
&\quad-\frac{M_KM_\pi}{144\pi^2}\Bigg[\frac{16M_K^2-17M_KM_\pi-8M_\pi^2}{(M_K+M_\pi)\sqrt{(2M_K+M_\pi)(M_K-M_\pi)}}\\
&\qquad\qquad\times\arctan\left(\frac{2(M_K+M_\pi)}{M_K-2M_\pi}\sqrt{\frac{M_K-M_\pi}{2M_K+M_\pi}}\right)\\
&\qquad+\frac{32M_K^4+35M_K^3M_\pi-108M_K^2M_\pi^2-40M_KM_\pi^3+44M_\pi^4}{3(M_K-M_\pi)^3\sqrt{(2M_K-M_\pi)(M_K+M_\pi)}}\\
&\qquad\qquad\times\arctan\left(\frac{2(M_K-M_\pi)}{M_K+2M_\pi}\sqrt{\frac{M_K+M_\pi}{2M_K-M_\pi}}\right)\\
&\qquad-\frac{113M_K^2-245M_KM_\pi-10M_\pi^2}{2(M_K-M_\pi)^2}\Bigg]\Bigg\}\\
&- \frac{2M_K}{ZF^2}\Bigg\{\left[\frac{4}{3}(K_1^r+K_2^r)+K_3^r-\frac{1}{2}K_4^r+\frac{1}{9}(10K_5^r+K_6^r)\right]M_\pi\\
&\qquad+\left[\frac{1}{3}(K_5^r+K_6^r)-2(K_{10}^r+K_{11}^r)\right]M_K
\end{aligned}
$$

$$+\frac{3}{64\pi^2}\left[\frac{2M_K^3 - M_K^2 M_\pi + 4M_K M_\pi^2 - 4M_\pi^2}{M_K^2 - M_\pi^2}\log\frac{M_K}{\lambda} + \frac{4M_K^2 - 6M_K M_\pi + M_\pi^2}{M_K^2 - M_\pi^2} M_\pi \log\frac{M_\pi}{\lambda} - \frac{4}{3}\left(M_K - 3M_\pi\right)\right]\Bigg\} .$$

We point out again that $\tilde{C}_0$ has already been given in Eq. (5.20). Comparing the two sets of coefficients, we note that L_4^r cancels in all $\tilde{C}$, which is due to the renormalisation of the pion decay constant. In addition, the dependence on the electromagnetic low–energy constants K_i^r simplifies strongly in $\tilde{C}_{e^2}$ as compared to C_{e^2}.

B.4 $a_0(\pi^- K^+ \to \pi^- K^+)$

The strong isospin violating contribution to the scattering length $a_0(\pi^- K^+ \to \pi^- K^+)$ can be expressed in terms of the constant $\tilde{D}_\epsilon$ defined in Eq. (5.70), which is found to be:

$$\begin{aligned}\tilde{D}_\epsilon = \frac{M_\pi}{8\pi^2 F^2}\Bigg\{ & \frac{6M_K^3 - 24M_K^2 M_\pi + 19M_K M_\pi^2 - 3M_\pi^3}{2(M_K^2 - M_\pi^2)}\log\frac{M_\pi}{\lambda} \\ & - \frac{64M_K(M_K - M_\pi)}{9(M_K + M_\pi)}\log\frac{M_K}{\lambda} \\ & + \frac{74M_K^3 - 40M_K^2 M_\pi - 43M_K M_\pi^2 + 27M_\pi^3}{18(M_K^2 - M_\pi^2)}\log\frac{M_\eta}{\lambda} \\ & + \frac{160M_K^3 - 180M_K^2 M_\pi - 43M_K M_\pi^2 + 45M_\pi^3}{9(4M_K^2 - M_\pi^2)} \\ & + \frac{2M_K(16M_K + 5M_\pi)}{9(M_K + M_\pi)} \\ & \times\sqrt{\frac{M_K - M_\pi}{2M_K + M_\pi}}\arctan\left(\frac{2(M_K + M_\pi)}{M_K - 2M_\pi}\sqrt{\frac{M_K - M_\pi}{2M_K + M_\pi}}\right)\Bigg\} . \end{aligned} \tag{B.61}$$

We do not spell out D_ϵ separately here, as the relation $\tilde{D}_\epsilon = D_\epsilon + 2\delta_F^\epsilon$ with δ_F^ϵ as given in Eq. (5.49) does not allow for any further simplifications.

Furthermore, the electromagnetic corrections can be written as

$$\begin{aligned}D_{e^2} = 1 - \frac{1}{F^2}\Bigg\{ & 8L_4^r M_K(2M_K - 3M_\pi) + 4\Big(L_5^r + 8L_6^r + 4L_8^r\Big)\Big(M_K^2 + M_\pi^2\Big) \\ & + \frac{1}{16\pi^2}\Bigg[\frac{4M_K^3 + 2M_K^2 M_\pi - 19M_K M_\pi^2 - 3M_\pi^3}{2(M_K^2 - M_\pi^2)} M_\pi \log\frac{M_\pi}{\lambda} \\ & + \frac{9M_K^3 + 103M_K^2 M_\pi - 23M_K M_\pi^2 - 17M_\pi^3}{9(M_K^2 - M_\pi^2)} M_K \log\frac{M_K}{\lambda} \\ & + \frac{16M_K^3 + 8M_K^2 M_\pi + 36M_K M_\pi^2 + 7M_\pi^3}{18(M_K + M_\pi)}\log\frac{M_\eta}{\lambda}\end{aligned}$$

$$
\begin{aligned}
&+\frac{8M_K^4-228M_K^3M_\pi+12M_K^2M_\pi^2+57M_KM_\pi^3-2M_\pi^4}{18(4M_K^2-M_\pi^2)}\\
&+\frac{M_KM_\pi\,(16M_K^2-17M_KM_\pi-8M_\pi^2)}{9(M_K+M_\pi)\sqrt{(M_K-M_\pi)(2M_K+M_\pi)}}\\
&\qquad\times\arctan\left(\frac{2(M_K+M_\pi)}{M_K-2M_\pi}\sqrt{\frac{M_K-M_\pi}{2M_K+M_\pi}}\right)\Bigg]\Bigg\}\\
-\;&\frac{2}{ZF^2}\Bigg\{\left[\frac{1}{3}(K_1^r+K_2^r)-2K_3^r-K_4^r+\frac{1}{9}(4K_5^r-5K_6^r)\right]2M_KM_\pi\\
&+\left[2K_2^r+\frac{1}{6}(K_5^r+7K_6^r)-3\left(K_{10}^r+K_{11}^r\right)\right]\left(M_K^2+M_\pi^2\right)\\
&-K_8^r\left(4M_K^2+3M_\pi^2\right)\\
&-\frac{3}{32\pi^2}\Bigg[\frac{4M_K^2-M_KM_\pi+M_\pi^2}{M_K^2-M_\pi^2}\,M_\pi^2\log\frac{M_\pi}{\lambda}\\
&-\frac{M_K^2-M_KM_\pi+4M_\pi^2}{M_K^2-M_\pi^2}\,M_K^2\log\frac{M_K}{\lambda}+\frac{2}{3}(M_K^2-M_KM_\pi+M_\pi^2)\Bigg]\Bigg\}
\end{aligned}
$$

in terms of "pure" e^2 corrections, see Eq. (5.69), and as

$$
\begin{aligned}
\tilde{D}_{e^2}\;=\;&1+\frac{1}{F^2}\Bigg\{16\Big(L_4^r-2L_6^r-L_8^r\Big)\Big(M_K^2+M_\pi^2\Big)-4L_5^r\Big(M_K-M_\pi\Big)\Big(M_K+3M_\pi\Big)\\
&+\frac{1}{16\pi^2}\Bigg[\frac{4M_\pi^3+2M_K^2M_\pi+11M_KM_\pi^2-M_\pi^3}{2(M_K^2-M_\pi^2)}\,M_\pi\log\frac{M_\pi}{\lambda}\\
&-\frac{9M_K^3+85M_K^2M_\pi-23M_KM_\pi^2+M_\pi^3}{9(M_K^2-M_\pi^2)}\,M_K\log\frac{M_K}{\lambda}\\
&-\frac{16M_K^3+8M_K^2M_\pi+36M_KM_\pi^2+7M_\pi^3}{18(M_K+M_\pi)}\log\frac{M_\eta}{\lambda}\\
&-\frac{8M_K^4-444M_K^3M_\pi-60M_K^2M_\pi^2+111M_KM_\pi^3+16M_\pi^4}{18(4M_K^2-M_\pi^2)}\\
&-\frac{M_KM_\pi\,(16M_K^2-17M_KM_\pi-8M_\pi^2)}{9(M_K+M_\pi)\sqrt{(M_K-M_\pi)(2M_K+M_\pi)}}\\
&\qquad\times\arctan\left(\frac{2(M_K+M_\pi)}{M_K-2M_\pi}\sqrt{\frac{M_K-M_\pi}{2M_K+M_\pi}}\right)\Bigg]\Bigg\}\\
-\;&\frac{2}{ZF^2}\Bigg\{\left[\frac{1}{3}(K_1^r+K_2^r)-2K_3^r-K_4^r+\frac{1}{9}(4K_5^r-5K_6^r)\right]2M_KM_\pi\\
&+\left[2(K_2^r-K_8^r)+\frac{1}{6}(K_5^r+7K_6^r)\right]\left(M_K^2+M_\pi^2\right)\\
&-\left(K_3^r-\frac{1}{2}K_4^r\right)M_\pi^2-(K_{10}^r+K_{11}^r)\left(3M_K^2+M_\pi^2\right)\Bigg\}
\end{aligned}
$$

$$-\frac{3M_K}{32\pi^2}\left[\frac{5M_K-M_\pi}{M_K^2-M_\pi^2}M_\pi^2\log\frac{M_\pi}{\lambda}-\frac{M_K^2-M_KM_\pi+4M_\pi^2}{M_K^2-M_\pi^2}M_K\log\frac{M_K}{\lambda}\right.$$
$$\left.+\frac{2}{3}(M_K-M_\pi)\right]\Bigg\}$$

for the corrections in terms of physical masses and decay constants according to Eq. (5.70).

B.5 Infrared divergent loop diagrams

In this and the following appendix, we discuss the explicit cancellation of infrared divergences in the combined total cross section for $\pi^-K^-\to\pi^0K^0(\gamma)$. The essential loop function containing an infrared divergence, stemming from the photon exchange diagram (a) in Fig. 5.1, is

$$G^{\pi K\gamma}(s)=-i\int\frac{d^4k}{(2\pi)^4}\frac{1}{\Big((q_\pi+k)^2-M_{\pi^\pm}^2\Big)\Big((q_K-k)^2-M_{K^-}^2\Big)\Big(k^2-m_\gamma^2\Big)}\ , \tag{B.62}$$

where $s=(q_K+q_\pi)^2$. This was evaluated explicitly in Chapter 6 in the kinematical region needed for the process in question, $s>(M_{K^\pm}+M_{\pi^\pm})^2$, yielding for the infrared divergent part

$$G^{\pi K\gamma}(s) \;=\; -\frac{1}{32\pi^2\sigma s}\left\{\log\frac{1-z_1}{1-z_2}+\log\frac{z_2}{z_1}-2\pi i\right\}\log\frac{m_\gamma^2}{s}+\mathcal{O}(m_\gamma^0)\ , \tag{B.63}$$

with $z_{1/2}$ as defined in Eq. (6.10). Other infrared divergent loop contributions stem from the wave function renormalisation of the charged pions (see e.g. [KM00b]) and kaons,

$$\begin{aligned}Z_{\pi^\pm} &= -\frac{e^2}{4\pi^2}\log\frac{m_\gamma}{M_{\pi^\pm}}+\mathcal{O}(m_\gamma^0)\ ,\\ Z_{K^\pm} &= -\frac{e^2}{4\pi^2}\log\frac{m_\gamma}{M_{K^\pm}}+\mathcal{O}(m_\gamma^0)\ .\end{aligned} \tag{B.64}$$

We write the tree level amplitude for $\pi^-K^+\to\pi^0K^0$ as

$$T^{(2)}=c_0+c_s\,s+c_t\,t+c_u\,u\ , \tag{B.65}$$

where

$$\begin{aligned}c_0 &= \frac{B}{6\sqrt{2}F^2}\left((m_u-m_d)\cos\epsilon+(m_u+m_d-2m_s)\frac{\sin\epsilon}{\sqrt{3}}\right)-\frac{Ze^2}{\sqrt{2}}\left(\cos\epsilon+\frac{\sin\epsilon}{\sqrt{3}}\right)\ ,\\ c_s &= -\frac{1}{2\sqrt{2}F^2}\left(\cos\epsilon+\frac{\sin\epsilon}{\sqrt{3}}\right)\ ,\quad c_t=\frac{\sin\epsilon}{\sqrt{6}F^2}\ ,\quad c_u=\frac{1}{2\sqrt{2}F^2}\left(\cos\epsilon-\frac{\sin\epsilon}{\sqrt{3}}\right)\ .\end{aligned} \tag{B.66}$$

(We do not expand these expressions to leading order in ϵ just for generality and demonstration matters.) The infrared divergent piece of the real part of the one loop amplitude $T^{(4)}$ is then given by

$$\begin{aligned}\left(\mathrm{Re}\,T^{(4)}\right)^{\mathrm{div}} &= T^{(2)} \times \frac{e^2}{8\pi^2}\left\{\frac{s-\Sigma}{\sigma s}\left[\log\frac{1-z_1}{z_1} + \log\frac{z_2}{1-z_2}\right]\log\frac{m_\gamma}{\sqrt{s}}\right. \\ &\qquad\left. - \log\frac{m_\gamma}{M_{\pi^\pm}} - \log\frac{m_\gamma}{M_{K^\pm}}\right\} \\ &\equiv T^{(2)} \times \frac{e^2}{8\pi^2}\,L(m_\gamma)\ . \end{aligned} \tag{B.67}$$

The total cross section is obtained from the amplitude via

$$\sigma = \frac{1}{64\pi^2 s}\frac{|\mathbf{q}_{\mathrm{out}}|}{|\mathbf{q}_{\mathrm{in}}|}\int |T|^2 d\Omega\ , \tag{B.68}$$

with $|\mathbf{q}_{\mathrm{in}}|$ and $|\mathbf{q}_{\mathrm{out}}|$ defined as in Eqs. (5.16), (5.17). The infrared divergent part of the total cross section can be calculated from Eq. (B.68) to be

$$\begin{aligned}\sigma^{\mathrm{div}} &= \frac{e^2}{(4\pi)^3}\frac{|\mathbf{q}_{\mathrm{out}}|}{|\mathbf{q}_{\mathrm{in}}|s}\left\{\left[c_0 + \left(c_s - \frac{c_t+c_u}{2}\right)s + \frac{c_t+c_u}{2}\left(M_{K^+}^2+M_{K^0}^2+M_{\pi^+}^2+M_{\pi^0}^2\right)\right.\right. \\ &\quad \left.\left. - \frac{c_t-c_u}{2}\frac{(M_{K^+}^2-M_{\pi^+}^2)(M_{K^0}^2-M_{\pi^0}^2)}{s}\right]^2 + \frac{4}{3}(c_t-c_u)^2|\mathbf{q}_{\mathrm{in}}|^2|\mathbf{q}_{\mathrm{out}}|^2\right\}L(m_\gamma)\ . \end{aligned} \tag{B.69}$$

B.6 The radiative cross section

The amplitude for the process

$$\pi^-(q_\pi)\,K^+(q_K) \to \pi^0(p_\pi)\,K^0(p_K)\,\gamma(l) \tag{B.70}$$

is given, to lowest order, by

$$\begin{aligned} T^\gamma &= \frac{e\,\epsilon^*\cdot(2q_K-l)}{2q_K\cdot l - m_\gamma^2}\Big(c_0 + c_s\,s_2 + c_t\,t_\pi + c_u\,u_\pi\Big) \\ &- \frac{e\,\epsilon^*\cdot(2q_\pi-l)}{2q_\pi\cdot l - m_\gamma^2}\Big(c_0 + c_s\,s_2 + c_t\,t_K + c_u\,u_K\Big) \\ &+ \frac{e}{2\sqrt{2}F^2}\,\epsilon^*\cdot\left\{\Big(q_K - q_\pi + p_K - p_\pi\Big)\cos\epsilon + \Big(q_K - q_\pi - 3p_K + 3p_\pi\Big)\frac{\sin\epsilon}{\sqrt{3}}\right\}\ , \end{aligned} \tag{B.71}$$

where

$$s_2 = (p_\pi + p_K)^2\ , \quad t_{\pi/K} = (q_{\pi/K} - p_{\pi/K})^2\ , \quad u_{\pi/K} = (q_{\pi/K} - p_{K/\pi})^2\ . \tag{B.72}$$

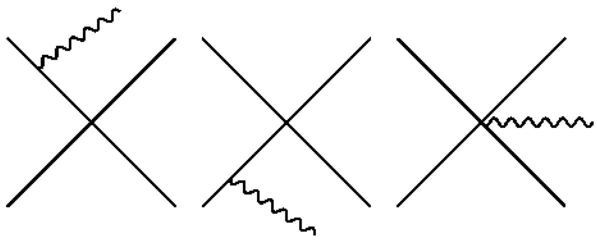

Figure B.1: Diagrams contributing to $\pi^- K^+ \to \pi^0 K^0 \gamma$ at tree level.

The three terms in Eq. (B.72) correspond to the three diagrams in Fig. B.1. The total cross section can be calculated from this amplitude by

$$\sigma^\gamma = \frac{1}{(2\pi)^5}\frac{1}{4|\mathbf{q}_{\rm in}|\sqrt{s}}\int dE_l \int d\Omega_{p_\pi}\int d\Omega_{p_\pi l}\frac{|\mathbf{p}_\pi||\mathbf{l}|}{8\left(E_{K^0}+E_{\pi^0}\left(1+\frac{|\mathbf{l}|}{|\mathbf{p}_\pi|}\cos\theta_{p_\pi l}\right)\right)}|T^\gamma|^2 \,, \tag{B.73}$$

where θ_{p_π} refers to the the angle between the outgoing pion and the axis of the incoming particles (in their center of mass system), and $\theta_{p_\pi l}$ denotes the relative angle between the outgoing pion and the photon.

B.6.1 Infrared divergence

One important check resulting from the exact calculation of the radiative cross section is that the infrared divergences indeed cancel when combining radiative and non radiative cross sections, we therefore demonstrate how to isolate the infrared divergent parts in the cross section Eq. (B.73). These stem exclusively from the lower integration bound of the E_l–integration, therefore it suffices to collect the leading powers in $1/E_l$ of the integrand. The squared matrix element simplifies considerably in this approximation, one may set $s_2 \to s$, $t_{\pi/K} \to t$, $u_{\pi/K} \to u$, and obtains

$$|T^\gamma|^2 = e^2\left\{-\frac{M_{\pi^\pm}^2}{(l\cdot q_\pi)^2}-\frac{M_{K^\mp}^2}{(l\cdot q_K)^2}+\frac{s-M_{\pi^\pm}^2-M_{K^\mp}^2}{l\cdot q_\pi\; l\cdot q_K}\right\}\Big(c_0+c_s s+c_t t+c_u u\Big)^2+\mathcal{O}(E_l^{-1}) \,. \tag{B.74}$$

As is well known from Quantum Electrodynamics, infrared divergences arise only from diagrams with soft photon radiation *from external legs* (diagrams (a), (b) in Fig. B.1), and indeed contributions from the diagram where the photon is radiated from the πK–vertex (diagram (c) in Fig. B.1) play no role here. Furthermore, we can set $|\mathbf{p}_\pi| = |\mathbf{q}_{\rm out}|$ (which is, as above, the modulus of the outgoing momentum of the *non–radiative* process), and use the abbreviations $y = \cos\theta_{p_\pi l}$, $z = \cos\theta_{p_\pi}$, to obtain

$$\sigma^\gamma = \frac{e^2}{(4\pi)^3}\frac{|\mathbf{q}_{\rm out}|}{4|\mathbf{q}_{\rm in}|s}\int_{m_\gamma}^{E_\gamma^{\rm max}} dE_l\, E_l\int_{-1}^{1}dz\int_{-1}^{1}dy\int_0^{2\pi}\frac{d\phi_{p_\pi l}}{2\pi} \tag{B.75}$$

$$\times \;\left\{-\frac{M_{\pi^\pm}^2}{(l\cdot q_\pi)^2}-\frac{M_{K^\pm}^2}{(l\cdot q_K)^2}+\frac{s-M_{\pi^\pm}^2-M_{K^\pm}^2}{l\cdot q_\pi\; l\cdot q_K}\right\}\Big(c_0+c_s s+c_t t+c_u u\Big)^2+\mathcal{O}(m_\gamma^0)\;.$$

Note that in this approximation, the term $c_0+c_s s+c_t t+c_u u$ depends, of all integration variables, only on z (via t and u). The $\phi_{p_\pi l}$ integration is relatively straightforward when using

$$l\cdot q_{\pi/K}=E_l\,|\mathbf{q}_{\rm in}|\,\Big(S_{\pi/K}\mp\cos\alpha\Big)\;, \tag{B.76}$$

where

$$S_{\pi/K}=\frac{s\mp M_{K^\pm}^2\pm M_{\pi^\pm}^2}{2|\mathbf{q}_{\rm in}|\sqrt{s}}\;,\qquad \cos\alpha=yz-\sqrt{1-y^2}\sqrt{1-z^2}\cos\phi_{p_\pi l}\;\;, \tag{B.77}$$

such that, for example, the first term in the curly brackets in Eq. (B.76) yields

$$M_{\pi^\pm}^2\int_{-1}^1 dy\int_0^{2\pi}\frac{d\phi_{p_\pi l}}{2\pi}\frac{1}{(l\cdot q_\pi)^2}=\frac{M_{\pi^\pm}^2}{E_l^2|\mathbf{q}_{\rm in}|^2}\int_{-1}^1 dy\frac{S_\pi-yz}{(S_\pi^2-1-2S_\pi yz+y^2+z^2)^{3/2}}=\frac{2}{E_l^2}\;, \tag{B.78}$$

and the other terms can be evaluated similarly. The only remaining z–dependence is the one which is also inherent in the integration of the non radiative cross section,

$$\int_{-1}^1 dz\Big(c_0+c_s s+c_t t+c_u u\Big)^2\;. \tag{B.79}$$

Altogether, one ends up with

$$\begin{aligned}\sigma^\gamma \;=\;& \frac{e^2}{(4\pi)^3}\frac{|\mathbf{q}_{\rm out}|}{|\mathbf{q}_{\rm in}|s}\log\Big(\frac{E_\gamma^{\rm max}}{m_\gamma}\Big)\left\{\frac{s-M_{K^\pm}^2-M_{\pi^-}^2}{2|\mathbf{q}_{\rm in}|\sqrt{s}}\Big(\log\frac{S_K+1}{S_K-1}+\log\frac{S_\pi+1}{S_\pi-1}\Big)-2\right\}\\ &\times\left\{\Big[c_0+\Big(c_s-\frac{c_t+c_u}{2}\Big)s+\frac{c_t+c_u}{2}\Big(M_{K^\pm}^2+M_{K^0}^2+M_{\pi^\pm}^2+M_{\pi^0}^2\Big)\right.\\ &\left.-\frac{c_t-c_u}{2}\frac{(M_{K^\pm}^2-M_{\pi^\pm}^2)(M_{K^0}^2-M_{\pi^0}^2)}{s}\Big]^2+\frac{4}{3}(c_t-c_u)^2|\mathbf{q}_{\rm in}|^2|\mathbf{q}_{\rm out}|^2\right\}+\mathcal{O}(m_\gamma^0)\;,\end{aligned} \tag{B.80}$$

which cancels the m_γ divergence in Eq. (B.69).

B.6.2 The radiative cross section at threshold

The other aspect of the radiative cross section on which one would like to have analytical information is the remainder at threshold. As the incoming charged particles are at rest at threshold, the angular integration for the total cross section simplifies considerably: the integration $d\Omega_{p_\pi}$ is trivial, and so is the integration $d\phi_{p_\pi l}$, hence the only angular variable to integrate is $dy=d\cos\theta_{p_\pi l}$, which is most conveniently done in the center–of–mass frame of the outgoing π^0K^0 system. Large cancellations take place, such that one obtains a surprisingly simple expression:

$$\begin{aligned}\int_{-1}^1 dy\,|T^\gamma|^2_{\rm thr} \;=\;& \frac{e^2}{24F^4}\Big(\cos\epsilon-\sqrt{3}\sin\epsilon\Big)^2\frac{(M_{K^-}+M_{\pi^-})^2}{M_{K^+}M_{\pi^-}}\\ &\times\;\frac{\Big(s_2-(M_{K^\pm}-M_{\pi^\pm})^2\Big)\Big(s_2-(M_{K^0}-M_{\pi^0})^2\Big)\Big(s_2-(M_{K^0}+M_{\pi^0})^2\Big)}{s_2^2}\;.\end{aligned} \tag{B.81}$$

In order to obtain Eq. (B.82), it is essential to take the radiation from the four–meson vertex (diagram (c) in Fig. B.1) into account, the vertex of which is linked to the $\pi^- K^+ \to \pi^0 K^0$ vertex by gauge symmetry. In fact, we find that just by expressing the coefficients for the 5 point vertex (the third term in Eq. (B.72)) by c_t and c_u, any dependence on c_0 and c_s drops out completely. This is why for the case of $\pi^+\pi^- \to \pi^0\pi^0\gamma$, the cross section vanishes at threshold: the lowest order $\pi^-\pi^- \to \pi^0\pi^0$ vertex is proportional to $s - M_{\pi^0}^2$ (in the σ gauge), and the $\pi^-\pi^- \to \pi^0\pi^0\gamma$ point vertex vanishes (again in the σ gauge). Furthermore, the result of Eq. (B.82) is proportional to $(c_t - c_u)^2$ which demonstrates that only the particular "asymmetry" of the reaction in question allows a finite remainder to survive at threshold.

Transforming the remaining integration over the energy of the outgoing photon into an integration of s_2, we obtain the total cross section at threshold via

$$\sigma^\gamma_{\text{thr}} = \frac{1}{(8\pi)^3} \frac{|\mathbf{q}_{\text{out}}|}{|\mathbf{q}_{\text{in}}| s} \int_{s_2^{\text{thr}}}^{s} ds_2 \left(\frac{s - s_2}{s_2}\right) \sqrt{\frac{(s_2 - (M_{K^0} - M_{\pi^0})^2)(s_2 - (M_{K^0} + M_{\pi^0})^2)}{(s - (M_{K^0} - M_{\pi^0})^2)(s - (M_{K^0} + M_{\pi^0})^2)}} \times \int_{-1}^{1} dy \, |T^\gamma|^2_{\text{thr}} \ , \tag{B.82}$$

where $s_2^{\text{thr}} = (M_{K^0} + M_{\pi^0})^2$ is the minimal energy (squared) for the final $\pi^0 K^0$ system. Eq. (B.82) is evaluated to leading order in isospin violation parameters, yielding the result

$$\sigma^\gamma_{\text{thr}} = \frac{e^2}{105(2\pi)^3 F_\pi^4} \frac{|\mathbf{q}_{\text{out}}|}{|\mathbf{q}_{\text{in}}| s} \frac{M_{K^-} M_{\pi^+}}{M_{K^+} + M_{\pi^+}} \Big(M_{K^-} - M_{K^0} + M_{\pi^+} - M_{\pi^0}\Big)^3 + \mathcal{O}(\delta^5) \ . \tag{B.83}$$

In terms of fundamental isospin breaking parameters, the meson mass difference in Eq. (B.83) can be expressed as

$$M_{K^-} - M_{K^0} + M_{\pi^-} - M_{\pi^0} = \frac{B(m_u - m_d)}{2M_K} + Ze^2F^2\left(\frac{1}{M_K} + \frac{1}{M_\pi}\right) + \mathcal{O}(\delta^2) \ . \tag{B.84}$$

Acknowledgements

At the end of this thesis, I would like to express my gratitude towards all those who, in one way or another, were involved in my scientific work during the last three years.

First of all, I would very much like to thank my thesis advisor Prof. Ulf-G. Meißner: for his interest in my work, for sharing his insights into physics with me, for the collaboration on the various publications that emerged from this research, and for his encouragement during the inevitable difficult periods of a long PhD work.

I thank Prof. H.R. Petry for agreeing to carefully read and assess this thesis.

My thanks, furthermore, go to the various members of our group for interesting discussions and help on all sorts of questions during the various stages of my work: Dr. Paul Büttiker, Dr. Nadia Fettes, Matthias Frink, Dr. Thomas Hemmert, Hermann Krebs, Dr. José-Antonio Oller, Lucas Platter, Markus Walzl, Priv.-Doz. Andreas Wirzba. Nadia, thank you also for all the help on proof reading drafts of publications and of this thesis! Furthermore, also Dr. Christoph Hanhart, Prof. Nikolai N. Nikolaev, Felix Sassen, and Sonja Schneider were always open for questions. As a short–term visitor in Jülich, Thomas Becher was most helpful, as were discussions with Prof. Véronique Bernard via email.

I would very much like to thank Prof. Jürg Gasser for offering me the opportunity to visit the Institute of Theoretical Physics in Bern. The discussions with, in particular, him, Dr. Akaki Rusetsky, and Julia Schweizer were most stimulating and encouraging for my research.

I am very grateful to several people who made my visit at the University of Massachusetts in Amherst such a pleasant experience: Prof. Barry R. Holstein, Prof. John F. Donoghue, Dr. Martin Mojžiš, Tobias Huber, Andreas Roß were a wonderfully lively group, sharing so many thoughts and insights that I profited immensely from those three months. And thank you, Tobi, Andi, Martin and your family, for also making life in Amherst so much more interesting.

This thesis would not have been possible without the financial support of the scholarships granted by the "Studienstiftung des deutschen Volkes" and by the Graduiertenkolleg "Die Erforschung subnuklearer Strukturen der Materie" at Bonn University, as well as additional support by the Forschungszentrum Jülich. In particular, I would like to thank the Graduiertenkolleg for allowing me to participate at the Chiral

Dynamics 2000 conference at Jefferson Lab, and the Studienstiftung for their generous support of my stay at UMass.

A big thank you to Dominik Giel, Reinhard Priber, Simon Trebst, and Anja Wille for keeping up my friendship bonds to our common university town. Thanks also to Sonja, Felix, and Andreas Motzke for proving that there is life in Jülich.

My parents and my brother gave me all the help and support in "real life" I could ever ask for. Their voices of sanity and reason from outside science and research were both encouraging and helped to keep me grounded.

Nadia, thank you for everything. I would never have come this far without you.

Bibliography

[A102] MAMI A1 collaboration, H. Merkel et al., *Phys. Rev. Lett.* **88** (2002) 012301.

[A4] MAMI A4 collaboration, D. v. Harrach (spokesperson), F.E. Maas (contact person), et al. (unpublished).

[AB01] B. Ananthanarayan and P. Büttiker, *Eur. Phys. J.* **C19** (2001) 517.

[ABT01] G. Amoros, J. Bijnens, and P. Talavera, *Nucl. Phys.* **B602** (2001) 87.

[Ad94] B. Adeva et al., CERN-SPSLC-95-1, CERN-SPSLC-P-284, Dec. 1994.

[Ad99] M. Adamovich et al., *Eur. Phys. J.* **C8** (1999) 59.

[Ad00] B. Adeva et al., CERN-SPSC-2000-032, CERN-SPSC-P-284-ADD-1, Aug. 2000.

[BCT98] J. Bijnens, G. Colangelo, and P. Talavera, *J. High Energy Phys.* **9805** (1998) 014.

[Be97] S.R. Beane, V. Bernard, T.-S.H. Lee, U.-G. Meißner, and U. van Kolck, *Nucl. Phys.* **A618** (1997) 381.

[Be02] S.R. Beane, V. Bernard, E. Epelbaum, U.-G. Meißner, and D.R. Phillips, `hep-ph/0206219`.

[BEG95] J. Bijnens, G. Ecker, and J. Gasser, in: L. Maiani, G. Pancheri, and N. Paver (eds.), *The second DAΦNE Physics Handbook* (INFN, Frascati) (1995).

[BFHM98] V. Bernard, H.W. Fearing, T.R. Hemmert, and U.-G. Meißner, *Nucl. Phys.* **A635** (1998) 121; (E) *Nucl. Phys.* **A642** (1998) 563.

[BGT97] J. Bijnens, P. Gosdzinsky, and P. Talavera, *Nucl. Phys.* **B501** (1997) 495; *JHEP* **9801** (1998) 014; *Phys. Lett.* **B429** (1998) 111.

[BHM02] V. Bernard, T.R. Hemmert, and U.-G. Meißner, `hep-ph/0203167`; work in progress.

[BKKM92] V. Bernard, N. Kaiser, J. Kambor, and U.-G. Meißner, *Nucl. Phys.* **B388** (1992) 315.

[BKLM94] V. Bernard, N. Kaiser, T.-S.H. Lee, and U.-G. Meißner, *Phys. Rept.* **246** (1994) 315.

[BKM91a] V. Bernard, N. Kaiser, and U.-G. Meißner, *Phys. Rev.* **D43** (1991) R2757.

[BKM91b] V. Bernard, N. Kaiser, and U.-G. Meißner, *Nucl. Phys.* **B357** (1991) 129.

[BKM95a] V. Bernard, N. Kaiser, and U.-G. Meißner, *Int. J. Mod. Phys.* **E4** (1995) 193.

[BKM95b] V. Bernard, N. Kaiser, and U.-G. Meißner, *Phys. Rev.* **C52** (1995) 2185.

[BKM95c] V. Bernard, N. Kaiser, and U.-G. Meißner, *Nucl. Phys.* **B457** (1995) 147.

[BKM96a] V. Bernard, N. Kaiser, and U.-G. Meißner, *Z. Phys.* **C70** (1996) 483.

[BKM96b] V. Bernard, N. Kaiser, and U.-G. Meißner, *Nucl. Phys.* **A607** (1996) 379; (E) *Nucl. Phys.* **A633** (1998) 695.

[BKM96c] V. Bernard, N. Kaiser, and U.-G. Meißner, *Nucl. Phys.* **A611** (1996) 429.

[BKM97] V. Bernard, N. Kaiser, and U.-G. Meißner, *Nucl. Phys.* **A615** (1997) 483.

[BKM01] V. Bernard, N. Kaiser, and U.-G. Meißner, *Eur. Phys. J.* **A11** (2001) 209.

[BKY88] M. Bando, T. Kugo, and K. Yamawaki, *Phys. Rept.* **164** (1988) 217.

[BL99] T. Becher and H. Leutwyler, *Eur. Phys. J.* **C9** (1999) 643.

[BL00] T. Becher and H. Leutwyler, *JHEP* 0106 (2001) 017.

[BM96] B. Borasoy and U.-G. Meißner, *Int. J. Mod. Phys.* **A11** (1996) 5183.

[BM00] P. Büttiker and U.-G. Meißner, *Nucl. Phys.* **A668** (2000) 97.

[BNL01] BNL E865 Collaboration, S. Pislak et al., *Phys. Rev. Lett.* **87** (2001) 221801.

[BU97] R. Baur and R. Urech, *Nucl. Phys.* **B499** (1997) 319.

[BZ72] M.A.B. Bég and A. Zepeda, *Phys. Rev.* **D6** (1972) 2912.

[CCWZ69] S. Coleman, J. Wess, and B. Zumino, *Phys. Rev.* **177** (1969) 2239; C. Callan, S. Coleman, J. Wess, and B. Zumino, *Phys. Rev.* **177** (1969) 2247.

[CGL00] G. Colangelo, J. Gasser, and H. Leutwyler, *Phys. Lett.* **B488** (2000) 261; *Phys. Rev. Lett.* **86** (2001) 5008.

[CK85] C.G. Callan and I. Klebanov, *Nucl. Phys.* **B262** (1985) 365.

[Da67] T. Das, G.S. Guralnik, V.S. Mathur, F.E. Low, and J.E. Young, *Phys. Rev. Lett.* **18** (1967) 759.

[De54] S. Deser, M.L. Goldberger, K. Baumann, and W. Thirring, *Phys. Rev.* **96** (1954) 774.

[DGS00] S. Descotes, L. Girlanda, and J. Stern, *JHEP* **0001** (2000) 041; S. Descotes and J. Stern, *Phys. Lett.* **B488** (2000) 274; S. Descotes, *JHEP* **0103** (2001) 002; S. Descotes, L. Girlanda, and J. Stern, `hep-ph/0207337`.

[DH98] L. Durand and P. Ha, *Phys. Rev.* **D58** (1998) 013010.

[DHB99] J.F. Donoghue, B.R. Holstein, and B. Borasoy, *Phys. Rev.* **D59** (1999) 036002.

[Dr00] D. Drechsel, in: D. Drechsel and L. Tiator (eds.), *Gerasimov-Drell-Hearn Sum Rule and the Nucleon Spin Structure in the Resonance Region* (GDH 2000, Mainz, Germany, June 14–17 2000), World Scientific (2001).

[Ec89] G. Ecker, J. Gasser, A. Pich, and E. de Rafael, *Nucl. Phys.* **B 321** (1989) 311; G. Ecker, J. Gasser, H. Leutwyler, A. Pich, and E. de Rafael, *Phys. Lett.* **B223** (1989) 425.

[Ec94] G. Ecker, *Phys. Lett.* **B336** (1994) 508.

[Ec00] G. Ecker, G. Müller, H. Neufeld, and A. Pich, *Phys. Lett.* **B477** (2000) 88.

[Ed66] R.J. Eden, P.V. Landshoff, D.I. Olive, and J.C. Polkinghorne, *The Analytic S-Matrix*, Cambridge University Press (1966).

[Ed94] T. Eden et al., *Phys. Rev.* **C50** (1994) R1749; M. Meyerhoff et al., *Phys. Lett.* **B327** (1994) 201; C. Herberg et al., *Eur. Phys. J.* **A5** (1999) 131; I. Passchier et al., *Phys. Rev. Lett.* **82** (1999) 4988; M. Ostrick et al., *Phys. Rev. Lett.* **83** (1999) 276; J. Becker et al., *Eur. Phys. J.* **A6** (1999) 329.

[EGM98] E. Epelbaum, W. Glöckle, and U.-G. Meißner, *Nucl. Phys.* **A637** (1998) 107; *Nucl. Phys.* **A671** (2000) 295.

[ET98] H.-B. Tang, hep-ph/9607436; P.J. Ellis and H.-B. Tang, *Phys. Rev.* **C57** (1998) 3356.

[FF60] W.R. Frazer and J.R. Fulco, *Phys. Rev.* **117** (1960) 1603, 1609.

[FKM02] M. Frink, B. Kubis, and U.-G. Meißner, *Eur. Phys. J.* **C25** (2002) 259.

[FKS00] N.H. Fuchs, M. Knecht, and J. Stern, *Phys. Rev.* **D62** (2000) 033003.

[FMMS00] N. Fettes, U.-G. Meißner, M. Mojžiš, and S. Steininger, *Ann. Phys. (NY)* **283** (2000) 273; (E) *Ann. Phys. (NY)* **288** (2001) 249.

[FMS98] N. Fettes, U.-G. Meißner, and S. Steininger, *Nucl. Phys.* **A640** (1998) 199.

[FSS91] N.H. Fuchs, H. Sazdjian, and J. Stern, *Phys. Lett.* **B269** (1991) 183.

[G0] G0 collaboration, D.H. Beck (spokesperson) et al. (unpublished).

[G201] Muon $g-2$ collaboration, H.N. Brown et al., *Phys. Rev. Lett.* **86** (2001) 2227.

[Ga99] A. Gall, J. Gasser, V.E. Lyubovitskij, and A. Rusetsky, *Phys. Lett.* **B462** (1999) 335; J. Gasser, V.E. Lyubovitskij, and A. Rusetsky, *Phys. Lett.* **B471** (1999) 244; J. Gasser, V.E. Lyubovitskij, A. Rusetsky, and A. Gall, *Phys. Rev.* **D64** (2001) 016008.

[Ga02] J. Gasser, I. Mgeladze, A. Rusetsky, and I. Scimemi, in: J. Bijnens, U.-G. Meißner, and A. Wirzba (eds.), *Effective Field Theories of QCD* (Bad Honnef, Germany, Nov. 26–30 2001), hep-ph/0201266.

[Ge84] H. Georgi, *Weak Interactions and Modern Particle Theory*, Addison-Wesley (1984).

[GH] G. Gellas and T.R. Hemmert, unpublished.

[GJJ01] V. Gadiyak, X.-D. Ji, and C.-W. Jung, *Phys. Rev.* **D65** (2002) 094510.

[GL82] J. Gasser and H. Leutwyler, *Phys. Rept.* **87** (1982) 77.

[GL83] J. Gasser and H. Leutwyler, *Phys. Lett.* **B125** (1983) 325.

[GL84] J. Gasser and H. Leutwyler, *Ann. Phys. (NY)* **158** (1984) 142.

[GL85a] J. Gasser and H. Leutwyler, *Nucl. Phys.* **B250** (1985) 465.

[GL85b] J. Gasser and H. Leutwyler, *Nucl. Phys.* **B250** (1985) 517.

[GL85c] J. Gasser and H. Leutwyler, *Nucl. Phys.* **B250** (1985) 539.

[GM91] J. Gasser and U.-G. Meißner, *Nucl. Phys.* **B357** (1991) 90.

[Go01a] J. Golak et al., *Phys. Rev.* **C63** (2001) 034006.

[Go01b] J.L. Goity, D. Lehmann, G. Prézeau, J. Saez, *Phys. Lett.* **B504** (2001) 21.

[Gr68] R.W. Griffith, *Phys. Rev.* **176** (1968) 1705.

[GS02] J. Gasser and J. Schweizer, work in progress.

[GSS88] J. Gasser, M.E. Sainio, and A. Švarc, *Nucl. Phys.* **B307** (1988) 779.

[Ha99] HAPPEX collaboration, K.A. Aniol et al., *Phys. Rev. Lett.* **82** (1999) 1096; *Phys. Lett.* **B509** (2001) 2117.

[Ha02] H.-W. Hammer, S.J. Puglia, M.J. Ramsey-Musolf, and Shi-Lin Zhu, `hep-ph/0206301`.

[HB01] B.R. Holstein and D.H. Beck, *Int. J. Mod. Phys.* **E10** (2001) 1.

[HKM99] T.R. Hemmert, B. Kubis, and U.-G. Meißner, *Phys. Rev.* **C60** (1999) 045501.

[HMD96] H.-W. Hammer, U.-G. Meißner, and D. Drechsel, *Phys. Lett.* **B385** (1996) 343.

[HMS98] T.R. Hemmert, U.-G. Meißner, and S. Steininger, *Phys. Lett.* **B437** (1998) 184.

[Ho76] G. Höhler et al., *Nucl. Phys.* **B114** (1976) 389.

[Ho90] B.R. Holstein, *Phys. Lett.* **B244** (1990) 83.

[IZ80] C. Itzykson and J.-B. Zuber, *Quantum Field Theory*, McGraw–Hill, New York (1980).

[Je93] E. Jenkins, M. Luke, A.V. Manohar, and M.J. Savage, *Phys. Lett.* **B302** (1993) 482; (E) *Phys. Lett.* **B388** (1996) 866.

[JM91] E. Jenkins and A.V. Manohar, *Phys. Lett.* **B255** (1991) 558; E. Jenkins and A.V. Manohar, in: U.-G. Meißner (ed.), *Effective Field Theories of the Standard Model*, World Scientific (1992).

[JMW95] E. Jenkins, A. Manohar, and M. Wise, *Phys. Rev. Lett.* **97** (1995) 2272.

[JS98] H. Jallouli and H. Sazdjian, *Phys. Rev.* **D58** (1998) 014011; (E) *Phys. Rev.* **D58** (1998) 099901.

[KBM00] V. Bernard, H. Krebs, and U.-G. Meißner, *Phys.Rev.* **C61** (2000) 058201; H. Krebs, V. Bernard, and U.-G. Meißner, `nucl-th/0207072`.

[KHM99] B. Kubis, T.R. Hemmert, and U.-G. Meißner, *Phys. Lett.* **B456** (1999) 240.

[KM00a] J. Kambor and M. Mojžiš, *Phys. Lett.* **B476** (2000) 344.

[KM00b] B. Kubis and U.-G. Meißner, *Nucl. Phys.* **A671** (2000) 332; (E) *Nucl. Phys.* **A692** 647.

[KM01a] B. Kubis and U.-G. Meißner, *Nucl. Phys.* **A679** (2001) 698.

[KM01b] B. Kubis and U.-G. Meißner, *Eur. Phys. J.* **C18** (2001) 747.

[KM02a] B. Kubis and U.-G. Meißner, *Nucl. Phys.* **A699** (2002) 709.

[KM02b] B. Kubis and U.-G. Meißner, *Phys. Lett.* **B529** (2002) 69.

[Kn93] M. Knecht, H. Sazdjian, J. Stern, and N.H. Fuchs, *Phys. Lett.* **B313** (1993) 229.

[KN02] M. Knecht and A. Nehme, *Phys. Lett.* **B532** (2002) 55.

[KSFR66] K. Kawarabayashi and M. Suzuki, *Phys. Rev. Lett.* **16** (1966) 255; Fayyazuddin and Riazuddin, *Phys. Rev.* **147** (1966) 1071.

[KSW98] D.B. Kaplan, M.J. Savage, and M.B. Wise, *Phys. Lett.* **B424** (1998) 390; *Nucl. Phys.* **B534** (1998) 329.

[KU98] M. Knecht and R. Urech, *Nucl. Phys.* **B519** (1998) 329.

[Le94] H. Leutwyler, *Ann. Phys. (NY)* **235** (1994) 165.

[LP01] D. Lehmann and G. Prézeau, *Phys. Rev.* **D65** (2001) 016001.

[LR00] V.E. Lyubovitskij and A. Rusetsky, *Phys. Lett.* **B494** (2000) 9.

[LWD91] D.B. Leinweber, R.M. Woloshyn, and T. Draper, *Phys. Rev.* **D43** (1991) 1659.

[Ma93] P. Markowitz et al., *Phys. Rev.* **C48** (1993) R5; H. Gao et al., *Phys. Rev.* **C50** (1994) R546; H. Anklin et al., *Phys. Lett.* **B336** (1994) 313; E.E.W. Bruins et al., *Phys. Rev. Lett.* **75** (1995) 21; H. Anklin et al., *Phys. Lett.* **B428** (1998) 248; W. Xu et al., *Phys. Rev. Lett.* **85** (2000) 2900; G. Kubon et al., *Phys. Lett.* **B524** (2002) 26.

[Me88] U.-G. Meißner, *Phys. Rept.* **161** (1988) 213.

[Me98] U.-G. Meißner, in: J. Goity (ed.), *Themes in strong interaction physics*, World Scientific (1998), hep-ph/9711365.

[Me00] U.-G. Meißner, *Nucl. Phys.* **A666&667** (2000) 51c.

[Me01] K. Melnikov, *Int. J. Mod. Phys.* **A16** (2001) 4591.

[MM97] G. Müller and U.-G. Meißner, *Nucl. Phys.* **B492** (1997) 379.

[MMD96] P. Mergell, U.-G. Meißner, and D. Drechsel, *Nucl. Phys.* **A596** (1996) 367.

[MMS97] U.-G. Meißner, G. Müller, and S. Steininger, *Phys. Lett.* **B406** (1997) 154.

[MO00] U.-G. Meißner and J.A. Oller, *Nucl. Phys.* **A673** (2000) 311.

[MR00] K. Melnikov and T. van Ritbergen, *Phys. Rev. Lett.* **84** (2000) 1673.

[MS97] U.-G. Meißner and S. Steininger, *Nucl. Phys.* **B499** (1997) 349.

[MS98] U.-G. Meißner and S. Steininger, *Phys. Lett.* **B419** (1998) 403.

[Mu94] M.J. Musolf et al., *Phys. Rept.* **239** (1994) 1.

[Ne02] A. Nehme, *Eur. Phys. J.* **C23** (2002) 707.

[NR95] H. Neufeld and H. Rupertsberger, *Z. Phys.* **C68** (1995) 91.

[NT02] A. Nehme and P. Talavera, *Phys. Rev.* **D65** (2002) 054023.

[Ou01] S.M. Ouellette, hep-ph/0101055.

[PDG02] Particle Data Group, K. Hagiwara et al., *Phys. Rev.* **D66** (2002) 010001.

[Pe89] R.D. Peccei, in: C. Jarlskog (ed.), *CP violation*, World Scientific (1989) (*Adv. Ser. Direct. High Energy Phys.* **3** (1989) 503).

[Pe00] G.G. Petratos, *Nucl. Phys.* **A666&667** (2000) 61c.

[PR00] S.J. Puglia and M.J. Ramsey-Musolf, *Phys. Rev.* **D62** (2000) 034010.

[PRZ01] S.J. Puglia, M.J. Ramsey-Musolf, and Shi-Lin Zhu, *Phys. Rev.* **D63** (2001) 034014.

[Ra99] P.G. Ratcliffe, *Phys. Rev.* **D59** (1999) 014038.

[RI97] M.J. Ramsey-Musolf and H. Ito, *Phys. Rev.* **C55** (1997) 3066.

[Ro99] A. Roessl, *Nucl. Phys.* **B555** (1999) 507.

[Ro00] R. Rosenfelder, *Phys. Lett.* **B479** (2000) 381.

[RS76] F.S. Roig and A.R. Swift, *Nucl. Phys.* **B104** (1976) 533.

[Sa97] SAMPLE collaboration, B. Mueller et al., *Phys. Rev. Lett.* **78** (1997) 3824; R. Hasty et al., *Science* **290** (2000) 211.

[Sa01] M.E. Sainio, `hep-ph/0110413`.

[Sc99] H.-Ch. Schröder et al., *Phys. Lett.* **B469** (1999) 25.

[Se01] SELEX collaboration, I. Eschrich et al., *Phys.Lett.* **B522** (2001) 233.

[TE02] K. Torikoshi and P.J. Ellis, `nucl-th/0208049`.

[tHo76] G. 't Hooft, *Phys. Rev. Lett.* **37** (1976) 8.

[Ur95] R. Urech, *Nucl. Phys.* **B433** (1995) 234.

[We66] S. Weinberg, *Phys. Rev. Lett.* **17** (1966) 616.

[We67] S. Weinberg, *Phys. Rev. Lett.* **18** (1967) 507.

[We77] S. Weinberg, *Trans. New York Acad. Sci.* **38** (1977) 185.

[We79] S. Weinberg, *Physica* **96A** (1979) 327.

[We90] S. Weinberg, *Phys. Lett.* **B251** (1990) 288; *Nucl. Phys.* **B363** (1991) 3.

[Wi96] M. Wicky, Diploma Thesis, University of Bern (1996), unpublished.

Forschungszentrum Jülich
in der Helmholtz-Gemeinschaft

Jül-4007
Oktober 2002
ISSN 0944-2952